

# **New Applications of Organic Polymers in Chemical Gas Sensors**

## **Neue Einsatzmöglichkeiten organischer Polymere in chemischen Gassensoren**

DISSERTATION

der Fakultät für Chemie und Pharmazie  
der Eberhard-Karls-Universität Tübingen

zur Erlangung des Grades eines Doktors  
der Naturwissenschaften

2005

vorgelegt von

MIKA HARBECK

Tag der mündlichen Prüfung: 18.11.2005

- Dekan: Prof. Dr. S. Laufer  
1. Berichterstatter: PD Dr. U. Weimar  
2. Berichterstatter: Prof. Dr. G. Gauglitz

# Contents

<b>1. Introduction</b>	<b>1</b>
1.1. Introduction to the Field . . . . .	1
1.2. Motivation and Scope . . . . .	4
1.3. Overview of the Presented Work . . . . .	5
<b>2. Theoretical Background and Related Work</b>	<b>7</b>
2.1. Sorption Processes . . . . .	7
2.2. Electrochemical Aspects of Interfaces . . . . .	11
2.3. The Chemical and Physical Structure of the Electrical Double Layer . . . . .	16
2.4. Measuring the Work Function and Surface Potentials . . . . .	30
2.5. Chemical Sensing with Field Effect Devices . . . . .	41
<b>3. Experimental Details</b>	<b>51</b>
3.1. Instrumental Equipment . . . . .	51
3.2. Materials for the Preparation of the Sensing Layers . . . . .	59
3.3. Polymer Deposition . . . . .	64
3.4. Measurement Procedure . . . . .	70
<b>4. Sensitive Layer Morphology: Characterisation and Optimization</b>	<b>73</b>
4.1. Polyacrylic Acid Layers . . . . .	74
4.2. Polystyrene Layers . . . . .	81
4.3. Poly-(4-vinylphenol) Layers . . . . .	84
4.4. Poly-(acrylonitrile-co-butadiene) Layers . . . . .	86
4.5. Poly-(cyanopropyl-phenyl-siloxane) Layers . . . . .	87
4.6. Summary . . . . .	87
<b>5. Response to Analyte Gases</b>	<b>89</b>
5.1. Inert Reference Material and Uncoated Substrates . . . . .	89
5.2. Polyacrylic Acid Coated Substrates . . . . .	91
5.3. Polystyrene Coated Substrates . . . . .	114
5.4. Poly-(4-vinylphenol) Coated Substrates . . . . .	122
5.5. Poly-(acrylonitrile-co-butadiene) Coated Substrates . . . . .	129
5.6. Poly-(cyanopropyl-phenyl-siloxane) Coated Substrates . . . . .	133

5.7. Summary of the KP and QMB Experiments . . . . .	135
5.8. A Model for the Origin of the Observed KP Signals . . . . .	141
<b>6. Conclusion and Outlook</b>	<b>149</b>
6.1. General Conclusions . . . . .	149
6.2. Outlook . . . . .	150
<b>A. The Grahame Equation</b>	<b>151</b>

## List of Acronyms

<b>AFM</b>	Atomic Force Microscope
<b>BAW</b>	Bulk Acoustic Wave
<b>CCFET</b>	Capacitively Coupled Field Effect Transistor
<b>ChemFET</b>	Chemical Field Effect Transistor
<b>CMOS</b>	Complementary Metal Oxide Semiconductor
<b>CVD</b>	Chemical Vapour Deposition
<b>DCM</b>	Dichloromethane
<b>DL</b>	(Electrical) Double Layer
<b>FET</b>	Field Effect Transistor
<b>GasFET</b>	Gas Sensitive Field Effect Transistor
<b>IC</b>	Integrated Circuit
<b>IGFET</b>	Isolated Gate Field Effect Transistor
<b>IR</b>	Infrared
<b>ISFET</b>	Ion Selective Field Effect Transistor
<b>ITO</b>	Indium Tin Oxide
<b>KFM</b>	Kelvin Force Microscope
<b>KP</b>	Kelvin Probe
<b>KPFM</b>	Kelvin Probe Force Microscope
<b>LB</b>	Langmuir-Blodgett
<b>LOD</b>	Limit of Detection, i. e. lower limit
<b>MFC</b>	Mass Flow Controller
<b>MIS</b>	Metal Insulator Semiconductor
<b>MISCAP</b>	Metal Insulator Semiconductor Capacitor
<b>MISFET</b>	Metal Insulator Semiconductor Field Effect Transistor
<b>MOSFET</b>	Metal Oxide Semiconductor Field Effect Transistor

<b>OM</b>	Optical Microscope
<b>PAA</b>	Polyacrylic Acid
<b>PAB</b>	Poly(acrylonitrile-co-butadiene)
<b>PCPhS</b>	Poly-(cyanopropyl-phenyl-siloxane)
<b>PDMS</b>	Polydimethylsiloxane
<b>PEG</b>	Polyethyleneglycol
<b>PES</b>	Photoelectron Emission Spectroscopy
<b>PMAA</b>	Poly(methyl acrylic acid)
<b>PMMA</b>	Poly(methyl methacrylate)
<b>PS</b>	Polystyrene
<b>PTFE</b>	Poly(tetrafluoroethylene)
<b>PVA</b>	Polyvinylalcohol
<b>PVPh</b>	Poly(4-vinylphenol)
<b>pzc</b>	Point of Zero Charge
<b>QMB</b>	Quartz (Crystal) Micro Balance
<b>SAM</b>	Self-Assembled Monolayer
<b>SAW</b>	Surface Acoustic Wave
<b>SEM</b>	Scanning Electron Microscope
<b>SGFET</b>	Suspended Gate Field Effect Transistor
<b>SPV</b>	Surface Photo Voltage
<b>TLM</b>	Triple Layer Model
<b>UHV</b>	Ultra High Vacuum
<b>UPS</b>	Ultraviolet Photon Spectroscopy
<b>UV</b>	Ultraviolet
<b>VOC</b>	Volatile Organic Compound

## Notation

List of the most common symbols used throughout the text.

$C$	Concentration
$\chi$	Surface potential
$e$	Electron charge
$E_C$	Conduction band edge
$E_F$	Fermi energy level
$E_{pot}$	Potential energy
$\varepsilon$	Relative permittivity
$\varepsilon_0$	Permittivity of vacuum
$E_V$	Valence band edge
$E_{vac}$	Vacuum energy level
$F$	Faraday's constant
$h$	Planck's constant
$K$	Equilibrium constant
$k$	Boltzmann's constant
$\tilde{\mu}_i$	Electrochemical potential
$\mu_i$	Chemical potential
$\nu$	Frequency of electro-magnetic radiation
$p$	Partial pressure
$p_0$	Saturation vapour pressure
$\Phi$	Galvani potential
$\phi$	Work function
$\varphi$	Work function (potential)
$\Psi$	Volta potential
$R$	General gas constant
$R_a$	Surface profile: average roughness

## Notation

---

$R_p$	Surface profile: height of peaks
$R_q$	Surface profile: rms average roughness
$R_v$	Surface profile: depth of valleys
$R_{zi}; R_t$	Surface profile: peak-to-peak roughness
$T$	Absolute temperature
$t$	Temperature
$T_g$	Glass transition temperature
$\theta$	Relative surface coverage
$\tau_{off}$	Recovery time constant
$\tau_{on}$	Response time constant
$V_b$	KP backing potential
$V_{CPD}$	Contact potential
$V_{K,S}$	Sum of contact potential and KP backing potential
$V_S$	Band bending
$\tilde{\zeta}$	Electron affinity
$z_i$	Charge number



# 1. Introduction

## 1.1. Introduction to the Field

### 1.1.1. Chemical Micro Gas Sensors

Chemical gas sensors have been of much scientific and commercial interest already for several decades. Metal oxide semiconductor sensors based on ZnO and SnO<sub>2</sub> were first developed by Seiyama et al. [1] and Taguchi [2] in the beginning 1960s as detectors for liquid petroleum gases (LPG) in homes. This sensor type was soon followed by others, e. g. quartz micro balance (QMB) sensors for the detection of volatile organic compounds (VOC) as reported by King [3]. Since then, chemical gas sensors have undergone a long development and they are nowadays in use in several application fields.

New application areas provoke a steady development of new sensor types to meet the additional requirements. At the same time, new sensor types open up new applications areas. Hence, much effort has been spent among others on the development of microsensors. The miniaturization of sensor devices offers substantial advantages such as low power consumption, small size, and batch fabrication at industrial standards like complementary metal oxide semiconductor (CMOS) compatible processes. Those are very crucial issues, for example, in battery-operated systems and infer low costs to the sensor user. Besides, the production technique allows easy addition of signal acquisition and data evaluation circuitry, partly a necessity due to the small signal of the transducer and partly an advantageous step in integration. Nevertheless, the very common CMOS microsensors inherit some disadvantages of CMOS devices like a limited operation temperature range and high development costs. The development and production of CMOS microsensors only pays off in mass market applications.

Microsensors based on several transduction principles are known and developed, as there are cantilevers, thermopiles, or capacitive/resistive structures for polymer layers or micro hotplates for metal oxides. A very prominent example of a microsensor is the chemical field effect transistor (Chem-FET), namely the gas sensitive field effect transistor (GasFET) as introduced by Lundström et al. [4] for the detection of hydrogen. Meanwhile, many other designs of the GasFET have been developed and a wide range of new sensitive materials has been tested. A common derivation of the Lund-

ström field effect transistor (FET) is the suspended gate field effect transistor (SGFET), known for almost twenty years. Several SGFET types are described in the literature, but there has been no significant commercialization of this sensor type, as yet. However, for SGFETs a prospective future is envisioned, as they allow cheap production, low-power operation, and are flexible in the choice of the sensitive material, and suitable for many new applications [5, 6]. A very personal view on the future of the GasFET together with a summary of its possible application is given by Janata [7].

### 1.1.2. Polymeric Sensitive Layers

The performance of a chemical gas sensor is generally judged on several criteria. The most common performance criteria are the classical factors of sensitivity, selectivity, and stability as well as reversibility and fast response & recovery. If a sensor device can keep to the actual limits depends on the overall performance of the transducer and the chemically active layer. Sensitive layers based on organic polymers inhibit many positive features and, consequently, are of wide interest and widely used in chemical gas sensors. The existing experience in the field is a proof that they fulfil many of the aforementioned requirements.

Polymers are available in many kinds having different chemical and sorption properties. The main approach for tuning sensitivity and selectivity is a chemical modification of side groups attached to the polymer backbone. More advanced strategies like the use of cage structures or chiral molecules, to name a few, are pursued in special cases. The size exclusion principle of analyte molecules and specific interactions are in those cases the main reason for a selectivity towards certain analytes.

The versatility of polymers makes them usable in many sensor types based on different transduction principles for the detection of a variety of analytes. Most commonly, polymers are used in bulk acoustic wave (BAW) and surface acoustic wave (SAW) sensors, cantilevers, capacitive and resistive sensors, and thermopiles for the detection of VOCs. Commercially exploited to a larger extent are, for example, polymeric layers in capacitive humidity sensors.

Additional criteria not directly related to the gas sensing properties may be imposed on the sensitive material, the sensitive layer, and the deposition technique. The sensitive layers must be mechanically and chemically stable. In many cases the coverage of the sensitive layer needs to be restricted to certain areas of the sensor device. For certain sensor structures the morphology of the sensitive layer is very important and there are strict limits on surface roughness and other layer parameters. All this implies restrictions

to the choice of the material and the deposition technique.

Quite many coating technologies for the deposition of polymer films are available, as the deposition of organic material is required in many applications outside the sensor field. Those techniques can be adapted to coat sensor substrates with films of desired thickness, shape, and morphology. Some techniques, normally used in electronics for deposition of glue and soldering paste or in the production of organic electronics, allow deposition of small and structured layers, which is especially crucial for microsensors.

Normally, simple deposition methods, if applicable, are preferred. The most common ones are spin casting, spray deposition, and electrospraying. The later yields layers of highest quality in terms of uniformity and roughness, as it produces very small droplets. It has other advantages as well like little waste and consumption of the spraying solution. Other methods are screen printing of pastes, microdrop deposition techniques, and thermal evaporation for non-soluble and thermally stable compounds. However, the most simple and an established method for sensitive layer preparations is the spray deposition with a spraying nozzle. It yields good results depending on polymer and solvent, which are sufficient for most sensor types. Besides, there is a possibility of (semi-)automation. Small areas of arbitrary shape can be produced using shadow masks. The main disadvantage is the high usage of polymer and limitations in the coating of small areas.

### 1.1.3. Ammonia as Target Analyte

Ammonia is a natural gas that is present throughout the atmosphere in concentrations of low-ppb to sub-ppb levels as the result of emission from anthropogenic and natural sources. It is produced in large quantities by chemical industry for the production of fertilizers and other nitrogen-containing compounds and for the use in refrigeration systems as cooling agent. Natural source include production by bacteria.

In the environment, high concentrations of ammonia lead to eutrophication and acidification of both ground and water, whereas in indoor environments it is a health hazard to humans. Therefore ammonia is an important target gas in applications like leakage control in refrigeration systems and air conditioners on one hand or in the emission control and quality monitoring of waste and drinking water on the other hand. Other application areas for ammonia sensors include high temperature sensing in the exhaust of cars and, as it is a product of biochemical processes, ammonia is also a useful reporter molecule in a variety of medial applications. This need have supported the development of devices capable of the detection and quantification of gaseous and dissolved ammonia. Many aspects of ammo-

nia sensing are summarized in a recent review by Timmer et al. [8] and information on ammonia sensing in solution can be found in [9].

For the use in work place safety and indoor monitoring applications devices capable of detecting ammonia in concentrations of 1 – 50 ppm in ambient air are required. These devices must not be prone to strong humidity interferences. Several regulations on the allowed ammonia concentration and exposure times exist, as there are the acceptable exposure limit (AEL) in Germany/Switzerland, the long time (LTEL) or short time (STEL) exposure limits in the UK, or the permissible exposure limit (PEL), usually a time-weighted average (TWA), in the USA. The values given therein are in the range from 25 to 50 ppm. Many commercial ammonia gas sensors as well as analytical devices are offered for this application area and concentration range.

The scientific literature describes the development of many sensor types. Optical ammonia sensors detect ammonia by the change in absorbance of an acid-base indicator, fluorescence of an ammonia complex, or a change in refractive properties of a coating. Infrared (IR) based gas sensors measure the absorbance change induced by the ammonia molecule. Electrochemical sensors rely on a change in resistance, capacitance or potential of the sensitive layer. Finally, resonator devices measure the mass of absorbed ammonia. Reported as sensitive layers in chemical gas sensors are different metal oxides, CuBr [10], TiN [11], and many different polymers and polymer blends [12–19].

### 1.2. Motivation and Scope

In spite of the large number of already available sensing layers for chemical gas sensors and the existing technology, new materials needs to be tested for special applications and new sensors are being developed. This thesis is focused on the development of ammonia sensitive layers for the future use in a SGFET. The SGFET device itself is under development by project partners [20].

Microsensors including the GasFET can be used in principle with many available gas sensitive materials: polymeric, inorganic or metallic. The main advantage of polymer sensitive layers over metal oxides is the operation at room temperature as they do not require heating. This is in line with the low-power goal of microsensors. Thus, they are very suitable for the use in GasFETs and the material of choice in this work.

The SGFET and the GasFET in general rely on potential changes upon gas exposure of a sensitive material deposited on the gate electrode. This po-

tential change can be in the same way measured with the so-called Kelvin probe (KP), introduced by Lord Kelvin [21] already more than 100 years ago. The KP served in this work as a test tool to determine the gas responses of the self-made samples. The test samples are made of a polymer film on a conducting substrate. Several polymer/substrate combinations were tested and characterized in their gas sensing performance with the KP. Polymers were preferred over metal oxides as sensitive layers to make low temperature operation of the SGFET possible. As required by the future use in the GasFET, the morphology of the layers was checked and optimized in a series of deposition experiments with the spraying nozzle. In the presented work the layer preparation and morphology characterisation and the results of the gas sensing experiments with the KP and additionally with QMB sensors and the IR technique are described in much detail.

It is the exploration of a new field. As of now, hardly any data is available on KP measurement of substrates coated with thin films of non-conducting polymers as used in this work. Neither an explanation of the observed phenomena was found. At this early stage, the focus was set on the investigation of this new sensing principle rather than detailed performance characterisation and optimisation. The QMB and IR experiments were carried out to gather additional data for the explanation of the sensing mechanism. The obtained data base allows a first modelling of the sensing mechanism and a basic model is presented in this work.

Next to the scientific interest, the experiments are expected to provide enough data to be able to choose the best sensing layer as of now for the detection of ammonia with the GasFET and to give an prognosis of the performance.

### 1.3. Overview of the Presented Work

The chapter **Theory and Related Work** serves as an introduction into the scientific fields related to this work. It presents the relevant theories and it discusses the related works by other authors available in the scientific literature. Such an introduction can never be exhaustive. It is mainly aimed to provide the reader with the necessary background knowledge and tools to set a starting point for further readings.

In this chapter the most common sorption processes occurring on polymers films are described. For the understanding of the Kelvin probe method it is helpful to recall the occurring terms related to electrical and chemical potentials of charged species in condensed phases and the potential differences across phase boundaries. Next, the chemical and physical nature of

the electrical double layer (DL) is explained on hand of selected cases for solid/gas and solid/liquid interfaces. It is also shown, how surface modifications and especially gas adsorption processes can change the DL of a solid and thus the work function of the material.

Several methods are described used for the measurement of work functions, among which the KP method is explained in more detail as it is the main tool of this work.

The chapter concludes with a presentation of important sensing devices based on the work function and gives an overview of sensitive layers used in KP and GasFET gas sensing experiments.

The chapter **Experimental Details** describes all the necessary equipment for the conducted experiments, lists all materials, and gives an overview of the standard parameters, experimental conditions, and procedures. Deviations from those standard values are noted later in the respective sections. The focus is set on the description of the deposition system and the Kelvin probe measurement set-up.

The presentation of the results is twofold. In the first part, **Sensitive Layer Morphology: Characterisation and Optimization**, the experimental data and results of the polymer layer characterisation and the optimization of the deposition process is presented. The results are best discussed on hand of individual selected samples and experiments, each of which is typical for the respective polymer and covers the whole range of observations.

The second part, chapter **Response to Analyte Gases**, presents the experimental data obtained in the KP, QMB, and IR measurements individually for all the polymers that were tested positively with the KP. The polymers were exposed to pulses of ammonia and humidity. Additionally, the humidity influence on the ammonia signal and the signal stability are of major interest as well as the stability of the signal over time. The results are again discussed on hand of selected samples different in layer thickness and substrate showing the whole range of the observations. The presentation of the experiments is followed by an interpretation of the observed effect.

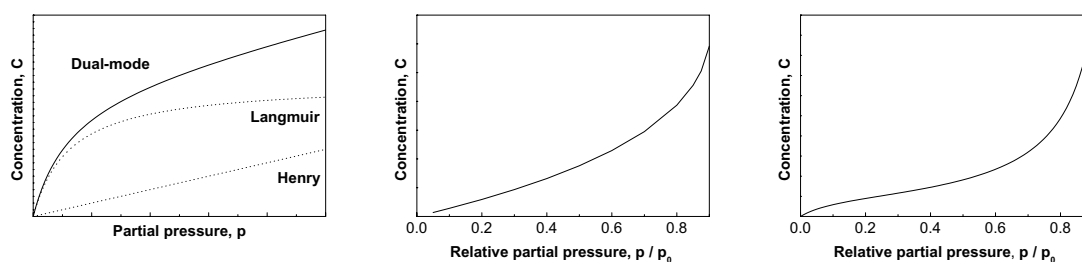
In **Summary and Outlook** a word on the current status and an outlook to further research possibilities finishes the work.

## 2. Theoretical Background and Related Work

### 2.1. Sorption Processes

When a gas or vapour is brought into contact with a solid, it will be partly taken up by the solid until an equilibrium of the concentrations in the two phases is reached. The molecules either enter the inside of the solid, called absorption or dissolution, or remain on the outside attached to the surface, named adsorption. The general term for all possible processes is sorption. It includes adsorption, absorption, clustering of sorbate molecules, and incorporation into microvoids of the sorbent. Several modes of sorption may occur simultaneously depending on the nature of the sorbate and sorbent, the ambient conditions, namely pressure and temperature, and the concentration of the sorbate in the gas phase.

The amount of sorbed molecules as a function of the partial pressure in the gas phase at a fixed temperature is modelled by a sorption isotherm. Several isotherms have been developed to describe the individual modes, some of which are plotted in figure 2.1, relevant for sorption into polymer matrices.



(a) Henry, Langmuir, and dual-mode sorption models

(b) Flory-Huggins isotherm

(c) BET isotherm

**Figure 2.1.:** Illustration of common sorption isotherms applicable to sorption into a polymer matrix. Isotherms give a relation between the concentration of the sorbate in the sorbent,  $C$ , and the partial pressure,  $p$ , at constant temperature.

In the case of polymeric sorbents the predominant chemical interaction with the sorbate and the sorption capabilities of the polymer, which are different for e. g. rubbery or glassy polymers, play a very decisive role in the shape of the isotherm. Also the mechanism of diffusion is very different

in rubbery and glassy polymers. Diffusion of absorbed molecules is faster in polymers in the rubbery than in glassy state, thus, rubbery polymers are preferred in chemical sensing applications.

Polymers may change their physical state with temperature. They are in a glassy state below the glass transition temperature,  $T_g$ , and in a rubbery state above this temperature. The value of  $T_g$  itself is e.g. depending on the degree of cross linking or the molar mass of the polymer. Similarly, sorbed gas molecules may cause a phase transition, as the glass transition temperature is lowered by sorbates like  $\text{CO}_2$  [22] or water molecules [23].

In the following, the models are applied to sorption from a gaseous phase, but they may be equally well employed to sorption processes of nonelectrolytes from solution.

**Bulk Sorption by Partitioning** Sorption into the bulk of a rubbery polymer matrix may be described like sorption into liquids following Henry's law. This simplest type of sorption holds, when interaction forces are non-specific and weak between sorbate/polymer and sorbate/sorbate and the partial pressure is much lower than the saturation pressure. The concentration of the sorbate in the polymer matrix,  $C$ , is then a linear function of the partial pressure  $p$  above the polymer phase (see plot in figure 2.1(a))

$$C = k_h p \quad (2.1)$$

The solubility coefficient  $k_h$  is a constant for a given temperature. Deviation from linearity are possible, e. g. by swelling of the matrix.

The distribution of sorbate molecules defines the partition coefficient  $K$ , as the ratio of the concentration in the polymer phase  $C^\beta$  and the gas phase  $C^\alpha$

$$K = \frac{C^\beta}{C^\alpha} \quad (2.2)$$

If sorption follows strictly Henry's law  $K$  is a constant for all concentrations, depending only on temperature. In the field of chemical gas sensing  $K$  is sometimes estimated by the linear solvation energy relationship (LSER) as introduced by Grate and Abraham [24]. This model includes several interaction parameters and is more advanced than the simple Hildebrand solubility theory. It was recently used by Hierlemann et al. [25], Grate [26] and previously by others as described in references [27–29] to choose the best coatings and to predict the response of gravimetric sensors based on known interaction parameters.



**Bulk Sorption Considering Sorbate/Sorbate Interactions** A more complex bulk sorption model is based on the Flory-Huggins theory of mixing. The amount of sorbed gas molecules depends on the entropy of mixing rather than on enthalpic effects. The entropy of mixing is calculated from the lattice theory and it accounts for the number of ways of arranging polymer and solvent molecules on a lattice, where each molecule occupies a number of sites proportional to its molecular volume. This type of isotherm arises when the interactions between the sorbate molecules are stronger than the sorbate/sorbent interactions and it is suitable to describe, for example, sorption of water molecules in hydrophobic polymer matrices or condensation in microvoids of glassy polymers. As a result of this the solubility increases with increasing partial pressure (see figure 2.1(b)).

The isotherm is implicitly defined by

$$\ln \frac{p}{p_0} = \ln \phi_1 + (1 - \phi_1) + \chi(1 - \phi_1)^2 \quad (2.3)$$

where  $p_0$  is the saturation vapour pressure,  $\phi_1$  the volume fraction of sorbate in the polymer and  $\chi$  the Flory-Huggins interaction parameter. The concentration of the sorbate is proportional to the volume fraction.

The Scatchard–Hildebrand equation for regular solutions is the simplest way of estimating  $\chi$ . The interaction strength depends on the solubility parameters  $\delta_1$ ,  $\delta_2$  (index 1 sorbate, index 2 polymer) and the partial molar volume  $V_1$  of the sorbate

$$\chi = \frac{V_1}{RT}(\delta_1 - \delta_2)^2 \quad (2.4)$$

**Adsorption and Occupation of Specific Sites** A kinetic model for adsorption and desorption leads to the Langmuir isotherm. It was initially developed to model adsorption to a fixed number of available surface sites, but it is commonly transferred to describe occupation of some kind of specific pre-existing sites in a matrix. The concentration of molecules  $C$  on the surface or bound to specific sites is given by

$$C = \frac{A b p}{1 + b p} \quad (2.5)$$

where  $A$  is a site saturation number and  $b$  is the rate constant for adsorption divided by that for desorption (i. e.  $b$  is the equilibrium constant for the adsorption process). It is thus the affinity to occupy surface or specific sites. The limited number of available sites is the cause of saturation (see plot in figure 2.1(a)) at high concentrations of the sorbate.

In the original context, this simple monolayer adsorption model is based on the assumptions, that each surface site can be only singly occupied, there are no lateral interactions between the adsorbed species, the enthalpy of adsorption is independent of surface coverage, and there is a dynamic equilibrium between the adsorption and desorption processes. This means that all sites are equivalent and the sticking probability is independent of the neighbouring sites.

The Freundlich and Temkin isotherms (see table 2.1) consider a change of enthalpy of adsorption to overcome some shortcomings of the Langmuir model, but they have limited physical background. The models include a adjustable parameter,  $n$ , to fit the data.

The Frumkin and the BET models (see table 2.1 and explanation below) extend the Langmuir model, as they consider interaction between the molecules or multilayer adsorption.

**Table 2.1.:** Adsorption isotherms considering interaction between sorbate molecules.  $\theta$  is the relative surface coverage.

Isotherm		Assumptions
Freundlich	$\theta = k_f p^n$	logarithmic fall in the enthalpy of adsorption with surface coverage
Temkin	$\theta = k_t \ln(np)$	linear fall in the enthalpy of adsorption with surface coverage
Frumkin	$k_f p = \frac{\theta}{1-\theta} e^{-2\gamma\theta}$	polar interactions between adsorbed particles considered

In the Frumkin isotherm the interaction between analyte molecules is expressed by the interaction parameter  $\gamma$  leading to a correction of the Gibbs free adsorption energy as a function of the surface coverage  $\theta$ :  $\Delta G = \Delta G_0 + \gamma\theta$ . A positive value of  $\gamma$  includes attractive, a negative repulsive interactions. In the case  $\gamma = 0$  the Frumkin isotherm reduces to the Langmuir isotherm.  $\gamma$  is modelled differently for ionic and dipolar interactions and depends on the charge and dipole moment of the neighbouring molecules. The model and an experimental example for thiosulfate on silver in solution is found in [30].

**Multilayer Sorption Model** The isotherms in table 2.1 account for interactions between the permeant molecules, but still do not consider multilayer formation on the surface. The model of Brunauer, Emmett, and Teller (BET isotherm, see figure 2.1(c)) incorporates multilayer adsorption by applying

the Langmuir equation to more than one layer, but using two different affinity constants for the first layer and all consecutive layers. In case of multi-layer adsorption there will be no saturation for high pressures. A kinetic model with rate constants for each layer leads to the following expression

$$\frac{V}{V_m} = \frac{c p}{(p_0 - p)[1 - (1 - c)\frac{p}{p_0}]} \text{ or } \frac{p}{(p_0 - p)V} = \frac{1}{c V_m} + \frac{(c - 1)}{c V_m} \frac{p}{p_0} \quad (2.6)$$

where  $V$  denotes the volume occupied by the sorbate,  $V_m$  the volume of one monolayer and  $c$  a specific constant. This isotherm is often observed in the case of water sorption by highly hydrophilic polymers such as poly(vinyl alcohol) or poly(acrylic acid).

**The Dual-Mode Model** A dual-mode sorption model as well as variations and derivations of the Flory-Huggins and the BET concept are commonly used to describe the sorption behaviour of polymers with phenomena other than pure partitioning as filling of microvoids in glassy polymers or specific sorbate/polymer interactions. The later is a common phenomenon in chemical gas sensing with organic layers providing specific interaction sites to govern selectivity and sensitivity [31–33].

The dual sorption mechanism (see figure 2.1(a)) is defined in terms of Henry's law of solubility,  $C_H$ , and Langmuir type of sorption,  $C_L$ ,

$$C = C_H + C_L = k_h p + \frac{A b p}{1 + b p} \quad (2.7)$$

In the case of  $b p \ll 1$  (limit of low concentration), the gas solubility is proportional to the applied gas pressure and the initial slope is given as  $k_h + A b$ . In the region of  $b p \gg 1$ , the saturation region of the Langmuir isotherm, the concentration of the sorbate in the sorbent increases linearly with a slope of  $k_h$ .

Although the dual sorption model provides a conceptual reference for studying gas sorption in polymers, it fails to correlate the sorption parameters to known properties of the polymer and the gas. Also, the presence of only two distinct modes is an oversimplification when considering the presence of sorption site size or affinity distribution.

## 2.2. Electrochemical Aspects of Interfaces

### 2.2.1. The Potential of Charged Species in Condensed Phases

**Electrical Potentials** For the full description of the potential of a charged species in condensed phases separation of chemical work and electrical

work makes the understanding easier, always bearing in mind, that they cannot be separated experimentally. Thus, let us consider only electrical potentials and electrostatic work for a moment.

Commonly, the electrical potential  $\Phi$  effecting charges inside a condensed phase, called inner potential or Galvani potential, is subdivided into the outer potential  $\Psi$ , often called Volta potential, and the surface potential  $\chi$

$$\Phi = \Psi + \chi \quad (2.8)$$

For an illustration refer to figure 2.2.

The inner potential arises as a result of the (hypothetical) work needed to take a test charge  $q$  from infinity across the electrical double layer (DL) at the surface into the phase without any chemical interactions.

The DL may be described as a region at the surface, where a potential drop arises due to excess charges (contributed to  $\Psi$ ) or the formation of a dipole layer of any kind (summarized in  $\chi$ ). This dipole layer may be the result of adsorption of ions or dipolar species at the surface or it is due to the ion and electron distribution in the topmost atomic layers of the solid and just above the surface.

The outer potential is defined by the work  $q\Psi$  necessary to take the charge near the surface of the phase against the electrical field of the present charges not yet interacting with the surface. This is reached practically at a distance of 1  $\mu\text{m}$  from the surface. This value is most commonly given in the literature. The surface potential is determined by the work  $q\chi$  needed to take the charge into the phase through the surface potential. By definition,  $\chi$  is positive if the positive ends of the dipoles are pointing away from the surface.

$\Phi$  and  $\chi$  are not measurable absolutely as a phase transition is involved and charges are unavoidably bound to chemical species (ions) or electrons. The mass transport across the phase boundary includes always chemical work  $\mu_i$ . Both chemical and electrostatic work are put together in the electrochemical potential.

**The Electrochemical Potential and the Real Potential** The electrochemical potential is defined as the total work of bringing one mole of species  $i$  of total charge  $z_iF$  from infinity (characterised by zero potential energy) into the phase, this is in vacuum without any other fields or forces working on the particle. It is frequently given formally as a sum of the chemical potential  $\mu_i$  and an electrostatic work  $z_iF\Phi$

$$\tilde{\mu}_i = \mu_i + z_iF\Phi = \mu_i + z_iF(\Psi + \chi) \quad (2.9)$$

The work necessary to take one mole of species  $i$  across the surface potential alone (starting from about  $1\ \mu\text{m}$  from the surface where no chemical interactions take place) bearing the total charge  $z_i F$  is called the real potential  $\alpha_i$

$$\alpha_i = \mu_i + z_i F \chi \quad (2.10)$$

Since  $\tilde{\mu}_i$  and  $\Psi$  are experimentally measurable it is convenient to write this in another way using the definition of the electrochemical potential

$$\alpha_i = \tilde{\mu}_i - z_i F \Psi \quad (2.11)$$

**The Work Function** The work function  $\phi_i$  of a species  $i$  is defined as the negative value of the real potential  $\alpha_i$

$$\phi_i = -\alpha_i \quad (2.12)$$

Thus, the work function is the difference between the potential in the phase  $\tilde{\mu}_i$  and just outside  $z_i F \Psi$ . The thermionic electronic work function  $\phi$  is the negative of the real potential for electrons ( $z_e = -1$ )

$$\phi = -\alpha_e = -\mu_e + F \chi \quad (2.13)$$

The energy level that is associated with the electrochemical potential of electrons in a solid is called Fermi level,  $E_F$ . The energy level in the proximity of the surface is referred to as the vacuum level,  $E_{vac}$ . The work function is directly given by the difference between the vacuum level and the Fermi level. For an illustration of the terms used in this context see figure 2.2.

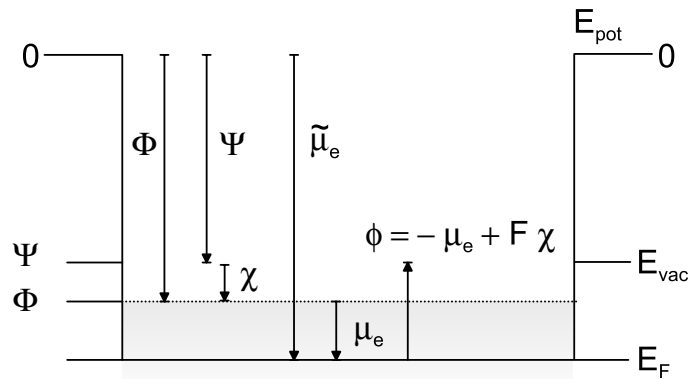


**Figure 2.2.:** Illustration of the relations among Galvani, Volta and outer potential,  $\Phi$ ,  $\Psi$ , and  $\chi$ , electrochemical,  $\tilde{\mu}_e$ , chemical work,  $\mu_e$ , and the work function,  $\phi$ , of electrons.

The work function is here defined as a molar quantity following the definition of the electrochemical potential, but more commonly the work function is related only to one electron, consequently, in the remaining text this convention is adopted. In some instances the work function has the dimension of a potential (then denoted with  $\varphi$ ) and the work is given as  $e\varphi$ .

The experimental value of the work function for a particular material varies slightly depending upon the process of emission. For example, the energy required to extract an electron out of a heated platinum filament (thermionic work function) differs slightly from that required to eject an electron from platinum that is struck by electromagnetic radiation (photoelectric work function). Work functions of common metals span a range from 1.8 eV (Cs) to 5.3 eV (Pt).

### 2.2.2. The Volta and Galvani Potential Differences at Phase Boundaries

As the main measurement technique in this work, the Kelvin probe (KP) method, is based on electrical phenomena occurring at contact of two phases, denoted with  $\alpha$  and  $\beta$ , we need to look at the potential difference across phase boundaries. At contact, all species—often common in both phases from the beginning—reach an equilibrium concentration in both phases.

The general equilibrium condition in respect to species  $i$  requires that the electrochemical potential is equal in all phases in contact

$$\tilde{\mu}_i^\alpha = \tilde{\mu}_i^\beta \quad (2.14)$$

The thermodynamic equilibrium is reached by a flow of ions or electrons from one phase to the other. The direction is given by the energy per particle  $\alpha_i/N_A$  in the phase resulting in a flow from the phase with higher energy to the one with lower energy. This flow of charged particles results in a charging of the two phases and in two opposite outer potentials  $\Psi_\alpha$  and  $\Psi_\beta$ . As a consequence the Galvani potentials will be influenced as well.

**The Volta Potential Difference** The Volta potential difference as the difference of  $\Psi$  in the two phases

$$\Delta\Psi = \Psi^\beta - \Psi^\alpha \quad (2.15)$$

is often called surface or contact potential. However, this quantity is not to be confused with the surface potential  $\chi$  introduced at the beginning of this section despite the name.

After starting with the equilibrium condition (2.14) and the definition of the electrochemical potential (2.9)

$$\mu_i^\alpha + z_i F(\Psi^\alpha + \chi^\alpha) - \mu_i^\beta - z_i F(\Psi^\beta + \chi^\beta) = 0 \quad (2.16)$$

and rearrangement of terms

$$z_i F(\Psi^\beta - \Psi^\alpha) = (\mu_i^\alpha + z_i F\chi^\alpha) - (\mu_i^\beta + z_i F\chi^\beta) \quad (2.17)$$

the Volta potential difference can be written as

$$\Delta\Psi = -(\alpha_i^\beta - \alpha_i^\alpha)/(z_i F) = (\phi_i^\beta - \phi_i^\alpha)/(z_i F) \quad (2.18)$$

recalling the definition of  $\alpha_i$  (2.10) and  $\phi_i$  (2.12) and substituting into (2.17).

The Volta potential difference is the measured quantity in the KP method. According to the above, the KP measures the difference between the electronic work functions of the sample and the reference electrode.

**The Galvani Potential Difference** At contact of two phases one may also look at the Galvani potential difference

$$\Delta\Phi = \Phi^\beta - \Phi^\alpha \quad (2.19)$$

From the above this can be written as

$$\Delta\Phi = \Delta\Psi + \Delta\chi = (\alpha_i^\beta - \alpha_i^\alpha)/(z_i F) + \Delta\chi \quad (2.20)$$

The Galvani potential difference is only measurable in special cases, e. g. when the two phases have the same potential determining species. This is the case in electrochemical half-cells, when a metal is immersed in a solution of metal ions of the same chemical element.

The equilibrium condition  $\tilde{\mu}_i^\alpha = \tilde{\mu}_i^\beta$  becomes

$$\mu_i^\alpha + z_i F\Phi^\alpha = \mu_i^\beta + z_i F\Phi^\beta \quad (2.21)$$

using the definition of the electrochemical potential.

The chemical potential of a species in a mixed phase as the function of chemical activity  $a_i$  can be calculated by

$$\mu_i = \mu_i^0 + RT \ln a_i \quad (2.22)$$

when the potential is referenced to a standard state, defined as the state in which  $a_i = 1$ . This may be a solid metal phase ( $a_i$  is set by definition to unity) or a solution with a concentration of ions such that  $a_i = 1$ .

Equation (2.21) becomes

$$\mu_i^{\alpha,0} + RT \ln a_i^\alpha + z_i F \Phi^\alpha = \mu_i^{\beta,0} + RT \ln a_i^\beta + z_i F \Phi^\beta \quad (2.23)$$

and finally

$$\Delta\Phi = \frac{\mu_i^{\alpha,0} - \mu_i^{\beta,0}}{z_i F} + \frac{RT}{z_i F} \ln \frac{a_i^\alpha}{a_i^\beta} \quad (2.24)$$

$\Delta\Phi$  is the Galvani voltage of a half-cell. The first term is independent of concentration and called the standard Galvani potential difference. It is a constant for a given reaction



at standard conditions and is already tabulated for many chemical systems.

### 2.3. The Chemical and Physical Structure of the Electrical Double Layer

In the preceding description of the potential and the DL no assumption was made about the real distribution of charges and dipoles at the phase boundary. Thus, models of the potential jumps have to be presented to fully describe the potential difference at phase boundaries. These are important for the understanding of potential changes occurring upon gas adsorption.

#### 2.3.1. The Potential Drop at the Surface of Metals and Semiconductors

The crystal structure of a solid metal or semiconductor deviates at the surface from the structure of the bulk. In covalent crystals surface atoms have different valencies as bulk atoms and electron density reaches out of the crystal as the result of an unsaturated valency (dangling bond); on ionic crystals the surface is also unsaturated from an electrostatic point of view, as the charges of ions at the surface are not fully compensated. The unequal distribution of positive and negative charges leads to a formation of an intrinsic dipole layer and to a non-zero value of the surface potential  $\chi$ . Any net charge on the surface is compensated by counter charges in the bulk.

In the band model for the electronic structure of solids the deviation of the electronic structure at the surface from the one of the bulk is taken into account by addition of localised surface states: even at adsorbate free surfaces intrinsic surface states are present. All deviations from the ideal



crystal structure, as there are impurities, non-stoichiometric composition, adsorbates and other surface defects as the reconstruction of surface atoms to allow electron pairing and neutralization of electric fields further influence the electronic structure in the surface region.

Those surface states are able to accept free charge carriers from the bulk. The density of available charge carriers (electrons or holes) is an important factor for the dimensions of the DL. Metals have a high density of available charge carriers, thus charges are fully compensated within the first few monolayers. The DL can be described by two sheets of charges forming a compact condenser structure. The work function of a metal depends on this dipole layer as well.

In semiconductors less charge carriers are available and compensation takes place over a larger region. The charges at the surface are compensated not by a sheet of charges but by the total charge in a so-called space charge region of finite depth extending to a distance  $x_0$ . The deviation of the density of available charge carriers from the density of in the bulk increases or decreases the escape potential for further electrons. This energy barrier is denoted with  $V_S$ .

To better describe the individual contributions to the work function of a semiconductor and changes thereof a new representation is helpful, which is equivalent to the one introduced in section 2.2.1.

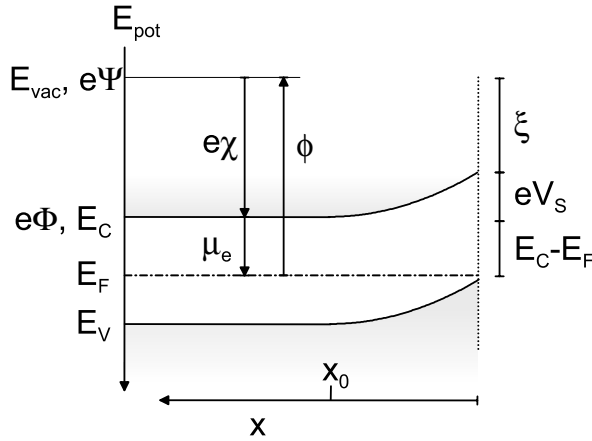


**Figure 2.3.:**

The DL of a semiconductor: contribution of electron affinity  $\zeta$ , band bending  $eV_S$ , and the bulk chemical potential ( $E_C - E_F$ ) to the work function.

The work function is then represented by the sum of three terms: the bulk chemical potential ( $E_C - E_F$ ), band bending  $eV_S$ , and the surface dipole potential or electron affinity  $\zeta$

$$\phi = (E_C - E_F) - eV_S + \zeta \quad (2.26)$$

as is illustrated in figure 2.3.  $E_C, E_V$  are the energy of the lower edge of the

conduction band and the higher edge of the valence band, respectively. The potential change due to the formation of a space charge layer is described by band bending. The contribution of a dipole layer is ascribed to  $\zeta$ .

An insulator has even less carriers and one can consider this as a semiconductor with a very large Debye length, extending over the whole material. Some aspect concerning the work function of an insulating layer on a conducting substrate are discussed later in section 2.4.3.2 in the context of KP measurement on poorly conducting samples.

### 2.3.2. Surface Potential Changes Induced by Adsorption and Surface Modifications

The work function is the least amount of energy required to remove an electron from the surface of a condensed phase to a point just outside. As the electron has to move through the surface region, its energy is influenced by the characteristics of the surface double layer. Hence, the work function is an extremely sensitive indicator of surface condition and is affected by adsorbed molecules, evaporated layers, surface reconstruction, surface charging, layer imperfections, surface and bulk contamination, surface orientation in single crystals to name a few. Most relevant for chemical gas sensing is the adsorption-induced change of the work function by interaction with adsorbates.

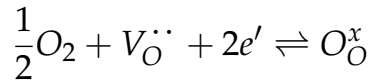
All three terms of the work function given in (2.26) may change depending on the electronic properties of the solid and the strength and the kind of interaction

$$\Delta\phi = \Delta(E_C - E_F) - \Delta(eV_S) + \Delta\zeta \quad (2.27)$$

Adsorbates on metallic solids may change the intrinsic dipole layer and add to the surface dipole through a dipole moment in the adsorbate molecules itself and a consequential modification of  $\zeta$  occurs. Furthermore, adsorbates on semiconductors and poorly conducting materials may change all three terms in (2.27): in the case of weak interactions (physisorption) a net surface dipole of the adsorbed molecules changes  $\zeta$ ; in case of stronger interactions and electron transfer the electronic structure of the surface region is altered. A local electron exchange with surface states as in the case of chemisorption forms a dipole layer. Ionosorption leads to both band bending and changes in the electron affinity, as electron transfer occurs with the bulk. Rarely, the bulk term ( $E_C - E_F$ ) is influenced.

### 2.3.2.1. Fermi Level Shift and Band Bending

**Fermi Level Shift Upon Gas Adsorption** The quantity  $(E_C - E_F)$  is a characteristic property of the bulk, and is therefore only changed by molecules diffused into the bulk. Textbook examples are  $ZrO_2$  and  $SrTiO_3$  having oxygen vacancies,  $V_O^{\cdot\cdot}$ , in the lattice due to a non-stoichiometric composition. These defects create donor levels energetically located in the band gap near the conduction band edge (n-type semiconductor). At high temperatures the mobility of oxygen ions is high and they are in equilibrium with ambient oxygen molecules according to



This chemical equilibrium reaction can be utilized in potentiometric and conductometric high temperature oxygen sensors. Potentiometric devices based on  $ZrO_2$  consist of two half-cell exposed to a fixed oxygen concentration on one side and to the unknown concentration on the other side. The electromotoric force changes logarithmically the oxygen concentration—a Nernstian behaviour. In the field of work function sensors, oxygen sensing with  $ZrO_2$  [34] and  $LaF_3$  [35, 36] is reported. In conductometric sensors the variation of the available free charge carrier due to a change in the density of oxygen vacancies in the lattice change the modulate the conductance of the device.

For potentiometric sensors with conducting polymers the same logarithmic response curve is observed [37, 38], but explaining the Nernstian behaviour is not straight forward. An attempt was made by Janata [39], Janata and Josowicz [40] for the Fermi level shift in semiconducting polymers in the presence of an analyte gas of partial pressure  $p$

$$E_F = E_D^* + \frac{kT}{2\delta} \ln p \quad (2.28)$$

where  $E_D^*$  describes the energy of the dopant modified by the affinity for a charge transfer,  $\delta$  is a measure for the partial charge transfer and is supposed to be between -1 and 1. However, larger values were measured indicating the limitations of this theory.

**Band Bending and Changes in Electron Affinity** Changes in  $eV_S$  and  $\zeta$  are often encountered in gas sensing, as conductive semiconductor sensors based on metal oxides rely on these phenomena. Refer to [41] for a detailed coverage of this topic. Adsorbed molecules acting as electron acceptors or donors create new surface states upon adsorption being involved in a

charge transfer to/from the bulk. Oxygen species on SnO<sub>2</sub> surfaces are, for example, electron acceptors. Band bending occurs as a result of a space charge region at the surface. The concentration of oxygen species at the surface is changed by adsorbed analyte molecules. A net dipole moment, if present, of the adsorbed molecules contributes additionally to changes in  $\zeta$ .

Band bending can occur at contact of a metal and a semiconductor, as well. Studies of interface phenomena with the Kelvin probe of organic semiconductors at contact with metals forming a Schottky-contact are reported by various authors, e. g. the charge distribution of polyimide [42–45] and polyethylene [46] films. Band bending and Fermi level alignment of several other organic semiconductors at contact with metals was studied recently with the KP by Ishii et al. [47], as well.

### 2.3.2.2. The Influence of a Dipole Layer on the Work Function

The focus is set on illustrating  $\Delta\zeta$  by a formation of an additional dipole layer due to the interaction with molecules adsorbed or deposited on the surface. This term is relevant for sensing hydrogen and hydrogen containing compounds with the classical Pd-FET or in the control of the behaviour of Schottky diodes. The electrical structure of the substrate itself is of less interest. The resulting dipole moment or changes thereof modify the work function according to the Helmholtz equation

$$\zeta = -\frac{1}{\epsilon\epsilon_0} N_s \mu \cos \theta \quad (2.29)$$

where  $\mu \cos \theta$  is the dipole moment perpendicular to surface and  $N_s$  the surface density of the adsorbed molecules. If the negative end of the dipole moment points away from the surface (negative surface potential) the work function is increased and vice versa.

**Adsorption** Adsorption studies on metals were carried out mainly on clean single crystal surfaces with the KP or ultraviolet photon spectroscopy (UPS) in ultra high vacuum (UHV) conditions. Thus, the results are of limited use for non ideal surfaces under ambient atmosphere where contamination and oxidation of the surface occurs and water vapour is always present, but they show the mechanism and possibilities of the origin of work function changes.

Changes in the work function can occur especially on metals with d orbitals forming bands able to interact with occupied  $n$ -orbitals and unoccupied  $\sigma^*$ -orbitals of adsorbates either as Lewis acid (electron acceptor) or

Lewis bases (electron donors). There is a decreasing tendency from  $\text{Rh} > \text{Pd} > \text{Pt} > \text{W} > \text{Ni} > \text{Fe} > \text{Cr}$  in parallel to the decreasing d character of the metal bond. Metals without d orbitals are far less reactive. Any charge transfer to or from adsorbed molecules to the surface alters the potential barrier of the DL by changing  $\zeta$ . For example, CO increases the work function whereas ammonia decreases the work function of Ni surfaces indicating an electron density transfer from and to the metal. However, in many cases only a weak interaction leads to a dipole layer of the adsorbed molecules. Metals or semiconductors without d-orbitals like silicon may, on the other hand, react with ammonia under formation of  $\text{SiNH}_2$  [48].

The effect of water vapour on freshly evaporated gold was first reported by Wells and Fort [49]. They found that a gold layer covered with water has a largely reduced work function due to chemisorbed and physisorbed water molecules. However, this change is not fully reversible by heating the sample. Not only water vapour but also ammonia and CO change the work function of gold films. This was studied by Surplice and Brearley [50] on freshly evaporated and baked gold layers. They found that the work function was altered by wet air, CO, and ammonia. Ammonia adsorption following a Tempkin isotherm always reduces the work function by several hundred millivolts reversibly. The work function change by CO is ten times lower, but in the same direction as ammonia, according to a Langmuir isotherm. Physisorbed water molecules changed the work function by 0.5 eV. Using the dipole moment of water, 1.85 D, a coverage of 0.25 ML accounts for this change of the surface potential.

Bilic et al. [51] calculated the work function changes on single crystal Au(111) surfaces induced by ammonia adsorption. According to their model the change in the work function of the gold layer originates not from a charge transfer between adsorbate and substrate. The interaction is truly dispersive. They calculate a decrease of the work function by 1.90 and 1.15 eV for a coverage of 1/4 ML (saturation) and 1/9 ML, respectively. While the sign of the change as well as its increase with coverage are typical for ammonia on transition metal surfaces, the magnitude of the change for the Au(111) surface is somewhat lower than for most others. The work function of Rh(111) and Pt(111) surfaces is changed by 2.5 and 3.0 eV, respectively. Using the Helmholtz equation an effective dipole moment of 2.15 D per molecule is obtained for the 1/9 ML coverage of ammonia on Au(111). This is significantly enhanced from the value of 1.47 D observed for free ammonia. For the adsorption on Rh(111) and Pt(111) values of 1.9 D and 2.0 D, respectively, were obtained in the same manner in the high-coverage limit.

Metal oxides or oxide layers on metals can react as Lewis and Brønsted

centres depending on the presence of water. Water modifies the surface by  $\text{OH}^-$  adsorption to metal centres and  $\text{H}^+$  to oxygen atoms by hydroxylation of the surface. This effect is generally studied with pyridine and ammonia as probe molecules by IR spectroscopy. Interactions of ammonia with strong Brønsted acid sites yields a surface ammonium cation, while interactions with Lewis acid sites give coordinated ammonia. The different species are clearly distinguishable in the spectra.

Work function changes can also occur during reactions on catalysts. Monitoring the work function can help to clarify the reaction path [52]. Adsorption of azomethane occurs on Pd and its decomposition takes place in several steps. Azomethane itself adsorbs in a cis configuration and decreases the work function of the metal, if it is trapped at low temperature. The decomposition at low temperatures leads to an adsorbed intermediate product,  $\text{CH}_3\text{N}$ , and a positive change of the work function. This intermediate product desorbs at higher temperatures under further decomposition.

**Surface Modifications** The aim of this section is to show how surface modification can change the work function according to the Helmholtz equation by formation of a dipole layer. In the following examples the surface modification was achieved by pure deposition of organic materials or by chemical bonding. An ordered layer has to be formed. Thin layers already induce large effects, as there is no contribution from the bulk of thick amorphous layers.

The first example is taken from corrosion studies performed by Nazarov and Thierry [53]. The deposited polymer layer modifies the substrate and the work function change occurs at the surface of the substrate. The deposition of polymers with acidic and basic groups interacting with oxides of iron and other metals lead to a formation of surface charges and dipoles, by abstraction or donation of protons from/to the surface. The reaction takes place only in humid air. The changes of the work function due to the deposition are in the range of several hundred millivolts.

The dipole moment is more commonly present in the deposited layer. A deposition of thin layers of poly(tetrafluoroethylene) (PTFE) polymers with polar groups resulted in an effective dipole moment [54]. The larger the dipole moment of the substituent the larger the change in the work function. The signal saturates already after deposition of layer thicker than 10 nm. Other possibilities of surface modifications include the deposition of Langmuir-Blodgett (LB) films and the formation of self-assembled monolayers (SAM) by a reaction of thiols with gold or chlorosilanes with silicon substrates. These highly ordered molecules carrying polar groups result in

a significant change of the surface potential. KP measurements can be used to estimate dipole moments of such layers [55, 56].

The modification of Schottky diodes or light emitting diodes as means to control the barrier height with organic compounds is of general interest in organic electronics. Consequently, surface modification of indium tin oxide (ITO) and other electrode/substrate materials have received wide attention. Tin complexes of phenoxide ligands having different dipole moments were prepared by Guo et al. [57] and LB films of acids by Zuppiroli et al. [58]. Metals like Au and Pt influence similarly the barrier height [59]. Campbell et al. [60] studied the work function changes after modification of the Ag substrates with SAMs. The modification of GaAs by substituted tartaric acids show clearly that the organic monolayer increases the current of a Schottky diode if the dipole is positive ( $-\text{CF}_3$  and  $-\text{CN}$  substituents), and decreases for negative dipoles ( $-\text{CH}_3$  and  $-\text{OCH}_3$ ) compared to the unmodified junction [61].

#### 2.3.3. The Solid/Liquid Interface

Similar considerations can be made for the solid/liquid interface as adsorption may also occur from solution. Additionally, in solution the possibility of charged particles adsorbing at the surface exists giving rise to a surface potential. To some extent the models presented here can be used to describe surfaces exposed to humid air and covered unavoidably with a layer of liquid water. The amount of water is further increased by polar polymers deposited on the surface.

##### 2.3.3.1. The Nernst Equation of Surface Potential

Firstly, a short general approach for calculating the surface potential for any charged species in equilibrium between the surface and the solution is represented by the Nernst equation for the surface potential. The AgI/Ag system is the best example for the validity as it exhibits a Nernst-type of electrode behaviour (59 mV per pAg unit at 25 °C) over more than 10 decades. This approach will be applied for protons as potential determining ions adsorbing at the surface. Whether the Nernst equation can be equally applied to protons and other systems than AgI/Ag is under discussion. Larson and Attard [62] introduce some aspects on this topic. It is claimed that the Nernst equation is a good approximation in all cases providing an upper boundary for the real value.

In equilibrium the electrochemical potentials are equal in solution (phase  $\alpha$ ) and at the surface of the solid (phase  $\beta$ ). The Nernst surface potential

$\psi_s^N$  is defined as the Galvani potential difference between the solid and the solution  $\Delta\Phi$  related to  $\Delta\Phi_{pzc}$ , the same quantity at the point of zero charge (pzc)

$$\psi_s^N = \Delta\Phi - \Delta\Phi_{pzc} \quad (2.30)$$

where  $\Delta\Phi_{pzc}$  is a possible difference in the Galvani potentials caused solely by dipoles, not by charges at the interface. The pzc is defined by the concentration of the potential determining species in the solution at which no net charge is present at the surface.

Using (2.24) this becomes

$$\psi_s^N = \frac{RT}{z_i F} \ln \frac{a_i^\alpha}{a_i^\beta} \cdot \frac{a_{i,pzc}^\beta}{a_{i,pzc}^\alpha} = \frac{RT}{z_i F} \ln \frac{a_i^\alpha}{a_{i,pzc}^\alpha} \quad (2.31)$$

making the valid assumption that  $a_i^\beta$ , the chemical activity in the solid phase, is constant at all concentrations of species  $i$ .

For a proton exchange reaction ( $z_H = 1$ ) as the potential determining reaction



the surface potential can be expressed in terms of the pH of the solution setting the activity equal to the concentration.

$$\psi_s^N = \frac{RT}{F} \ln \frac{[H^+]^\alpha}{[H^+]_{pzc}^\alpha} = 2.3 \frac{RT}{F} (pH - pH_{pzc}) \quad (2.33)$$

Different assumptions can be made to relate the surface charge to the surface potential, the simplest of which is a compact capacitor model. Net surface charges can be determined in potentiometric or conductometric titration experiments. Starting from high pH values an acid is added to the solution and the measured pH is compared to the theoretical one without proton absorption at the surface. All missing protons are absorbed at the surface of the solid. This procedure is continued until a low pH is reached. The whole experiment is repeated at different ionic strengths of the solution starting over from high pH. All curves intersect at the  $pH_{pzc}$ .

### 2.3.3.2. The Origin of Surface Charge: Surface Complexation Models for Oxidic Surfaces

The Nernst model does neither consider all chemical conditions at the surface nor the effect of other ions in the solution. A more physical model for



the origin of surface charges describing the surface reactions of many metal oxides and metals immersed in solution is necessary and shall be presented here for the proton exchange involving surface MOH groups.

The “proton adsorption” at the surface of oxidised materials or oxidic compounds surfaces is a common case and the charging mechanism is described by site-binding models. These models allow to calculate the relation between the pH of the solution and the surface charge density  $\sigma_s$ , thus the surface potential. The models for the surface charging mechanism are combined with models for the solution side based on the ideas by Gouy-Chapman-Stern-Grahame (see next section).

The surface MOH groups are amphoteric in character and may donate or accept protons from the solution, leaving a negatively charged or a positively charged surface group, respectively. The exchange of protons can be describes by means of one or several surface reactions.

Following Yates et al. [63] and Davis et al. [64] two possible surface reactions occurring at the metal/electrolyte interface (2-pK model) are considered, neglecting a possible specific adsorption of electrolytes directly at the surface



The 1-pK model [65] makes use of only one relation for the proton exchange



This convention means that protonation occurs only at every second hydroxyl group (active sites in the model are  $\text{HO} - \text{X} - \text{OH}_2$ ). The MUSIC model includes more species and multiple chemical proton exchange reactions [66].

The corresponding equilibrium constants  $K_1$  and  $K_2$  for the two reactions are defined in the usual way and are depending on the surface concentration of the involved species

$$K_1 = \frac{[\text{MOH}][\text{H}^+]^\beta}{[\text{MOH}_2^+]} \quad \text{and} \quad K_2 = \frac{[\text{MO}^-][\text{H}^+]^\beta}{[\text{MOH}]} \quad (2.36)$$

The surface concentration of protons is denoted with  $[\text{H}^+]^\beta$  to distinguish it from the concentration in solution  $[\text{H}^+]^\alpha$ . The model does include other electrolytes in solution. The interaction of all charged surface site with the

## 2. Theoretical Background and Related Work

---

electrolytes in solution, presented by  $C^+$  and  $A^-$ , are incorporated similarly to the relations in (2.36).

The total number of sites per unit area,  $N_s$ , (mass balance of surface groups) is assumed to remain constant

$$N_s = [MOH] + [MOH_2^+] + [MO^-] + [MOH_2^+ A^-] + [MO^- C^+] \quad (2.37)$$

In the model  $N_s$  is fixed, however, for oxidised metals and metal oxides  $N_s$  is often depending on the pH: a decreasing pH causes a decreasing number of hydroxyl groups, whereas a increasing pH creates more surface sites.

The net surface charge density  $\sigma_s$  is given by

$$\sigma_s = e([MOH_2^+] - [MO^-]) \quad (2.38)$$

The concentration of hydrogen ions at the surface is linked to the concentration of hydrogen ions in solution by a Boltzmann distribution function

$$[H^+]^\beta = [H^+]^\alpha e^{\frac{-e\psi_s}{kT}} \quad (2.39)$$

where  $\psi_s$  is the surface potential relative to potential in the liquid.

At the point of zero charge no net charge is present on the surface,  $\sigma_s = 0$  and  $\psi_s = 0$ . Using (2.36), (2.39), and (2.38) one can derive the following expression to calculate the  $pH_{pzc}$  from the equilibrium constants  $K_1$  and  $K_2$

$$pH_{pzc} = -\log(K_1 K_2)^{\frac{1}{2}} \quad (2.40)$$

When the pH differs from  $pH_{pzc}$  the surface potential  $\psi_s$  and the pH are linked using (2.36) and (2.40) via

$$\psi_s = -2.3 \frac{kT}{e} (pH - pH_{pzc}) + 2.3 \frac{kT}{2e} \log\left(\frac{[MO^-]}{[MOH_2^+]}\right) \quad (2.41)$$

One can model the last term in (2.41) assuming a Gouy-Chapman-Stern-Grahame model resulting in

$$2.3(pH_{pzc} - pH) = \frac{e\psi_s}{kT} + \sinh^{-1}\left(\frac{e\psi_s}{kT}\beta\right) \quad (2.42)$$

where  $\beta$  is a sensitivity factor

$$\beta = \frac{2e^2 N_s (K_1 K_2)^{\frac{1}{2}}}{kT C_{DL}} \quad (2.43)$$

and  $C_{DL}$  the capacitance of the DL.

A linearisation of (2.42), valid especially near the pzc, yields

$$2.3(pH_{pzc} - pH) = \frac{1 + \beta e\psi_s}{\beta kT} \quad (2.44)$$

and Nernstian response is reached only for large values of the sensitivity factor  $\beta$ .

The  $pH_{pzc}$  for many metal oxides and hydroxides are listed by Parks [67], which is used as reference in recent publications.

This charging mechanism is not the only effect of pH. In the case of Ir, W, and Pt also oxidation of the surface may take place.

### 2.3.3.3. The Potential Drop in Solution

After the understanding of the origin of the surface charge a description of the solution side of the interface is necessary. In electrochemistry, the charge and potential distribution at the electrode solution interface is most often described by the classical Gouy-Chapman-Stern-Grahame (GCSG) model although there has been extensive work on alternative models of the double layer as this is a mean field theory that neglects interactions between the ions.

The Triple Layer Model (TLM), based on the full Gouy-Chapman-Stern-Grahame description of the DL structure, is a common model in the context of the site-binding models. It defines three layers, hence the name, two compact capacitors and a diffuse layer, and several planes separating the layers. However, the modelling can be done on various levels of sophistication, depending on the demands of the matter under study. The simplest models are assuming only the presence of either a compact capacitor, the Constant Capacitance Model, or a diffuse layer, the Diffuse Double Layer Model. They may be considered as limits for very high or low electrolyte concentrations, respectively.

The TLM subdivides the Stern layer in two compact layers in series, the inner and outer Helmholtz layer. The Helmholtz layers comprise the layer of adsorbed hydrogen ions and strongly bound anions and cations. The innermost plane, the 0-plane (see figure 2.4), is located at the solid surface and in this plane the charges developed by the potential determining ions are located. In the case of the oxide surface this are all surface hydroxyl groups involved in the proton exchange mechanism:  $MOH$ ,  $MOH_2^+$ ,  $MO^-$ . The surface groups are exposed to the potential  $\psi_0$ .

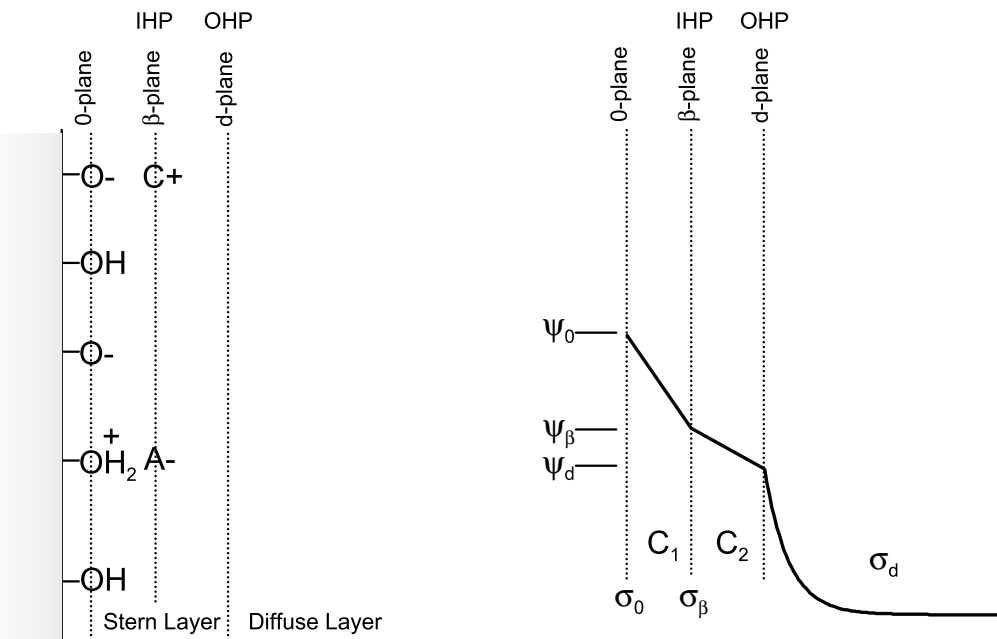


**Figure 2.4.:** The structure of the electronic double layer in solution for oxidic surfaces (see text for explanation).

The centres of associated counter ions are located at the  $\beta$ -plane at potential  $\psi_\beta$ . This is the plane of closest approach of the tightly bound ions without a hydration shell and also called the inner Helmholtz plane (IHP). The first plane of ions that carry a hydration shell and are still tightly bound to the surface is designated as the outer Helmholtz plane (OHP) or d-plane.

The d-plane is the onset of the diffuse layer extending to the solution at the potential  $\psi_d$ . In the diffuse region the ion distribution is determined by a balance of electrostatic forces and random thermal motion. The potential in this region, therefore, decays as the distance from the surface increases until, at sufficient distance, it reaches the bulk solution value, conventionally taken to be zero. This layer is characterized by the Debye length  $1/\kappa$  and the zeta potential  $\zeta$ . The Debye length is a measure for the width of the diffuse layer. The electric potential at the shear plane is called zeta potential and measured in zeta analysers based on electrophoresis. The shear plane is an imaginary surface separating the thin layer of liquid bound to the solid surface and showing elastic behaviour from the rest of liquid showing normal viscous behaviour.

In the diffusive layer ion concentrations are governed by the Poisson-Boltzmann equation; counter-ions are attracted to the surface and co-ions are repelled. The distribution of ions is strongly dependent on the valency of the ions. It should be mentioned that the potential,  $\psi_d$ , at the outer

Helmholtz or Stern plane is one of the most important parameters in discussing colloid stability and double-layer interaction.

No charges are assumed to be present inside the Helmholtz layers. The charged particles are accumulated at the 0-plane and  $\beta$ -plane and distributed in the diffuse layer. The neutrality condition for the charges imposes

$$\sigma_0 + \sigma_\beta + \sigma_d = 0$$

The net surface charge density  $\sigma_s$  is neutralized by the charge in the diffuse layer  $\sigma_d$

$$\sigma_s = e([MOH_2^+] - [MO^-]) = -\sigma_d \quad (2.45)$$

and  $\sigma_d$  can be calculated using the Grahame equation (see appendix A)

$$\sigma_d = -\sqrt{8\varepsilon\varepsilon_0c_0kT} \sinh \frac{e\psi_d}{2kT} = -\frac{4c_0e}{\kappa} \sinh \frac{e\psi_d}{2kT} \quad (2.46)$$

The layer are characterized by the corresponding capacitances  $C_1$  and  $C_2$ , generally defined as differential capacitances. Using this the potential at the surface can be written as

$$\psi_0 = \psi_d - \frac{\sigma_d}{C_2} + \frac{\sigma_0}{C_1} \quad (2.47)$$

$\psi_d$  may be written in terms of the inverse function of  $\sinh y/2$  using (2.46). However, it is often used in literature in an equivalent expression as the following

$$\psi_d = \frac{2kT}{e} \ln \left[ \frac{\sigma_d}{\sqrt{8\varepsilon\varepsilon_0c_0kT}} + \sqrt{1 + \frac{\sigma_d^2}{8\varepsilon\varepsilon_0c_0kT}} \right] \quad (2.48)$$

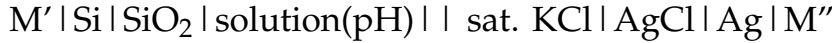
which is derived from (2.46) by substituting  $\sinh y/2$  by the two exponential functions and solving the occurring quadratic equation for  $\psi_d$ . The diffuse layer potential is available experimentally e. g. by the atomic force microscope (AFM) technique.

The often made simplification lies in the assumption that the onset of the diffuse layer is identical to the plane associated to the counter ions such that  $\psi_\beta = \psi_d$ . Then the model reduces to the Basic Stern Model (BSM).

**Other Potentials in Solution** In more complex systems additional potentials in solution add up to the full potential drop. Liquid/liquid junctions

and potentials of ion selective membranes, described by equations according to the Henderson and Donnan model, have to be considered.

One example, where surface potentials of metal electrodes immersed and emersed from solution are characterized by the KP method is reported by Samec et al. [68], but additional potentials are most common in potential sensors for liquid sensing, e.g. the ion selective field effect transistor (IS-FET) , between the potentiometric device and a reference electrode. A pH sensitive ISFET with a SiO<sub>2</sub> or any other oxidic surface is characterized by the following presentation



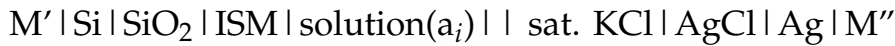
using a Ag/AgCl reference electrode.

The total potential drop of the device includes the interfaces between the liquid and the insulator and between the liquid and the reference electrode

$$V_T = E_{ref} + E_j - \psi_0 + \chi_{sol} + V_{ss} \quad (2.49)$$

where  $E_j$  is the liquid junction potential, which is commonly calculated by the Henderson equation, due to diffusion of ions across the interface,  $\psi_0$  is the potential difference between the insulator surface and the bulk of the solution and  $\chi_{sol}$  is the constant surface dipole potential at the insulator-solution interface.  $V_{ss}$  is the potential drop given by the device itself (see section 2.5.2 and equation (2.73)).  $\psi_0$  is depending on the pH of the solution. The sensitivity of a SiO<sub>2</sub> surface can be modelled according the site-binding model.

If one includes an ion sensitive membrane (ISM) the system is



and the governing equation is given by

$$V_T = E_{ref} + E_j - \frac{\mu_{i,sol}}{z_i F} - \frac{a_i^{ISM}}{z_i F} + V_{ss} \quad (2.50)$$

where  $\mu_{i,sol}$  standard chemical potential of ion  $i$  in the solution and  $a_i^{ISM}$  the real potential in the membrane.

## 2.4. Measuring the Work Function and Surface Potentials

Many techniques have been developed based on different physical effects to measure the electronic work function of a sample. We may distinguish

between two groups of experimental methods for work function measurements: absolute and relative. Methods of the first group employ electron emission from the sample induced by photon absorption (photoemission), by high temperature (thermionic emission), due to an electric field (field emission), or using electron tunnelling. All relative methods make use of the contact potential difference between the sample and a reference electrode. Experimentally, either an anode current of a diode is used or the displacement current between the sample and reference, created by an artificial change in the capacitance between the two, is measured (the KP method).

However, more often than determining the absolute value of the work function, changes are of interest during adsorption of molecules, layer deposition, light illumination, and other processes or treatments, and an indirect or relative determination of the work function is sufficient for recording changes thereof.

These methods take in a wide range of application fields, allowing to measure possibly any kind of sample under the desired set of conditions. Some methods are designed to scan surfaces performing work function imaging, others are more macroscopic providing an average over a larger area.

The principles of selected techniques applied widely nowadays are discussed briefly below. The focus is set on the Kelvin probe method as the method of choice in this work.

### 2.4.1. Photo Emission Spectroscopy

Photoelectron emission spectroscopy (PES) is the general term for spectroscopic techniques based on the outer photoelectric effect. In the case of UPS, the surface of a solid sample is irradiated with ultraviolet (UV) light and the kinetic energy of the emitted electrons is analysed. As UV light is electromagnetic radiation with an energy  $h\nu$  lower than 100 eV it is able to extract only valence electrons. Due to limitations of the escape depth of electrons in solids UPS is very surface sensitive, as the information depth is in the range of 2 – 3 monolayers. At the same time the measurement principle restricts PES to be used in UHV conditions.

The resulting spectrum reflects the electronic structure of the sample providing information on the density of states and the occupation of states. The representation of the energy states is high in resolution due to the highly monochromatic emission of the radiation source and capabilities of the analyser.

The measured spectrum allows the calculation of the work function of the

sample as shown in the following. In case of metallic or semiconducting samples the Fermi levels of the sample  $\phi$  and analyser  $\phi_{sp}$  are expected to be equilibrated at contact. If the work functions are different an electric field proportional to  $\Delta\phi$  between the two results (contact potential), which adds extra energy to the kinetic energy of the electrons. If  $\phi$  is smaller than  $\phi_{sp}$  an additional bias is applied to make  $\phi - \phi_{sp} > 0$ . Electrons leave the sample with a kinetic energy of  $h\nu - I$ , but the kinetic energy measured by the analyser is given by

$$E_{kin} = h\nu - E_B - \phi_{sp} \quad (2.51)$$

where  $I$  is the ionisation energy of the electron, and  $E_B$  the electron binding energy in the sample relative to the Fermi level.

In case of a metallic sample the lower edge of the spectrum (lowest kinetic energy) is determined by electrons that have a binding energy  $I$  of  $h\nu$ . They leave the sample with zero kinetic energy and their measured kinetic energy  $E_i$  is only determined by the electric field due to the contact potential. At the higher edge of the spectrum  $E_f$  electrons originating from the Fermi level are measured ( $E_B = 0$ )

$$E_i = \phi - \phi_{sp} \quad \text{and} \quad E_f = h\nu - \phi_{sp} \quad (2.52)$$

The spectral width  $\Delta E = E_f - E_i$  and the work function of the sample result as the following

$$\Delta E = h\nu - \phi \quad \text{and} \quad \phi = h\nu - \Delta E \quad (2.53)$$

If the work function of the spectrometer is unknown, it can be determined using (2.52).

In the case of semiconducting samples electrons emitted with a kinetic energy of  $E_f = h\nu - (E_F - E_V) - \phi_{sp}$  from the upper edge of the valence band,  $E_V$ , build the high energy port of the spectrum and with a kinetic energy  $E_i = \phi - \phi_{sp}$  the lower edge. Hence the width of the energy spectrum  $\Delta E$  is

$$\Delta E = E_f - E_i = h\nu - \phi - (E_F - E_V) \quad (2.54)$$

and the work function of the sample

$$\phi = h\nu - \Delta E - (E_F - E_V) = E_f + \phi_{sp} - \Delta E \quad (2.55)$$

The work function of a semiconductor sample can be calculated if the work function of the spectrometer  $\phi_{sp}$  was determined in a previous measurement on a metallic sample.



The interaction of gases at the sample surface changes the work function of the sample. This change of the work function is reflected in the spectrum as portrayed in figure 2.5. The spectral width  $\Delta E$  is changed by  $\Delta\zeta$  and the spectrum ends are shifted by  $\Delta\phi$  and  $\Delta(eV_s) + \Delta(E_C - E_F)$ , respectively.

$$E_i = \phi - \phi_{sp} + \Delta\phi \quad (2.56)$$

$$E_f = h\nu - (E_F - E_V) + \Delta(eV_s) + \Delta(E_C - E_F) - \phi_{sp} \quad (2.57)$$

$$\Delta E = E_f - E_i = h\nu - \phi - (E_F - E_V) - \Delta\zeta \quad (2.58)$$

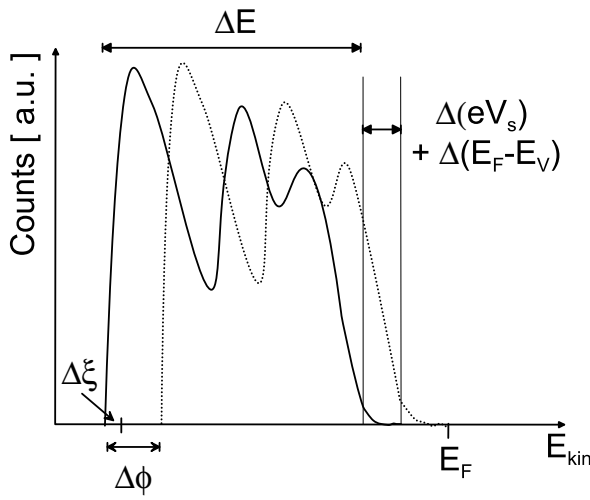


**Figure 2.5.:**

Schematic UPS spectrum of a semiconducting sample (solid line) and the result of work function changes by adsorbates on the spectrum (dotted line).

### 2.4.2. Methods Based on Thermionic Emission

The retarding diode method is one of the simplest and oldest method of measuring work functions. It is based on the thermionic emission of electrons from an emitter. The current density  $J$  of the electrons collected by the sample depends on the work function  $\phi$  of the sample and is given by the Richardson–Dushman equation

$$J = AT^2 e^{-\frac{\phi}{kT}} \quad (2.59)$$

where  $A$ , the Richardson constant, is a specific material constant. The current density increases rapidly with temperature and decreases exponentially with the work function. Changes of the work function can be easily determined by applying a retarding potential  $V$  between the sample and the electron emitter;  $\phi$  is replaced by  $e(\phi + V)$  in equation (2.59). The difference in the retarding potential measured at constant current is equivalent to the work function change, assuming that the work function and the temperature of the emitter is constant.

One can use (2.59) directly to determine the work function by temperature variation of the sample, as well. Rearranging the equation yields

$$\ln(J/T^2) = \ln(A) - \frac{\phi}{kT} \quad (2.60)$$

The line produced by plotting  $\ln(J/T^2)$  vs.  $1/T$  will have a slope of  $-\phi/k$  allowing to determine the work function of the sample.

### 2.4.3. The Kelvin Oscillator

The Kelvin method (“vibrating capacitor/condenser method”, “capacitive probe method”), using a so-called Kelvin probe or Kelvin oscillator, is an established tool for measuring the work function of a sample or, more precisely, the contact potential between the sample and a reference. A major asset of this method is that it is a non-contact and non-destructive way of measuring. Additionally, it is not expected to influence the electrical or chemical structure of the material. The technique is very simple, but fast, accurate, and versatile: it can be used in principle in many environments and applied to any solid or liquid sample.

Traditional application areas cover surface science, tribology, and material science: investigation of adsorption or deposition processes, determination of surface layer imperfections, wear and corrosion studies [69, 70, and references therein]. It is also used as a testing tool in gas sensing applications or surface photo voltage (SPV) measurements during illumination. Nowadays, Kelvin probes are being more and more exploited to investigate organic materials and conduct interfaces studies: determination of barrier heights in Schottky contacts, Fermi level determination, influence of doping, studies of film growth and multilayer structures.

The traditional KP, as described by Lord Kelvin [21], consists of a flat circular electrode (termed the reference electrode) suspended above and in parallel to a stationary electrode (the sample under study), thus creating a simple capacitor. The charge on the capacitor due to the contact potential needs to be measured awkwardly with an electrometer or via the discharging current when moving one plate away. In 1932, Zisman [71] introduced an improved measurement procedure. He mounted a vibrating reference surface just above the sample and the discharging current varies then periodically as the tip vibrates, and the amplitude depends on the difference between the contact potential and an external voltage. This technique led to the development of systems that automatically track shifts in the contact potential and, thus, the work function of the sample, if the reference electrode is unaffected.

Several designs have been developed to serve different purposes and several mechanisms have been used to achieve the required variation in spacing between the tip and sample among which piezoelectric [72] and voice-coil [73] drivers are the most convenient and the most used.

Other models are reported in [74–82]. Reviews on the topic given by Engelhardt et al. [80], Surplice and D’Arcy [83], Kronik and Shapira [84] list and compare many different types available at the time of writing.

Most probes are rather macroscopic with a reference electrode of the size of a few millimetres or centimetres. Smaller probes are necessary to conduct localized measurements or be able to do scanning of samples. Scanning Kelvin probes (SKP) are reported in [69, 70, 85, 86], and miniaturized devices developed for special applications in [87–89].

### 2.4.3.1. General Working Principle

The Kelvin oscillator consists of a metallic reference electrode of work function  $\phi_K$ , which is in electrical contact with the sample (work function denoted with  $\phi_S$ ). If these materials are made into a parallel plate capacitor, equal and opposite surface charges form, resulting in a contact potential, commonly denoted with  $V_{CPD}$ , as explained in section 2.2.2

$$V_{CPD} = \frac{(\phi_K - \phi_S)}{e} \quad (2.61)$$

If in addition a bias voltage  $V_b$  is applied (often called “backing” or “bucking” voltage), a total voltage drop,  $V_{K,S}$ , as the sum of the two results.

Changes in the distance (mean distance  $d_0$ ) of the reference electrode from the sample due to the periodic oscillation of the grid of frequency  $\omega$  and oscillation amplitude  $d_1$ , result in changes in the distance by  $d(t) = d_0 + d_1 \sin(\omega t)$  and consequently in the charge  $q(t)$  on the capacitor and the capacity  $c(t)$  of the sample-grid capacitor according to

$$c(t) = \frac{q(t)}{V_{K,S}} = \epsilon\epsilon_0 \frac{A}{d(t)} = \epsilon\epsilon_0 \frac{A}{d_0 + d_1 \sin(\omega t)} \quad (2.62)$$

where  $A$  denotes the area of the reference electrode, normally the common area.

Using

$$i(t) = \frac{dq(t)}{dt} \quad (2.63)$$

the variation of the electrical current  $i(t)$  flowing between the reference electrode and the sample can be expressed as

$$i(t) = V_{K,S} \frac{dc(t)}{dt} \quad (2.64)$$

and  $\frac{dc(t)}{dt}$  determines the sensitivity of the Kelvin probe.

Calculating the derivative  $\frac{dc(t)}{dt}$  leads to

$$i(t) = -V_{K,S} \frac{\epsilon\epsilon_0 A}{d_0^2} \frac{d_1 \omega \cos(\omega t)}{\left(1 + \frac{d_1}{d_0} \sin(\omega t)\right)^2} \quad (2.65)$$

For small vibrations one can assume  $d_1 \ll d_0$  and the above simplifies to

$$i(t) \approx -V_{K,S} \frac{\epsilon\epsilon_0 A}{d_0^2} d_1 \omega \cos(\omega t) \quad (2.66)$$

However, in the normal operating region, the assumption  $d_1 \ll d_0$  is often invalid and the form of the equation is much more complicated. An improvement of (2.65) may be given by a Fourier analysis as reported by Wolff et al. [90] and Baumgärtner and Liess [87]. Their approach is still approximative as higher harmonics are neglected. Fourier analysis yields the optimal vibration amplitude  $d_1 = d_0/\sqrt{2}$ . A large vibration amplitude is favourable due to a higher sensitivity, but the amplitude of higher harmonics increases as well. At this ratio the most efficient working point of the KP is reached and the contribution of the fundamental to the signal is the highest.

During the measurement the bias voltage is continuously readjusted to keep the current zero. Hereby, the contact potential is calculated as  $-V_b$ . Commonly a lock-in amplifier set to the probe oscillation frequency is used to detect the null condition and variations from it, regardless of higher harmonics. A band pass filter before the amplifier is commonly used to further reduce higher harmonics and noise.

This highlights one problem for a KP which relies on lock-in techniques: unless working in the range where  $d_1 \ll d_0$ , and thus the signals are very small, much of the signal is not in the fundamental frequency, but in higher harmonics, and is therefore lost. This leads to an error in the measured contact potential.

To overcome this drawback a “off-null” method is proposed by some authors [91]. Since the amplitude of the KP output signal,  $i(t)$ , varies linearly with the potential difference between the probe and sample, a plot of the

signal amplitude versus the backing potential yields a straight line, with the x-axis intercept being the contact potential. The null point at which the backing potential is equal to  $-V_{CPD}$  is calculated by interpolation (or extrapolation) between measurements made away from the null. The non-null points have a far superior signal-to-noise ratio than the null point, and thus can be measured with great accuracy. This method is considered particularly important where the signal to noise ratio is small due long connecting cables, shielding problems, and reduced probe dimensions, or for very high accuracy measurements.

### 2.4.3.2. Poorly Conducting Samples and the Influence of Trapped Charges

When the sample under investigation is an electrical conductor, the surface of the sample works as the plate of the capacitor, i. e., the charges resulting from the contact potential and the applied bias voltage are accumulated at the surface. In the case of a poorly conducting sample, a semi-conductor or even an insulator, the potential is not fully compensated at the surface of the layer, but the potential drop occurs at the layer surface,  $\chi_1$ , and the interface to a conducting substrate,  $\chi_2$ , due to polarization effects as well as a distribution of charges in the bulk and at the surface,  $V_\sigma$ . Thus, the situation is quite different from that of a conducting sample. However, during the KP measurement the charge and the charge distribution in the layer remain constant as a charge transfer with the substrate may occur, but such an effect can be completely neglected in the case of the null-detection condition (no electric field) and high vibration frequencies (larger than the relaxation time constant).

Analogous to (2.8) the electrical potential of the conducting substrate becomes

$$\Phi^\beta = \Psi^\beta + \chi_2 + \chi_1 + V_\sigma \quad (2.67)$$

and the Volta potential differences to the reference electrode of the KP becomes

$$e(\Psi^\beta - \Psi^\alpha) = (\mu^\beta - e\chi^\beta - e\chi_1 - e\chi_2 - eV_\sigma) - (\mu^\alpha - F\chi^\alpha) \quad (2.68)$$

$$= \Delta\phi - e\chi_1 - eV_\sigma \quad (2.69)$$

instead of (2.18).

Pfeiffer et al. [92] report that the KP method gives the correct surface potential of a poorly conducting sample only, if the capacitance of the sample film is larger than that of the gap between the sample and reference electrode. Ishii et al. [47] argue that the KP method probes the precise surface potential of such a layer in all cases.

It should be noted that the observed potential reflects the total charge distribution in the sample layer and the substrate surface. If there exist trapped charges in or on an insulator layer, a  $V_{CPD}$  which includes the effect of the charges, is measured. How this charges on the insulator influence the measured contact potential by the KP was first described by Reedyk and Perlman [93]. The following derivation of the influences of charges on insulating layers was derived by Harris and Fiasson [94] developed to describe charge measurements with the KP on surfaces of ionic crystals. This model was later used among others by Luo et al. [95, 96] and Ostrick et al. [11, 97].

The value of  $V_b$  at null balance will be given by the contact potential difference  $V_{CPD}$  between the probe and the electrode and a term depending on the charge density,  $V_\sigma$ .

The gap  $d$  between the layer surface and the reference electrode and the dielectric layer of thickness  $D$  constitute capacitors in series that divide up any voltage applied across them according to

$$V_{CPD} + V_b = E_d d + E_D D \quad (2.70)$$

where  $E_d$  and  $E_D$  are the electric fields across the gap and the dielectric respectively.

If free charges exist on the surface, they will affect the polarization within the insulator. The electric displacement is continuous across the surface. Using Gauss's law the variation of the electric displacement across this surface becomes  $\varepsilon\varepsilon_0 E_D - \varepsilon_0 E_d = \sigma$ , where  $\varepsilon$  is the dielectric constant of the dielectric layer. Using this and the fact that  $E_d = 0$  in the null condition of the KP the above leads to

$$-V_b = V_{CPD} - \frac{\sigma D}{\varepsilon\varepsilon_0} = V_{CPD} - V_\sigma \quad (2.71)$$

If no net charges are present the null balance obtained by adjusting  $V_b$  until  $E_d$  is zero gives  $-V_b = V_{CPD}$ . This is precisely the result obtained when no dielectric at all is present on the electrode. The dielectric surface might, however, contain free charges of surface density  $\sigma$ , in which case  $V_b$  is different from the real  $V_{CPD}$  between the sample and the probe.

The charges may be accumulated not only on the surface but can be present through the whole film. Then  $\sigma$  is a charge density across the film according to Sessler et al. [98]

$$\sigma = \frac{1}{\varepsilon\varepsilon_0} \int_0^D x\rho(x)dx \quad (2.72)$$

This relation was used in the investigation of insulating organic films being charged due to a displacement of electrons from the substrate to the layer at deposition [42–44, 46].

Residing charges on poorly conducting samples and surfaces like the measurement chamber in proximity of the KP are a disturbing effect, which has to be accounted for in the determination of the contact potential. Several sources of charges and the effect on KP results are mentioned by Luo et al. [95].

### 2.4.3.3. Advanced Signal Analysis and Sources of Error

A more advanced analysis of the raw signal output of the Kelvin method than given in section 2.4.3.1 was attempted by many authors. The KP signal is modelled on hand of a simple equivalent circuit similar to figure 2.6 by solving the characteristic differential equations. The first treatment of this problem is reported by Anderson and Alexander [99]. This approach of signal analysis can be found, for example, in [100–103] in different variations.

The equivalent circuit incorporates the capacitance of the KP capacitor  $C_{KP}$  and the contact potential as a voltage source  $V_{KP}$ ;  $C_M$  and  $R_M$  are accounted to the driving electronics, and  $C_s$  and  $R_s$  are sources of errors. Additional terms may be added depending on the desired level of sophistication.

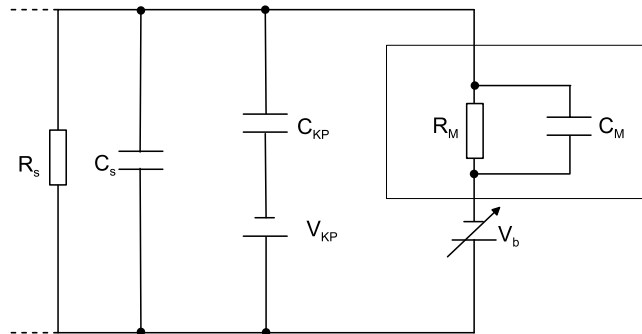


Figure 2.6.: Equivalent circuit for the Kelvin probe set-up.

Signal analysis leads to a model for the influences of error sources on the KP signal. [101, 102, 104–107]. Main sources of error are capacities in parallel to the sample as capacitances of cables and variable stray capacitances due to coupling to distant surfaces as well as non-parallel sample-reference electrode arrangements, fringe fields, charge accumulation on insulating surfaces. The sources of error result in spacing dependent errors due to the

non-ideal behaviour as derived by Rossi [104], which has to be compensated for in determination of absolute work functions.

A multiple capacitor model was developed to correct for those effects as well as inhomogeneous samples surfaces. The measured contact potential is an area weighted contribution of all individual influences. Also non-planar geometries can be modelled. A very problematic issue in gas test with the KP is a possible gas adsorption at the walls of the measurement chamber, which may influence the measured KP.

Finally, one has to consider pick-up noise and the influence on the results [91, 101].

### 2.4.4. Kelvin (Probe) Force Microscopy

The Kelvin probe force microscope (KPFM) or Kelvin force microscope (KFM) is based on an AFM set-up and the determination of the work function is based on the measurement of the electrostatic forces between a small tip and the sample. The conducting tip and the sample are characterised by different work functions. When both elements are brought in contact, a net electric current will flow between them until the Fermi levels are aligned, as discussed previously. An electrostatic force between tip and sample builds up, resulting from the net charge transfer.

For the measurement a voltage is applied between tip and sample, consisting of a DC-bias  $V_{DC}$  and an AC-voltage  $V_{AC} = \sin \omega_2 t$  of frequency  $\omega_2$  at the second resonance frequency of the AFM cantilever.

$$V = (V_{DC} - V_{CPD}) + V_{AC} \sin(\omega_2 t)$$

Tuning the AC-frequency to the second resonance frequency of the cantilever results in an improved sensitivity and allows the independent and simultaneous imaging of topography and the contact potential.

As a result of these biasing conditions, an oscillating electrostatic force appears, inducing an additional oscillation of the cantilever with the characteristic frequency  $\omega_2$ . The general expression of such electrostatic force not considering coulomb forces due to charges can be written as

$$F = \frac{1}{2} \frac{dC}{dz} V^2$$

The electrostatic force can be split up into three contributions, as the total electrostatic force  $F$  acting on the tip has spectral components at the frequencies  $\omega_2$  and  $2\omega_2$ .

$$F = F_{DC} + F_{\omega_2} + F_{2\omega_2}$$



The DC component,  $F_{DC}$ , contributes to the topographical signal, the term  $F_{\omega_2}$  at the characteristic frequency  $\omega_2$  is used to measure the contact potential and the contribution  $F_{2\omega_2}$  can be used for capacitance microscopy

$$F_{DC} = -\frac{dC}{dz} \left[ \frac{1}{2} (V_{DC} - V_{CPD})^2 + \frac{1}{4} V_{AC}^2 \right]$$

$$F_{\omega_2} = -\frac{dC}{dz} (V_{DC} - V_{CPD}) V_{AC} \sin(\omega_2 t)$$

$$F_{2\omega_2} = +\frac{dC}{dz} \frac{1}{4} V_{AC}^2 \cos(2\omega_2 t)$$

For contact potential measurements a lock-in amplifier is used to detect the cantilever oscillation at  $\omega_2$ . During the scan  $V_{DC}$  will be adjusted so that the electrostatic forces between the tip and the sample become zero and thus the oscillation amplitude of the cantilever at the frequency  $\omega_2$  becomes zero. Since the electrostatic force at  $\omega_2$  depends on  $V_{DC} - V_{CPD}$ ,  $V_{DC}$  corresponds to the contact potential. Absolute values of the sample work function can be obtained if the tip is first calibrated against a reference sample of known work function. Apart from this, one can use the normal topographic scan methods at the resonance frequency  $\omega_1$  independently of the above. Thus, in one scan, the topography and the contact potential of the sample are determined simultaneously.

## 2.5. Chemical Sensing with Field Effect Devices

UP spectrometer and Kelvin probes are well established tools to study the gas interaction at surfaces, but for practical sensor applications they are not suitable due to the necessary instrumentation and the limits in miniaturisation. The same holds for KFM devices.

The Kelvin probe is more widely used as a test tool to screen and characterize possible sensing layers for field effect devices. The experiments are focused on the gas sensing performance and on basic studies of the sensing mechanism. An exception is a miniature KP device described by Bergstrom et al. [88] developed for oxygen sensing.

Microsensors based on thermionic emission are feasible and a device has been developed. However, the effect is only in rare cases usable [108], as normally higher temperatures than desired are necessary. Thus, the most commonly used devices are based on the field effect, some of which are introduced in the following, preceded by a overview of materials used in such devices.

### 2.5.1. Sensitive Layers in Work Function Type Sensors

Only a few organic and inorganic materials have been tested with the KP during the past years and much less data are available as for conducting metal oxide sensors or polymer coated quartz micro balances (QMB). In the following, examples found in the recent literature are introduced tested with a Kelvin probe and used in metal oxide semiconductor field effect transistors (MOSFET). For the sensitive layers work function shifts upon gas adsorption in the order of several hundred millivolts are possible, however, in many cases the signal is only in the range of 10 – 50 mV.

**Organic layers** The most exhaustively studied organic material are the conducting polymers polypyrrol [37, 109–112] and polyaniline [38] in interaction with volatile organic compounds (VOC) like methanol, ethanol, hydrocarbons, and chlorinated hydrocarbons. Other studies investigate the effect of dopants [113].

More recent reports focus on LB or SAM thin films of porphyrins [114–117]. They are found to be sensitive to ethanol and triethylamine. Phthalocyanines work as ozone [118] and NO<sub>2</sub> [119] sensitive layers. Non-conducting polymers other than the ones used in this work like polyvinylpyrrolidone as humidity sensitive layer are reported by Simon et al. [120].

**Inorganic layers** Semiconducting inorganic layers include thin and thick layers of SnO<sub>2</sub> [121–123] and many other oxides like iron oxide [124], mixed aluminium and nickel oxides [125], iridium oxide [126]. Normally, studies are concentrated on simple gases like CO, NO<sub>2</sub>, NH<sub>3</sub> and humidity. Elevated temperatures are necessary for proper operation of the sensing layers. A novel observation is the ability of Pt activated SnO<sub>2</sub> and Ga<sub>2</sub>O<sub>3</sub> layer to work as CO sensor at room temperature [127].

Chemically inert layers are used as reference layers to investigate the response of the KP itself, and in MOSFETs as protective coatings to limit the gas interaction to the sensitive layer [128].

Studies on gas sensitive insulating materials are reported for KI being ozone sensitive [129], carbonates, especially BaCO<sub>3</sub>, being sensitive to CO<sub>2</sub> and NO<sub>2</sub> [97, 130, 131], and TiN as well as TiO<sub>2</sub> [11] as ammonia sensitive layers. ZrO<sub>2</sub> [34] and LaF<sub>3</sub> [35, 36] function as oxygen sensing layers in field effect transistor (FET) devices.

**Metallic layers** Next to the classical Pd gate [4, 132] of the first MOSFET, recently Au and Pt were used as ozone sensing layers [133]. Au is also

known to be sensitive to NO<sub>2</sub> [134]. A mixed phase of Pt/Cu in interaction with CO was under study by Kiss et al. [135].

Examples are available, but the materials are not comparable to the layers used in this work. However, some hints for the understanding the obtained results can be obtained from the interpretation of the insulator layers.

### 2.5.2. Gas Sensitive Field Effect Transistors

Integrated and small sensor structures are desirable, which at best should be prepared by conventional CMOS technology. In this context various sensor types based on the field effect have been developed. The use of a MOSFET, metal insulator semiconductor capacitor (MISCAP), and Schottky diode as a chemical gas sensor is discussed below. An introduction to this field can be found in [136]. In the following, we confine ourself to describing historic milestones and recent developments.

**Principles of a MOSFET** The metal insulator semiconductor field effect transistor (MISFET) is the most prominent device based on a metal insulator semiconductor (MIS) structure next to the so-called MISCAP. If the insulator layer is chosen to be an oxide like silicon dioxide it is termed MOSFET. A high temperature design is based on SiC as semiconductor. Chemically sensitive field effect transistors are built on the conventional isolated gate field effect transistor (IGFET) platform. The MOSFET is generally not used as a instrument to determine the work function of a sample. It is an electronic device and part of many integrated circuits (IC) being a switch, either used for logical functions or to provide current and voltage gain in electronic circuits. The general working principle of a MOSFET is quite simple. A MOSFET consists of a source, a drain, and a gate. A voltage is applied between the source and drain contact resulting in a current, the source-drain current  $I_{DS}$ . The current can be regulated by a potential applied to the gate,  $V_{GS}$ .

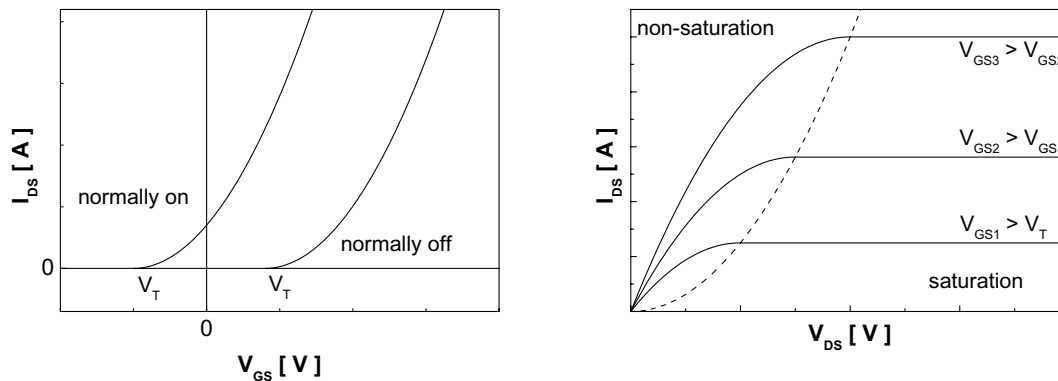
The term metal oxide semiconductor describes the three principal layers of a MOSFET: a metal (the gate) on top of an oxide insulator and a semiconductor substrate (including source and drain) as illustrated in figure 2.8(a). The regions of the source and drain are made of the same semiconductor material but are oppositely doped resulting in a n-p-n or p-n-p structure. The source provides charge carriers and the drain collects charge carriers, whereas the substrate between the two acts as a conductive channel. For a n-channel MOSFET the charge carries are electrons. For a p-channel MOSFET the charge carriers are positively charged holes. Note: a n-channel MOSFET is based on a n-p-n structure. In some designs the transistor is

## 2. Theoretical Background and Related Work

embedded in a transistor well to allow several independent transistors on one single substrate.

There are basically four different types of MOSFET, depending on the type of the conductive channel. If, at zero gate bias  $V_{GS}$ , a conductive n-channel exists ( $I_{DS} > 0$ ) and a negative voltage has to be applied to the gate to reduce the channel conductance, then the device is a n-channel “normally on” MOSFET (illustrated in figure 2.7(a)). If the channel conductance is very low at zero gate bias and a positive voltage larger than the threshold voltage  $V_T$  must be applied to the gate to form a n-channel, then the device is a n-channel “normally off” MOSFET. Similarly, p-channel normally on and p-channel normally off MOSFETs are available.

The channel geometry, charge carrier mobility, and the number of available charge carriers determine the conductance of this channel. The later can be modulated by varying the gate voltage  $V_{GS}$  or a substrate bias voltage. The electric field established by  $V_{GS}$  across the dielectric layer, in the direction traverse to the current flow, influences the type and concentration of charge carriers. Let us consider a n-channel MOSFET. If a low positive potential is applied to the gate the major carriers in the substrate (holes) are repelled and a depletion region is formed. At high potential the minor charge carriers (electrons) are attracted to the semiconductor surface (inversion layer). The inversion layer occurs if  $V_{GS} > V_T$ . Now the channel is again conducting significantly and a current can flow due to the existing n-n-n structure. Increasing  $V_{GS}$  further increases the number of charge carriers and with it the current through the channel.



(a) Transconductance curves for a “nor- (b) Output conductance curves for different values of  $V_{GS}$ .

**Figure 2.7.:** Characteristics of a MOSFET device.

The actual current through the channel is determined by the applied source-drain potential and two regions are distinguished: the non-saturation

and the saturation mode as shown in figure 2.7(b). Two semi-quantitative equations describe these two modes. The current-voltage characteristics in the non-saturation mode ( $|V_{DS}| \leq |V_{GS} - V_T|$ ) of a long gate FET can be modelled using the square law approximation leading to

$$I_{DS} = \mu_{eff} C_{ox} \frac{W}{L} \cdot (V_{GS} - V_T - \frac{V_{DS}}{2}) V_{DS}$$

In saturation mode ( $|V_{DS}| \geq |V_{GS} - V_T|$ ) the current is given by

$$I_{DS} = \mu_{eff} C_{ox} \frac{W}{2L} \cdot (V_{GS} - V_T)^2$$

where  $\mu_{eff}$  the charge carrier mobility,  $W, L$  the channel width and length, respectively, and  $C_{ox}$  the insulator capacitance. The drain current is near zero if the gate voltage is less than the threshold voltage. For a more detailed description of the device physics see e. g. [137].

The performance of a MOSFET device is characterised by two terms: the transconductance quantifies the drain current variation with a gate-source voltage variation while keeping the drain-source voltage constant. This is an important parameter as it determines the device sensitivity and contributes to the overall sensitivity of the sensor device. The output conductance quantifies the drain current variation with a drain-source voltage variation while keeping the gate-source voltage constant.

The threshold voltage  $V_T$  as the onset of the inversion layer is determined among other factors by the properties of the materials and by the work functions of the gate material  $\varphi_M$  and the bulk semiconductor  $\varphi_S$

$$V_T = \varphi_M - \varphi_S - \frac{Q_i}{\varepsilon_i} d_i + 2\varphi_F - \frac{Q_B}{\varepsilon_i} d_i \quad (2.73)$$

where  $Q_i$  denotes the charge of the insulator at the insulator-semiconductor interface,  $d_i$  the thickness of the insulator,  $\varepsilon_i$  its permittivity,  $Q_B$  the depletion charge in the semiconductor, and  $\varphi_F$  the potential drop across the depletion region.

**The ChemFET** The term chemical field effect transistor (ChemFET) is the generic term for chemical sensors based on the MOSFET design. This class is commonly divided into two major subgroups: gas sensitive field effect transistor (GasFET) for gas sensing and ISFET for sensing in liquids. The ISFET is the first MOSFET sensor and was proposed by Bergveld [138]. Both sensor types have undergone a long development and were just topic of a review recognizing their 30th anniversary [7, 139].

## 2. Theoretical Background and Related Work

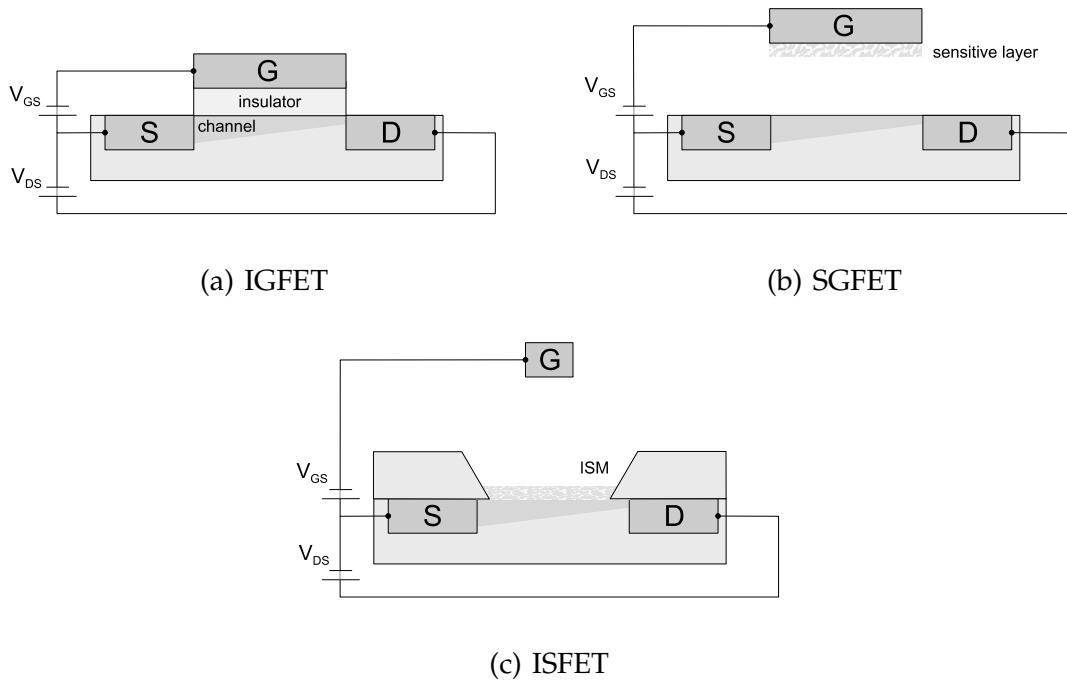


**Figure 2.8.:** Schematics of different MOSFET types used as chemical sensor.

In order to come up with a gas sensitive FET, the influence of gases on the gate or, more precisely, on the gate-insulator interface must be ensured. The best-known example is the Pd-FET (“Lundström FET”) reported by Lundström et al. [4] as a variant of the IGFET. In the case of the Pd-FET the gate is made of palladium, which is highly permeable to hydrogen. Hydrogen molecules dissociate at the gate surface, diffuse to the interface and become polarised. The resulting dipole layer changes the contact potential by  $\Delta V$ .

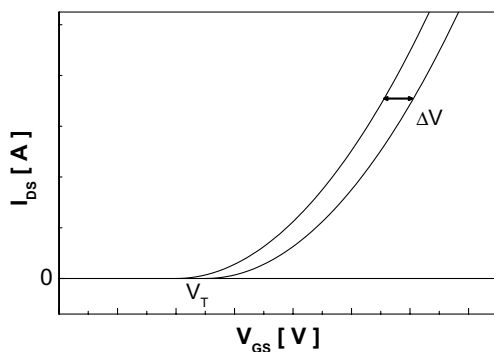


**Figure 2.9.:**

A shift of the I-V curve of a Gas-FET induced by gas adsorption and a change of work function at the metal/insulator interface.

$V_T$  is altered by the analyte gas by influencing the work function of the metal gate,  $\varphi_M$ , and consequently  $I_{DS}$ : the I-V curve is shifted by  $\Delta V$  (see

figure 2.9). The MOSFET sensors are usually operated under the constant drain current mode, which means that the change of the drain current due to the change of the work function is compensated for by the adjustment of the gate voltage.

One limitation of the Pd-FET is the fact, that only hydrogen can diffuse through the gate and therefore only few gases can be detected like hydrocarbons and ammonia. Variations in sensitivity and selectivity are possible by different operation temperatures.

To overcome this limitation ultra thin, non-continuous layers of metals (among others Pt, Au, Ir) or porous materials can be used as gate materials. The palladium gate has been replaced by SnO<sub>2</sub> [121], conducting polymers [112], ZrO<sub>2</sub> [34], LaF<sub>3</sub> [35, 36], phthalocyanines [118], and porphyrins [117].

Apart from a modification of the gate material, structuring of the gate is applied successfully leading to the suspended gate field effect transistors (SGFET) device: the gate is suspended over the insulator and optionally coated with a sensitive material. A sketch is shown in figure 2.8(b). The idea of a SGFET was introduced by Josowicz and Janata [111], Cassidy et al. [132] and until recently under investigation [38]. In a SGFET the gases come into direct contact with the insulator face of the gate electrode. This type of MOSFET is in principle more versatile and some designs have been developed, where the gate material can be deposited in a separate process on the gate before mounting to the device. The first flexible design was reported by Flietner et al. [123]. The first designs of the SGFET were based on a fixed micromachined gate. The SGFET has recently gained new interest and new developments are reported by Fleischer et al. [5], Eisele et al. [140], Wilbertz et al. [141].

A variation of the SGFET is the capacitively coupled field effect transistor (CCFET). In case of the CCFET the gate itself is not in contact with analyte gases, but the potential drop is occurring on an electrode which is coupled to a floating gate, often buried in a passivation layer [142, 143]. The actual transistor is a regular MOSFET.

For liquids a similar design as is used. Essentially, the ISFET construction is the same as the one of an SGFET, except for the fact that the standard gate is replaced by a more complex structure (see figure 2.8(c)). Namely, the gate structure, consists of a reference electrode at constant potential. The selectivity is governed by the chemical activity of the insulator surface or a ion selective membrane. The ion concentration in the electrolyte influences the potential drop across this region, which in turn modifies the transistor threshold voltage.

### 2.5.3. MIS Capacitors

Another sensor device using the field effect is the MISCAP. The layer structure is made of a metal electrode separated by an insulator layer from the semi-conductive substrate (see figure 2.10 a). The sensor is electrically connected on both sides and the capacitance is measured.

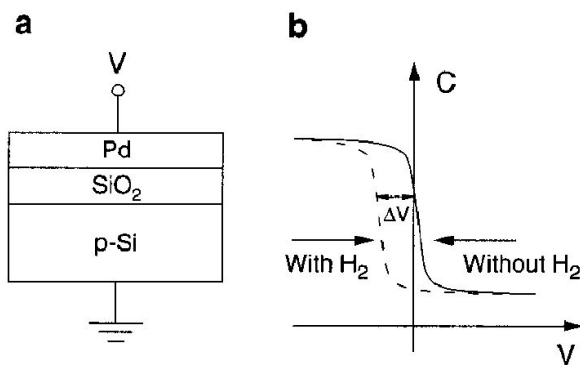


**Figure 2.10.:**

a) The description of the MISCAP structure: an oxidized silicon wafer (p-doped in this case) is covered with a thin layer of palladium. The structure is electrically connected on both sides. b) When exposed to hydrogen, a shift by  $\Delta V$  is observed in the C-V curve [taken from 144].

Normally, the metal is gas sensitive and often the same layers are used as in the Lundström FET. During gas adsorption the characteristic C-V curve of the device is shifted by  $\Delta V$  (see figure 2.10 b), which is the shift in the work function induced by the gas due to a dipole layer at the metal/insulator interface. A device with a palladium layer is reported to have similar H<sub>2</sub> sensing capabilities as the FET based on the same mechanism [144].

Kreisl et al. [145] operate a capacitor in a non-stationary temperature pulse mode to be able to detect hydrocarbon species. During the phase of high-temperature the chemical interaction of analyte gases with a catalytically active electrode takes place and at low-temperature the C-V characteristic is read out. Another possibility of changing and enhancing selectivity and sensitivity is the deposition of a thin catalytically active layer on the Pt metal gate. TiN, SiO<sub>2</sub>, Al<sub>2</sub>O<sub>3</sub>, SnO<sub>2</sub> are reported to enhance the sensitivity of the capacitor device towards hydrogen, ammonia and other selected analytes [146, 147], thus, using the same strategies as for the MOSFET.

### 2.5.4. Schottky-Diodes

Schottky-Diodes are based on a Schottky type electrical contact between a metal and a semiconductor. The current through the device at constant applied voltage is determined by the barrier height for electrons across this contact. Schottky diodes are preferred over capacitors as sensor devices



due to the simple electronic circuitry. In order to use them as a gas sensor the metal/semiconductor interface needs to be accessible by the analyte gas and a change in work function must occur either in the metal or in the semiconductor side of the interface.

The rectifying J–V behaviour of Schottky barrier devices is usually assumed to follow the standard thermionic emission theory for conduction across the junction. The current is assumed to be controlled only by the transfer of carriers across the interface regulated by an applied voltage. The relation between the current density  $J$  and applied forward bias voltage  $V$  is given by

$$J = J_0 \left( e^{\frac{eV}{kT}} - 1 \right)$$

where  $J_0$  represents the reverse leakage current density and  $V$  the applied forward-bias voltage. From  $J_0$  the barrier height  $\phi_B$  can be calculated

$$J_0 = AT^2 e^{-\frac{e\phi_B}{kT}}$$

where  $A$  is the Richardson constant. The barrier height depends on the work function  $\phi_M$  of the metal and the electron affinity of the semiconductor for n-type semiconductors

$$e\phi_B = \phi_M - \zeta$$

and for a p-type semiconductor as the difference between the valence band edge of the semiconductor and the work function of the metal

$$e\phi_B = E_G + \zeta - \phi_M$$

where  $E_G$  is the band gap.

The metals used in gas sensitive Schottky diodes are mostly the same as in GasFETs. Typical semiconductors are silicon,  $\text{TiO}_2$ ,  $\text{SnO}_2$ , and  $\text{WO}_3$ . Examples for applications of this type of sensor are ozone and nitric oxide sensing with InP [148] or the detection of ammonia and urea as ammonia by discontinuous platinum films [149, 150].

The choice of materials is not limited to metals or inorganic materials, also organic materials, for example polyaniline, can be used. It is known that it forms an ohmic contact with gold or a Schottky contact with Al. Campos et al. [151] describe the properties of such an Al/polyaniline/ITO device influenced by the changes of the Al/polymer interface induced by gas absorption. Methane increases the barrier height by 0.7 – 0.8 eV in the concentration range of 0.25 – 0.6% and consequently the current is decreased. The result of one methane measurement is illustrated in figure 2.11.

## 2. Theoretical Background and Related Work

---

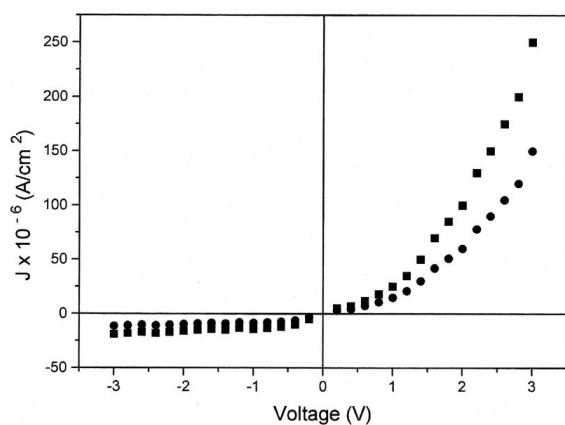


**Figure 2.11.:**

Plot of current density vs. applied voltage rectification characteristic for 0.6 M doped Al/polyaniline/ITO device in nitrogen (squares) and in 0.6% v/v of methane (circles) [taken from 151].

## **3. Experimental Details**

### **3.1. Instrumental Equipment**

#### **3.1.1. Optical Microscope**

The Olympus BX60 is an optical microscope for measurements in reflection and transmission mode. The maximum magnification factor in the present configuration is 1000x (in steps of 50x, 100x, 200x, 500x). Documentations are possible by the attached digital camera able to capture images. The supplied AnalySIS software was used to capture and process the optical microscope (OM) images. The system is calibrated for lateral distance measurements.

#### **3.1.2. Atomic Force or Scanning Probe Microscope**

In scanning probe microscopy (SPM) or more commonly called atomic force microscope (AFM), the interaction of a stylus probe and sample surface is quantified and mapped across a sample. The probe or “tip” is of nanometer-scale sharpness and the standard image is a 3D surface topography at resolution approaching the atomic or molecular scale. An AFM by Digital Instruments (Nanoscope III Multimode) was used in a special mode, called tapping or non-contact mode, which allows the characterization of sensitive or soft materials, like polymers, lipid structures, proteins or even cells. Measurements are available in a maximal lateral range of 20  $\mu\text{m}$ .

#### **3.1.3. Scanning Electron Microscope**

In the scanning electron microscope (SEM) a finely focused beam of electrons is scanned across the specimen generating secondary electrons, back-scattered electrons, and characteristic X-rays. The detected secondary electrons show the topography of surface features a few nm across in magnifications up to several 100,000x with a dramatically better resolution and depth of view than an optical microscope has to offer. A Zeiss DSM 962 was used with an electron acceleration voltage of 5 kV.

### 3.1.4. Stylus Surface Profilometer

The KLA Tencor Alpha Stepper 500 surface profilometer is a stylus profilometer. It is intended to be a versatile system for precise measurement of very thin step heights on wafers and small samples. The measurement is done by a stylus, which touches the surface of a sample and runs across a prescribed length.

To measure the thickness of a film, a step that is comparable to the film thickness must be produced before the measurement. This can be done in many ways, such as scratching the film with a sharp metal piece or covering part of the sample with a slide during film deposition, lifting it off for the measurement.

Before characterising the samples in terms of roughness the most relevant and commonly used definitions shall be given here for completeness:

The roughness average  $R_a$  is the arithmetic average of the absolute values of the roughness profile ordinates  $Z_i$

$$R_a = \frac{1}{n} \sum_{i=1}^n |Z_i - \bar{Z}| \quad \text{or in integral form} \quad R_a = \frac{1}{l} \int_0^l |Z(x)| dx \quad (3.1)$$

The root means square (rms) average roughness  $R_q$  is the root mean square average of the roughness profile ordinates

$$R_q = \sqrt{\frac{1}{n} \sum_{i=1}^n (Z_i - \bar{Z})^2} \quad \text{or in integral form} \quad R_q = \sqrt{\frac{1}{l} \int_0^l Z^2(x) dx} \quad (3.2)$$

The rms roughness represents the standard deviation of the profile heights and is used in computations of skew and kurtosis.

The maximum profile peak height  $R_p$  and the maximum profile valley depth  $R_v$  are the distances from the mean line/surface to the highest/lowest point in the evaluation length/area (see figure 3.1(a)).

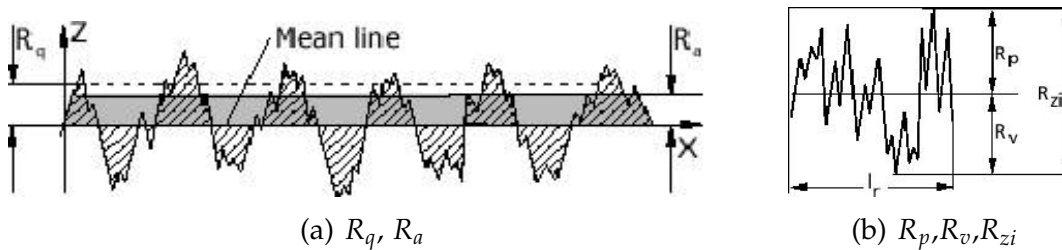


Figure 3.1.: Illustration of the roughness parameters.

The single roughness depth or maximum height  $R_{zi}$  or more commonly denoted with  $R_t$  is the vertical distance between the highest and lowest points in the evaluation length/area (see figure 3.1(b))

$$R_t = R_p + R_v \quad (3.3)$$

The skewness  $R_{sk}$  is a measure of the asymmetry of the profile about the mean line. Negative skew indicates a predominance of valleys, while positive skew is seen on surfaces with peaks

$$R_{sk} = \frac{1}{n R_q^3} \sum_{i=1}^n (Z_i - \bar{Z})^3 \quad (3.4)$$

The kurtosis  $R_{ku}$  is a measure of the distribution of spikes above and below the mean line. For spiky surfaces,  $R_{ku} > 3$ , for bumpy surfaces,  $R_{ku} < 3$ , and perfectly random surfaces have kurtosis 3

$$R_{ku} = \frac{1}{n R_q^4} \sum_{i=1}^n (Z_i - \bar{Z})^4 \quad (3.5)$$

The later two measures are not very robust in calculation and not used in this work.

### 3.1.5. Gas Mixing System

Testing gas sensing properties of new materials and first stage sensor tests require controllable and reproducible conditions in terms of temperature, air flow, and composition of the gas atmosphere. This allows thorough testing of the responses to individual gases and studies of the influences of temperature, changing humidity, and cross interferences. In gas mixing systems all those parameters can be adjusted with high accuracy and reproducibility.

A gas mixing system (see figure 3.2) consist of several gas channels controlled by a set of mass flow controllers operated by a computer. The system used in this work similar to the one described in [152] consists of eight channels each of which is equipped with a mass flow controller (MFC) and solenoid valves under control of a personal computer, running the home-made software programme POSEIDON, through a D/A card. An A/D card is used to monitor the gas mixing bench by reading back the actual gas flows from the MFCs for documentation purposes.

### 3. Experimental Details

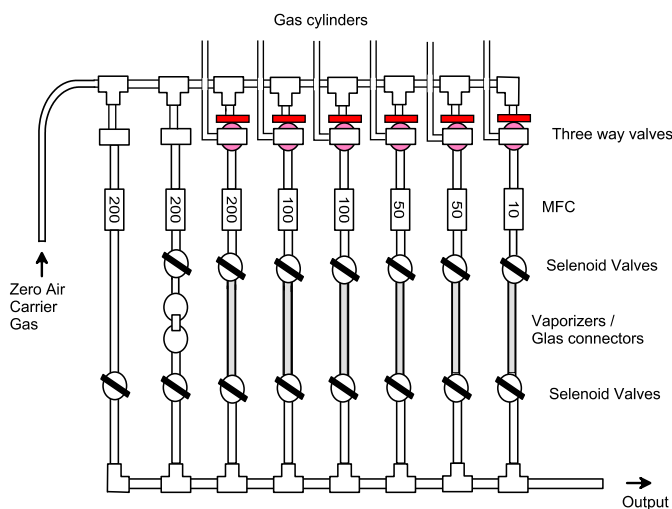


**Figure 3.2.:** Schematic sketch of an eight channel gas mixing system. The analytes are either added to the carrier gas from gas cylinders or by carrier gas fed through vaporizers. The latter method is also used to adjust the relative humidity.

The tubing of the gas mixing system consists mainly of stainless steel pipes with an inner diameter of 4 mm and partly of gas tight poly(tetrafluoroethylene) (PTFE) tubing. The interconnections between the solenoid valves are made via either glass tubes or U-shaped vaporizers filled with an adsorbent of a high specific surface area (Chromosorb P-NAW 80/100 mesh, Macherey-Nagel). Each channel is then fed either by a gas cylinder with analyte gas or by carrier gas swept through a vaporizer, with the chemical compound (in liquid phase) under investigation or water adsorbed on the surface of the adsorbent. The vaporizers for the analytes are immersed in a thermostated bath of ethylene glycol (ethanediol). The carrier gas gets saturated with the vapour of the analyte. The actual concentration in the gas stream is determined by the saturation vapour pressure at the temperature of the thermostat, which is calculated by Antoine's equation

$$\log p = A - \frac{B}{t + C} \quad (3.6)$$

where  $p$  is the vapour pressure in Torr,  $t$  the temperature in  $^{\circ}\text{C}$ , and  $A$ ,  $B$ ,  $C$  are specific constants found in reference [153] valid in a certain temperature range. A typical temperatures is  $-15^{\circ}\text{C}$  to have an adequate saturation vapour pressure for the analytes in this work. This principle is used for humidifying the carrier gas and the ethanol, toluene, and n-butylamine channels.

Ammonia was supplied from gas cylinders with a certified concentration of analyte gas as a product of Messer Griesheim. The carrier gas was produced by a zero-air generator from pressured air.

The calibration of all channels was on a regular basis checked with a flow meter (Sensirion Flow Meter ASF1400). The composition of the fi-

nal gas mixture was monitored with an electrochemical cell (3AM CiTiCel Ammonia, no cross sensitivity to humidity, 0 – 50 ppm range and 0.5 ppm resolution) and a high precision hygrometer.

### 3.1.6. Kelvin Probe Set-up

The Kelvin probe (KP) measurement set-up includes an oven, which is hosting the Kelvin probe in a special measurement chamber, and the KP driving electronics. The measurement data is acquired by a digital multimeter connected via the serial port to a PC running computer software written in Agilent Vee.

#### 3.1.6.1. Kelvin Probe

In this work a KP manufactured by Besocke-Delta Phi was used. The Kelvin probe type S is an improvement of the initially developed type, described by Besocke and Berger [72]. The probe material is a gold covered stainless steel grid of 3 mm diameter fixed to a steel rod, but electrically insulated. The vibrations are produced by a piezoceramics. The piezoceramics is shielded by a grounded metal tube to minimize pick-up of the driving potential by the probe. A schematic drawing of the measurement set-up is presented in figure 3.3.

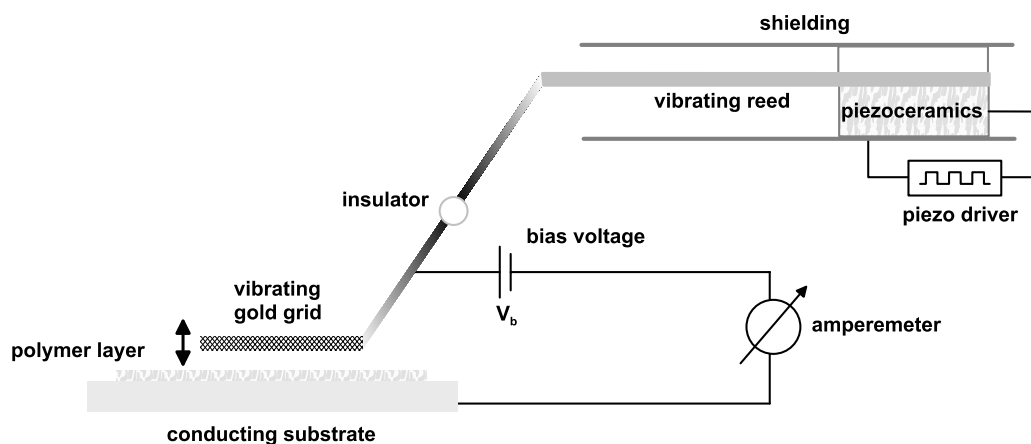


Figure 3.3.: Sketch of the measurement set-up with the Besocke Kelvin probe.

The base resonance frequency of 160 Hz (overtones near 900 Hz) is set by the dimensions of the probe and the piezoelectric constant of the piezoceramics. In this set-up the Kelvin probe is operated in the ground resonance mode. The amplitude can be varied via the electronics in an estimated

range of 1 mm. The optimal sample–probe distance is according to the manufacturer about 1 mm.

#### 3.1.6.2. Driving Electronics

The Kelvin probe was controlled by an electronics (Kelvin Control 7) manufactured by the same company. The electronics has outputs for driving the piezoelectric actuator, for the raw signal visualised by an oscilloscope, and for the KP signal connected to the data acquisition system.

In the automatic modus the DC bias voltage  $V_b$  is adjusted by the circuitry to minimize the charging current of the KP probe head-sample capacitor (null method). For the determination of the contact potential the raw signal is amplified with a lock-in amplifier and optionally filtered with a build-in filter. The output of the Kelvin Control is  $-V_b$  that minimizes the current equal to the contact potential between the probe head and the sample. The maximal accuracy is about 1 mV in optimal, this is in a ultra high vacuum (UHV) set-up, conditions at an integration time of 1 s. The manual mode can be used to manually adjust the contact potential to zero. In this case the current is displayed on an integrated gauge.

The settings for amplitude, integration time, and gain were fixed for all experiments to: integration time (“Time Con”) 2, signal amplification (“Gain”) 2, oscillation amplitude (“Oscillator”) 3, filter on. The possibility of adjusting the probe-sample distance by the means of a DC voltage (“Distance”) was not used. The shorter integration time is causing a lower accuracy of 1 to 3 mV.

#### 3.1.6.3. Measurement Chamber

The measurement chamber for the Kelvin probe is made of an aluminium cross fitting with a tube inner diameter of 25 mm to host both the sample and the Kelvin probe. Due to the size and shape of the device the cell volume is large (80 ml) and the inside is fissured in shape. The KP chamber is positioned in a programmable oven to ensure a constant and defined temperature of the sample and the measurement instrument. In the photograph image in figure 3.4 the measurement chamber can be seen standing inside the oven.





**Figure 3.4.:**

Picture of the KP measurement chamber (left) and the coil for preheating the carrier gas (right) located in the programmable oven.

On the sides of the cross the gas connections with the gas mixing system and the exhaust system is put up. A coil can be added to the gas flow before the chamber to allow preheating the carrier gas at higher measurement temperatures (also shown in the picture). In the back the two necessary gas tight electrical feedthroughs are made for the electrical connections to the KP. The sample fixed on a micrometre screw for height adjustment is introduced from below. The position of the sample can be monitored from the opening in front and from above. The openings are closed after the mounting the sample with two sealed caps.

The grid of the Kelvin probe was centred in the measurement chamber and after the initial mounting kept at a fixed position. A micrometer screw can be used for the necessary height adjustment of the sample. The sample probe distance is always kept minimal to have a maximal sensitivity of the KP. The sample is directly connected to the ground of the Kelvin Probe driving electronics to have only one common ground. Careful grounding of sample and measurement chamber is crucial to minimize error.

#### **3.1.6.4. Validation of the KP Set-up at High Humidity Levels**

The Besocke KP was designed for the use in very low pressure environments at ambient temperatures. However, it is specified for working temperatures up to 80 °C and it is expected to work in a relative humidity range up to 80% rh. To ensure proper operation and reliability of the later obtained results potential changes were simulated by applying known and constant potentials to a test sample at high humidity and temperature levels. For this test a substrate with a sensitive layer was used like for the real gas experiments. The result for the high humidity test (70% rh) is shown in figure 3.5.

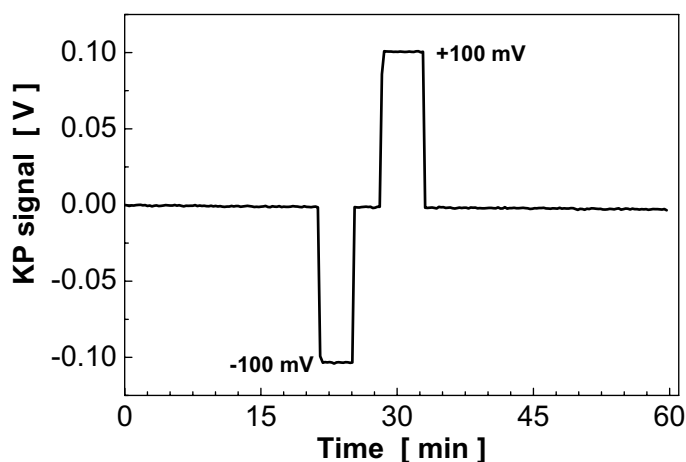


**Figure 3.5.:**

Validation of the KP functionality at high humidity levels (in this case 70% rh). Response of the KP to voltage pulses of  $\pm 100$  mV simulating a CPD change induced by gas exposure: raw KP signal with the first data point set to zero.

Further can be said that the signal has a negligible drift within 1 h in comparison with the expected signals and is stabilizing further after an equilibration time of hours. The noise level in the baseline is lower than  $\pm 0.3$  mV.

The linearity of the KP response was tested by applying several voltage pulses up to  $\pm 5$  V to the sample and by comparing the KP output with the applied voltage. The response of the KP to the applied pulses is excellent, accuracy and linearity are sufficient with an error smaller than 3%. At the ambient conditions with a polymer sample voltage pulses smaller than 2 mV were detectable. The response time is determined only by the driving electronics. The temperature test proved the operability of the set-up in a similar way.

In general the signal of the KP is stable after a equilibration time of several hours, having a long time drift at high humidity levels.

#### 3.1.7. QMB Set-up

Commercially available quartz crystals manufactured by Kristallverarbeitung Neckarbischofsheim were used as quartz micro balance (QMB) sensors. These so-called AT-cut crystals have a fundamental frequency near 30 MHz (thickness 56  $\mu\text{m}$ , density 2.6  $\text{g}/\text{cm}^3$ ) and are partially covered with gold electrodes (diameter 3 mm) on both sides.

The driving oscillator circuitry is integrated in the QMB sensor holder. A coaxial cable provides the driving voltage and transmits the signal. The output signal is mixed with a reference and then read out by a frequency counter card. The data acquisition system allows measuring ten QMB sensors at a time. Data points are stored every ten seconds as an average of ten individual recordings. The system resolution is 1 Hz.

The QMB measurement chamber is designed for a maximum of 11 QMB sensors aligned in two opposite, interlacing rows leading to a cell volume of 20 ml. The sensors are close to a water filled cooling/heating coil integrated in the walls of the measurement chamber. The temperature control is achieved by a Julabo F 32 MH thermostat.

#### 3.1.8. Infrared Spectrometer

The infrared (IR) spectra were recorded on a Bruker Equinox 55 FT-IR spectrometer. The measurement of single channel spectra in transmission with a resolution of  $2\text{ cm}^{-1}$  were taken every five minutes with 256 scans. The accompanying software package (OPUS 4) was used to calculate the absorbance spectra using the corresponding reference. The spectra were calculated using the last but one spectrum before the analyte/humidity pulse and the last but one spectrum during the pulse.

A gas tight measurement cell with two IR radiation transparent NaCl windows in front and back was designed hosting samples of an area of  $15 \times 15\text{ mm}^2$ . The air gap above the sample is 3 mm. A gas inlet was connected to a gas mixing system as described in section 3.1.5. The polymer layers were prepared on a silicon wafer substrate in spray coating process. The deposition of polymer was stopped at a frequency shift of the QMB witness of 30 kHz. The substrate was carefully fixed in the chamber to ensure a vertical position.

### 3.2. Materials for the Preparation of the Sensing Layers

All organic materials and chemicals used in the preparation of the sensing layers and in the gas sensing experiments are commercially available and were used as delivered.

#### 3.2.1. Organic Polymers

##### 3.2.1.1. Polyacrylic acid (PAA)

Polyacrylic acid (PAA) (for the chemical structure see figure 3.6(a)) is a plastic polymer having a relatively elevated glassy point in the range of  $76 - 106\text{ }^\circ\text{C}$  not so much favourable for the use in chemical sensors as for example the rubbery poly(methylacrylate) ( $T_g$  of  $7\text{ }^\circ\text{C}$ ); the reported values of the glass transition temperature differ often in the literature for PAA and the other polymers. The physical data for all the polymers was taken from references [154] and [155]. The later serves also as an introduction

### 3. Experimental Details

to technical applications of polymers with a lot of information on some of the polymers used in this work. Only limited data is available on the data sheets provided by the supplier.

Due to PAA's polar and acidic character with a  $pK_a$  of 6.2 (similar to acetic acid) significant specific interactions with bases are expected. Additionally, the acid functional group is capable of hydrogen bonding via the oxygen atom. PAA is soluble in acetone, water and other polar solvents, but not soluble in the monomer. The polymer (CAS No. 9003-01-4,  $M_w$  2000 g/mol, no cross linking, density 1.05 g/cm<sup>3</sup>) was provided by Sigma-Aldrich.

PAA belongs chemically to the large group of acrylates, which are widely used in technical applications: acrylic glass made of poly(methyl methacrylate) (PMMA) and fibres or soft contact lenses made from polyacrylonitrile (PAN). PAA can be synthesised by electrochemical polymerisation, chemical vapour deposition (CVD) processes or chemical polymerisation in solution initiated by oxidation or radicals. Diisocyanates, polyethyleneglycol (PEG) or polyvinylalcohol (PVA) are commonly used as cross link agents. Cross linked with PEG or diisocyanates PAA itself is technically used as a hydrogel and functions as a superadsorbant in diapers and other hygiene products.

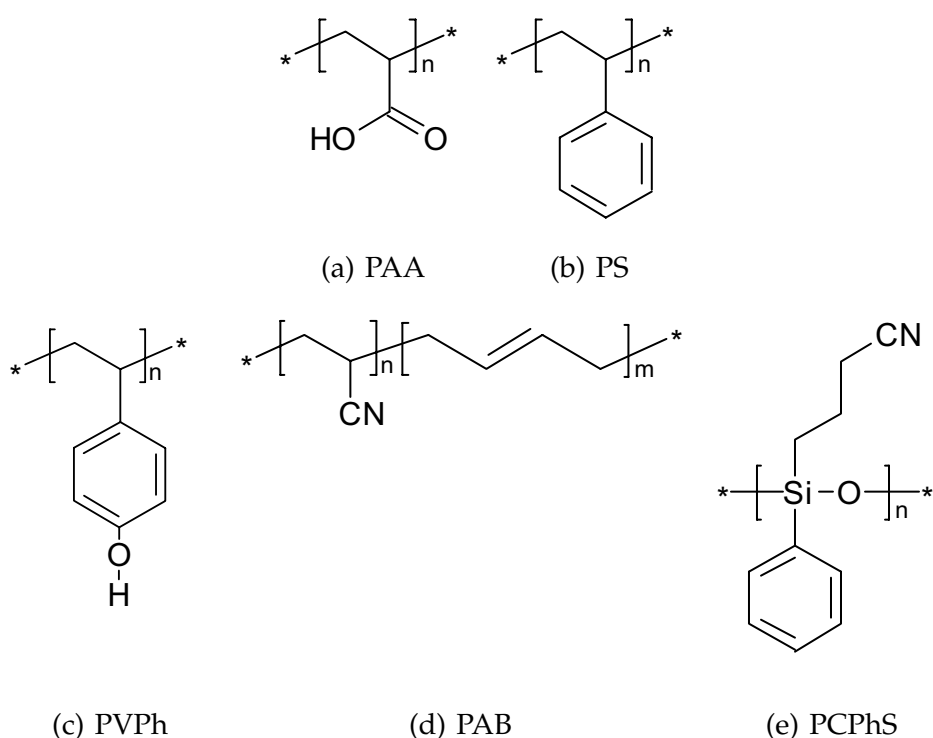


**Figure 3.6.:** Chemical structures of the organic polymers introduced as ammonia sensitive layers in the KP and QMB experiments.

### 3.2.1.2. Polystyrene, bimodal (PS)

The stable and chemically rather inert polymer polystyrene (PS) (see figure 3.6(b)) is a very common plastic material with thermoplastic properties having a melting point of 240 °C. It is of great technical importance for the production of plastic goods. In contact with analytes the phenyl group can provide specific interactions of the  $\pi$ - $\pi$  type. The polymer is soluble in dichloromethane and trichloromethane (chloroform) and similar solvents. Polystyrene (CAS No. 9003-53-6,  $T_g$  80 – 90 °C, density 1.05 g/cm<sup>3</sup>) was produced by Sigma-Aldrich.

### 3.2.1.3. Poly-(4-vinylphenol) (PVPh)

Poly(4-vinylphenol) (PVPh) or poly(4-hydroxystyrene) (see figure 3.6(c)) is a solid, thermoplastic material which melts and decomposes at temperatures of 360 °C. This soluble reactive polymer has excellent dimensional stability and chemical resistance. It finds applications for printed circuits as electric insulator or as dielectric in organic electronics and is used as resin in UV lithography and support polymer for peptide synthesis and antibody binding. PVPh is soluble in acetone and other polar solvents. Poly-(4-vinylphenol) (CAS No. 24979-70-2,  $T_g$  134 °C or 170 – 180 °C depending on the source, density 1.16 g/cm<sup>3</sup>,  $M_w$  8000 g/mol) was obtained from Sigma-Aldrich.

### 3.2.1.4. Poly-(acrylonitrile-co-butadiene), amine terminated (PAB)

Poly(acrylonitrile-co-butadiene) (PAB) with an acrylonitrile fraction of 18% (see figure 3.6(d)) is a viscous and amorphous polymer. It has capabilities of polar interactions via the CN group. This elastomer is used as a rubber modifier in epoxy compositions or as a component of epoxy adhesives, coatings and fiberglass reinforced compositions. It is soluble in dichloromethane (DCM). PAB (CAS No. 68683-29-4,  $T_g$  –51 °C, density 0.96 g/cm<sup>3</sup>) was supplied by Sigma-Aldrich

### 3.2.1.5. Poly-(cyanopropyl-phenyl-siloxane) (PCPhS)

Poly(cyanopropyl-phenyl-siloxane) (PCPhS) (see figure 3.6(e)) is a derivative of siloxane like the very commonly used polymer polydimethylsiloxane (PDMS). Through the CN group a polar interaction and via the phenyl group  $\pi$ - $\pi$  interactions are possible. It is soluble in DCM. The fraction of

both side groups is 50%. The compound, a stationary phase in gas chromatography, was provided by Ohio Valley Specialty Chemicals.

Siloxanes are available in a variety of derivatives modified in the side groups. PDMS is one of the chemically simplest siloxanes and widely used as stationary phase in gas chromatography and in the detection of volatile organic compounds (VOC) with chemical sensors, namely QMB sensors. Their chemical stability and their low  $T_g$  (PDMS has a  $T_g$  of  $-123\text{ }^\circ\text{C}$ ) as the result of their flexible back plane are advantageous for the application field of chemical gas sensing.

#### 3.2.2. Substrates

The planned experiments made the use of two different types of substrates necessary which were based either on alumina plates or on silicon wafers.

##### 3.2.2.1. Alumina Based Substrates: Au/Al<sub>2</sub>O<sub>3</sub>

The alumina substrates, kindly provided by the Siemens AG in Munich, are made of sintered and polished polycrystalline alumina plates covered with a quite thin gold layer on top of a platinum layer. This gold layer was either thermally evaporated or screen printed on the substrate covering the whole area. The plate was laser cut into pieces of  $8 \times 6.5\text{ mm}^2$  for the KP experiments.

The evaluation of the surface profilometer data yielded that the surface of the Au/Al<sub>2</sub>O<sub>3</sub> substrate is very rough. For the different roughness parameters the following values were determined, derived from surface profiles like in figure 3.7 taken with a stylus profilometer:  $R_q$  80 nm,  $R_v$  240 nm,  $R_p$  310 nm, and  $R_t$  550 nm.

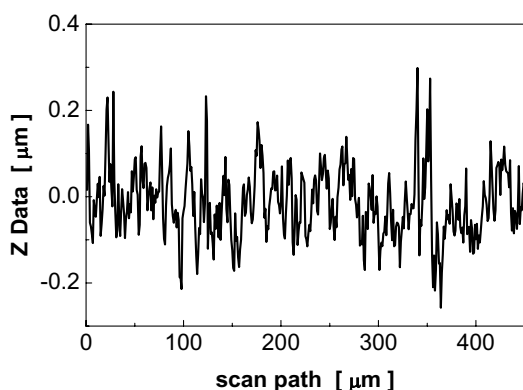


**Figure 3.7.:**  
Surface profile of a bare alumina substrate (Au/Al<sub>2</sub>O<sub>3</sub>) recorded with a stylus profilometer.

This profile structure made the determination of the surface roughness of the polymer layers impossible as long as the thickness of the polymer layer

was in the range of the roughness of the substrate, because the layer surface structure was very much superimposed by the nature of the substrate. As a consequence this type of substrate was considered not suitable for the polymer layer characterisation.

The reason for using this type of substrate are the field effect transistor (FET) sensors, which are designed to use this inexpensive material as support with a specially structured gold layer as gate and electrical contacts. The Au/Al<sub>2</sub>O<sub>3</sub> substrate was partly used for the KP measurements to reproduce the same material conditions as in the FET devices.

#### 3.2.2.2. Silicon Wafer based Substrate: Au/Si

The silicon substrates were prepared from silicon wafers covered with a thin gold layer of about 100 nm on a thin layer of titanium. The wafers were hand cut to the desired size for the KP measurements (around 5x5 mm<sup>2</sup>). Pieces of larger size of a bare silicon wafer were used in the IR measurements and in some special KP experiments.

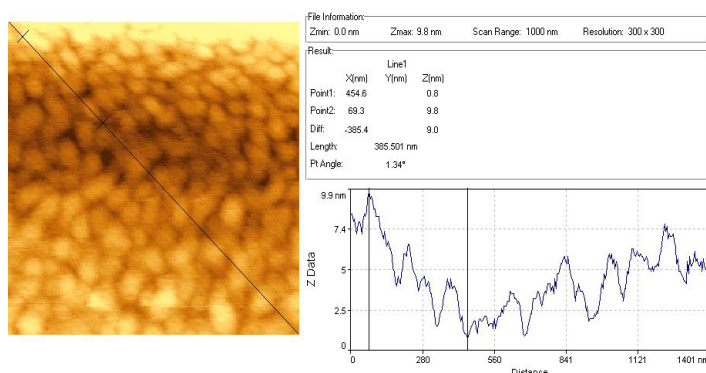


**Figure 3.8.:**  
AFM image and surface profile of the Au/Si substrate.

The very limited degree of surface roughness of the silicon wafers allowed an accurate investigation on the intrinsic polymer layer properties, as the Au/Si substrates have a roughness of less than 10 nm, which is the result of the AFM measurements. An AFM image is presented in figure 3.8. The gold layer consists of grains of the size of 50 nm.

#### 3.2.3. Other

All solvents (DCM, acetone, ethanol, toluene, and n-butylamine (n-BuNH<sub>2</sub>)) used for cleaning purposes, layer preparation, and as analytes were of highest available grade and used as delivered.

### 3.3. Polymer Deposition

All polymer layers were prepared by the spray coating technique. Using a conventional spraying nozzle with nitrogen as propellant the polymers dissolved in an organic solvent were sprayed onto a substrate. The progress of the coating processes was monitored on-line by a QMB sensor used as a thickness monitor. The samples were heated up overnight after preparation to 60 °C to remove remaining solvent traces and were openly stored at room temperature in ambient air.

Two deposition systems were in use: a manual system and a semi-automatic system [156]. Initially a standard hand-held air-brush was used for the preparation of the samples. In a parallel arrangement of the substrate and a QMB thickness monitor the polymer solution was sprayed from a distance of 8 to 10 cm using a air pressure of 1.3 bar in a waving motion.

Later it was made use of the semi-automatic system to overcome the limitations and drawbacks of the manual system especially the fact that it was not possible to prepare a larger set of samples in one single process under constant conditions.

**Table 3.1.:** System parameters of the Düsen-Schlick Model 970 S8 taken from the data sheet provided by the manufacturer.

Parameter	Value
Carrier gas flux	1.5 m <sup>3</sup> /h at 1 bar
Liquid phase flux	100 ml/h at 1 bar
Droplets size	30 μm
Nozzle diameter	0.3 mm

A mountable spraying nozzle (a two substance nozzle Model 970 S8 manufactured by Düsen-Schlick, see table 3.1) was fixed in a distance of 5 to 12 cm in front of a rotating disk (rotating frequency about 0.2 Hz) holding the samples. This peculiar spraying nozzle model was chosen for its low consumption of spraying solution and the small size of the droplets (around 30 μm) producing a fine spray mist.

This set-up is depicted in figure 3.9: the spraying nozzle (right) pointing at the QMB witness is mounted in front of the rotating disk (middle) functioning as the sample holder, here also equipped with a shadow mask; the QMB holder can be seen on the left connected to a frequency counter and to a conventional oscilloscope via a coaxial cable to monitor change in frequency and amplitude of the quartz crystal during the deposition process.



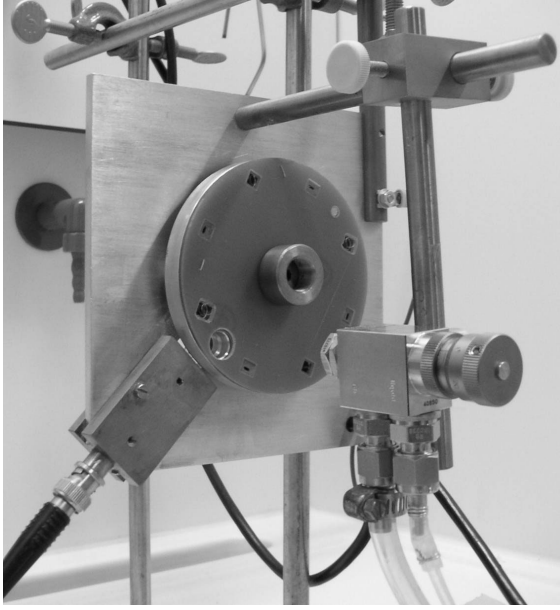


**Figure 3.9.:**

Photograph image of the semi-automatic deposition system: the spraying nozzle (right) mounted in front of the rotating disk (middle) functioning as sample holder and additionally equipped with a shadow mask. The QMB holder with the connection to the frequency counter is seen on the left.

The exchangeable disk holds up to eleven samples and can be additionally equipped as shown with a shadow mask for samples other than for the KP experiments. In this set-up the QMB thickness monitor is positioned in line with the nozzle behind the disks and is reached by the air stream of the propellant through an opening in the disks.

The frequency shift  $\Delta f$  of the QMB witness is according to Sauerbrey's equation proportional to the additional mass load on the crystal and indirectly to the thickness of the deposited layer [157].

$$\Delta f = -\frac{f_q^2}{N \rho_q A_q} \cdot M_p \quad (3.7)$$

The frequency shift  $\Delta f$  due to the mass load  $M_p$  can be calculated according to equation 3.7 using the base frequency  $f_q$ , density  $\rho$ , area  $A$  (indices  $q$  for quartz and  $p$  for polymer) and a constant  $N$  for the given crystal (for the specific type of crystal and cut direction used here  $N$  equals 1668 kHz mm).

Using

$$M_q = \frac{N \cdot \rho_q \cdot A_q}{f_q} \quad (3.8)$$

equation 3.7 becomes

$$\frac{\Delta f}{f_q} = -\frac{M_p}{M_q} = -\frac{\rho_p \cdot A_p \cdot d_p}{\rho_q \cdot A_q \cdot d_q} \quad (3.9)$$

and using the fact that  $A_p = A_q$  the thickness of the polymer layer can be estimated to  $d_p$

$$d_p = \frac{|\Delta f|}{f_q} \cdot \frac{d_q \cdot \rho_q}{\rho_p}. \quad (3.10)$$

However, this procedure assumes a compact and homogeneous layer composition, requires the knowledge of the density of the produced layers, which can differ from the bulk density for the polymer material given by the manufacturer, and is only valid for thin, inelastic layers without lateral stress.

#### 3.3.1. Characterization of the Deposition System

The semi-automatic deposition system was designed and build for the preparation of the polymer layers described in this work. It proved to be superior to the old manual system in terms of comfort and sample throughput. The manual coating system was therefore used only initially for the preparation of the sensitive layers. The disadvantage of the new system is mainly the much higher consumption of organic solvents in the range of 100 ml/h. This makes the system not suitable for expensive materials and environmentally problematic chemicals. However, no negative changes in the quality of the layers using the semi-automatic device were observable compared to the established one.

The first time use made a detailed testing necessary to find the optimal settings before the coating of the actual sensitive layers was attempted. Adjustable spraying parameters are the flux of the polymer solution (on a scale from 1 – 10), the spraying pressure (0.3 – 2 bar), the position of the air cap at the nozzle opening (on a scale from 1 – 10), sample-nozzle distance—all influencing coating rate, particle size, formation of large airborne particles, uniformity of the layer, and thus the quality of the polymer layer. The sample-nozzle distance (6 cm), nozzle air cap position (2) and liquid phase flux (3) were kept fixed after the optimisation process. The influence of the pressure of the carrier gas was studied as well as of the concentration of the spraying solution and the used solvent (or solvent mixture) for each individual polymer.

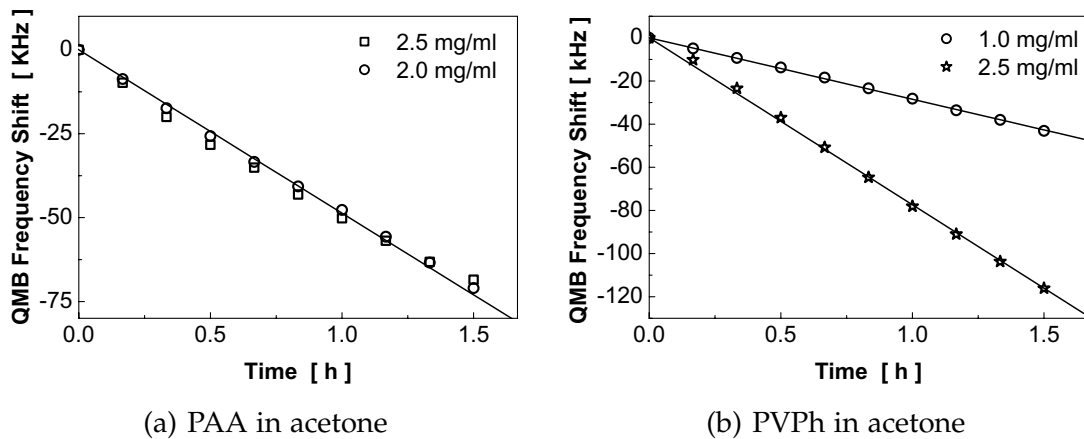


**Figure 3.10.:** Example results for the frequency shift of the QMB witness as a function of spraying time for two examples (1 bar, flux 3, air cap 2, distance 6 cm).

Pre-tests were made to determine the consumption of the spraying solution and—more important—the amount of deposited polymer per hour and were focused on linearity, repeatability, and reliability of the set-up. This tests are illustrated in figure 3.10 on hand of two examples for PAA and PVPh. The frequency shift of the QMB witness during the coating process is plotted versus the time for different concentrations of the polymers.

The frequency decrease (proportional to the amount of deposited material) is very linear in time and the slope is in the range of 20 – 100 kHz/h depending on polymer, concentration, and solvent for a fixed set of the other parameters listed above. After some testing it became obvious that the spraying time is a not sufficient parameter for exact repeatability due to variations in the consumption and, subsequently, coating rate for the same concentration of the polymer solution. Therefore, the thickness monitor had to be used in every coating run. In some rare cases the nozzle was blocked by the polymer which is only detectable with the QMB witness. Thus, the use of a QMB witness is not only convenient, but it also makes the deposition more reliable.

The overview in table 3.2 gives an idea of the achievable coating rates expressed in kHz/h and  $\mu\text{m}/\text{h}$  for the polymers (both linearly scaled if necessary to a concentration of 1 mg/ml). There are some fluctuations around the straight line, which are also visible in figure 3.11(d). The relative error for the deposition rate is around 5% for a single coating process. The growth rate was calculated using the data from table 3.3 in the next section.

**Table 3.2.:** Polymer deposition rates for the semi-automatic deposition system.

Polymer	Deposition rate [ kHz/h ]	Growth rate [ $\mu\text{m/h}$ ]
PAA	17	0.3
PS	27	0.6
PVPh	31	-
PAB	17	0.1

However, one should not forget the larger deviations due to the spread in the consumption of spraying liquid of the device.

The comparison of achieved frequency shifts of QMB sensors placed at the position of the KP substrates and of the QMB thickness monitor during a deposition run gave a relation to the manual method. The frequency shift of the QMB witness is 3 to 4 times lower than that of the QMB positioned on the sample holder disk. This factor can be used to compare the old and new samples. All old samples were converted to the new system (divided by 3) and the frequencies are marked with an asterisk.

#### 3.3.2. Determination of Polymer Layer Thickness

In general, calculating the layer thickness from the frequency shift of a QMB sensor using equation 3.10 can give only an estimate of the layer thickness, if the made assumptions are not fully fulfilled. Therefore, the achieved layer thickness is always to be determined with a profiler after the deposition process. In our case a calibration step is necessary for a second reason, as the deposition system allows only the on-line monitoring of a witness QMB sensor as a thickness monitor and process indicator, which is positioned at a different position (distance) from the nozzle opening as the sample.

However, by measuring with the profilometer the layer thickness of a test set for each polymer, consisting of three to four samples of different degrees of thickness in the desired range, a conversion factor from frequency shift of the QMB witness to layer thickness of the actual sample can be estimated. The determined conversion factors can be then used for calculating the layer thickness of all future samples, if the geometrical and deposition parameters are kept constant. This simple method gives the layer thickness with sufficient confidence. The eventual effect of the concentration of the spraying solution on the conversion factor due to a different density of the layers is neglected.

In the cases when the determination of the conversion factor is not possi-

ble or data is not available, for example due to a different solvent as used in the calibration, the witness QMB frequency shift during deposition is given as the “thickness” of the layer.

The whole procedure assumes a layer growth that is leading to uniform, compact, and homogeneous layers. If this precondition is not fulfilled like for PVPh and PCPhS the layer thickness is not linearly dependent on the deposited amount of polymer. The deviations for those polymers are clearly the result of the layer structure described later in this work.

The factor for the calculation of the layer thickness from the frequency shift of the QMB witness is given in table 3.3 for all the polymers under study. For PAA, PS, and PAB layers a linear relationship was found with small deviations allowing to determine the layer thickness with sufficient accuracy. The relative error for the linear model is around 10% as deviations from the straight line (see figure 3.11(d)). PCPhS is omitted from the beginning as this polymer forms no closed layer and no attempts were made to estimate the conversion factor.

**Table 3.3.:** Conversion factors for calculating the layer thickness from the frequency shift of the QMB thickness monitor.

Polymer	Conv. Factor [ nm/kHz ]	Linearity
PAA	16	good
PS	24	good
PVPh	-	poor
PAB	8	very good

The determination of the conversion factor is demonstrated for PAA in more detail in the following and for all other polymers a similar procedure was applied. The deposition times were 1.5 to 0.5 h, and 2 to 1 h for PAB. The spraying parameters are 2 (nozzle air cap) and 3 (flux), distance 6 cm, and pressure 1 bar. The used concentrations are 2.5 mg/ml for PAA and PVPh and 1 mg/ml for the other polymers.

The achieved frequency shifts of the QMB witness in this time with the given parameters are 70 kHz for PAA, 40 kHz for PS, 115 kHz for PVPh and only 33 kHz for PAB. The achieved thickness of the individual layers in 2 to 1.5 h were 0.3 – 3  $\mu\text{m}$  and meaning that the deposition rates are very different, especially the PAB layers were very thin and deposition very slow.

The layer thickness was determined by the stylus profiler after scratching the layer down to the substrate with a sharp tool. This may cause artificial peaks near the scratch, which were not considered in the evaluation of the

### 3. Experimental Details

profiler data. Figures 3.11(a) to 3.11(c) show the profiler scans for three PAA layers of increasing thickness and the resulting calibration curve allowing to extract the conversion factor as the slope of a fitted straight line.

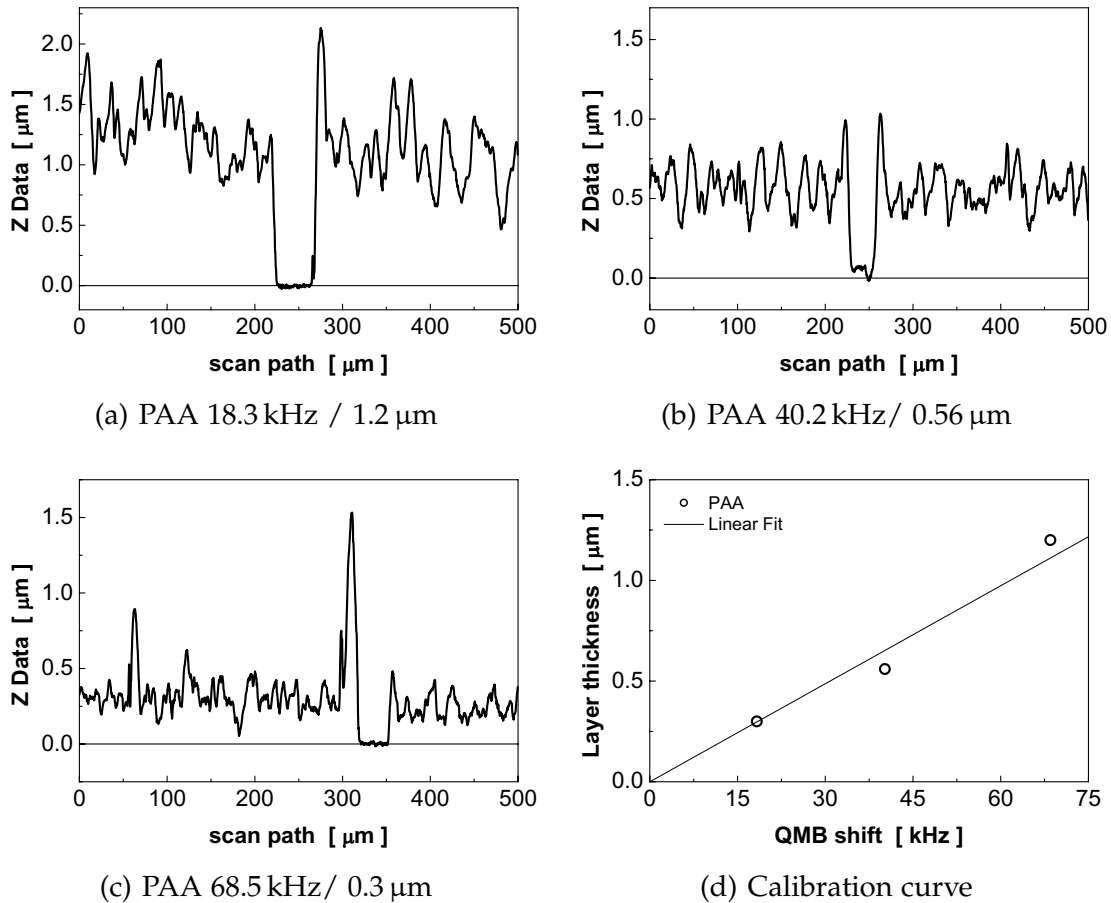


**Figure 3.11.:** Determination of the conversion factor of QMB frequency shift to layer thickness for PAA: layer profiles for different samples of increasing thickness and resulting calibration curve for calculation the conversion factor from the frequency shift of the QMB witness to the polymer layer thickness of the actual sample.

## 3.4. Measurement Procedure

### 3.4.1. KP Sample Positioning

A height adjustment of the KP sample is necessary each time the sample is changed. To get the optimal position of the sample the Kelvin electronics was put in manual mode and the raw signal amplitude displayed on the oscilloscope was maximized by bringing the sample closer to the KP electrode as long as a stable operation was ensured. The resulting air gap was

estimated to be smaller than 0.5 mm. Then the amplitude was manually minimized via the offset control. For the measurements the KP electronics was switched back to the automatic mode.

### 3.4.2. Measurement Protocol

A typical gas measurement protocol consists of several pulses of the target analyte alternating with pure carrier gas (zero air) to allow the sensor to recover. Prior to the first gas pulses the system was purged for typically four hours to equilibrate the system. Analyte pulses were mostly 30 min long followed by 120 min of cleaning with carrier gas. Before the analyte pulse the humidity level was adjusted for 120 min. The total gas flow through the system is a constant 200 ml/min.

The conditions and concentration ranges were chosen according to the requirements of possible applications. Measurements were conducted usually in dry air and also at 50% rh (only some older measurements were taken at 40% rh) to include the conditions of ambient air. The concentration range of interest for ammonia is 1 to 10 ppm, but measurements at lower and higher concentrations were conducted to characterize the sensitive layers in a broader range in order to be confident about the obtained results.

The concentration range fits to be in the limits given by the legal regulations in the countries worldwide. The values given therein are in the range from 25 to 50 ppm for ammonia. Toluene and ethanol were dosed lower than the stated values of 500 – 1000 ppm for ethanol and 50 – 200 ppm for toluene. The measurement temperature was kept constant at 30 °C. The humidity level mentioned in the experiments is given in terms of the ambient temperature of the laboratory (approximately 24 °C) as the vaporizer for humidifying the carrier gas is surrounded by ambient air.

### 3.4.3. Signal Processing and Feature Extraction

The signal was calculated by subtracting the reading of the KP electronics at the end of the analyte pulse from the value of the baseline. For this purpose a manual baseline correction was made. The baseline correction proved to be difficult in some cases, as there was not always full recovery of baseline, even after the long purging time. For convenience the resulting KP signal is always plotted positive regardless of the sign and so is the QMB frequency shift, even if it is always a decrease of frequency. In this work the signal strength for 10 ppm ammonia and the sensitivity in the KP experiment is reported for the polymers as features of interest.

The sensitivity is defined as the slope of calibration curve (signal versus concentration). In the case of a logarithmic dependency of the KP signal with concentration the sensitivity can be also calculated as the difference of the KP signal at a given concentration or partial pressure of the analyte to the signal at ten times this concentration. This sensitivity is then the change of the signal per decade of concentration change.

In an old set-up the KP recordings are superimposed by a relatively high degree of noise. No smoothening of the signal was carried out.

#### 3.4.4. Determination of Time Constants

For calculating the time constants an exponential model for response and decay were assumed. The response peak of the sensor was fitted using the built-in function “ExpDecay1” of the scientific software package Origin 7 by OriginLab. This function can be used using the constrain  $y_0 = -A_1$  for the onset of the signal resulting in

$$y(x) = A_1 \left[ 1 - e^{-\frac{x-x_0}{\tau_{on}}} \right] \quad (3.11)$$

and without the constrain in its original form for recovery

$$y(x) = y_0 + A_1 e^{-\frac{x-x_0}{\tau_{off}}} \quad (3.12)$$

The software implemented data markers were used to limit the fit range to the required data range.



## 4. Sensitive Layer Morphology: Characterisation and Optimization

A high substrate coverage and a smooth, homogeneous surface, especially without high spikes, are desired features and even required for the envisioned future application of the tested polymer layers in the actual sensor devices for the following reasons:

- Full coverage of the gold substrate leads to genuine sensor signals without any possibly disturbing direct interaction of the gold substrate and the analyte molecules. This undefined interaction of the target analyte or other present chemical compounds like water may be sources of unwanted noise and drift causing irreproducibility of the measurement results.
- A smooth surface minimizes the risks of (electrical) contact between the polymer layer and the gate. A  $R_p$  value smaller than approximately  $1\ \mu\text{m}$  is required for the use in field effect transistors (FET) with a suspended gate (see section 2.5.2 and figure 2.8(b)). The exact value is depending on the real geometry of the device. Large particles on the surface are surely fatal and must be avoided.

Therefore, measurements have been made to find qualitative and quantitative measures to describe the morphology of the polymer films, principally the substrate coverage, layer homogeneity, and surface roughness. Additionally, the influence of shadow masks was tested if they are eventually the cause for walls or areas of poor coverage at the edges of the coated area. This aspect is only presented very shortly here in one simple example, as this work is focused on the gas tests with the Kelvin probe (KP), where the shape and the homogeneity of the edges are of minor interest. To avoid an influence of the substrate structure in order to see the intrinsic properties of the polymer the silicon wafer based substrates were used for those investigations, and the results are compared in single instances with samples on the alumina substrate.

Optimal coating parameters are given as the result of the deposition tests for the individual polymers. The concentration of the spraying solution and the nature of the solvent are influential factors on the surface properties of the layer. The other variable parameters (liquid phase flux, nozzle air cap position, distance, and spaying pressure, see section 3.3) were kept fixed for

all later coating processes or were varied only in a limited range after an initial testing phase to reduce the dimensionality of the search.

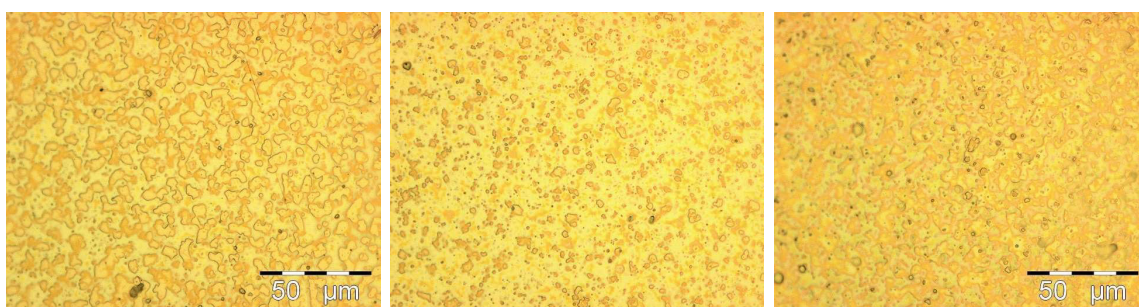
#### 4.1. Polyacrylic Acid Layers

Polyacrylic acid (PAA) polymer layers were investigated most thoroughly as this polymer proved to be most sensitive to the target analyte ammonia in the KP experiments and is from this point of view the most promising candidate.

In the following the results of the atomic force microscope (AFM), scanning electron microscope (SEM), optical microscope (OM), and surface profiler measurements are presented for layers of different thickness and layers prepared using different deposition parameters and the findings are discussed on hand of those representative examples.

##### 4.1.1. General Surface Properties and Influence of Deposition Parameters

The obtained results, when changing the concentration of the spraying solution, for PAA layers are presented in the this section. Spraying solutions of the polymer dissolved in acetone in the concentration range of 1 to 6 mg/ml were used for coating the substrates. Generally, a higher concentration of the spraying solution is desired as the coating time and consumption of solvent is reduced by nearly the same factor as the concentration is increased, but rapid coating may have in some cases a negative influence on the layer quality as described later.



(a) PAA 10 kHz\* / 160 nm    (b) PAA 20 kHz\* / 320 nm    (c) PAA 30 kHz\* / 480 nm

**Figure 4.1.:** OM (magnification 500x) images of PAA spray coated layers (1 mg/ml) of increasing thickness on Au/Si substrates.

Starting with a concentration of 1 mg/ml polymer the most representative OM images of the produced layers are shown in figure 4.1 for layers

of 10 – 30 kHz\* in thickness prepared using the manual deposition system. The calculated thickness using equation 3.10 is 150 – 460 nm, which is in good agreement with using the calibration data obtained for the new deposition system in table 3.3: 160 – 480 nm. From this one can infer that both deposition systems produce layers of the same consistency for PAA.

The reproduced area was always chosen to be in the middle of the coated area, even if the layers are quite uniform from the middle to the edges. At 10 kHz\*/160 nm the layer is not fully closed, as the substrate remains visible in parts, but seems to be totally closed at 30 kHz\*/480 nm with still a pertinent, noticeable surface structure. A perfectly even surface was never obtained with this polymer: very few larger particles and some impact holes of airborne particles (diameter 2  $\mu\text{m}$ ) are always present on the surface, as well as areas of lower layer thickness.

When one wants to increase the concentration of PAA in acetone the maximum is reached at about 6 mg/ml. The results for this concentration are presented in figure 4.2 in contrast to the layers in figure 4.1.

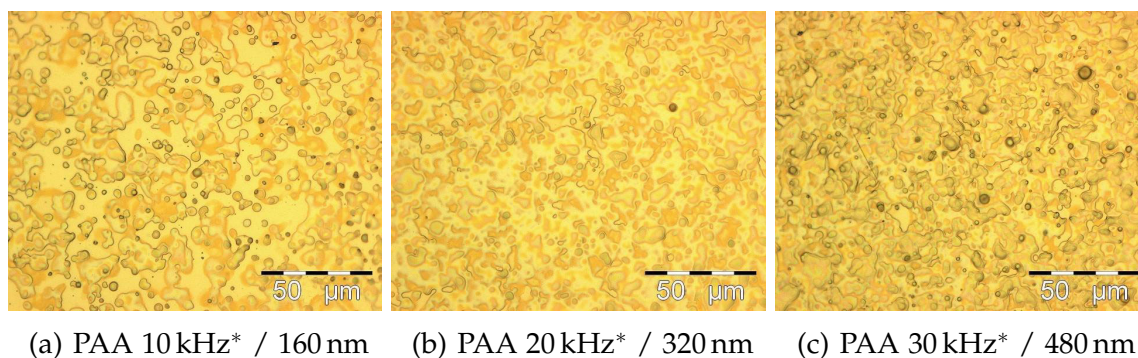


**Figure 4.2.:** OM (magnification 500x) images of PAA spray coated layers (6 mg/ml) of increasing thickness on Au/Si substrates.

The layer is deteriorated clearly in respect of number of larger particles and holes due to the impact of droplets or particles. As a result of this a concentration at the lower end of the tested range is preferred for the later gas sensitive samples. As a trade off between time and quality a concentration of 2 mg/ml was therefore used for the actual KP substrates with the exception of one sample.

In figure 4.3 the OM images of two layers for the Kelvin probe measurements on the same substrate (Au/Si) are shown for a thickness of 71 and 23 kHz, respectively. These layers were prepared with the semi-automatic system. A comparison of 4.1(b) and 4.3(a) reveals no apparent differences for the two layers ( $\approx$  20 kHz) and both deposition systems deliver layers of similar quality concluded from the OM images.

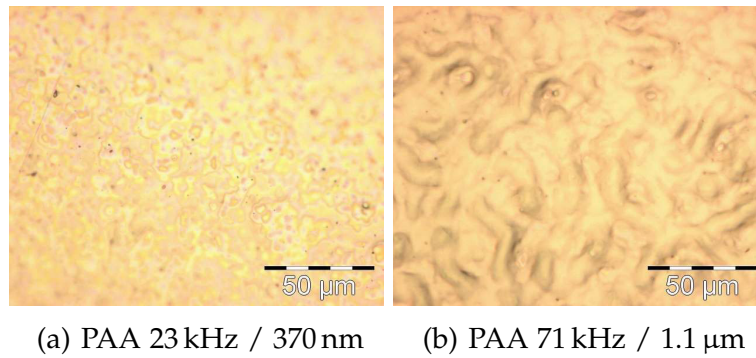


**Figure 4.3.:** OM (magnification 500x) images of PAA spray coated Kelvin probe samples (see table 5.1).

When the thickness is increased more than for the previous examples the layer is totally covering the substrate forming walls (see 4.3(b)) with a width of 10 µm. It seems that the substrate has now no influence on the layer properties any more, as a comparison with layers on the Au/Al<sub>2</sub>O<sub>3</sub> substrate shows a comparable structure. Kelvin Probe measurements of exact those two PAA samples will be presented in a later section.

#### 4.1.2. Substrate Coverage and Layer Homogeneity

The degree of substrate coverage and layer homogeneity can be better estimated in the SEM images than in the OM images due to the higher polymer–substrate contrast given by this method. Only very thin layers of polymer might be not distinguishable from uncoated regions as both appear nearly as bright also in this technique.

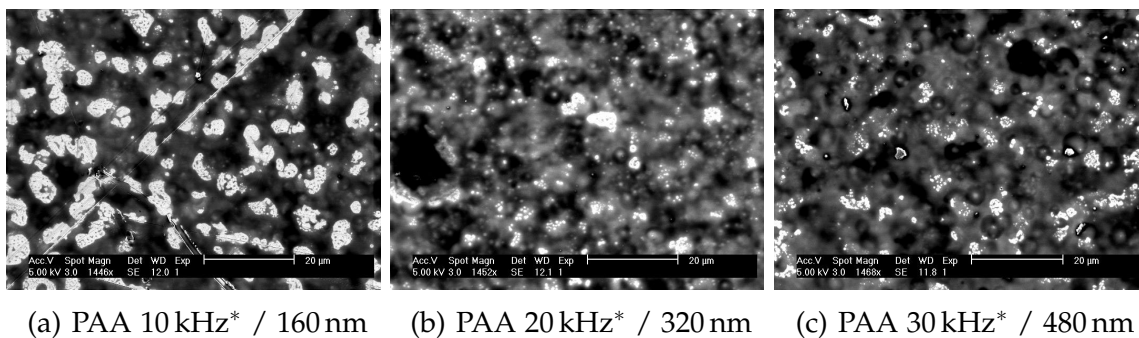


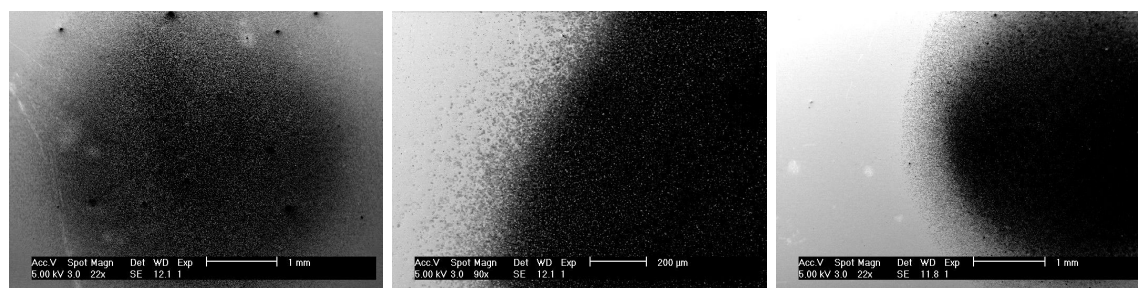
**Figure 4.4.:** SEM (magnification 1500x) images of PAA spray coated layers (1 mg/ml) of increasing thickness on Au/Si substrates.

SEM images are presented for the same layers as in the previous section. Images of centre regions of the layer are shown in figure 4.4 under high

magnification and of the layer edges in figure 4.5 under low magnification. In the first and thinnest layer the gold substrate is still dominant the polymer covering only half of the area, but the polymer is covering completely the substrate at 30 kHz as a confirmation of the OM measurements.

The remaining spots in the 30 kHz\* layer are of much lower brightness than before indicating at least a thin polymer coverage. The complete coverage of the substrate is supported by the AFM and the surface profiler runs as the tip and stylus were never touching down to the substrate.

The coverage and homogeneity on a larger scale can be judged in figures 4.5 as well as the effect of simple shadow mask on the homogeneity and coverage at the edges of the layers. A boundary region of approximately 0.4 mm remains and is not optimal covered by the polymer using the masks available at that time.



(a) PAA 10 kHz\* / 160 nm    (b) PAA 20 kHz\* / 320 nm    (c) PAA 30 kHz\* / 480 nm

**Figure 4.5.:** SEM (magnifications 22x and 90x) images of PAA spray coated layers (1 mg/ml) of increasing thickness on Au/Si substrates, effect of shadow masks.

This aspect is not further reported here because it is only of interest later in the final application of the polymer layers and out of the focus of this work. It will be only mentioned here that low pressure and even much lower concentration of the spraying solution proved to be helpful to minimize the height of walls at the edges of the coated area, which are in some cases present.

The task of optimisation when using shadow masks appears to be a purely technical issue, whereas the polymer layer properties are intrinsic in the material and can be influenced only in a limited range by choosing the most suitable deposition method or set of parameters. Therefore, the surface properties must be considered in the choice of prospective candidates.



4.1.3. Surface Roughness

The next and for the later use most important aspect of investigation is the surface roughness. The evaluations of AFM and surface profiler measurements give a quantitative measure for the surface profile.

AFM images of PAA samples with increasing thickness are depicted in figure 4.6. The samples were prepared identically as the ones presented before in figure 4.1 with a solution of a concentration of 1 mg/ml in acetone. In the 10 kHz\* layer (thickness 160 nm) the AFM tip reaches nearly down to the substrate.

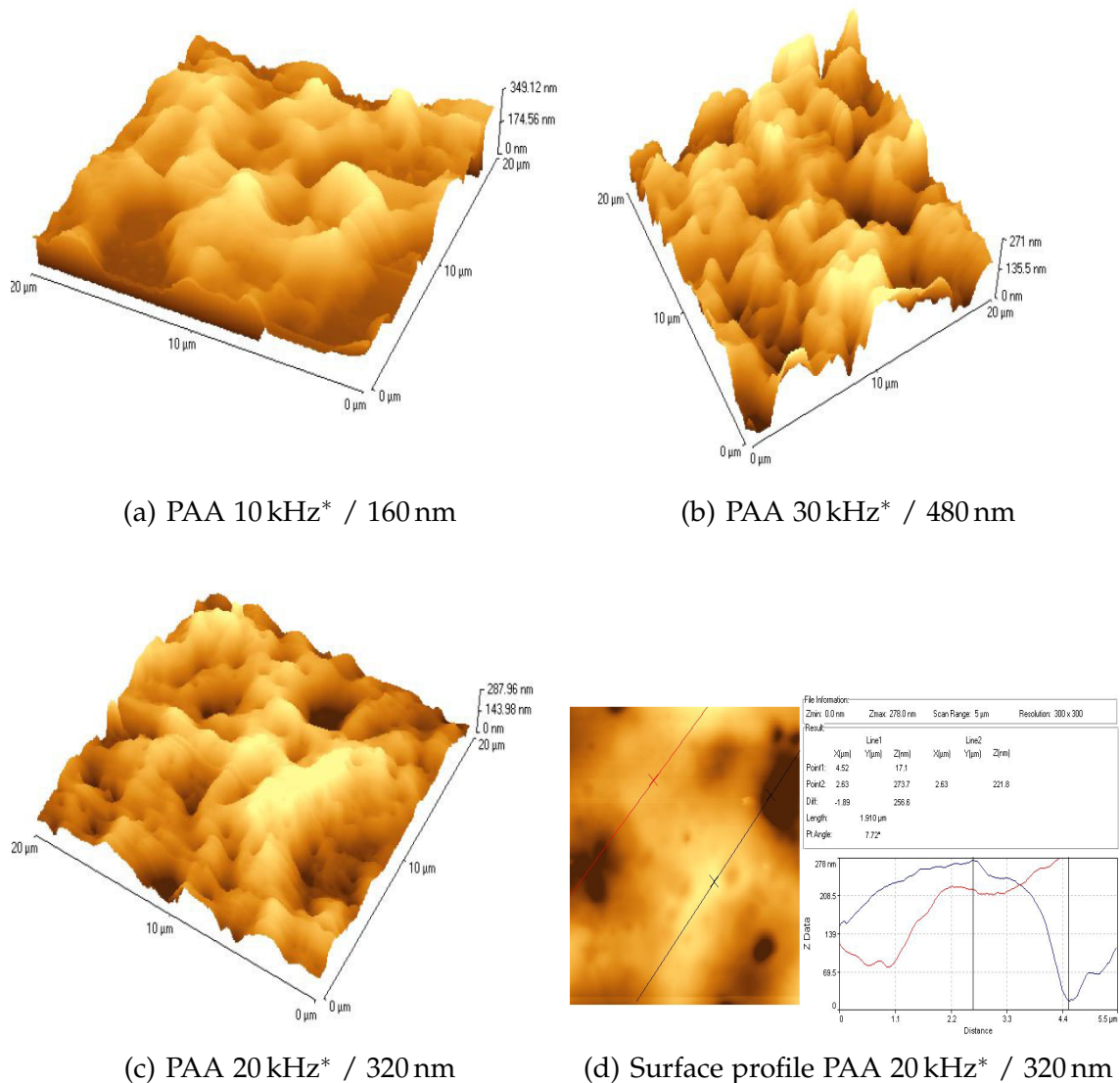


Figure 4.6.: AFM images and an example surface profile of PAA spay coated layers (1 mg/ml) on Au/Si substrates.

The data for the 30 kHz\* (480 nm) layer indicates a fully closed layer as the

roughness is lower than 300 nm. The maximum peak-to-valley roughness for the 20 kHz (320 nm) layer is around 250 nm indicating that the coverage is near completeness as the tip never reaches totally down to the substrate.

This result must be compared to stylus profiler measurements on a second set of samples of comparable and larger thickness prepared in the new semi-automatic system. The coating times were chosen to be 30 – 90 min, the concentration of the spraying solution was 2.5 mg/ml, and the pressure was 1 bar. The obtained witness QMB frequency shifts are 18, 40, and 69 kHz, equivalent to a layer thickness of 0.3 – 1.2  $\mu\text{m}$ . The optical inspection by OM showed again no difference to the samples prepared by the old system. The evaluation of the surface profiles taken with the stylus profiler over a longer distance than possible with the AFM yielded the data for the individual roughness parameters as listed in table 4.1.

**Table 4.1.:** Roughness parameters for PAA samples prepared in deposition times of 30 – 90 min (values in units of  $\mu\text{m}$ ).

	90 min	60 min	30 min
$R_a$	1.2	0.56	0.3
$R_q$	0.24	0.12	0.11
$R_v$	0.5	0.3	0.2
$R_p$	0.6	0.3	0.6
$R_t$	1.1	0.6	0.8

In the OM images and in the profiler data the surface of the PAA layers is relatively smooth without high spikes. The average roughness  $R_q$  is low but it is increasing with preparation time and thickness. Also the height of the peaks and the depth of the valleys are showing a trend to increase, but are in the set limits of 1  $\mu\text{m}$ . These layers are slightly rougher as the ones presented before with the AFM data.

Thinner PAA layers have a peak-to-valley roughness in the range of the Au/Al<sub>2</sub>O<sub>3</sub> substrate (compare with figure 3.7 and the calculated  $R_t$  roughness of 550 nm) and thicker layers have larger roughness but the parameters remain within the desired limits. Finally one should remember that this method as well fails to detect single large particles on the layer. Luckily this is not so much an issue for PAA according to the OM images.

#### 4.1.4. Effect of Ageing

Next to the influence of long storage times on the sensing properties the change in the physical surface properties of a sample was examined after

#### 4. Sensitive Layer Morphology: Characterisation and Optimization

storage under clean room conditions (at constant humidity and temperature) for about twenty months. The PAA spray coated layer has altered during this time, which can be clearly seen in the OM images in figure 4.7 on hand of a PAA sample on the silicon substrate. The layer appears now to be coloured as the result of interference effects indicating very homogeneous and compact layers (see image (a)). The surface has smoothed out, however, the layer has now numerous polymer free patches of  $150\ \mu\text{m}$  in diameter surrounded by walls (see image (b)).

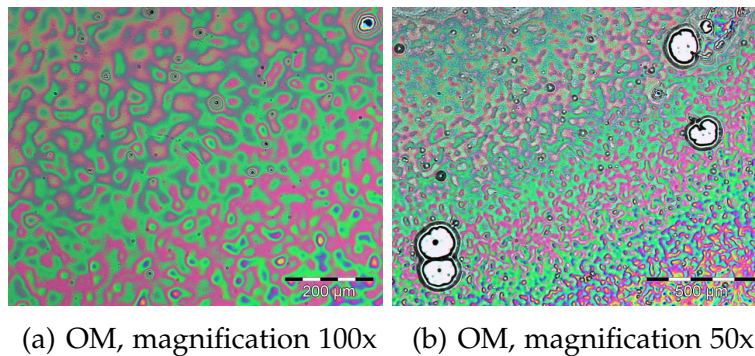


**Figure 4.7.:** Effect of ageing after twenty months of storage time on a PAA spray coated layer visible in the OM images of the aged layers.

The ageing becomes more clear by the comparison of the new surface profiles in figures 4.8(a) and 4.8(b) with the initial surface profile in figure 3.11(c) and the roughness data in table 4.1 with the data given here.

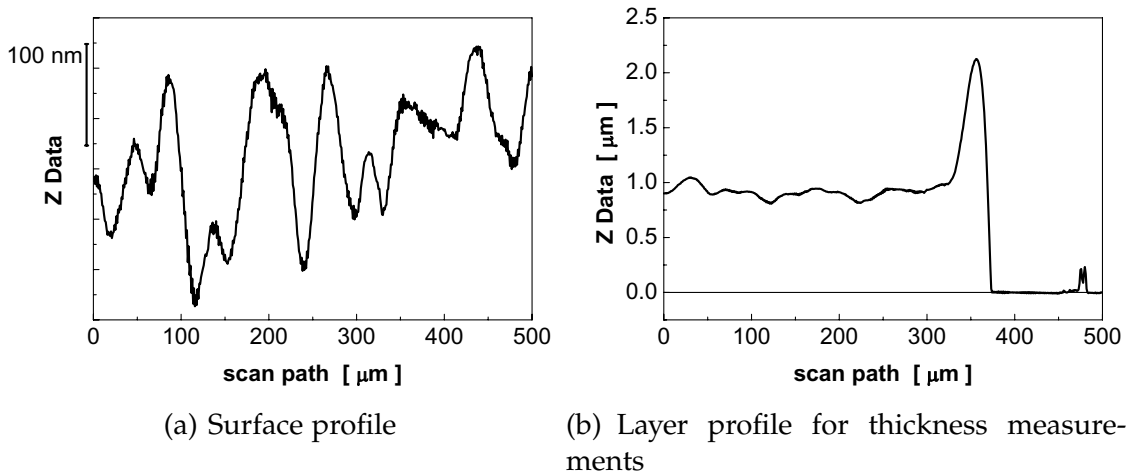


**Figure 4.8.:** Effect of ageing after twenty months of storage time on a PAA spray coated layer: surface profiler scans.

The calculated values for the roughness parameters of the aged layers are



60 nm for  $R_q$ , 150 nm for  $R_v$ , 100 nm for  $R_p$ , and 260 nm for  $R_t$ . This is a clear decrease to a quarter of the initial values, but the overall average layer height remains unchanged.

KP samples on substrates with a gold layer showed the same ageing behaviour, thus it can be excluded that this is caused by the silicon surface. Presumably the ageing process is accelerated by humidity, as the used PAA is not cross-linked and therefore very soluble in water. A pre-ageing in saturated atmosphere and under defined conditions as it was used by [158] could be used as a tool create more ideal layers and could minimize ageing effects if required.

## 4.2. Polystyrene Layers

### 4.2.1. General Surface Properties and Influence of the Deposition Parameters

The second extensively examined polymer is PS and a similar procedure was applied as before for PAA, but in contrast to the above only the OM images are presented. The concentration of polystyrene in dichloromethane (DCM) was varied in a range of 1 – 10 mg/ml.

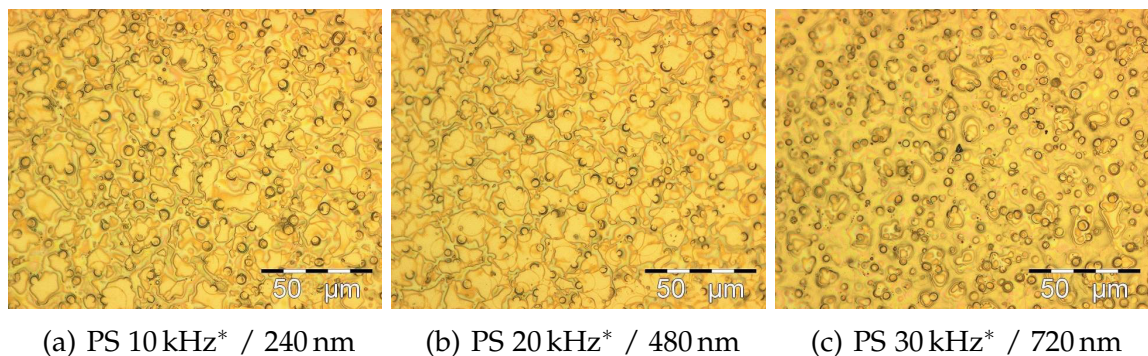


**Figure 4.9.:** OM (magnification 500x) images of PS spray coated layers (1 mg/ml in DCM) of increasing thickness on Au/Si substrates.

First, the results for the lowest concentration of 1 mg/ml are illustrated in figure 4.9 for layers of 10 – 30 kHz\* in thickness. This correspond to a thickness using the calibration data in table 3.3 of 240 – 720 nm. The density of the sprayed layers must be lower than the value for polystyrene (PS) material given by the manufacturer as equation 3.10 yields a much lower result.

In the images of the layers one can see knobs on the layer due to the impact of large particles (diameter around 2 μm) scattered densely on the

#### 4. Sensitive Layer Morphology: Characterisation and Optimization

surface. Additionally, large particles are sometimes present on the surface especially after long deposition times. Coverage seems to be complete already at 10 kHz (thickness 240 nm) in contrast to the PAA case before. The size of the knobs increases to 5  $\mu\text{m}$  the number being constant, when a higher concentrations is used. This is demonstrated with the next images of layers of the same thickness but prepared using a concentration of 10 mg/ml (figure 4.10). The surface is clearly less ideal, even when one considers the large domains of a relatively smooth surface. Thus, a low concentration is unavoidable if one wishes to obtain very smooth and homogeneous surfaces.

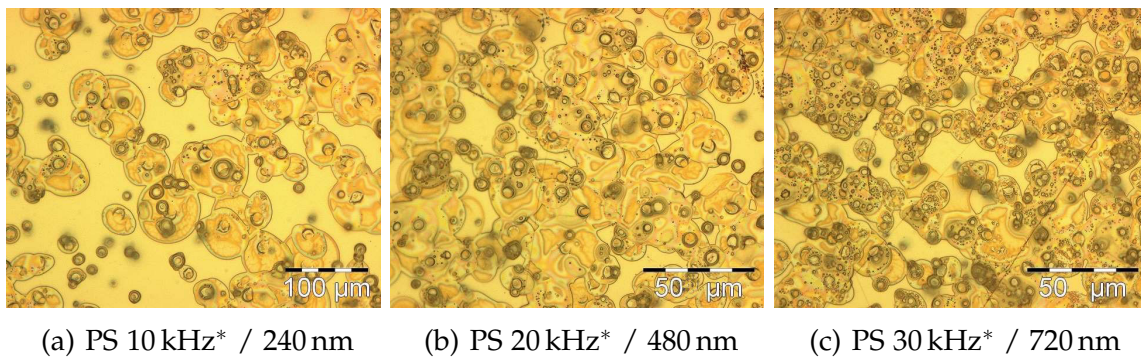


**Figure 4.10.:** OM (magnification 500x) images of PS spray coated layers (10 mg/ml in DCM) of increasing thickness on Au/Si substrates.

Additionally, a set of samples on the Kelvin substrate (Au/Al<sub>2</sub>O<sub>3</sub>) prepared with the semi-automatic system are presented (1 mg/ml in DCM, 1 bar). The images of the different layers are presented in figure 4.11.

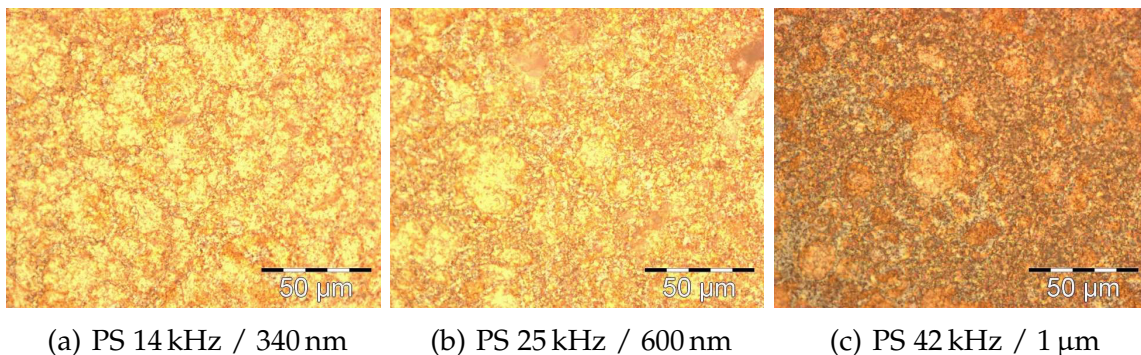


**Figure 4.11.:** OM (magnification 500x) images of PS spray coated layers (1 mg/ml in DCM, 1 bar) of increasing thickness on Au/Al<sub>2</sub>O<sub>3</sub> substrates.

The positive influence of the semi-automatic system is visible in the absence of impact holes and in the lower number of very large particles on the

surface. Compare, for examples, the image 4.11(b) with the images 4.9(b) and 4.9(c). The layer seems more homogeneous as before. There is only some area left, which is less covered indicated by the lighter colour in the images.

#### 4.2.2. Surface Roughness and Effect of Ageing

The coverage of the PS layers was almost complete but the texture of the surface seems to be critical. This time only stylus profiler measurements are presented. AFM seemed to be not appropriate due to the high degree of unevenness of the surface.

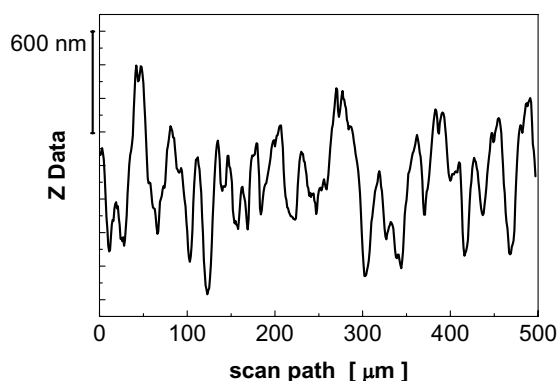


**Figure 4.12.:** Surface profiler scan of a PS spray coated layer of 1  $\mu\text{m}$  thickness.

A profile scan for a PS layer of about 1  $\mu\text{m}$  thickness is given in figure 4.12. The surface is much rougher as a comparable PAA layer and has several cases of a much higher peak-to-valley distance. With increasing layer thickness in the range from 300 nm to 1  $\mu\text{m}$  there is an increase of  $R_q$  from 0.16 to 0.29  $\mu\text{m}$  and there is trend for  $R_v$ ,  $R_p$ , and  $R_t$  to higher numbers.  $R_p$  is in the range of 0.5 – 1  $\mu\text{m}$  just at the limit of 1  $\mu\text{m}$ .

PS layers showed no observable ageing effect on the layer texture after storage time of more than one year under the same conditions as the PAA layers.

#### 4.2.3. Influence of the Solvent on the Surface Properties

To test if it is possible to overcome some of the negative findings of the PS layers, especially the large particles on the surface, other solvents than DCM were used in the coating process. The use of chloroform and a reduced spraying pressure lead to an improvement in the number of the unwanted, large airborne particles, but the layer is not only less homogeneous with deep and steep valleys almost down to the substrate, but also the cover-



age is poorer. The result for a PS layer (deposition of 35 kHz) is shown in figure 4.13. This layer can be compared to the images in figure 4.9(c).

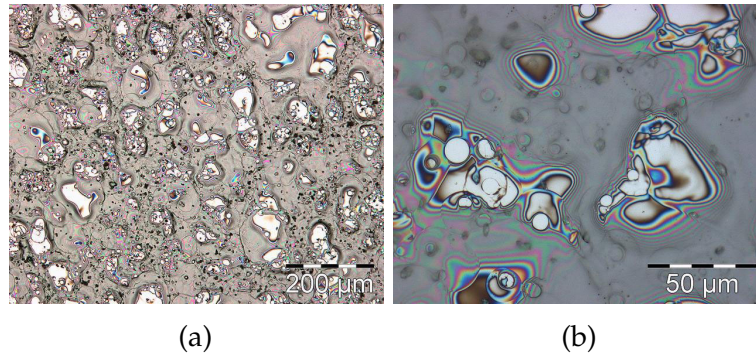


**Figure 4.13.:** OM (magnification 100x and 500x) images of a PS spray coated substrate using a solution of 1 mg/ml PS in chloroform (0.3 bar), deposition of 35 kHz.

If there are any differences in the KP experiments between the sample prepared with DCM or chloroform will be discussed later in the KP section. Tries with tetrachloroethene and mixtures with chloroform gave no improvement in the surface and layer properties.

### 4.3. Poly-(4-vinylphenol) Layers

#### 4.3.1. General Surface Properties and Substrate Coverage

The last three cases of polymer layers are characterised shortly by the results of OM images and profiler scans. The poly(4-vinylphenol) (PVPh) deposition never yielded homogeneous layers nor smooth surfaces for any concentration or for any choice of depositions parameters.

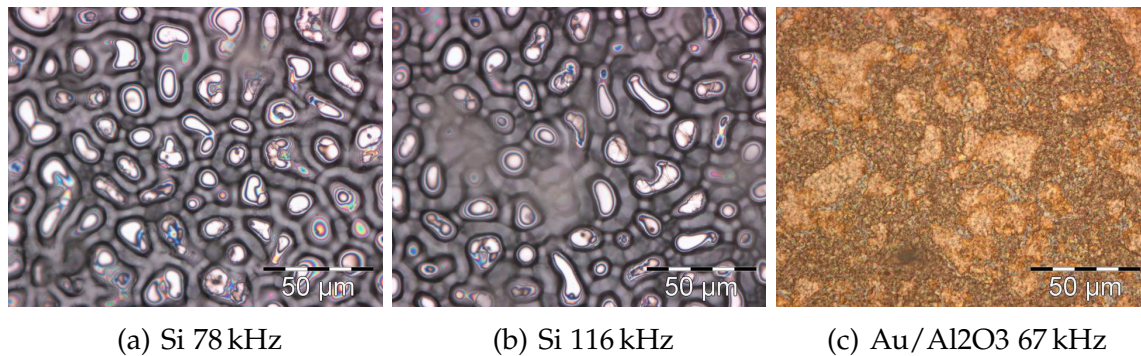


**Figure 4.14.:** OM (magnification 500x) images of PVPh spray coated layers of different thickness on Si and Au/Al<sub>2</sub>O<sub>3</sub> substrates.

Using the new deposition system was not an improvement in terms of layer quality: always a net structure without total coverage of the substrate as demonstrated in the OM images in figure 4.14(a) and figure 4.14(b) for two layers on a Si substrate was observed. The width of the walls is  $10\ \mu\text{m}$ . The samples presented here were prepared using  $2 - 2.5\ \text{mg/ml}$  of polymer in acetone at 1 bar of spraying pressure.

The substrate has in the case of PVPh an influence on the polymer's substrate wetting capabilities and as a result of this on the layer texture. To demonstrate this effect one samples on a Au/Al<sub>2</sub>O<sub>3</sub> substrate is presented in image 4.14(c) in comparison to samples on the Si substrate (4.14(a) and 4.14(b)); the results on a Au/Si substrate are the same as for the Si substrate. The net structure on the alumina based substrate is similar in nature, but broader and leading to a better overall coverage. This gives hope for improvement if modifications of the substrate are possible.

The images are blurry in parts due to larger particles on the surface, which are not in the focus of the OM any more. This problem of very large particles on the layer make this polymer hardly usable in the field effect transistor (FET) devices.

#### 4.3.2. Surface Roughness and Effect of Ageing

As already seen in the OM images the substrate is never totally covered and the stylus of the profilometer reaches down in the valleys to the substrate level even for layers of a thickness of several micrometers. This can be seen in the profile in figure 4.15(b) for the thickest prepared layer of a thickness of 116 kHz.

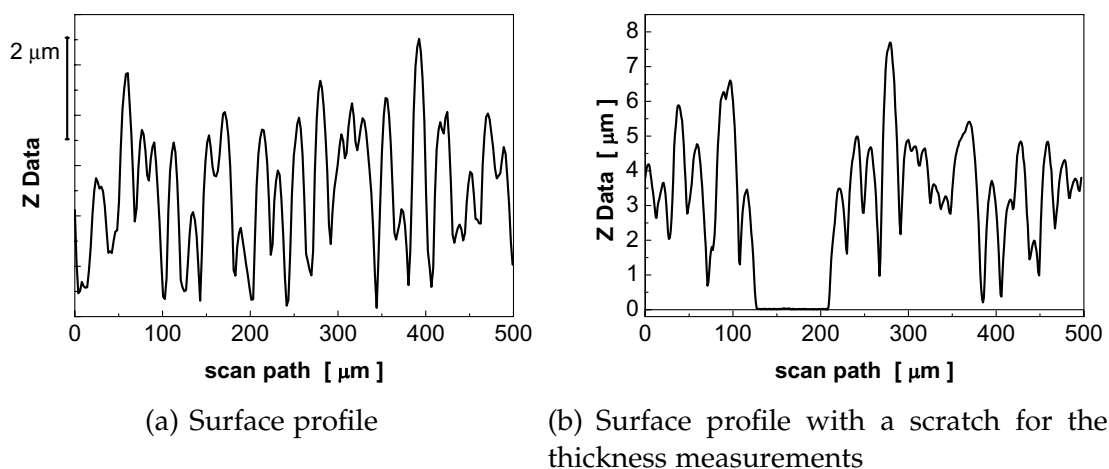


**Figure 4.15.:** Surface profiler scans of a PVPh spray coated layer (116 kHz).

The surface has a high roughness with peaks extending several micrometers from the surface. The thickest layer under investigation (thickness  $\approx 3 \mu\text{m}$ ) has a  $R_q$  roughness of  $1.2 \mu\text{m}$  and the values  $2.3 \mu\text{m}$  for  $R_v$ ,  $3.0 \mu\text{m}$  for  $R_p$ , and  $5.3 \mu\text{m}$  for  $R_t$ . This is clearly out of the given limits. The thinner layers have a lower roughness, but the coverage is unacceptably poor.

PVPh layers do not show any changes due to ageing after twenty months determined by optical inspection.

#### 4.4. Poly-(acrylonitrile-co-butadiene) Layers

A poly(acrylonitrile-co-butadiene) (PAB) layer has a very smooth surface as shown in figure 4.16(a) and covers the substrate completely in a similar way like the commonly used polymer polydimethylsiloxane (PDMS). PAB layers are very soft as the path of the stylus can be followed for short time on the layer surface after the profiler measurements. In the image of the layer (figure 4.16(b)) a few round spots (size  $10 \mu\text{m}$ ) are visible which are most probably the result of impacts of particles. The layer is coloured (the polymer PAB itself is not coloured) as a result of interference effects.

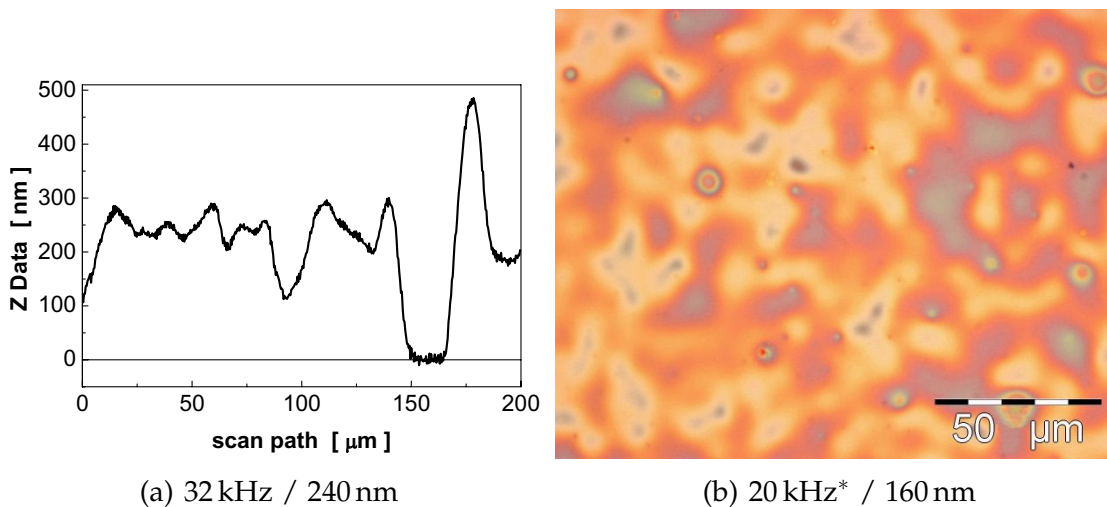


**Figure 4.16.:** Layer profile and OM (magnification 500x) image of two PAB spray coated layers (1 mg/ml) on Au/Si substrates.

The roughness is the lowest of the investigated polymers in this work, which becomes clear when looking at the calculated values for the profile above (excluding the gap):  $40 \text{ nm}$  for  $R_q$ ,  $120 \text{ nm}$  for  $R_v$ ,  $70 \text{ nm}$  for  $R_p$ , and  $190 \text{ nm}$  for  $R_t$ . As a consequence no further tests were considered necessary to improve the quality of the layer. It was noticed that a higher concentration did not change the perfect coverage and homogeneity of the

layer. However, degradation is visible over time similar to the PAA layers, but with a higher number of polymer free zones.

#### 4.5. Poly-(cyanopropyl-phenyl-siloxane) Layers

Poly(cyanopropyl-phenyl-siloxane) (PCPhS) is completing the list of polymer layer, which are presented in this work and proved to be sensitive in the KP experiments. The polymer covers the substrate very poorly (figure 4.17). Only less than half of the substrate is covered by polymer bumps (diameter up to 10  $\mu\text{m}$ ) resulting in an archipelagos like structure of small and large islands.

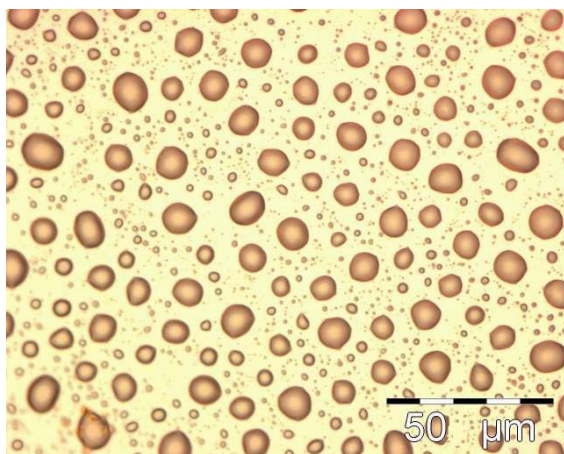


**Figure 4.17.:**  
OM image (magnification 500x) of PCPhS spray coated layer (1 mg/ml, 20 kHz\*) on the Au/Si substrate.

This finding is not unique to this polymer, also polyacrylonitrile and other cyano substituted siloxanes have same structure on gold or silicon. Surface modifications of the substrate, post deposition treatments or variations in the various deposition parameters were not attempted due to the discouraging performance in the KP and quartz micro balance (QMB) experiments.

#### 4.6. Summary

With the semi-automatic deposition system sample sets consisting of several substrates can be easily coated with polymers in the desired thickness and of the necessary quality. However, it is not avoidable, that the optimal deposition parameters must be determined individually for each polymer to yield the best layers in terms of coverage and roughness on the one hand and an efficient coating procedure on the other hand. A low concentration of the spraying solution enhances the homogeneity and minimizes the number of airborne particles on the surface. The new systems seems to

be a further improvement in this point as less airborne large particles are produced. A low spraying pressure (smaller than 1 bar) avoids walls at the edges of the polymer layer when using shadow masks, but additionally increases deposition time.

In the following a concise summary shall be given:

**PAA** PAA layers are generally of good quality with a low degree of surface roughness and a high degree of surface coverage already for low amount of deposited polymer and layers thicker than 400 nm on smooth substrates. As roughness increases with layer thickness the layer should be prepared in the range of 30 – 50 kHz (approximately 0.5 – 0.8  $\mu\text{m}$ ). Some spots on the surface due to airborne particles cannot be avoided. Concentrations of 2 mg/ml or higher are possible allowing rapid coating while maintaining the good layer properties. Long time storages causes visible ageing effects on the layer.

**PS** In the case of PS the concentration should be chosen as low as possible, however, the problems with larger particles on the layer surface is always remaining. Other than that, the coverage is complete from the very beginning and the roughness stays well in the given limit. In this terms it is sufficient to prepare sensitive layers of 15 kHz (approximately 0.35  $\mu\text{m}$ ). No visible ageing of the layer occurs.

**Other** For the remaining polymers one can conclude that in the case of PVPh there is room for improvement by changing the substrate or its surface properties, but the layers are not closed even after long depositions times; the PAB layers need no improvements due to the good intrinsic properties of this polymer, and for PCPhS a tedious optimization is not worth the effort when used in the KP for ammonia sensing due to its somewhat poor performance.



## 5. Response to Analyte Gases

### 5.1. Response of an Inert Reference Material and of the Uncoated Substrates

The Besocke Kelvin probe head is made of a non-replaceable gold grid as previously described. Gold surfaces are known to react with many different adsorbed molecules, among others with ammonia, even after a passivation process through ageing of the surface. For that reason, before measuring the polymer coated substrates with the Kelvin probe (KP) it had to be verified, whether or not an interaction of the analyte molecules and the gold grid is a source of error in the determined contact potential values. For this purpose, the response of a chemically rather inert material (silicon nitride,  $\text{Si}_3\text{N}_4$ ) was tested to estimate the contribution of the KP gold grid, thus one expects contact potential changes only to occur on the gold grid. Silicon nitride is commonly used as reference to eliminate the influence of the Kelvin Probe grid by subtracting the obtained signal from the signal of the actual sample under investigation. The problem of referencing the KP signal is described in [128]. Influential and problematic factors are the measurement history, degree of usage, and the age of the Kelvin Probe gold grid.

Additionally, the reactivity of the used substrates (Au/Si, Au/Al<sub>2</sub>O<sub>3</sub>, Si) was tested under the same conditions as the polymer samples. The response of the bare substrates can give hints to identify the origin of the KP signal for the polymer layers as well. Ammonia was exposed in the usual concentration range up to 10 ppm in dry and humid air (at 50% rh). The gold layers were also tested at higher ammonia concentrations up to 200 ppm.

#### 5.1.1. Results of the KP Experiments

##### 5.1.1.1. Si Substrate and Inert Reference Material

Firstly, the results for a bare silicon wafer and a silicon nitride covered wafer (10 nm LPCVD nitride, kindly provided by Universität der Bundeswehr, Munich) are presented. For both type of samples the response to ammonia is lower than 10 mV, but the water influence is substantial. The raw KP signals are plotted in figure 5.1 for both materials. The change from 0 to

50% rh gives rise to a signal of 20 mV for the silicon wafer and 60 mV for the nitride substrate.

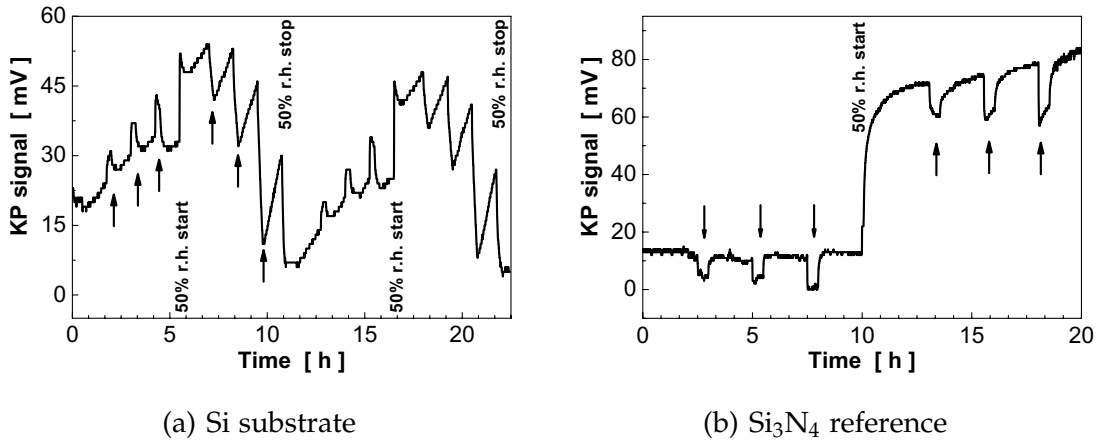


**Figure 5.1.:** Raw KP signals of (a) an uncoated Si substrate and (b) an inert material exposed to incremental concentration pulses of ammonia: 1, 3, and 10 ppm in dry and humid air (50% rh).

If the signal of a measurement with the silicon nitride is considered as the response of the gold grid all signals different from that must be from the actual sample consisting of a polymer layer and the substrate. In the following results on the polymer coated structures the total signal is given, the background determined on the inert material is not subtracted. This means that the data are not directly transferable to another system, which has a different background signal, as the measured KP signal is always the sum of all contributions.

### 5.1.1.2. Au/Si and Au/Al<sub>2</sub>O<sub>3</sub> Substrates

Secondly, gold covered substrates were exposed to ammonia and the KP signal was recorded. Comparing the raw KP recordings for the two types of samples similar in nature—both are gold layers—presented in the graphs in figure 5.2 shows that the response of a bare gold surface to ammonia is not very reproducible. It is sometimes as high as 30 mV (dry air) and 85 mV (at 50% rh) for 10 ppm ammonia, but mostly the signal is much lower in the range of 10 – 20 mV even for 200 ppm (dry air) like in the second example. Changing the humidity to 50% rh does not influence the systems and the KP signal is unchanged (see graph (a) in figure 5.2). The existence of a signal indicates that the processes on the gold surface of the sample and the KP grid do not neutralize each other in terms of the contact potential.

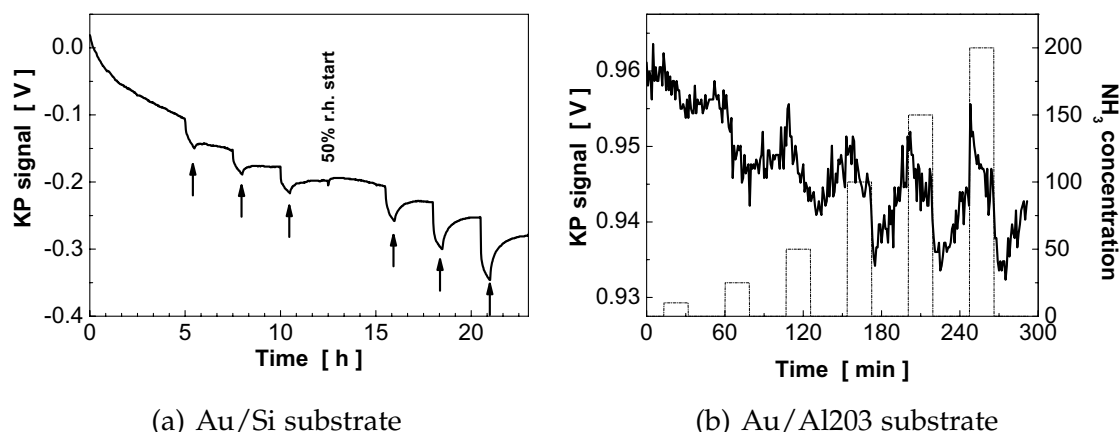


**Figure 5.2.:** Raw KP signal of uncoated substrates (Au/Si, Au/Al<sub>2</sub>O<sub>3</sub>) exposed to incremental concentration pulses of ammonia: (a) 1, 3, and 10 ppm in dry and humid air (50% rh), (b) 1 – 200 ppm in dry air.

The presence of a KP signal at ammonia exposure to the bare gold substrates gives a first hint to a possible origin of the KP signal: the substrate surface itself or the polymer/substrate interface. A detailed discussion follows the presentation of the experimental results. It further raises the question, if one should focus more on the substrate to improve the sensing performance.

### 5.1.2. Results of the IR Experiment on Si Substrates

IR experiments on the Si substrate were carried out for two reasons: it was expected to obtain some data for the explanation for the KP signal and the spectra were used as a reference to calculate absorbance spectra for the polymer coated samples. In the presence of humidity in the carrier gas, the spectra indicate some condensation of water on the substrate. No effects of ammonia in concentrations up to 200 ppm are visible neither in dry nor humid air.

## 5.2. Response of PAA Coated Substrates

### 5.2.1. Results of the KP Experiments on PAA Samples

Prior to a presentation of the experimental KP and quartz micro balance (QMB) results an overview of all presented Kelvin probe polyacrylic acid (PAA) samples is given in table 5.1. A choice of selected samples of different degree of thickness and on different types of substrates were chosen to illustrate the results obtained with PAA.

The classification code for the KP samples consists of an index number *i* (*ki*, *k* for KP sample) to group the samples by preparation date and by production batch, the material of the polymer layer (here PAA), the substrate material (AuSi, AuAl, Si, Fe), and the thickness of the layer in units of kHz (this is the frequency shift of the QMB witness). The table also lists the calculated thickness of the layers and the relevant preparation parameters like concentration and used pressure; acetone was used in all cases as solvent.

**Table 5.1.:** Overview on the presented PAA Kelvin probe samples.

Sample	Substrate	Note
k1.PAA.AuSi.71	Au/Si	1.1 $\mu\text{m}$ , 2 mg/ml, 1 bar
k1.PAA.AuSi.23	Au/Si	0.4 $\mu\text{m}$ , 2 mg/ml, 1 bar
k2.PAA.AuAl.X0	Au/Al203	0.2 – 1.5 $\mu\text{m}$ , 2 mg/ml, 1 bar
k2.PAA.Si.40	Si	0.6 $\mu\text{m}$ , 2 mg/ml, 1 bar
k3.PAA.Fe.40	Stainless steel	0.6 $\mu\text{m}$ , 2 mg/ml, 1 bar
k4.PAA.AuAl.20	Au/Al203	0.3 $\mu\text{m}$ , 10 mg/ml

On hand of these samples the sensitivity of PAA coated substrates to ammonia is demonstrated, the response to humidity, and cross interferences to ethanol and toluene are shown.

### 5.2.1.1. Response to Ammonia

First some general observations made in the KP experiments with ammonia will be reported. Next to the basic measures like sensitivity and signal strength, the humidity influence, the results at elevated temperatures, and the signal and baseline stability over time are of great interest. Besides, a set of five samples with a variation of thickness from 0.2 – 1.5  $\mu\text{m}$  plus two samples with silicon and stainless steel substrate are presented to demonstrate the influence of sensitive layer thickness and substrate material.

**General Observations** The raw KP output of the first sample, denoted with k1.PAA.AuSi.71, is shown in figure 5.3(a) during pulses of 0.4, 1, 3, 10, and 30 ppm ammonia alternately in dry air and at 50% rh. The measurement cycle was repeated three times over a time interval of five days to illustrate the stability and reproducibility of the ammonia response and the course of the baseline. The very first measurement cycle after preparation is always discarded due to initial instabilities and strong drift; at later time stabilisation is achieved by purging with carrier gas for several hours after mounting the sample.

In the raw KP signal in figure 5.3(a), which shows a typical signal during gas exposure for this sample, the drift of the baseline during the phases of humid air is plainly visible, whereas the baseline is stable in dry air. The signal heights were extracted after the baseline correction and the analysed data are plotted in figure 5.3(b) separately for dry and humid air.

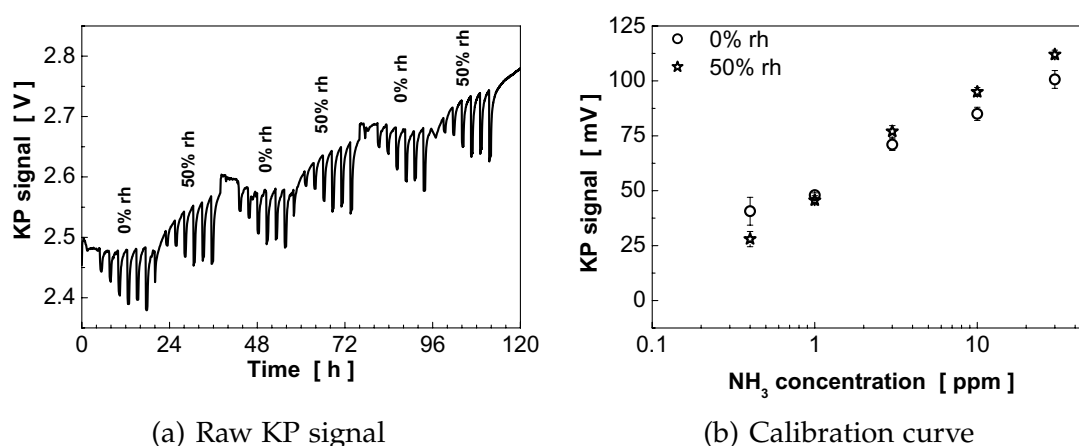


**Figure 5.3.:** KP measurement and results of a PAA spray coated substrate (k1.PAA.AuSi.71) for 0.4 – 30 ppm ammonia alternating in dry air and at 50% rh: (a) raw KP signal and (b) resulting calibration curves with calculated standard deviations for three repetitions.

One can see that there is only a very small deviation from the signal in dry air to the one obtained in humid air. The calculated error (given is the standard deviation) out of the repetition of the experiment is negligible showing a good reproducibility of the KP measurements in consecutive measurement cycles. The low error and the high sensitivity lead to a (extrapolated) limit of detection (LOD), defined as three times the standard deviation, in the sub-ppm range and with that lower than the lowest measured concentration. The signal for 10 ppm of ammonia is 85/95 mV in dry/humid air (50% rh). The calculated logarithmic sensitivity for the sample k1.PAA.AuSi.71 is 33 mV/decade in dry and 46 mV/decade in humid air.

The resulting calibration curves for the KP response are linear on the logarithmic concentration scale over the measured range of nearly two decades. However, one should keep in mind that a dual mode and a logarithmic isotherm are quite similar. The difference are apparent only in a wider concentration range. This fact is easily demonstrated in a way as presented in the plot in figure 5.4(a), where the different isotherms are plotted over the other using the actual parameters for the fit to the calibration curve above. Even though the error in the KP experiments is low one cannot measure accurately and precisely enough with the KP to distinguish between the two,

if ever possible (see figure 5.4(b)). A logarithmic response can only be fully confirmed if data were available over a much wider measurement range. This topic will be discussed at the end of this chapter on summarizing and modelling the response of the polymer coated substrates to the exposure of gaseous analytes. In general is difficult to infer the adsorption model from the measured isotherm.

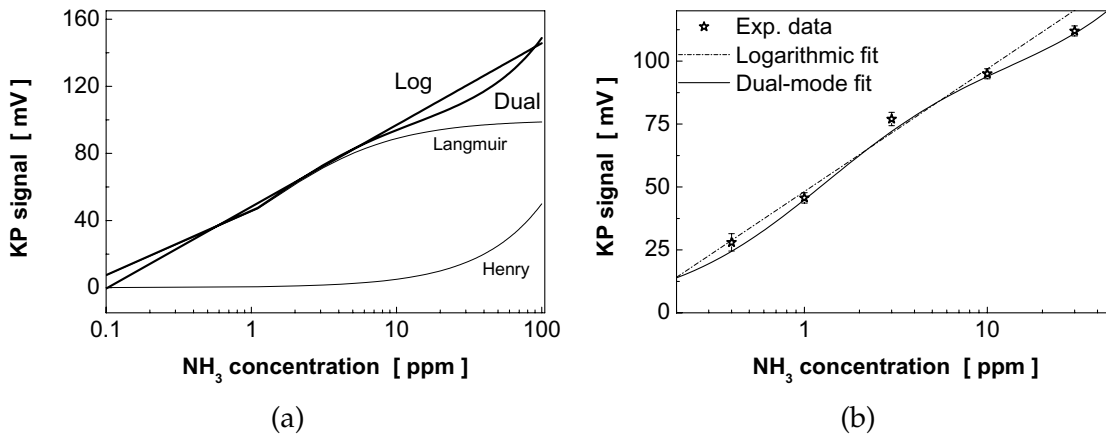


**Figure 5.4.:** Measurement data and fit: (a) illustration of the similarity of the dual-mode sorption isotherm (Langmuir-Henry) and a logarithmic isotherm, (b) experimental data and results of the two models in comparison.

To investigate more the origin of the KP signal additional experiments were carried out. The contribution of humidity to the origin of the KP signal of the samples was tested in an experiment, in which a PAA sample was measured after long time purging with dry air to minimize the residual humidity in the polymer layer to the limit of the system. In a measurement after purging the signal decreases only little, but the noise level is increased significantly. The signal (measured in dry air) can be fully recovered after purging for a short time with humid air. Traces of humidity seem to be enough to generate a KP signal in the polymer/substrate structures in conjunction with ammonia.

In the following the results for a second sample, thinner in layer thickness, from this sample series shall be described and compared to the previous results, as there are differences in the observed phenomena.

The uncorrected output of the KP during an experiment with this sample (k1.PAA.AuSi.23) is presented in figure 5.5(a) for 1, 3, and 10 ppm of ammonia in dry and humid air repeated over five days. The signal (10 ppm ammonia) is 75 mV in dry and 70 mV in humid air 50% rh. The obtained sensitivities are 32 and 30 mV/decade, respectively.

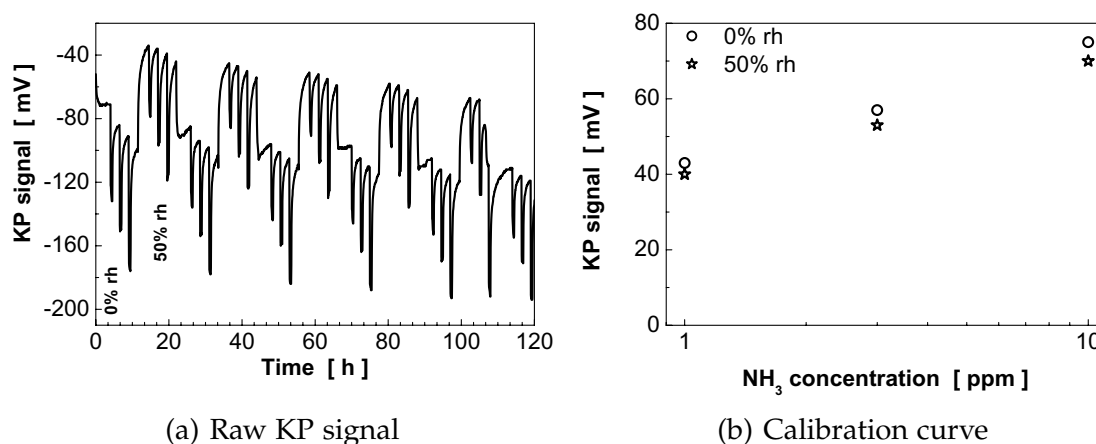


**Figure 5.5.:** KP results of a PAA coated substrate (k1.PAA.Al.AuSi.23) for 1, 3, and 10 ppm ammonia in dry air and at 50% rh: (a) raw KP signal and (b) calibration curve.

In the raw signals for this and the previous sample there is a clear difference in the humidity influence on the baseline. The thinner layer of the sample k1.PAA.AuSi.23 shows a faster water uptake at the switch to 50% rh than the sample k1.PAA.AuSi.71 resulting in a jump of 60 mV and a higher influence of humidity on the baseline. There is less drift in phases of humidity, but also drift present in times of dry air leading to an overall drift of the baseline of 20 mV per day in this time period of five days.

**Humidity Influence** The influence of humidity on the signal and the sensitivity was investigated more closely in a further measurement series. Ammonia was dosed in a concentration of 2, 10, and 50 ppm at humidity levels of 0, 5, 10, 30, 50, and 70% rh. The raw KP signal of one cycle is plotted in figure 5.6(a). The evaluation of the response is summarized in a graph in figure 5.6(b). It shows the sensitivity (left scale) and signal strength (right scale) for all the individual humidity levels.

Neither signal strength nor sensitivity seems to be influenced by a variation of the humidity level in the carrier gas. There is a deviation for the measurement in dry air from the others in sensitivity, but one could claim that sensitivity and the signal height are almost constant with a slight decrease, if humidity is present in the ambient atmosphere. The 10 ppm signal ranges from 70 to 100 mV and sensitivity from 22 to 54 mV/decade with a mean of 85 mV and 42 mV/decade, respectively.

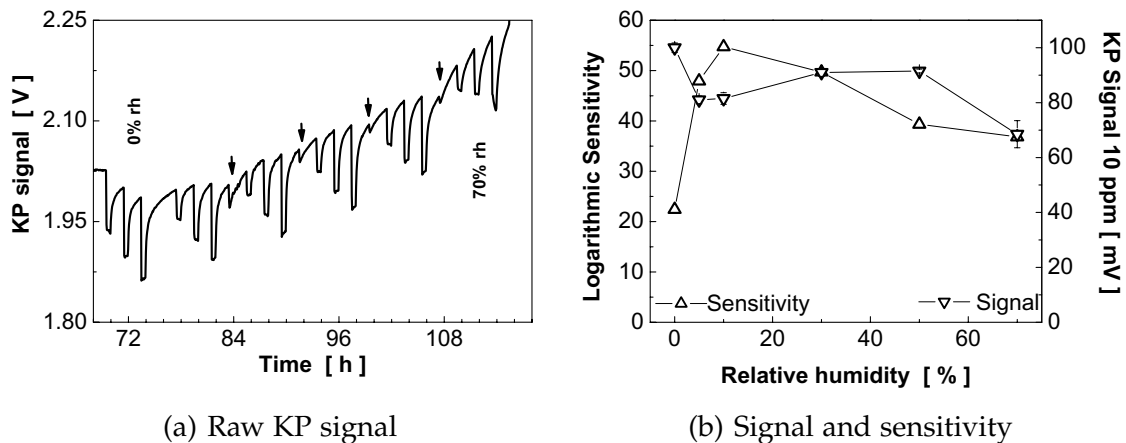


**Figure 5.6.:** Humidity influence on the KP ammonia signal of a PAA spray coated substrate (k1.PAA.Al.AuSi.71): (a) raw KP signal for 2, 10, and 50 ppm ammonia at 0, 5, 10, 30, 50, and 70% rh and (b) sensitivity (left scale) and 10 ppm ammonia signal (right scale) as a function of humidity.

The main difference lies in the course of the baseline. The drift in opposite direction as the ammonia signal increases with humidity. The drift at 70% rh is clearly higher than at the other humidity levels and the same holds for the recovery times. One common observation is present in the raw KP signal in this measurement as well. At switching the humidity content of the carrier gas (marked with arrow in the graph) the baseline is not directly changing to its new course. Very often two processes occur, the first being opposite in direction and stronger. The first process is rather fast, whereas the second spreads easily over a time of two hours. This behaviour is smaller at higher humidity levels and when the change in humidity is low. This effect was not present on the silicon nitride samples, thus, one might exclude that the KP itself is the origin of this effect.

**Response and Recovery Time Constants** An attempt was made to extract the time constants as there are of some importance in the final application field of the sensitive layers. The time constants for response and recovery were calculated by fitting the signal peak to an exponential function as described in section 3.4.4. The procedure was carried out not only with several PAA layers and measurements, but also with the other polymers. The results and numbers given here are typical for all polymers and experiments. The KP itself is very fast having a low integration time of the electronic circuitry (see the example of the humidity test in section 3.1.6.4). The systems should allow in principle the determination of time constants, but expected are the limitations of the measurement chamber.



The time constants,  $\tau_{on}$  and  $\tau_{off}$ , for the bare Au/Si substrate for ammonia (1 – 10 ppm) are: 6 – 4 min in dry air and 7 – 5 min at 50% rh for response and 34 – 40 min and 16 – 22 min for recovery, respectively. The peaks are fairly good approximated by a single exponential functions.

In the case of a polymer coated substrate the calculation of the time constants was not straight forward. The single exponential fit is still perfect for the onset as shown in figure 5.7 in a typical example for a analyte exposure time of 30 min and a purge time of 2 h. The response time constant  $\tau_{on}$  is in the range of 5 – 0.5 min decreasing with increasing concentration, but rather independent of humidity level, sample properties (layer thickness), and polymer material in general, when looking at all available data for all polymers. One must be aware that this is probably a limitation of the system as one might have expected from the large cell volume and the nature of the analyte (ammonia has a high sticking probability).

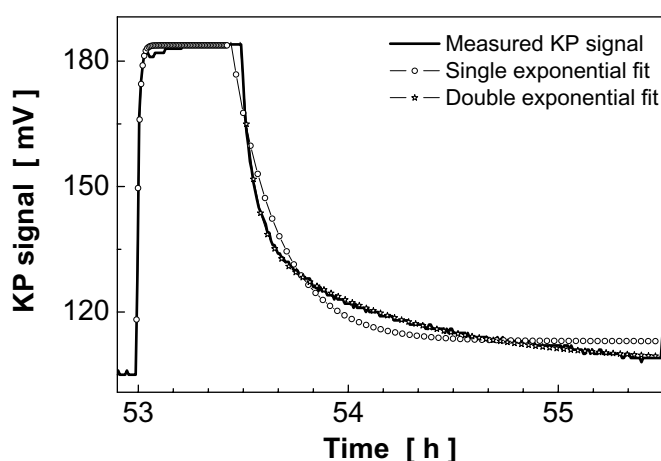


**Figure 5.7.:**

Example for fitting the KP signal to extract time constants for response,  $\tau_{on}$ , and recovery,  $\tau_{off}$ .

For the recovery time a single exponential fit is not a good representation of the peak as demonstrated in the plot (see deviations for the curve of open circles in the plot from the recorded signal). The recovery time constants  $\tau_{off}$  are in the range of 10 – 20 min, but without a clear trend other than that the recovery from ammonia exposure is little slower at higher humidity levels. In a double time constant model recovery time constants of 2 – 4 min and 35 – 45 min of equal weight are obtained.

**Long and Short Time Stability** As the optical investigation by optical microscope (OM) showed a ageing of the PAA layer after one year of storage the long time stability of the sensing properties were investigated by a repetition of the gas test after a certain time. Additionally, a sample was monitored from the very beginning after preparation time on for six months.

At this point one problem in this procedure becomes obvious: when the samples is remounted in the KP set-up, the same lateral position and distance of the KP sample to the KP grid cannot be ensured. This may cause additional deviations in the measured sensor response for the same sample, even if the layers appear to be homogeneous over the whole area in the OM and scanning electron microscope (SEM) investigations. It further remains unclear how large are the contributions of the KP device (gold grid) itself to drift and instabilities during long time measurements over a time period of several days and in repetitions after a long time. The KP was continuously purged in between the measurements with dry carrier gas to maintain constant starting conditions for all measurements.

The measurements of the two samples presented above were taken one year after sample preparation. If the values are compared to a measurement directly after preparation the signal and sensitivity remain the same over time: sensitivity was initially around 55 mV/decade and signal (10 ppm) 90 mV. From this, one expects only a little ageing of gas sensitivity for PAA layers.

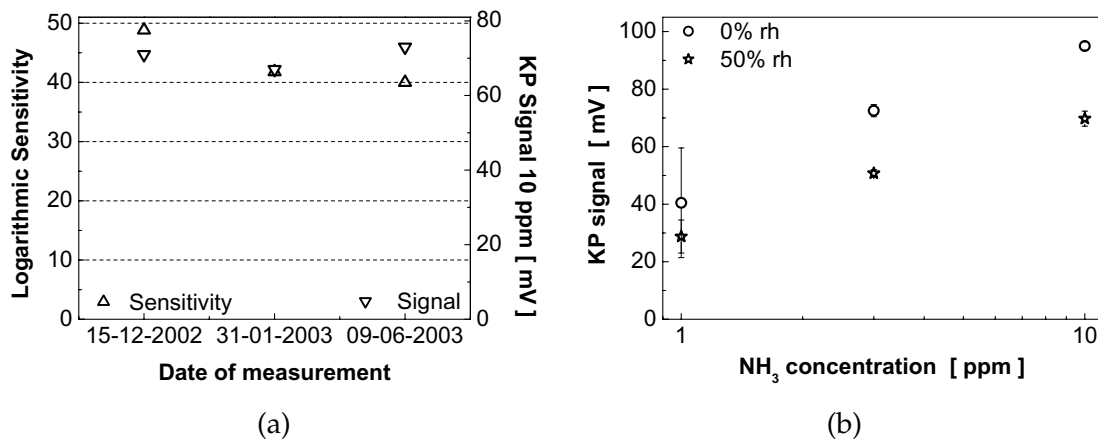


**Figure 5.8.:** KP results of measurements of 1, 3, and 10 ppm ammonia in dry and humid air for a PAA coated substrate (k4.PAA.AuAl.20): (a) signal and sensitivity for the individual measurements in dry air at the three measurements times and (b) calibration curve for a set of measurement over six months.

Another sample (k4.PAA.AuAl.20) was tested several times to obtain more detailed long time stability data from the very time after preparation. The KP sample was prepared only five days before first measurement and no change within the next six months is visible as shown in the diagram of figure 5.8(a) for dry air. In total six measurements over six months were made; the calibration curve over all those measurements is given in figure 5.8(b)

with the error calculated over all measurements. The 10 ppm signal is on average 95 mV and 70 mV for dry and humid air. The sensitivity decreases with humidity for this sample from 54 to 41 mV/decade similarly as before for the other PAA layers. The reason for the large spread in the measurement data of this sample at low concentration remains unclear when looking at the good performance of the other samples. An explanation might be the low layer thickness without guaranteed full coverage of the substrate as pointed out earlier.

**Temperature Influence** To test if and how the long response and especially recovery times can be shortened the temperature of the sample was increased from 30 to 70 °C using the programming feature of the oven hosting the Kelvin probe. It is assumed that the KP itself is not influenced by temperature other than in a shift of the baseline. The signal is expected to decrease due to the change in the partition coefficient. As the signal at 30 °C is very far from the noise level some loss can be accepted to still stay within the required signal range.

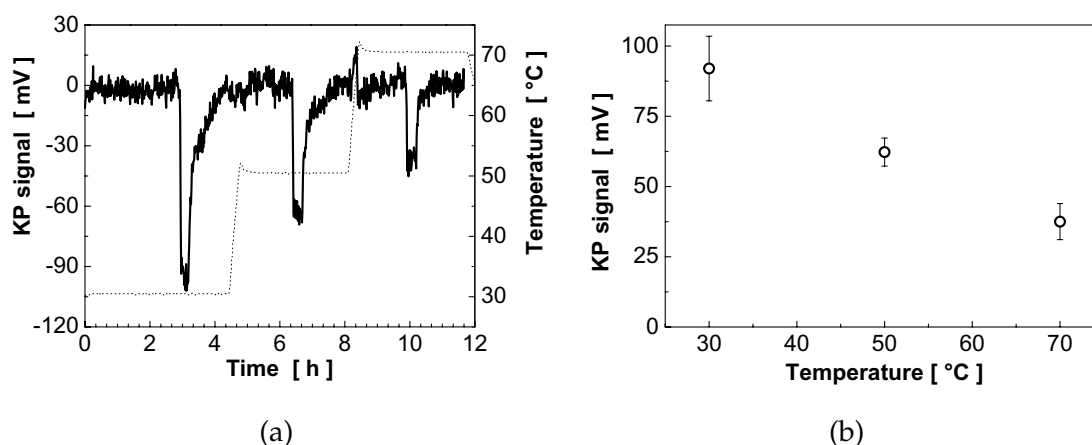


**Figure 5.9.:** KP measurements of 10 ppm ammonia in dry air at temperatures of 30, 50, and 70 °C for a PAA coated substrate (k4.PAA.AuAl.20): (a) KP signal (baseline corrected), (b) temperature dependency of the signal for 10 ppm of ammonia.

The resulting KP signal (baseline corrected) and the extracted signal for 10 ppm ammonia as a function of temperature obtained in two repetitions are plotted in figure 5.9 for a PAA sample. The course of the temperature during the measurement is indicated by the dotted line.

The signal and time constants were determined for the elevated temperatures of 50 and 70 °C in comparison to the usual 30 °C. With increasing

temperature the recovery time constant decreases linearly and is a quarter at 70 °C of the value at 30 °C going down to four minutes. The signal decreases to 35 mV at 70 °C from the initial value of 95 mV.

This experiments show that an increase of temperature to at least 70 °C is possible to achieve a faster kinetics, but to still maintain a signal, that is high enough to measure ammonia in the desired concentration range. However, relying on this puts one of the main advantages of polymer sensitive layers on risk, as they are capable of gas sensing at room temperature in contrast to metal oxides or many other inorganic materials.

**Layer Thickness Influence** In the following the sensitive layer thickness dependency of the signal and sensitivity of PAA layers were in the focus of the experiments. The five samples (k2.PAA.AuAl.X0) were prepared with 10, 30, 50, 70, and 90 kHz, which corresponds to a thickness of 160 – 1450 nm according to table 3.3. The signal strength for 10 ppm ammonia and sensitivity are plotted in figure 5.10 in (a) dry and (b) humid air (50% rh) as a function of layer thickness.

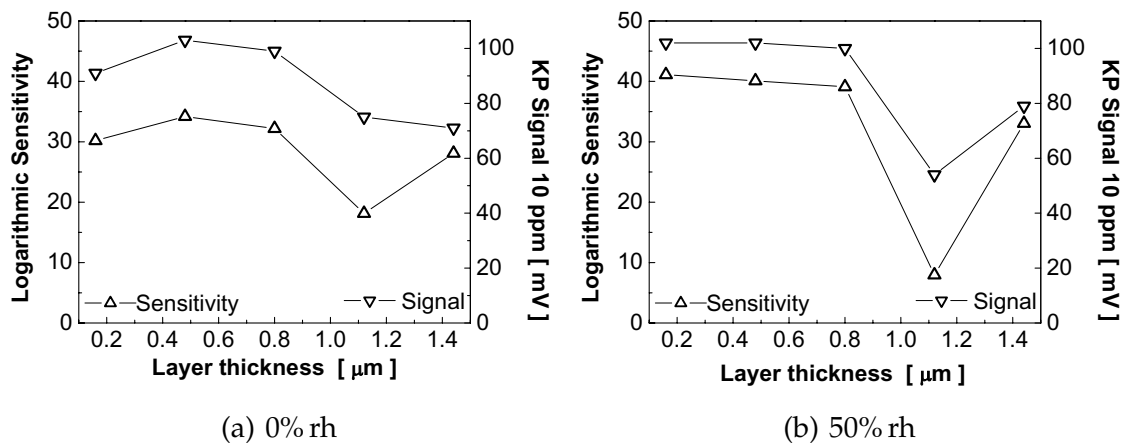


**Figure 5.10.:** Layer thickness dependency of the KP sensitivity and signal strength of PAA coated substrates of a thickness of 160 – 1450 nm at (a) 0% rh and (b) 50% rh.

The influence of the layer thickness on sensitivity and KP signal is very limited: signal and sensitivity are slightly smaller for thicker layers and there is only a variation in those two sensor parameters around the mean. This can be partly explained by unknown inter-sample deviations similar as the problem of repeating a measurement on the same sample as stated earlier. Not counting the 70 kHz sample (1.1 μm) the mean signal is 91/95 mV in dry/humid air and the sensitivities are 31/38 mV/decade. The sample

was considered an outlier and it showed the same behaviour in repeated measurements.

The humidity influence on the baseline at the switch from 0 to 50% rh is the smallest for the sample with the thickest polymer layer. The sudden change of humidity seems to result in two processes in the sample. As before for the other PAA sample there is often a sudden and strong change in the KP signal in the same direction as the ammonia signal and then a slow change in the opposite direction to the new baseline.

There was no measurable influence of the layer thickness on the time constants.

**Variation of the Substrate** At last the influence of a variation of the substrate on the sensing properties was investigated. The sample above were either based on the Au/Si and the Au/Al<sub>2</sub>O<sub>3</sub> substrate. Now a silicon wafer and a stainless steel substrate were coated with 0.6 μm of PAA and tested; the Si sample (k2.PAA.Si.40) is part of the series in the previous paragraph.

The silicon substrate was measured at 0 and 50% rh. The signal is 98 and 85 mV and the corresponding sensitivities 31 and 41 mV/decade. The humidity influence on the baseline is similar as on the Au/Al<sub>2</sub>O<sub>3</sub> based samples. The baseline changes about 40 mV switching from 0 to 50% rh.

The sample on the stainless steel substrate (k3.PAA.Fe.40) was measured at 0, 50, and 70% rh and the signals for 10 ppm are 65, 62, and 88 mV; the sensitivities at the different humidity levels are 36, 33, and 39 mV/decade. In case of this sample the influence of the humidity on the baseline is quite large (jump of 100 mV), but opposite in sign (this means in the same direction as the ammonia signal) going from 0 to 50% rh. Increasing the humidity content further from 50 to 70% rh the baseline goes back. A final comparison at the end of this section and data are summarized in a table.

**Summary of the Ammonia Results** Concluding the description of the KP measurements the results for the analyte ammonia are compiled in the following table to summarize the data obtained with the KP on the PAA samples.

Generally, the response to ammonia of the PAA layers in the KP experiments is very high and proved to be stable over time. Signals as high as 100 mV were observed for ammonia in a concentration of 10 ppm. In combination with a low error in repetitive measurements this leads to a LOD in the sub-ppm range, which is much lower than the measured 0.4 ppm.

**Table 5.2.:** Ammonia signal strength (10 ppm, in units of mV) and sensitivity (in units of mV/decade) for PAA samples in dry/humid air (50% rh). Juxtaposition of measurements on fresh and old samples.

Sample	Fresh		Old	
	Signal	Sensitivity	Signal	Sensitivity
k1.PAA.AuSi.71	94/91	60/54	85/95	33/46
k1.PAA.AuSi.23			75/70	32/30
k2.PAA.AuAl.50			99/100	32/39
k2.PAA.Si.40			98/85	31/41
k3.PAA.Fe.40			65/62	36/33
k4.PAA.AuAl.20	95/70	-/49	95/70	54/41

The signal decreases slightly if humidity is present in the measurement atmosphere, whereas the influence of all other factors is negligible. Humidity influences also the stability of the baseline: the higher the humidity level the higher the drift and the thicker the layer the smaller is the influence of humidity on the course of the baseline. The drift is acceptable and not affecting the sensing effect excessively.

The results were confirmed in many experiments on hand of several samples, but the apparent inter-sample deviations have to be evaluated in further test series. However, a extensive testing is limited by the fact that the measurements with the Kelvin Probe are tedious and very time consuming, as parallel measurements are not feasible. The most important parameters are better determined with the final sensor device when available, but the potential of the PAA layers makes them at the time being the most promising to be used in gas sensitive field effect transistor (GasFET) devices.

### 5.2.1.2. Response to Humidity

Measuring the response to water vapour itself with the KP exhibited some unexpected problems with the PAA and later on with the PS layers, which were not present in the ammonia experiments. The KP signal for humidity is not well behaved and not always reproducible.

The response can be as high as 50 mV as presented in figure 5.11, in which a measurement for pulses of humidity levels from 10 to 75% rh is shown for a thin PAA layer (sample k4.PAA.AuAl.20). The response is already high for low humidity concentrations and saturation of the signal occurs.

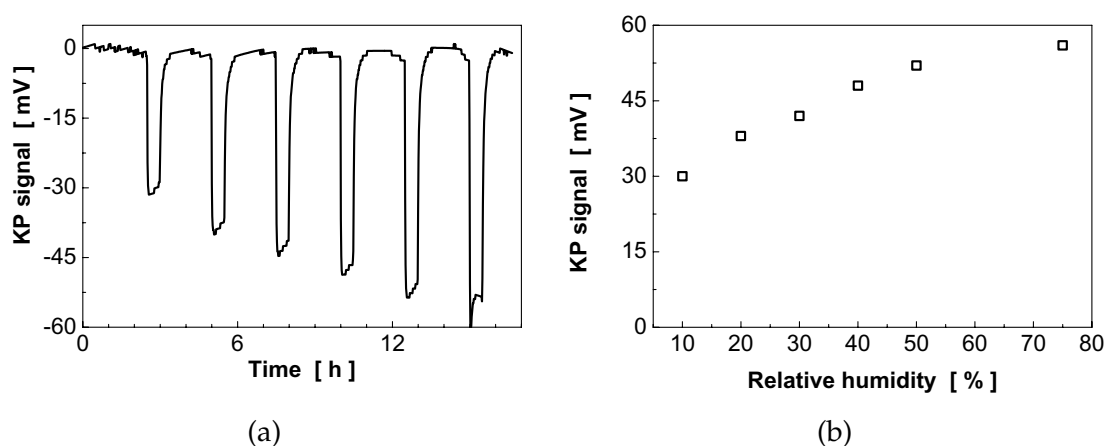


**Figure 5.11.:** KP response to short pulses of water vapour (10, 20, 30, 40, 50, and 75% rh) for a PAA coated substrate (thin layer of k4.PAA.AuAl.20): (a) KP signal (baseline corrected), (b) calibration curve for humidity.

At this point one also has to recall the course of the baseline in the ammonia experiments. The finding above represents only the response to short pulses of water vapour or a initial response to a changing humidity background. As described earlier on a longer time frame the response is in the opposite direction.

In case of a thick layer, for example k1.PAA.AuSi.71, the response to humidity is much lower. The peaks resemble more a transient response as a square pulse and there is shift of baseline during the pulse, especially at high humidity levels. The response to 60% rh is approximately 35 mV and to 10% rh it is lower than 35 mV. The two opposing effects on the response are more visible in the case of thick layers.

### 5.2.1.3. Response to Cross Interferents

Before reporting the results for ethanol and toluene another important finding should be included here. Ammonia is a very basic molecule and so is n-butylamine, which has a slightly higher  $pK_b$  as ammonia (cf. 4.75 and 3.2). This compound was chosen to check whether the basicity of the analyte ammonia is the cause for the signal in the KP samples forming ammonium and carboxylate ions in combination with water molecules.

n-Butylamine was added to the carrier gas to obtain concentrations of 200, 500, and 1500 ppm in dry and humid air. The corresponding signal heights in dry air are 159, 193, and 192 mV already showing saturation of the signal. The signal in humid air was not measurable as the peaks are cut off. The very high mass uptake, which becomes clear in the QMB

experiments, rises already the expectation of a large KP signal. The time constants are extremely large for this analyte.

At last the sensitivity to the omnipresent analyte ethanol (a polar compound) and a model compound toluene, chosen for its aromatic character, were determined and compared to the ammonia signal. The signal to ethanol and toluene is very low. The cross interference to the two analytes is less than 13 and 7 mV for 200 ppm. The KP signal is plotted in figure 5.12.

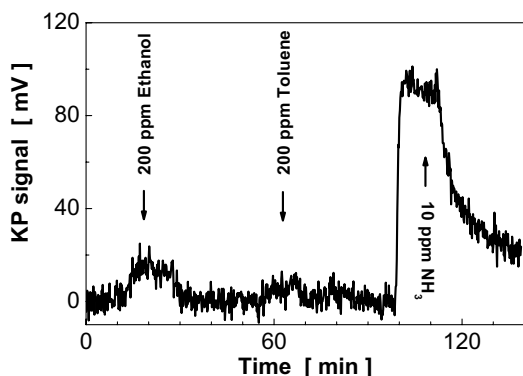


**Figure 5.12.:**

KP response to 200 ppm of ethanol and toluene in comparison to the ammonia signal for a PAA coated substrate.

The above may give an indication that basic analytes cause much higher signals than neutral compounds and changes in the pH or the formation of polar species may have an influence of the KP signal.

### 5.2.2. Results of the Experiments on PAA Coated QMB Sensors

The QMB measurements with PAA coated sensors were conducted with a set of sensors of an initial frequency shift by the polymer of 27 – 294 kHz. This is equivalent to a layer thickness of approximately 0.1 – 1.5  $\mu\text{m}$ . The layers were prepared from a solution of 2 mg/ml PAA in acetone. The thickness range was chosen to be similar as the one of the KP samples.

The sample index for the QMB sensors here and in the other cases to come is similar to the scheme of the KP samples: qmb.PAA.xy (where xy denotes the layer thickness in units of kHz, i. e. the frequency shift of the sensor itself during the coating process). The coating was applied on one side only, if not otherwise noted.

The QMB response to ammonia and the cross interferences to butylamine, ethanol, and toluene were tested as well as the humidity signal. As before, the first measurements during the stabilization phase of the layer were always discarded. The results are compared to the KP measurements and they are expected to give some additional information for modelling the KP effect observed on the polymers in this work. As the QMB experiments



were always conducted in parallel to the KP experiments, the available data base is limited.

### 5.2.2.1. Response to Ammonia

The main interest in the QMB experiments lies in the response to ammonia and in the humidity influence of the ammonia signal. Typical QMB results for 2 – 50 ppm ammonia are presented in figure 5.13. The two plots illustrate the data of measurements in dry and humid air (50 and 70% rh) for a single sensor and for four sensors with increasing layer thickness. The sensors were selected to cover the whole range of layer thickness.

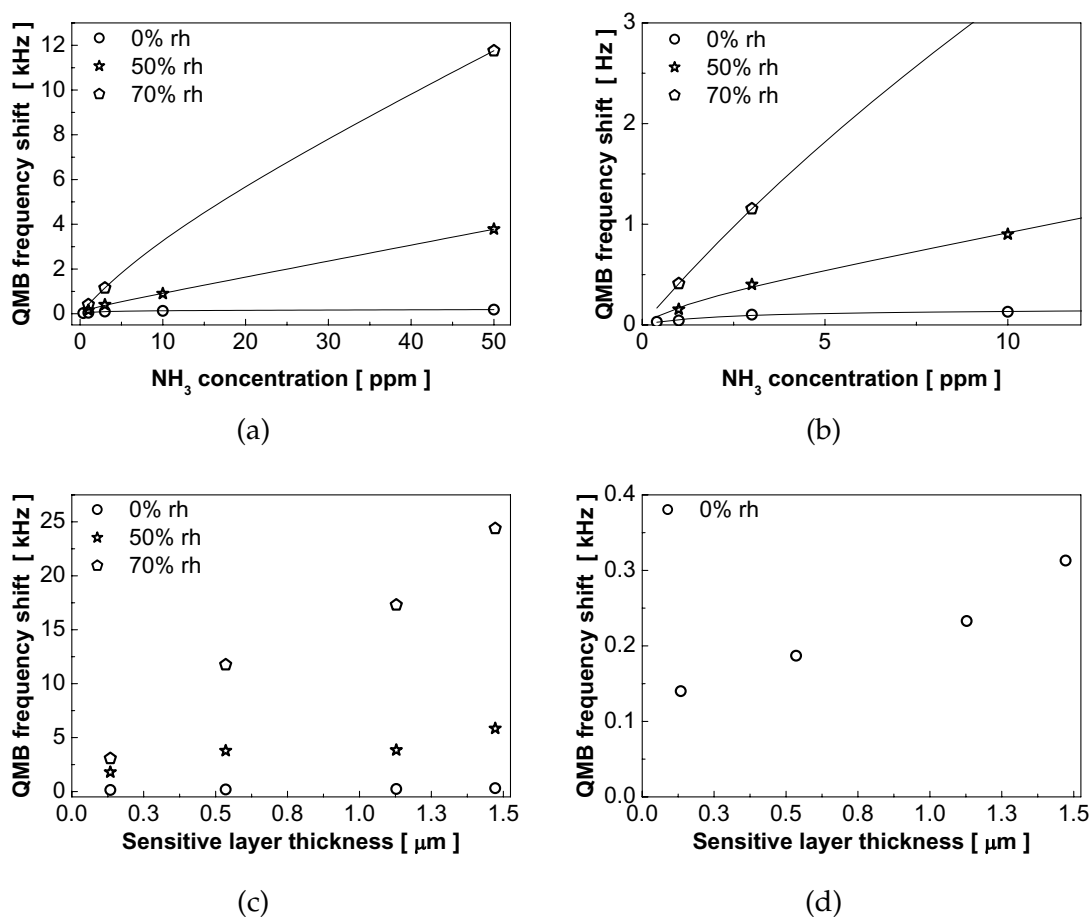


**Figure 5.13.:** QMB results for PAA coated sensors for 2 – 50 ppm ammonia in dry and humid air (50 and 70% rh): (a) calibration curve for a single sensor (qmb.PAA.107), (b) detail for low concentration, (c) thickness dependency of the ammonia signal for 50 ppm at different humidity levels demonstrated with four QMB sensors, (d) detail for measurement in dry air.

A dual-mode sorption isotherm gives the best representation of the calibration data (figure 5.13(a)). The response curve is clearly not linear on a logarithmic scale in contrast to the KP results of the same polymer. The very high mass load leading to a frequency shift in the order of 10 kHz for 50 ppm is striking.

The mass uptake is apparently higher in humid air, concluded from a higher sensor response by a factor of ten. To precisely obtain the individual parameter of the Langmuir-Henry isotherm more information would be necessary. However, the higher the humidity level the larger is the linear contribution to the isotherm. There seems to be a humidity threshold, above which PAA changes among others its sorption properties as reported by [159]. This might be the result of a shift of the glass transition temperature with humidity as explained by Arce et al. [23]. Thus, a transition from glassy to rubbery polymers' behaviour.

The signal increases almost linearly with layer thickness only for 70% rh with a small saturation effect (figure 5.13(c)). A bulk sorption is the most probable explanation, but for the other humidity levels and dry air the ammonia uptake is fairly—in comparison to the data at 70% rh—independent of layer thickness, especially for dry air (see figure 5.13(d)).

### 5.2.2.2. Response to Humidity

Next the QMB response to water vapour was investigated. Frequency shifts of several kilohertz were recorded for humidity levels of 10 to 70% rh shown for a single sensor (figure 5.14(a)) and for four sensors as a function of increasing layer thickness (figure 5.14(b)).

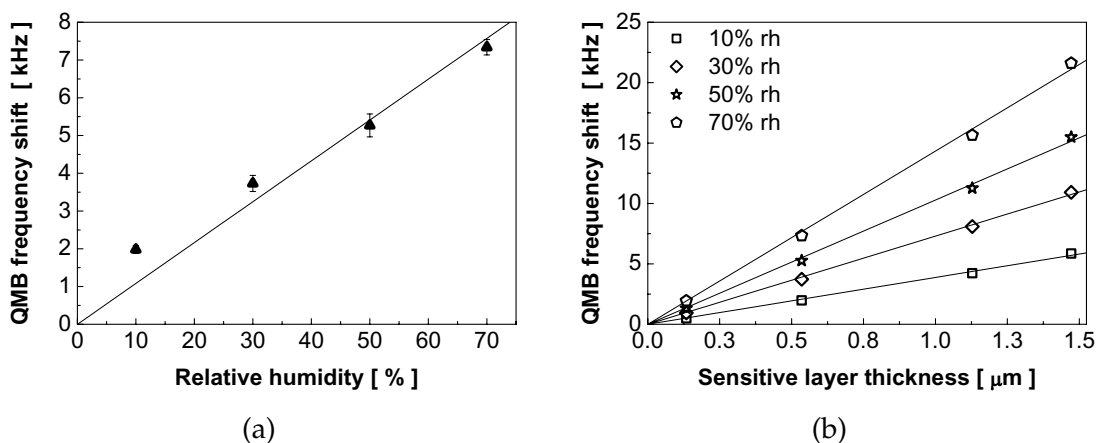


**Figure 5.14.:** QMB results for PAA coated sensors for humidity: (a) results for a single sensor (qmb.PAA.107) and (b) thickness dependency of the signal for humidity levels of 10 to 70% rh.

The humidity response is almost linear over the measured range, but a BET behaviour cannot be excluded for this polymer. The straight line in the diagram indicates the case of a bulk absorption process. A Flory-Huggins model for water adsorption in PAA was determined in other cases, where PAA of much higher molar weight was used in thinner films than here [23].

However, there is an increase of the sensitivity with thickness following the bulk absorption model. This increase in sensitivity explains the increase of the slope with higher humidities as expected.

### 5.2.2.3. Response to Cross Interferents

At last the results for ethanol and toluene are shown in figure 5.15 for two concentrations each (200 and 1500 ppm) and for 200 – 1500 ppm *n*-butylamine in figure 5.16. All measurements were carried out in dry and humid air. Presented is the result for one QMB and the thickness dependency of the signal for the four selected QMB sensors.

No signal at all was obtained in humid air for ethanol and toluene due to high baseline fluctuations and a relatively low response. The signals for ethanol and toluene are very similar in amplitude, showing a higher response to toluene. However, consideration of the saturation vapour pressures and molar weights of the two analytes results in a higher partition coefficient for ethanol.

The signal is an order of magnitude lower than for ammonia. Looking at the data for all QMBs a linear increase of the signal for both compounds with increasing layer thickness (see figure 5.15(b)) is found.

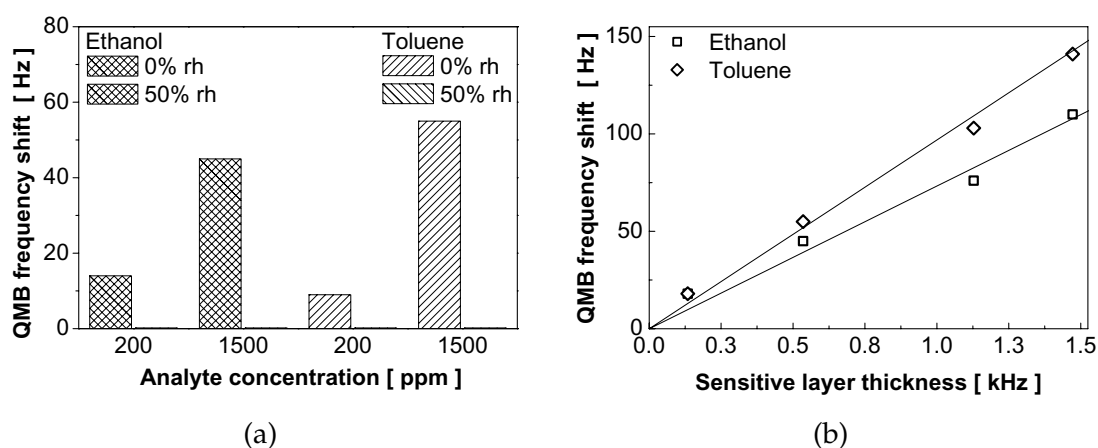


**Figure 5.15.:** QMB results for PAA coated sensors for ethanol and toluene in dry air; no signal was obtained in humid air (50% rh): (a) results for a single sensor (qmb.PAA.107) and (b) thickness dependency of the 1500 ppm signal in dry air.

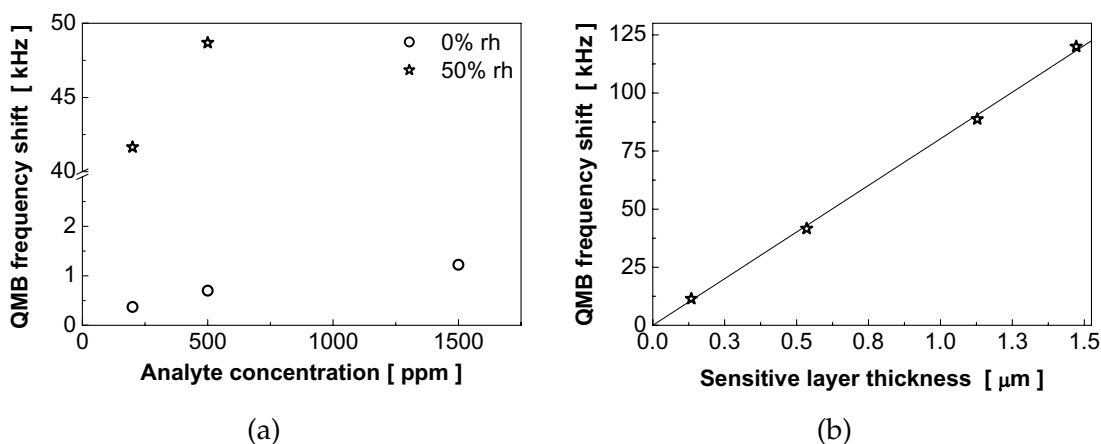


**Figure 5.16.:** QMB results for PAA coated sensors for n-butylamine in dry and humid air (50% rh): (a) results for a single sensor (qmb.PAA.107) and (b) thickness dependency of the 200 ppm signal in dry air.

The response to n-butylamine is similar as to ammonia: the mass uptake is very high and the signal in humid air is an order of magnitude higher than in dry air (see figure 5.16). No signal was obtained in humid air for concentrations higher than 500 ppm as the height of the signal was not measurable due to the instability of the signal. The QMB peaks were cut off. The evaluation of the peaks yields a calibration curve going into saturation (figure 5.16(a)) and again a linear dependency of the signal on the layer thickness (see figure 5.16(b)).

The results for the analytes ethanol, toluene, and butylamine indicate a bulk adsorption process. This is also the case for humidity, but clearly not for ammonia. In the later case may other effects than pure mass related interfere in the QMB response.

### 5.2.3. Results of the IR Experiments on PAA Layers

The infrared (IR) measurement technique is a useful tool to characterize and quantify the type and intensity of interactions between sorbate and sorbant molecules. Additionally, it can be used to identify new chemical species created in the sorption process or changes in the local environment as a result of sorption. Here it was expected to clarify whether, among other things, a possible formation of ammonium ions is the origin of the observed KP signal. However, as the absorption of IR radiation is related to the number of absorbing molecules, species only existing at the interface to the substrate or on the polymer surface will hardly be detected when measured in transmission, if they are not present in very large quantities or strongly absorbing IR radiation.

Two PAA samples were examined in the IR experiments and no significant differences occurred between their spectra. In the following the results are summarized for both samples. Before a new sample was measured the measurement system and the sample was purged with dry carrier gas. It was noticed that purging more than two hours did not have any influence on the spectra any more. If a spectrum of the bare silicon substrate is used as reference no peaks attributed to water are visible.

### 5.2.3.1. Peak Assignment and Exposure to Different Levels of Humidity

In the following the main peaks assigned to PAA are identified on hand on the spectra recorded in humid air. In figure 5.17 several spectra taken at increasing level of humidity are plotted. As reference a spectrum taken before humidity exposure was used. Consequently, not all peaks of PAA are necessarily observed, but only the ones that change their intensity and position during analyte gas or humidity exposure. A decrease in concentration of a species results in a negative peak and an increase in a positive peak. The assignment conforms to accepted results reported in the literature, e. g. by Santhiya et al. [160].

The broad band spanning from  $3600 - 3100 \text{ cm}^{-1}$  is assigned to associated water molecules. The visible bands in this region and below are due to stretching vibrations of certain distinctive O-H groups involved in hydrogen bonding: either of the carboxylic acid itself or of water molecules interacting with the polymer. From a spectrum of a PAA layer in dry air referenced to the spectrum of the uncoated silicon substrate (not shown here) the peaks at  $3230$  and  $2954 \text{ cm}^{-1}$  could be assigned directly to the polymer's O-H groups. Additionally, this region also corresponds to stretching vibrations of the N-H bonds of ammonia species. The O-H vibrations of hydronium ions fall also in this spectral range, but they cannot be clearly identified.

The band at  $1742 \text{ cm}^{-1}$  belongs to the C=O stretching vibration characteristic for carboxylic acids. The position of this band is very sensitive to the local environment of the COOH group. In the vapour phase, where the acid is present in a monomeric form, this band can be as high as  $1780 \text{ cm}^{-1}$ , whereas for cyclic dimers it is as low as  $1710 \text{ cm}^{-1}$ . At weak hydrogen bonding it is found around  $1725 \text{ cm}^{-1}$ . In our case one can see at higher humidity levels a second peak in addition to the one listed above. It appears at  $1717 \text{ cm}^{-1}$  and is an indication of an increased interaction of the carboxylic group with water molecules. The band at  $1640 \text{ cm}^{-1}$  is the C=O stretching vibration of the COOH group in the presence of intramolecular and other types of strong hydrogen bonding. The peak at  $1559 \text{ cm}^{-1}$  is the result of a O-C-O stretching vibration of the carboxylate group (asymmetric

stretching vibrations). The ratio of the  $\text{COO}^-/\text{COOH}$  bands can be used in principle to calculate the pH of the environment of the polymer molecule. However, if the polymer is not in solution deviations from the expected pH value are often observed [161]. The impossibility to exactly determine the baseline, as several species having IR peaks near to each other appear in the spectra, renders a quantification impossible here.

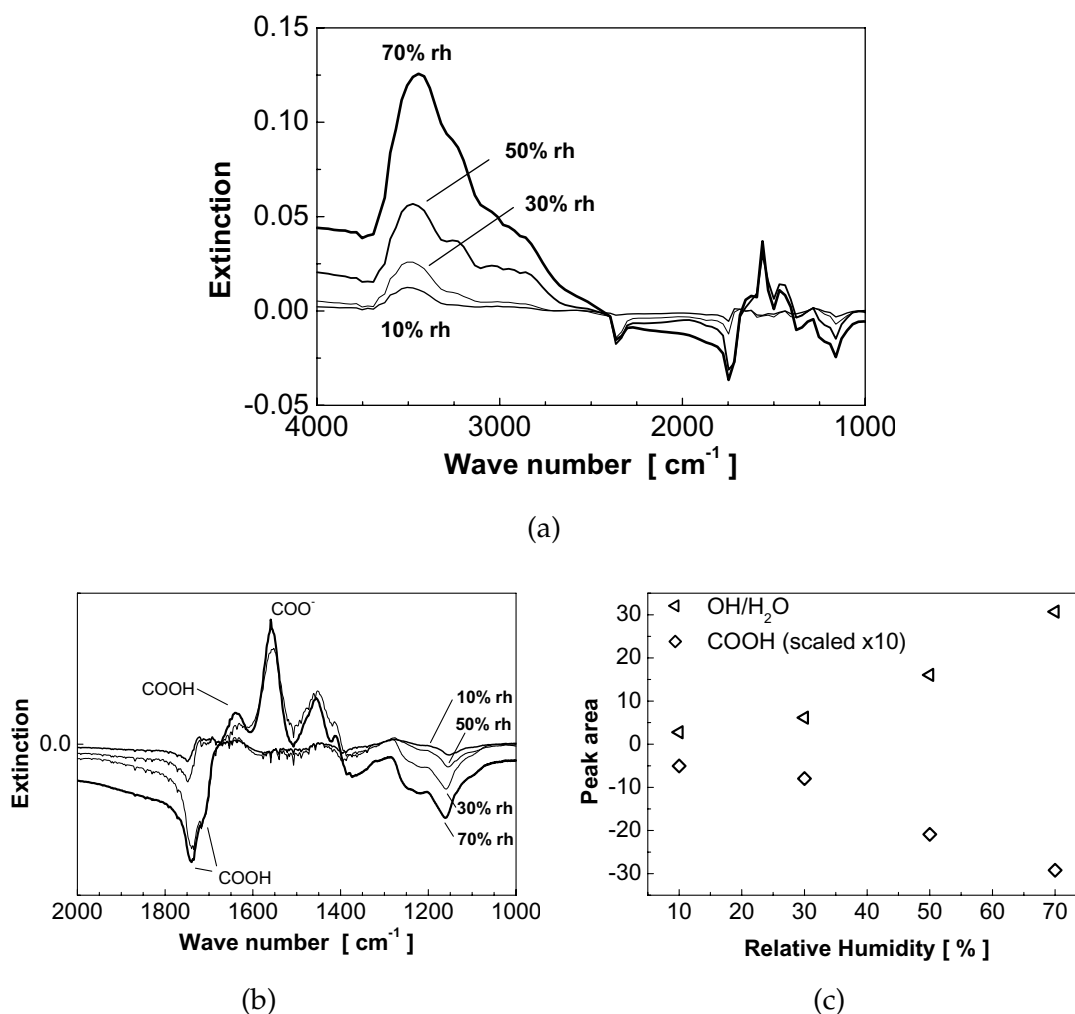


**Figure 5.17.:** IR spectra of PAA on silicon for increasing humidity levels (10 – 70% rh): (a) overview over the total spectral range, (b) close-up of the spectral range characteristic to carboxylic acids and carboxylates, (c) results of a band analysis for the peaks associated with OH groups and COOH (at  $1742\text{ cm}^{-1}$  and  $1717\text{ cm}^{-1}$ ).

The weak bands at  $1452$  and  $1412\text{ cm}^{-1}$  are assigned to combinations of C-O stretching and O-H deformation vibrations. The peaks at the lower end of the spectra are weak and the determination of the peak positions remains imperfect. The broad bands at  $1284$  and  $1203\text{ cm}^{-1}$  are due to the

CH<sub>2</sub> deformation mode. The weak bands at 1163 and 1010 cm<sup>-1</sup> indicate C-O stretching.

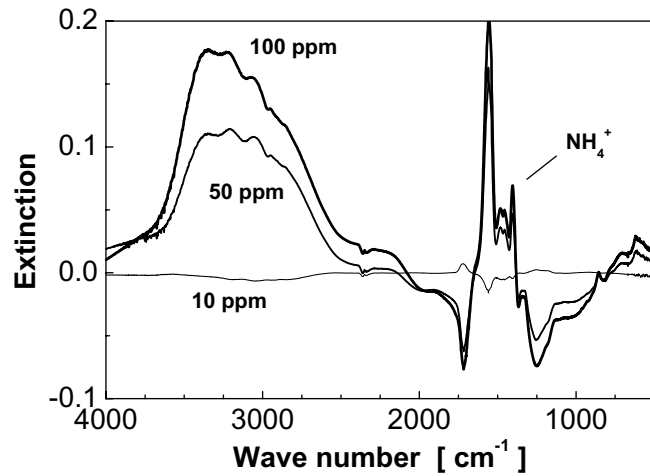
Now, the effect of exposure to different levels of humidity shall be discussed. The spectra for humidity levels up to 70% rh are presented in figure 5.17(a). The changes in the spectra due to sorption of water molecules are very strong in the case of PAA. Most obvious is the increase in intensity of the broad peak assigned to associated water molecules. This finding is in agreement with the known water sorption properties of PAA films.

The part 2000 cm<sup>-1</sup> – 1000 cm<sup>-1</sup> of the spectra is shown in figure 5.17(b). One can see a link of increasing humidity level to a decrease of the peak attributed to COOH and an increase of the COO<sup>-</sup> peak. This means a higher degree of dissociation of the weak acid PAA with an increase of water species in the PAA layer. The peak at 1640 cm<sup>-1</sup> of the COOH group involved in hydrogen bonding is clearly visible at humidity levels above 30% rh. A detailed investigation by calculating the individual peak areas shows that the areas of the peaks associated with O-H, COOH/COO<sup>-</sup> groups change at the same rate (see figure 5.17(c)).

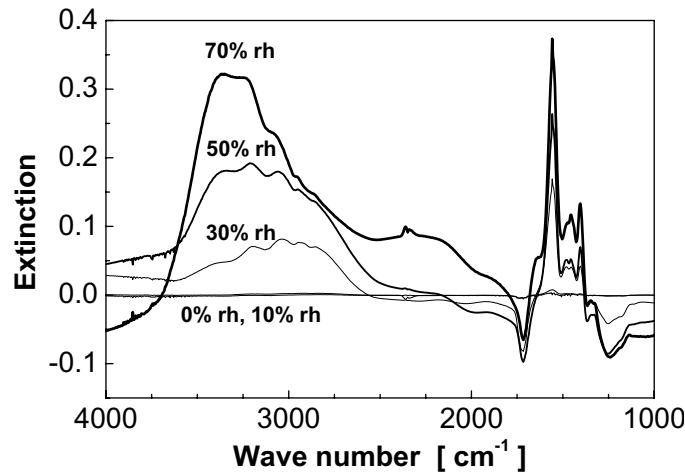
### 5.2.3.2. Ammonia Exposure

More important are the investigations of the effect of ammonia exposure in and without the presence of humidity. The ammonia induced changes in the spectra recorded in dry air are very small and thus not shown here. The changes in the spectra are more than ten times lower than in the case of humid air. Anyhow, a decrease in the number of COOH groups and similar increase in the number of COO<sup>-</sup> groups is observable. No peak for a COOH group involved in hydrogen bonding (expected at 1640 cm<sup>-1</sup>) was seen. More important is the fact, that no ammonia related species are detectable, except for the characteristic peak of gaseous ammonia at 950 cm<sup>-1</sup>. The proton exchange reaction between PAA and ammonia hardly takes place in dry air.

In humid air the changes in the spectra are much more intense. See the spectra in figure 5.18(a) for the results of measurements in an atmosphere of 10 – 100 ppm ammonia in humid air (50% rh). The reference is the respective spectrum just before ammonia exposure. It can be seen that ammonia sorption creates additional sorption possibilities for water molecules, as the peaks attributed to distinctive O-H vibrations have strongly gained intensity. Thus, one can conclude that the high mass load measured by the QMB sensor coated with PAA is not only caused by ammonia sorption alone, but also by additionally absorbed water molecules. Not increasing is, however, the peak linked to associated water molecules expected at 3480 cm<sup>-1</sup>.



(a)



(b)

**Figure 5.18.:** IR spectra of PAA on silicon: changes induced (a) by different levels of ammonia (at 50% rh) and (b) by a constant ammonia concentration (120 ppm, except at 70% rh) at different levels of humidity.

Furthermore, a strong decrease of the peak at  $1720\text{ cm}^{-1}$  and a strong increase of the peak at  $1550\text{ cm}^{-1}$  is observed. The sharp peak at  $1404\text{ cm}^{-1}$  assigned to a N-H deformation mode indicates the existence of  $\text{NH}_4^+$  ions. Both findings indicate a reaction of ammonia molecules with PAA to a large extent. Water molecules seems to enable the protonation of the ammonia molecules.

Similar are the results for a fixed concentration of ammonia at different levels of humidity as shown in figure 5.18(b). The ammonia concentration was chosen to be 120 ppm except at 70% rh, where the possible maximum concentration of ammonia was only 70 ppm. The two spectra for 100 ppm



and 120 ppm at 50% rh recorded in the two experiments are nearly identical in shape. There is a trend for the effect of ammonia addition with increasing humidity levels. The increase of the number of water species in the PAA layer induced by the presence of ammonia is stronger for higher humidity levels. The decrease of COOH and increase of COO<sup>-</sup> follows the increasing humidity level. The effect is low for 10% rh but very high for 70% rh, also considering the lower ammonia concentration at this humidity level.

**Response and Recovery Time Constants** The determined response time constants are similar to the KP case. For 120 ppm of ammonia the response time constants are about 6 min at 50% rh. This is a surprising result considering the small sample chamber and only little dead volume. The response time in the KP experiments is therefore not determined by the measurement chamber.

However, the decay times are generally very large, similar to the decay time constants in the QMB experiments and much larger than in the KP experiments. Recovery time constants around 30 min were determined in a fit to the IR data. A fit of a single time constant for the decay was representing the experimental data very well. All peaks change in parallel, so the fit can be made to all peaks for O-H, COOH or COO<sup>-</sup> without difference.

### 5.3. Response of PS Coated Substrates

#### 5.3.1. Results of the KP Experiments on PS Samples

On the basis of the samples listed in table 5.3 the results of the KP measurements on polystyrene (PS) layers will be discussed. Several samples of different thickness were prepared on various substrates and extensively tested with the KP for ammonia in dry and humid air (mostly 50% rh). All samples were prepared using the semi-automatic deposition system due to the clear improvement and better quality of the layers.

**Table 5.3.:** Overview of presented PS Kelvin probe samples.

Sample	Substrate	Note
k1.PS.AuAl.35	Au/Al203	0.8 $\mu\text{m}$ , 1 mg/ml, DCM, 1 bar
k1.PS.AuAl.13	Au/Al203	0.3 $\mu\text{m}$ , 1 mg/ml, DCM, 1 bar
k2.PS.AuSi.40	Au/Si	2 mg/ml, $\text{CHCl}_3$ , 1 bar
k2.PS.AuSi.30	Au/Si	2 mg/ml, $\text{CHCl}_3$ , 1 bar
k2.PS.Si.40	Si	2 mg/ml, $\text{CHCl}_3$ , 1 bar
k3.PS.Fe.40	Fe	1 $\mu\text{m}$ , 2 mg/ml, DCM, 1 bar

The short time stability/baseline of the signal was studied over sixteen days and the issues of ageing was followed over 15 months. The first order cross interference to ethanol and toluene, the humidity influence on the ammonia response and the humidity signal itself were examined. The outcome is compared to the results of the QMB experiments. Finally the results for sample using another solvent in the preparation process, which causes a departing layer structure, are reported.

##### 5.3.1.1. Response to Ammonia

**General Observations and Signal Stability** The first two samples listed in table 5.3 were studied in detail in their ammonia sensing properties. The main focus is set on the sensitivity and signal strength to ammonia in dry and humid air and additionally the influence of humidity and ageing processes of the polymer layer on the KP signal.

The baseline stability of the KP signal for the k1.PS.AuAl.13 sample in a continuous measurement over a duration of two weeks consisting of different experiments is shown in figure 5.19(a). After an initial start-up phase the baseline is very stable over time, with the exception of one occurrence of an irregularity after 11 d. In figure 5.19(b) one measurement for 0.4 –

50 ppm ammonia in dry and humid air (at 5, 10, 20, 30, 50, and 70% rh) is shown in more detail. One can see that the humidity influence on the baseline is very low. There is only a drift in the same direction as the ammonia signal for higher humidity levels than 50% rh. The sample k1.PS.AuAl.35 is similar in its stability, only the humidity influence on the baseline is more pronounced (30 – 40 mV for 70% rh).

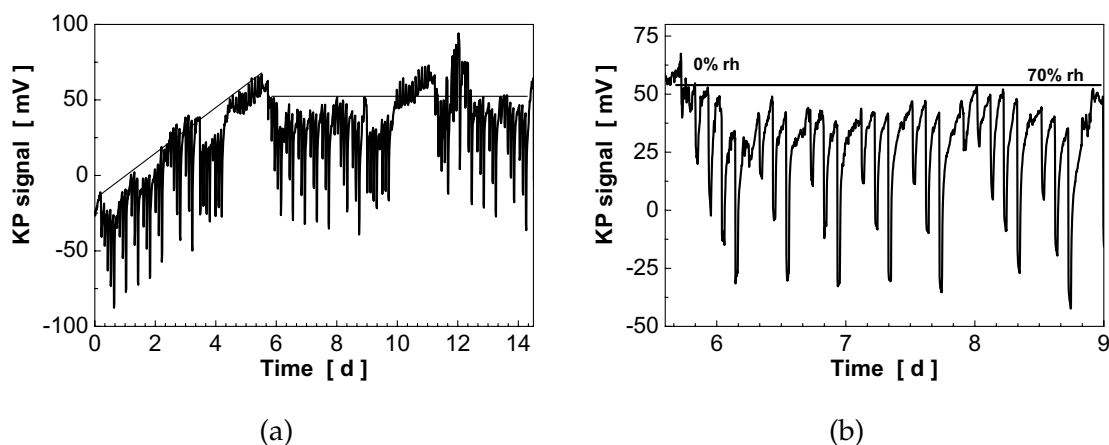


**Figure 5.19.:** KP measurement of 0.4 – 50 ppm ammonia in dry and humid air (at 5, 10, 20, 30, 50, and 70% rh), of ammonia and humidity, and of humidity (5 – 60% rh) for a PS coated sample (k1.PS.AuAl.13): (a) course of the KP response over a time of more than two weeks and (b) raw KP signal of one measurement cycle for ammonia.

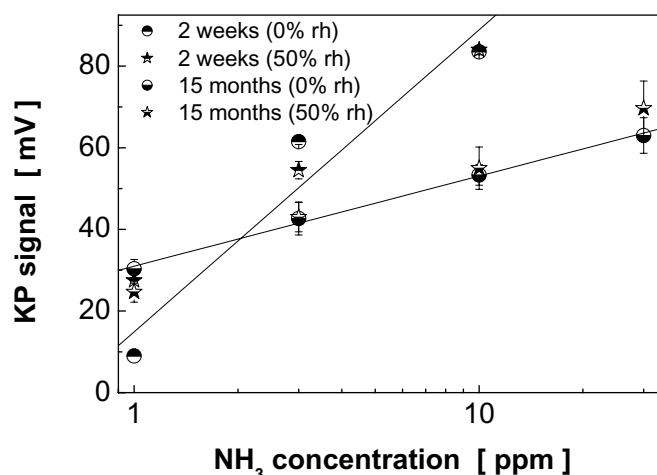


**Figure 5.20.:** KP results for measurements of 1, 3, 10, and 30 ppm ammonia in dry and humid air for a PS spray coated sample (k1.PS.AuAl.13): comparison of the measurements taken after two weeks after preparation and 15 months.

The sample k1.PS.AuAl.13 was measured the first time two weeks after preparation and then again 15 months later. The difference between the results taken on the two time points can be seen in the calibration data in figure 5.20.

A logarithmic fit was applied to the data and the resulting calibration curves in dry air are shown in the plot. The low error shows the good reproducibility in the repeated measurements. The sensitivity in dry/humid air (50% rh) is initially 74/56 mV/decade, but decreases to 22/29 mV/decade with time, whereas the signal height for 10 ppm is 84/84 mV and later 53/55 mV. All of this leads to a LOD in the low ppm range. In the table 5.4 the results for the two samples are summarized.

**Table 5.4.:** Ammonia signal strength (10 ppm, in units of mV) and sensitivity (in units of mV/decade) for PS samples in dry/humid air (50% rh). Comparison of measurements on the fresh and old sample.

Sample	Fresh		Old	
	Signal	Sensitivity	Signal	Sensitivity
k1.PS.AuAl.35	65/61	50/41	33/35	18/21
k1.PS.AuAl.13	84/84	74/56	53/55	22/29

Looking at the data reveals that the thinner layer has a higher sensitivity and signal strength. The loss of signal due to ageing seems to be a general issue for PS sensitive layers. One should remember that PS layer showed no ageing in the optical inspection, whereas in the KP experiments a considerable change in the signal and sensitivity has taken place.

**Humidity Influence** Of great interest is the humidity influence on the ammonia signal. The results on this matter are given in figure 5.21 for ammonia (0.4 – 50 ppm) at different levels of humidity (0 – 70% rh). The plots show the calibration curves for all humidity levels and the evaluation of the sensitivity and signal of a PS KP sample in a measurement after more than one year of sample storage time.

Both measures remain constant with humidity. The average signal is 53 mV and sensitivity 28 mV/decade. There is a slight trend of decreasing sensitivity and increasing signal strength with increasing humidity. The experimental data for the other sample confirm this result, but there is a strong deviation for the measurement at 70% rh, at which the signal is higher.

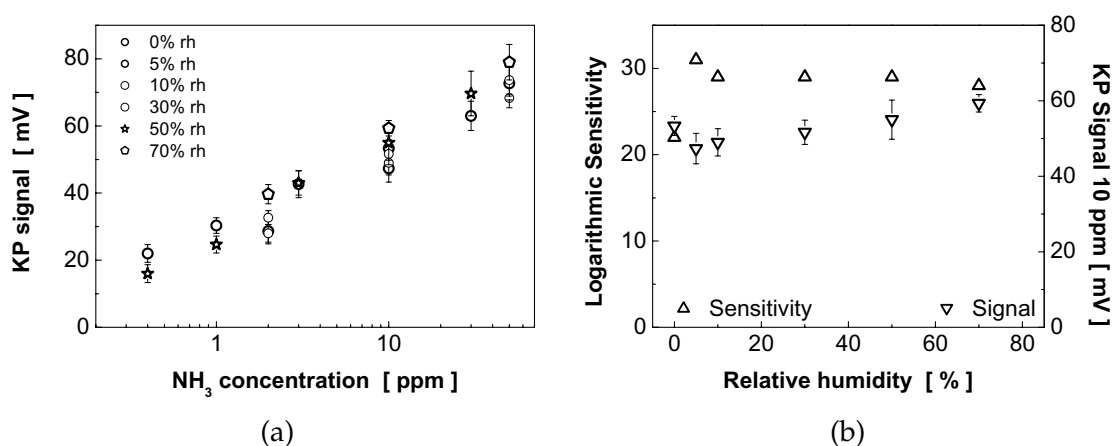


**Figure 5.21.:** KP results for measurements of 0.4 – 50 ppm ammonia at different levels of humidity (0 – 70% rh) for a PS spray coated sample (k1.PS.AuAl.13): (a) calibration curve and (b) ammonia signal and sensitivity as a function of humidity.

**Variation of Solvent** A second set of samples was prepared with trichloromethane as solvent. The solvent was varied due to the better layer quality in terms of large particles on the polymer layer surface as previously described. Two KP samples on the Au/Si substrate are being presented here. Measurement time and conditions are similar as before.

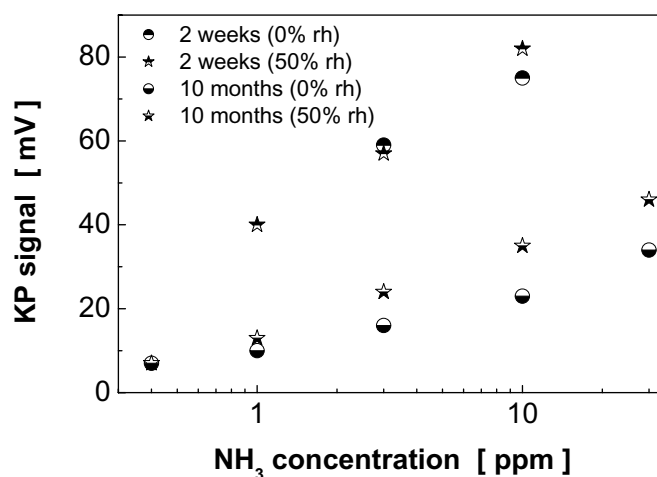


**Figure 5.22.:** KP results for measurements of 0.4, 1, 3, 10, and 30 ppm ammonia in dry and humid air for a PS spray coated sample (k1.PS.AuSi.40): comparison of the measurements taken at two weeks after preparation and ten months.

The ammonia signal in dry and humid air and ageing of signal over time (see figure 5.22) were investigated. The first measurement was taken two

week after preparation and the experiment was repeated after ten months.

The measurements show a minimal influence of humidity up to 50% rh when the signals for 0 and 50% rh are compared to each other. Again, a decrease of signal amplitude from 80 to 30 mV and in sensitivity from 31 to 14 mV/decade is evident due to long time storage and ageing of the sample. The results for these two samples are summarized in the following table.

**Table 5.5.:** Ammonia signal strength (10 ppm, in units of mV) and sensitivity (in units of mV/decade) for PS samples in dry/humid air (50% rh). Comparison of fresh and old samples.

Sample	Fresh		Old	
	Signal	Sensitivity	Signal	Sensitivity
k2.PS.AuSi.40	75/82	31/42	23/35	14/21
k2.PS.AuSi.30			43/56	21/31

Comparing the two samples with decreasing layer thickness shows that there is an increase of the response and sensitivity with decreasing layer thickness and with humidity in the carrier gas.

**Variation of Substrate** Finally, one can compare the results of a PS coated stainless steel substrate of 40 kHz thickness (k3.PS.Fe.40) to the data obtained on the regular gold covered substrate. The signal for 10 ppm ammonia is 19, 35, and 31 mV and the sensitivities 7, 18, and 15 mV/decade at humidity contents of 0, 50, and 70% rh. The sample was measured very shortly after preparation, thus the response is rather low. The baseline drift during phases of humidity is very pronounced. Samples based on the Si substrate were not successfully measured and therefore not further considered.

**Summary of the Ammonia Results** The PS samples were lower in response compared to the PAA samples, but the signal is still high enough to have a LOD in the low ppm range. The signal and sensitivity are affected by long storage times and decreased by initial ageing processes, but remain then stable over time. There are very limited humidity influences on signal and baseline making this polymer the best choice for higher concentrations at higher humidity levels. Samples with a thin polymer layer have a noticeably higher signal. The samples prepared with chloroform undergo the same ageing process and the humidity influence is larger. Other substrates seem not to be suitable.

### 5.3.1.2. Response to Humidity

After the ammonia investigations the KP signal to water vapour is shown in figure 5.23 for humidity levels from 0 to 70% rh for a PS sample. Low signals are expected from the above observations on the humidity influence on the baseline, especially for thin layers.

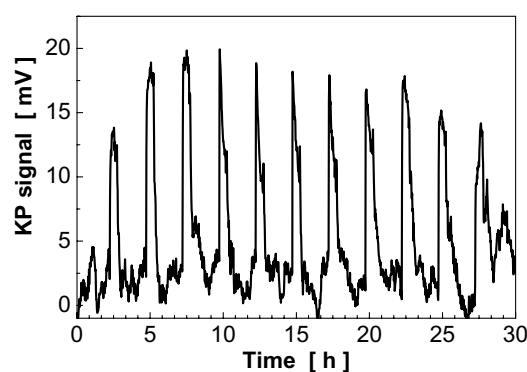


**Figure 5.23.:** KP measurement of different levels of humidity (5, 10, 20, 40, 50, 60, 50, 40, 20, 10, and 5% rh) for a PS spray coated sample (k1.PS.AuAl.13): KP signal (baseline corrected).

In this example of a thin layer (k1.PS.AuAl.13) the signal reaches a maximum of 20 mV independently of the humidity level. Already low levels (5% rh) of humidity give rise to a strong response of the KP. On the contrary to the expectations from the ammonia measurements at different humidity levels, the humidity signal for thicker layer is only little higher reaching only 25 mV. In all measurements saturation occurs at humidity levels higher than 10% rh. In the case of the stainless steel substrate the humidity response is lower, but the response to pulses of water vapour does not result in well shaped peaks.

One will notice later in the QMB section that the water time constant is very large.

### 5.3.1.3. Response to Cross Interferents

The cross interference to ethanol and toluene as well as to n-butylamine in comparison to the ammonia response is shown in figure 5.24 in bar charts for a PS sample. The dosed concentrations are 200 and 1500 ppm for the first two analytes. Butylamine was added in concentrations of 250 and 2500 ppm. One should pay attention to the different scales of the two charts for the signal.

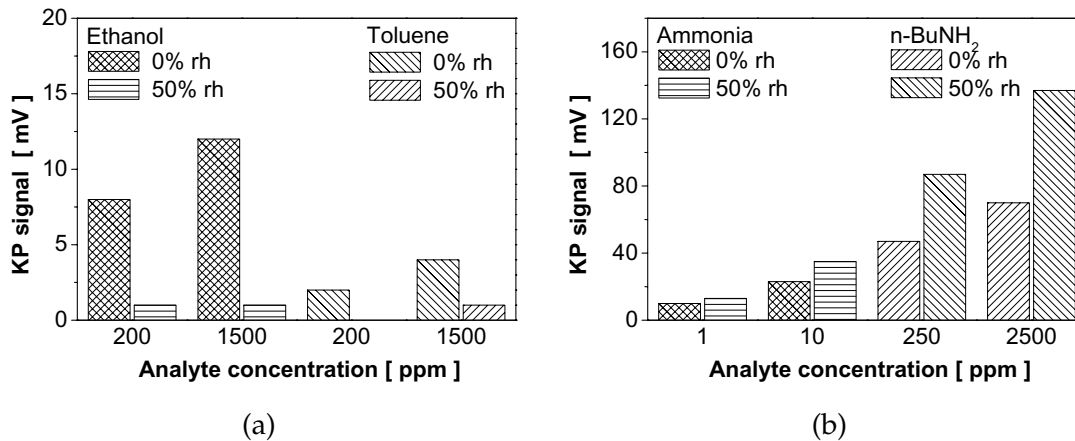


**Figure 5.24.:** KP results of measurements of ethanol, toluene, n-butylamine, and ammonia in dry and humid air for a PS spray coated sample (k1.PS.AuSi.40).

The signal to 200 ppm of the analyte ethanol is lower than 10 mV and lower than 5 mV for toluene. This must be compared to the response of 25 mV to ammonia (see table 5.5). However, the signal to butylamine is very high and even further increased by humidity: the signals for 250 ppm are 50 and 90 mV. This is lower than for PAA, but in contrast to PAA a signal in the presence of humidity was measurable as well. Assuming a logarithmic response the sensitivities are 23 mV/decade in dry and 50 mV/decade in humid air.

### 5.3.2. Results of the Experiments on PS Coated QMB Sensors

A series of QMB sensors with increasing amount of polymer from 14 – 178 kHz, corresponding to an approximated layer thickness of 0.1 – 1.4  $\mu\text{m}$  using equation 3.10 and a reduced density, were prepared using a solution of 1 mg/ml PS in DCM with 1 bar of pressure. The QMB response to ammonia and the cross interferences to humidity, butylamine, ethanol, and toluene were tested.

#### 5.3.2.1. Response to Ammonia and Humidity

First the response to ammonia was tested with the QMB sensors, but no response was detectable for this analyte with neither PS coated QMB in the normal range up to 50 ppm. It also became clear that the response time constant for humidity is in the range of hours not reaching equilibrium in a reasonable time. The response is approximately 200 Hz for the step from 0 to 50% rh taken from the ammonia measurement. The performance of the



PS sensors is generally poor with instabilities of the baseline and large drift and fluctuations.

### 5.3.2.2. Response to Cross Interferents

The presentation of the PS coated QMB sensors continues with the results for ethanol and toluene for two concentrations each (200 and 1500 ppm) and for 200 – 1500 ppm of n-butylamine. All measurements were conducted in dry and humid air. Presented is the result for one QMB and the thickness dependency of the signal for four selected QMB sensors.

The signal to toluene is very high in comparison to ethanol with little or no humidity influence (see figure 5.25(a)), as one might expect from the chemical nature of the analyte and polymer. Both compounds are chemically very much alike composed of an aromatic system capable of  $\pi$ - $\pi$  interactions. The layer thickness dependency is illustrated in a plot in figure 5.25(b). The signal increases linearly for toluene and is somewhat non-linear for ethanol including a offset for low concentrations. The straight lines are added to the plot to better judge the linearity.

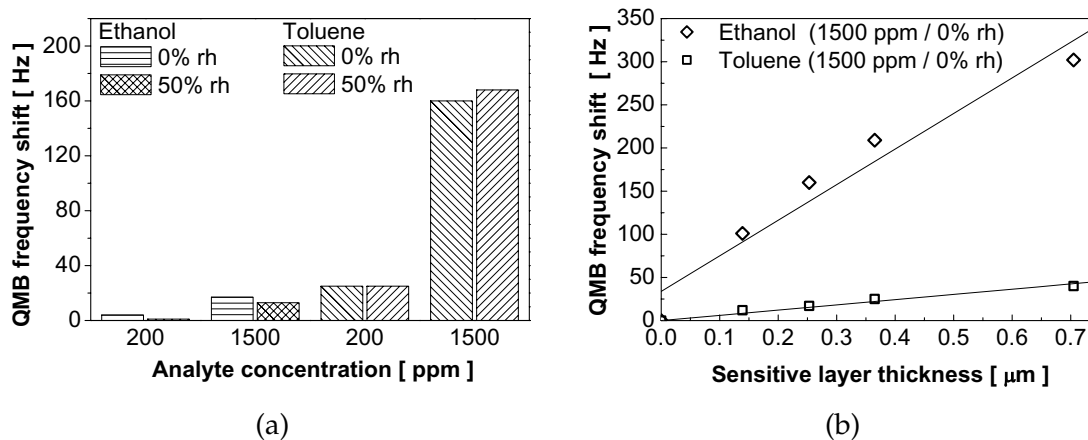


**Figure 5.25.:** QMB results for PS coated sensors for ethanol and toluene in dry and humid air (50% rh): (a) results for a single sensor (qmb.PS.52) and (b) thickness dependency of the 1500 ppm signal.

The signal to n-butylamine is very low compared to the response of the PAA layers. No influence of humidity was seen either as above for ethanol and toluene (calibrations curves in figure 5.26(a)), as the result of the low water uptake. The response curve resembles a Langmuir-Henry type of isotherm. With increasing layer thickness there is an increase of signal, but not in a way as expected for a bulk sorption process. There is a fast

saturation already at low concentrations and only a slight increase at higher concentrations with thickness (see figure 5.26(b)).

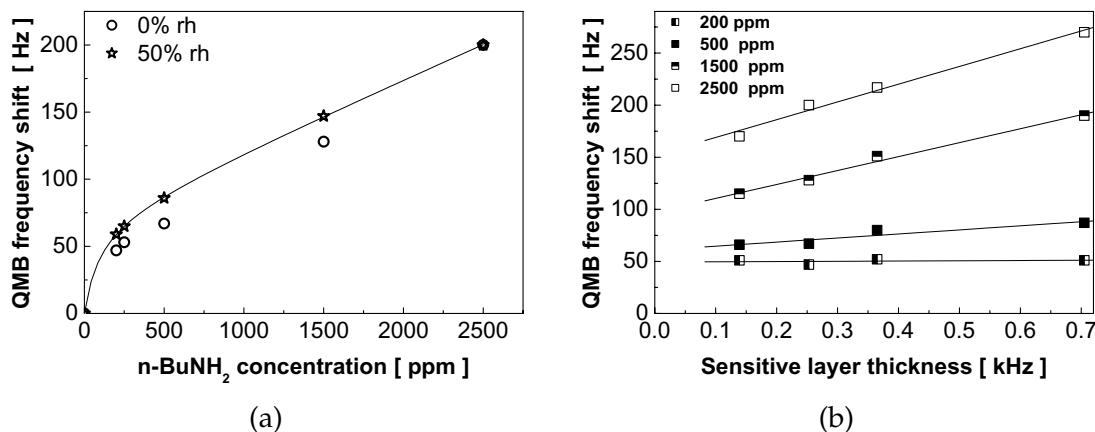


**Figure 5.26.:** QMB results for PS coated sensors for n-butylamine in dry and humid air (50% rh): (a) results for a single sensor (qmb.PS.52) and (b) thickness dependency at various concentrations.

### 5.3.3. Results of the IR Experiments on PS Layers

PS layers on the Si substrate were examined with the IR technique. However, no changes in the spectra were observable when humidity and ammonia was added to the carrier gas.

## 5.4. Response of PVPh Coated Substrates

After the very detailed investigations of the PAA and PS sensing layers the remaining polymers are only characterized in less depth, as they are considered less optimal in sensor performance or do not meet the stated requirements in their physical properties.

It is the rough surface and the imperfect coverage that make the polymer poly(4-vinylphenol) (PVPh) not optimal for later use in sensor devices. Nevertheless, PVPh coated substrates proved to be gas sensitive towards ammonia in the KP experiments. The results of two KP and one QMB samples (for details see table 5.6) are introduced in the following. Acetone was used as solvent for all samples. Earlier samples were prepared with the manual system, newer samples with the semi-automatic system.

**Table 5.6.:** Overview of the PVPh coated KP and QMB samples selected for presentation.

Sample	Substrate	Note
k1.PVPh.AuAl.20	Au/Al203	manual system
k2.PVPh.AuAl.43	Au/Al203	1 mg/ml, 1 bar
qmb.PVPh.60	QMB	2x 30 kHz, manual system

At first the characterisation of a sample in a concentration range of almost three orders of magnitude (1 – 900 ppm) of ammonia at different humidity levels (0 – 80% rh) will be discussed. Then the humidity influence on the ammonia signal was investigated more thoroughly, and finally the results of the QMB sensors are presented on the hand of one example.

#### 5.4.1. Results of the KP Experiments on PVPh Samples

##### 5.4.1.1. Response to Ammonia

**General Observations and Long Time Stability** The first PVPh sample, sample code k1.PVPh.AuAl.20, was characterised in dry and humid air (40, 50, and 80% rh) in a much wider range of ammonia concentration reaching from 1 to 900 ppm as before. The main results of these experiments are presented in figure 5.27.

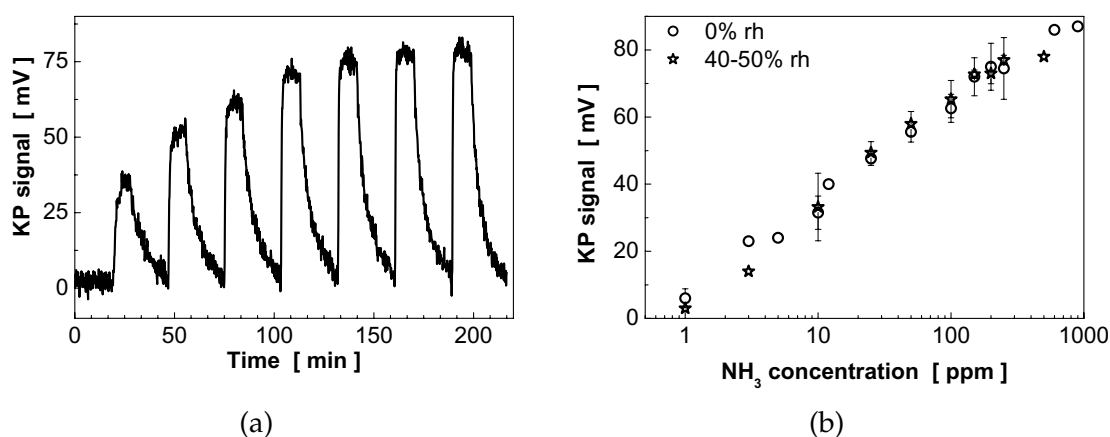


**Figure 5.27.:** KP results of measurements of ammonia in concentrations of 1 – 900 ppm in dry and humid air of a PVPh coated sample (k1.PVPh.AuAl.20): (a) example KP signal (baseline corrected) in humid air (40% rh) and (b) resulting calibration curves for all measurements.

The figure displays a plot of the baseline corrected KP signal for ammonia in dry air and the resulting calibration curves for dry air and humidity levels of 40 and 50% rh, the later two put together in one. The noise level in the KP signal is caused by an early KP set-up and is not a property of the polymer layer. One can see two things: the signal for ammonia is linear over the whole measured concentration range and the signal is hardly influenced by medium levels of humidity.

The first of the above presented measurements was taken after 13 months after sample preparation and the signal remained constant over the covered time period of 22 months. The calibration curves in figure 5.27(b) summarize ten measurements in this time window, not always taken over the full range. The logarithmic sensitivities are 28 mV/decade in dry and 30 mV/decade in humid air (aggregated for measurements at 40 – 50% rh). At 80% rh the values are only half as high, which might be an artefact of the KP itself. It is remarkable, that the humidity has no influence on the sensitivity and signal strength as it can be seen in the diagram above for this sample and later in figure 5.28(c) for a second sample up to humidity levels of 70% rh.

However, there was an initial ageing process on a short time scale going on as the response at the beginning, taken four weeks after preparation, was higher. The signal for 10 ppm ammonia was nearly the same, but sensitivity was 67 mV/decade in dry air.

**Humidity Influence** A PVPh sample was measured at several levels of humidity from 5 – 70% rh to closer investigate the influence of humidity on the ammonia response and to confirm the results of the first sample, that the humidity influence is the lowest for the tested polymers.

The raw KP signal for a measurement over eight days is plotted in 5.28(a). The baseline at low humidity levels is hardly influenced by humidity up to 50% rh as seen in the raw data for one cycle in figure 5.28(b). The signal for 1 ppm of ammonia not very distinct in this measurement leading to the large uncertainty in the calibration curve as it was common for this polymer. The overall drift of the baseline is 20 mV in six days, after an initial strong drift at the beginning of the measurement.

A humidity influence on the ammonia signal is not evident and therefore all data were taken to calculate the calibration curve in figure 5.28(c). The overall sensitivity is 35 mV/decade for this layer. This is higher than for the thinner layer above, but the error is larger for the lower end of ammonia concentration.

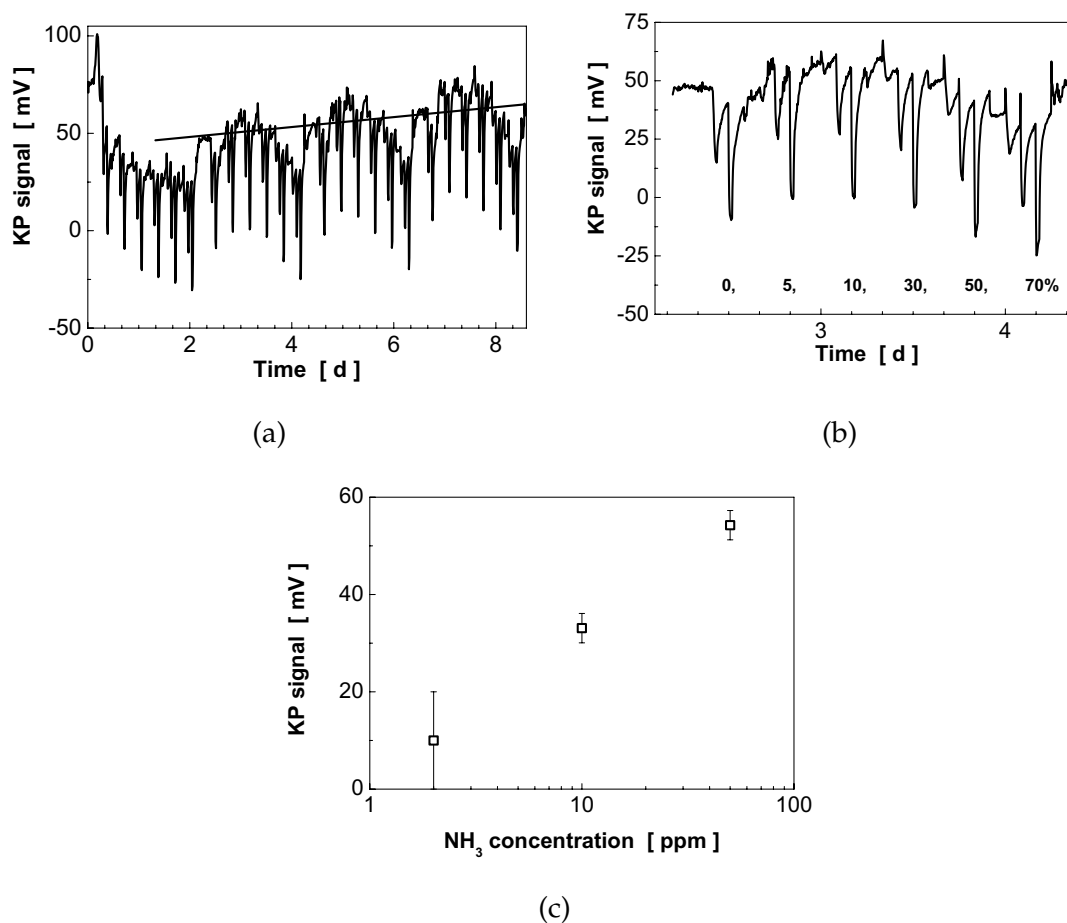


**Figure 5.28.:** KP measurement and results for ammonia in concentrations of 2, 10, and 50 ppm in dry and humid air (5 – 70% rh) for a PVPh coated sample (k2.PVPh.AuAl.43): (a) raw KP signal of a long time measurement over eight days, (b) blow-up of one measurement cycle, (c) resulting calibration curve for all cycles and all humidity levels.

The slight increase of the ammonia response was noticed in a set of spray-coated samples from 10 – 30 kHz\* and spin-coated samples of larger thickness. This example is not further elaborated here, but one can conclude from the observation made that the increasing coverage is the cause for the higher response, and this means the signal is not originating from the bare substrate but from the polymer coated areas.

**Summary of the Ammonia Results** PVPh layers prove to be stable in the KP experiments over time, after an initial ageing and loss of signal. The humidity influence is very limited. The measurements show a good linearity of the response on the logarithmic scale over 3 decades of concentration. However, there is a irreproducibility of the signal at the lower concentra-

tion end accompanied by a high error. Consequently, the LOD for PVPh is higher than for the previous polymers.

At last the results for ammonia are compiled in the following table to summarize the KP data.

**Table 5.7.:** Ammonia signal strength (10 ppm, in units of mV) and sensitivity (in units of mV/decade) for PVPh samples in dry/humid air (50% rh). Data for measurements on fresh and old samples.

Sample	Fresh		Old	
	Signal	Sensitivity	Signal	Sensitivity
k1.PVPh.AuAl.20	25	67	32	28/30
k2.PVPh.AuAl.43	-	-	33	35

#### 5.4.1.2. Response to Humidity and Cross Interferents

No cross interference to ethanol and toluene was measurable for PVPh samples with the KP. The humidity response is low. For details on the humidity signal see the experimental data in reference [162].

#### 5.4.2. Results of the Experiments on PVPh Coated QMB Sensors

##### 5.4.2.1. Response to Ammonia

The results of the ammonia experiments are shown in figure 5.29 for two measurements in a interval of 38 months, the first measurement being 13 months after preparation (in parallel to the KP experiment in figure 5.27(a)). Initially the response to ammonia is quite high as well as the humidity influence on the response, but both decrease significantly with time. The data indicate a Langmuir-Henry type of sorption behaviour.

PVPh coated QMB sensors show a poor performance when humidity was added to the carrier gas on the contrary to the KP measurements, where also at 80% rh a utilizable signal was obtained. The baseline is not stable and feature extraction difficult.

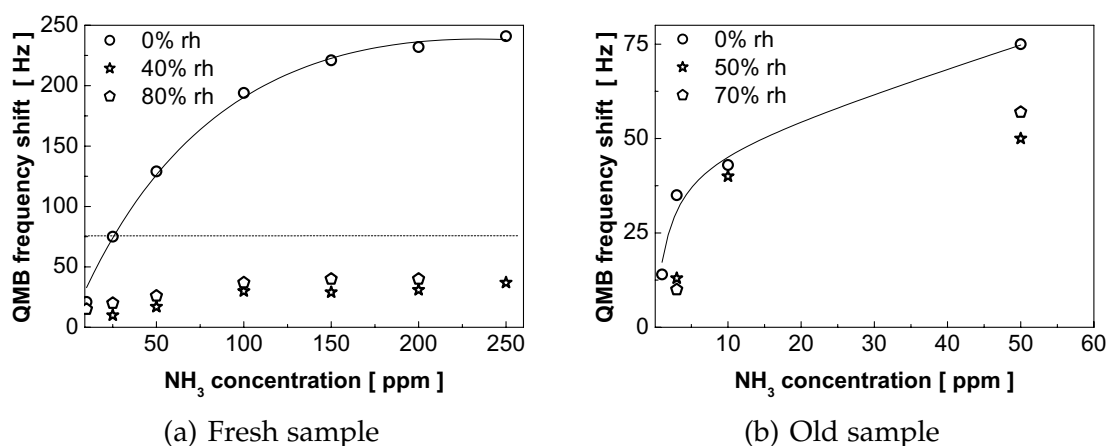


**Figure 5.29.:** QMB results for a PVPh coated sensor: ammonia at 0% rh and different humidity levels: (a) measurement of the freshly prepared QMB sensor and (b) after over three years. The line in the left graph indicates the full scale of the right graph.

#### 5.4.2.2. Response to Humidity and Cross Interferents

The response to humidity is large and follows a linear behaviour (see figure 5.30(a)) with an offset at low humidity levels. In additional experiments (not shown here) a linear increase of signal with increasing layer thickness was found.

The response to ethanol is high (200 Hz at 200 ppm) and much higher as for toluene (5 Hz) (see data in the bar chart of figure 5.30(b)), as one might expect the polar polymer PVPh. The signal decreases in humid air for ethanol, but remains constant on the low level for toluene.

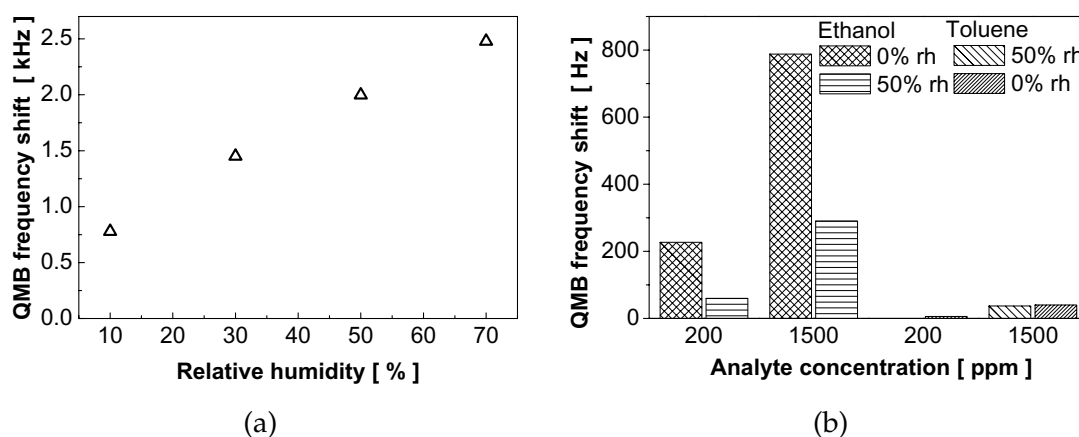


**Figure 5.30.:** QMB results for a PVPh coated sensor: (a) humidity signal for 10, 30, 50, 70% rh and (b) ethanol and toluene signal (at 0 and 50% rh).

Finally, the response to butylamine is reported. This analyte causes long adsorption times with large time constants. The signal is approximately 250 Hz for 200 ppm in dry air and only little affected by humidity leading to a slight increase of the signal.

### 5.4.3. Results of the IR Experiments on PVPh Layers

At last, PVPh coated substrates were characterized with the IR technique. The aforesaid experiments were repeated for ammonia and humidity with PVPh coated substrates. Ammonia exposure induces no changes in the spectra neither in dry nor in humid air. No peaks assigned to ammonium species could be identified in the spectra. Unfortunately, no further information is available for the interpretation of the KP results.

A spectrum of a PVPh layer is shown in comparison to a phenol spectrum (see figure 5.31(a).) One can observe that the peak corresponding to the OH group of the phenol group at  $3612\text{ cm}^{-1}$  is missing in the spectrum of the polymer probably due to a interaction between neighbouring chains and among next neighbours.

The change in the humidity level, on the contrary, can be followed with IR spectroscopy. Spectra for different humidity levels and dry air are presented in figure 5.31(b).

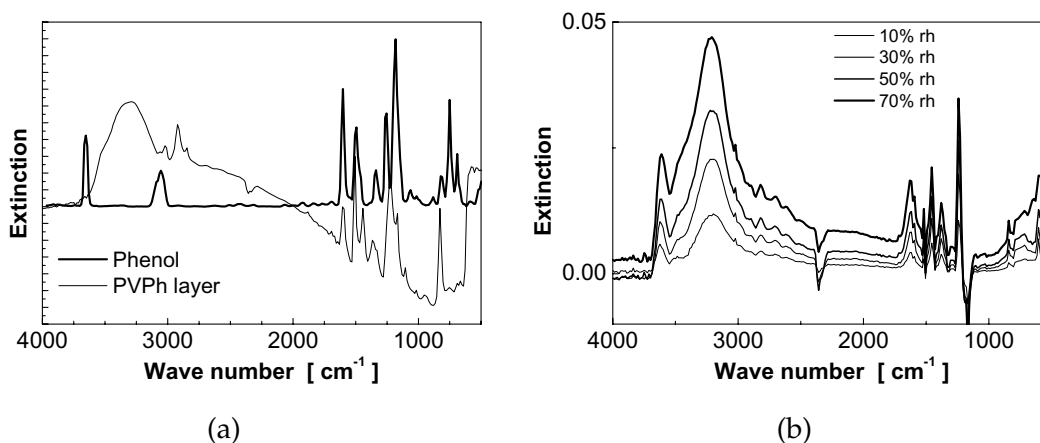


**Figure 5.31.:** IR spectrum of a PVPh layer on silicon: (a) the spectrum in dry air compared to a spectrum of phenol (both spectra normalized), (b) increasing levels of humidity.

At increasing level of humidity the peak at  $3612\text{ cm}^{-1}$  appears and grows. With increasing humidity in the ambient atmosphere more and more water is absorbed by the polymer. This results in an increasing broad peak at  $3210\text{ cm}^{-1}$ . Also all other peaks are increased in intensity. Thus, water



disturbs the interaction of the phenol OH groups. PVPh is a polar polymer and a high water uptake is expected similar as for PAA. In the region of  $3000 - 2500 \text{ cm}^{-1}$  peaks corresponding to hydrogen bonds between water and phenol groups appear. Water molecules are bridged between phenol OH groups.

## 5.5. Response of PAB Coated Substrates

Poly(acrylonitrile-co-butadiene) (PAB) layers were tested in measurements with ammonia in a concentration range of 1 – 200 ppm at 0% rh and at 40 – 50% rh. The layer ageing was evaluated in repetition of the experiments over 15 months to check whether the apparent ageing process influences the sensitivity. Additionally, an effort was made again to investigate the layer thickness dependency of the KP signal. The KP results are compared to the ones obtained with a QMB sensor. An overview of the tested KP and QMB samples is given in table 5.8. All samples were prepared from a solution of 10 mg/ml polymer dissolved in dichloromethane (DCM) using the manual deposition system.

**Table 5.8.:** Overview on the presented PAB coated KP and QMB samples.

Sample	Substrate	Note
k1.PAB.AuAl.XX	Au/Al	five samples, 0.03 – 0.5 $\mu\text{m}$
qmb.PAB.60	QMB	2x 30 kHz

PAB is one of the first positively tested examples with ammonia, but was abandoned after some instabilities of the signal and low response. Other than the ammonia response only the humidity influence and layer thickness influence on sensitivity are characterised.

### 5.5.1. Results of the KP Experiments on PAB Samples

**General Observations** In figure 5.32 a typical measurement (baseline corrected) is displayed for ammonia in dry and humid air for a sample with a calculated thickness of 160 nm. This measurement was recorded with an early KP set-up, which was causing the noise clearly seen in the KP signal. The baseline is quite stable, but the peak shape makes the evaluation of the signal difficult; this is considered as the source of the high error in the calibration curve.

## 5. Response to Analyte Gases

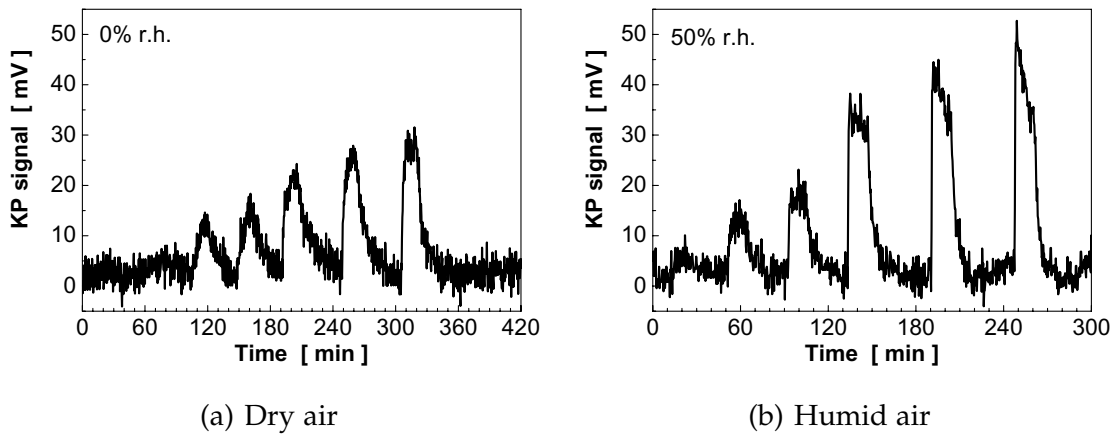


**Figure 5.32.:** KP results of a PAB spray coated substrate (k1.PAB.AuAl.20) for ammonia in concentrations of 1, 3, 10, 25, 50, and 100 ppm: KP signal (baseline corrected) (a) in dry air and (b) at 50% rh.

The plots in figure 5.33 show all available sensitivity data for this sample. It summarizes the results of two sets of measurements in dry and humid air over a time window of 15 months. The first ammonia measurement was taken only one year after preparation so the initial ageing of the layer can not be estimated. The data evaluation shows clearly that humidity enhances the sensing effect, but the sensitivity remains constant. A fit to the logarithmic representation of the data yields a sensitivity of 16 mV/decade and signal for 10 ppm of 10 mV in dry air and 20 mV/decade 20 mV in humid air.

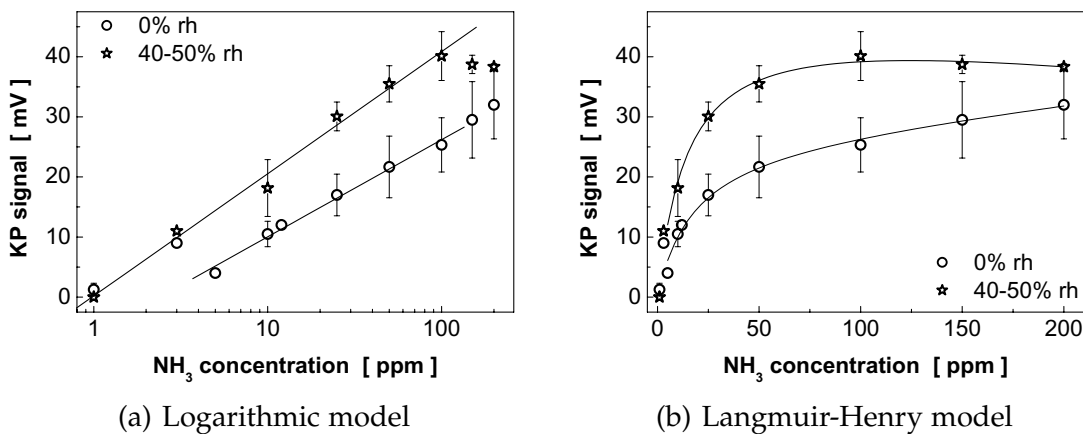


**Figure 5.33.:** KP results of a PAB spray coated substrate (k1.PAB.AuAl.20) for ammonia in concentrations of 1 – 200 ppm: a comparison of two models for the calibration curves.

In this case a saturation of the signal occurs and a dual mode isotherm fit

might be as suitable to represent the data. In figure 5.33 both possibilities are compared to each other. The Henry contribution is small and there is no linear term present.

**Layer Thickness Influence** In the next figure, 5.34(a), the effect of increasing layer thickness is shown on hand of the calibration curves for ammonia. The signal is lowered drastically by larger layer thickness and is inverted later in sign (5.34(b)). This is clearly a difference to the PAA samples, where there was no thickness influence, and to the PVPh samples, where the signal was increasing with layer thickness as substrate coverage was improved.

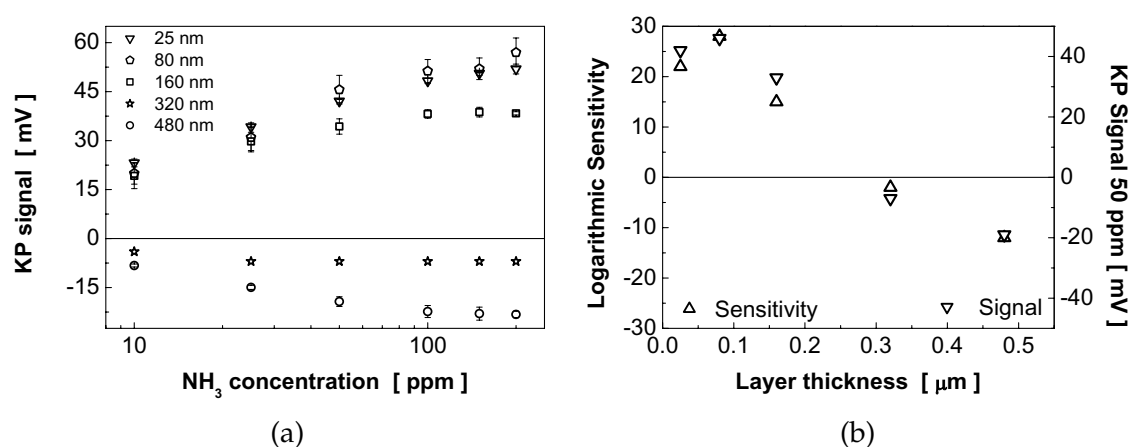


**Figure 5.34.:** KP results of PAB spray coated substrates of increasing thickness (30 – 500 nm.) for ammonia in concentrations of 10 – 200 ppm at 40% rh: (a) resulting calibration curves for the individual samples and (b) thickness dependency of signal and sensitivity.

In case of humidity the same course is observed. The lower the layer thickness the higher is the signal.

## 5.5.2. Results of the Experiments on PAB Coated QMB Sensors

The QMB responses to ammonia and the cross interferences to humidity, butylamine, ethanol, and toluene were tested. Typical QMB results of a QMB sensor coated with PAB are presented in this section.

### 5.5.2.1. Response to Ammonia

Figure 5.35 shows the evaluation of the QMB signal at 0, 50, 70% rh for ammonia in a concentrations of 2 – 50 ppm. One observes a strong increase of the QMB signal for ammonia with humidity from 30 to 180 Hz for 50 ppm.

There is not a linear dependency of the response with concentration, but more a Langmuir like isotherm getting more linear with humidity. The measurement was recorded after one year of sensor storage.

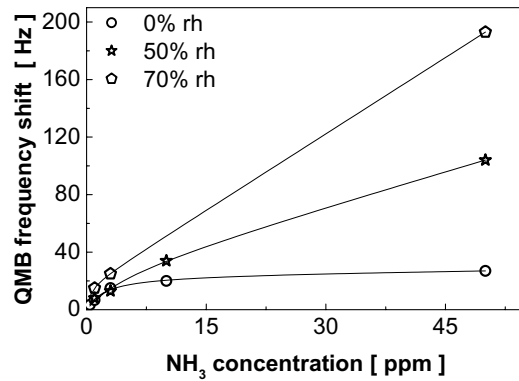


Figure 5.35.: QMB results for a PAB coated sensor: 2 – 50 ppm of ammonia at 0, 50, and 70% rh.

### 5.5.2.2. Response to Humidity and Cross Interferents

The signals for humidity, ethanol, and toluene are depicted in figure 5.36. The humidity signal is very strong. Frequency shifts up to 1.5 kHz for 70% rh were recorded. The response curve is linear over the tested range, but has an offset for low humidity levels.

Comparing the two test analytes shows that the signal is higher for ethanol than for toluene and decreased by humidity, whereas the toluene signal stays nearly constant.

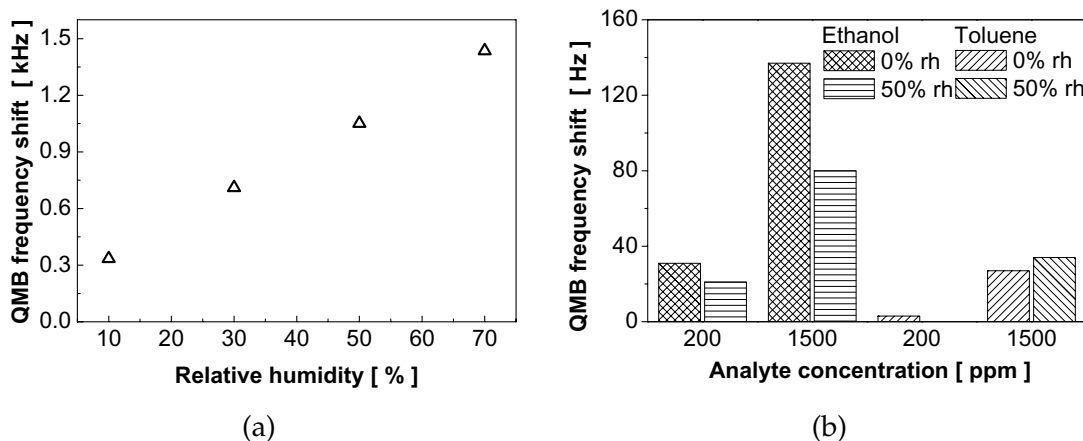


Figure 5.36.: QMB results for a PAB coated sensor: (a) humidity signal and (b) cross sensitivity to ethanol and toluene.

For n-butylamine the sorption processes are quite slow, not even nearly a equilibrium condition was reached during the normal exposure and purge time, making a signal extraction not possible. The estimated signal is higher than 150 Hz for 200 ppm ammonia in a dry atmosphere. Humidity increases the butylamine signal in a similar way as ammonia. The frequency shift is calculated to reach 600 Hz.

## 5.6. Response of PCPhS Coated Substrates

As the final example in this work of the positively tested polymers serves poly(cyanopropyl-phenyl-siloxane) (PCPhS). The most representative KP and QMB results for this polymer are presented shortly in this section for completeness. The gas testing experiments were concentrated on ammonia in a limited number of experiments as PCPhS was considered not ideal for sensor use after inspection of the substrate wetting capabilities presented in section 4. As a consequence, the sensitivity to other analytes than ammonia was not tested. The KP response to water vapour of this polymer is already reported in [162].

### 5.6.1. Results of the KP Experiments on PCPhS Samples

The presented KP sample (k.PCPhS.AuAl.20) is based on the alumina substrate Au/Al<sub>2</sub>O<sub>3</sub> coated with 20 kHz\* of PCPhS (10 mg/ml dissolved in DCM). Ammonia was dosed in a concentration of 10 – 200 ppm in experiments in dry and humid air, both at 40 or 50% rh. The results of the KP experiments are shown in figure 5.37 for the fresh sample and for the same sample after a storage time of 14 months. The initial response of the fresh KP sample is unstable in terms of baseline fluctuations and peak shape leading to large errors in the calibration curve for ammonia at 40% rh for repeated measurement cycles (see figure 5.37(a)).

As before for the other polymers a logarithmic response to ammonia in the KP experiments was found. In this case, however, saturation occurs at concentrations above 100 ppm. For PCPhS the signal for 10 ppm ammonia is in the order of 20 mV and the sensitivity was calculated to be around 23 mV/decade. In a repetition of the experiment in dry and humid air after 14 months (see figure 5.37(b)) no signal at all was obtained in humid air, whereas the signal in dry air is still present, but the lowest of the tested polymers. The signal for 10 ppm ammonia is 15 mV and the sensitivity was calculated to be 16 mV/decade.

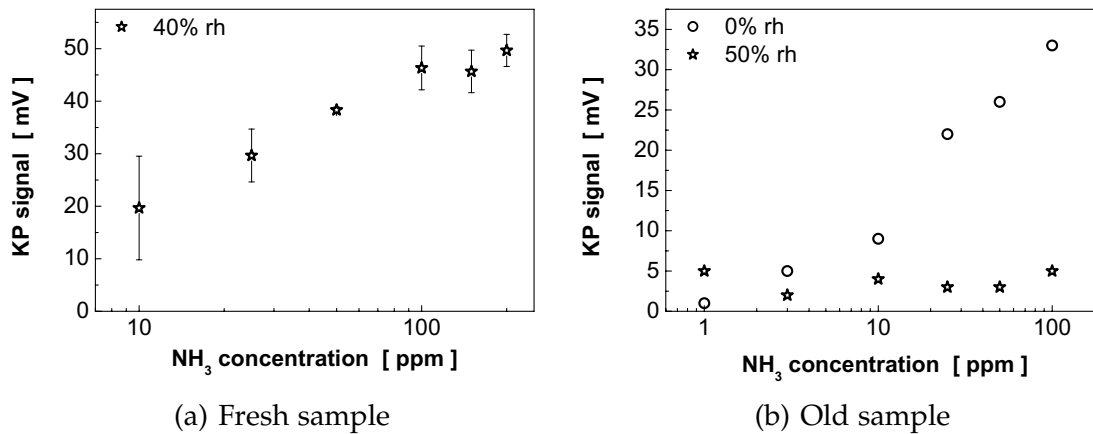


**Figure 5.37.:** KP results of a PCPhS spray coated substrate (k.PCPhS.AuAl.20) for ammonia in concentrations of 10 – 200 ppm at 40% rh: (a) initial signal after preparation and (b) signal after 14 months in dry and humid air.

Summarizing the findings means that the instability of the signal and the loss of signal, especially in the more important humid air condition, are remarkable and consequently PCPhS was omitted from the list of prospective candidates for a final sensor device. The high error even in directly repeated measurements allow only somewhat reliable ammonia detection in concentrations higher than 100 ppm.

### 5.6.2. Results of the Experiments on PCPhS Coated QMB Sensors

Typical QMB results of a sensor coated with PCPhS are depicted in figure 5.38 for 10 – 200 ppm ammonia and different levels of humidity. The QMB sensor signal for ammonia (figure 5.38(a)) at 40% rh and for humidity ranging from 0 to 80% rh (see figure 5.38(b)) are rather low, but relatively stable. One can observe a Langmuir type of response for ammonia and a highly linear response to humidity over the tested range typical for a bulk sorption process.

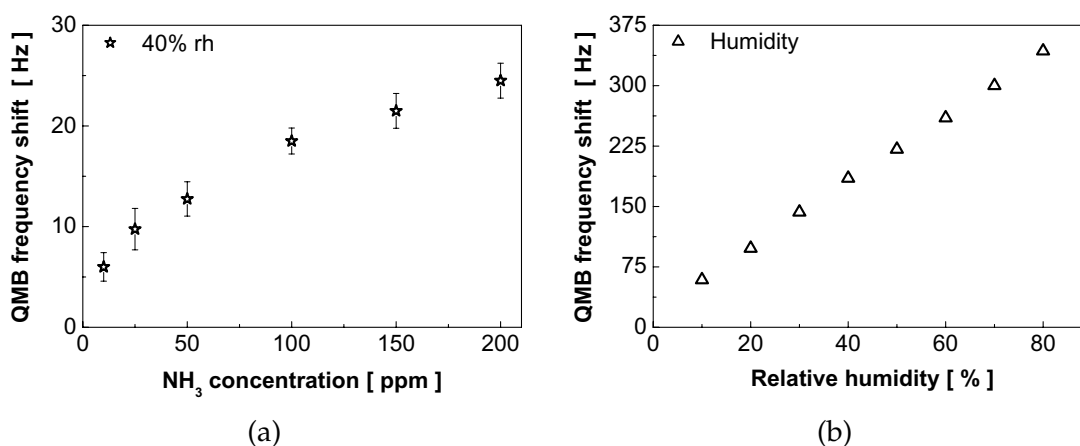


**Figure 5.38.:** QMB results for a PCPhS coated sensor (qmb.PCPhS.60): (a) ammonia in concentrations of 10 to 200 ppm at 40% rh and (b) different levels of humidity from 10 to 80% rh.

## 5.7. Summary of the KP and QMB Experiments

### 5.7.1. Results of the KP Experiments

The experiments have shown that conducting substrates coated with thin films of non-conducting organic polymers undergo potential changes upon gas adsorption, which can be read out with a KP and most probably potentiometric devices like the GasFET. This effect is not unique to the specific Kelvin probe used in this work, as the effect was already reproduced on other systems [163]. Furthermore, GasFETs with a suspended gate using the sensitive layers described in this work have already been tested and presented [164].

The KP results obtained so far are very promising and a good starting point for further investigations. It has been shown that a variety of polymer/substrate combinations exhibit potential changes in the range of 100 mV, when exposed to gases like ammonia in concentrations of only a few ppm. PAA was identified as the most suitable candidate for ammonia detection so far, but several other polymers show a nearly equal gas sensing properties.

The initially stated requirements—a signal higher than 10 mV for 10 ppm of ammonia and functionality at normal and high humidity conditions, operation at room temperature—concerning the gas sensing capabilities are mostly fulfilled. The response to ammonia is even higher than required. The measured 10 ppm ammonia signals range from 20 to 100 mV and the sensitivities from 15 to 50 mV/decade depending on polymer and measure-

ment condition. The most decisive factor is the kind of the polymer, the influence of the substrate is present, but minor. The determined detection limits are low and in the best case in the sub-ppm level. It was discovered that the response follows a logarithmic calibration curve, experimentally proven over 3 to 4 orders of magnitude.

The cross sensitivity to other analytes is quite low. Only other basic and presumably acidic compounds give a comparable response. This was clearly shown for n-butylamine. Humidity has only a minor influence on the ammonia signal and sensitivity. The influence is more indirect as the baseline stability is depending on the humidity content.

In the following, a concise summary for the individual polymer layers is given presenting the most prominent observations only. For details refer to the respective sections.

**PAA** PAA samples have the highest ammonia response in the KP experiments amongst the tested samples with a low cross sensitivity and influence of humidity. The LOD is in the sub-ppm range. The samples exhibit a good short time and long time stability. Several measurements cycles over weeks under operation show the high reproducibility in consecutive measurements. Additionally, the measurements were repeated over a long time period and no significant ageing of layers in terms of the sensing properties was found.

The response to analyte pulses is quite fast, but full recovery is quite slow. The time constants are rather independent of the physical properties like the thickness of the polymer layer. Recovery follows a two time constant model, one time constant is in range of minutes and the other one larger than 30 minutes.

The drift of the baseline is low, but increasing with humidity, especially for thin layers. There is no influence of layer thickness on the ammonia signal itself, only on the humidity influence on the stability of the baseline.

**PS** The PS samples show a lower response to ammonia than the PAA samples, but the LOD is still in the low ppm range. In contrast to PAA, there is a decay of the sensing properties in the first weeks after preparation. The response of the aged layers is very stable and hardly influenced by humidity. There is a small influence of humidity on the baseline and the drift behaviour is excellent. In the case of PS the KP signal decreases with increasing layer thickness.



**PVPh** PVPh samples have the lowest humidity influence in the ammonia exposure experiments. The medium high signal is stable over time after a small initial decrease of the signal. The error is high at the lower end of the tested concentrations range making PVPh more suitable of detecting high concentrations of ammonia. The response follows the logarithmic isotherm over a wide range at least up to 1000 ppm. The signal is increased with increasing layer thickness. This is explained by an increasing coverage of the substrate by the polymer, which is in general rather poor.

**Other Polymer Layers** The other sample types are much poorer in the ammonia sensing performance and not of interest in future studies. There is apparent ageing and poor performance in the presence of humidity.

### 5.7.2. Results of the QMB Experiments

All the different polymers used as sensitive layers on QMB sensors, except for PS, respond not only to ammonia but also to the other tested analytes and water vapour. Examples for ethanol, toluene, and n-butylamine are given in this work. Besides, the influence of background humidity on the analyte signal is often substantial. The cross sensitivity to humidity and the other analytes is often higher than the ammonia signal itself. It was noticed that the QMB sensors coated with the specific polymers of this work have in general a poor performance, especially at high humidity levels. The baseline is not very stable showing large fluctuations. This makes it difficult to confidently extract small signals.

The thickness dependency is as expected governed by a bulk sorption process. The QMB data give an indication that sorption of ammonia and the other analytes is not fully unspecific and includes some specific interactions. A dual-mode model was applied to fit the response data. The response and recovery times are longer than in the KP experiments, which is not only ascribed to the effect of the KP measurement chamber in series with the QMB set-up.

In the following, a short summary of the observation for the individual polymers is given. As the results are very different for the individual polymers, general values for the response cannot be given.

**PAA** The ammonia signal of PAA coated QMB sensors is very large. The ammonia signal reaches several thousand Hertz for 10 ppm of ammonia depending on the layer thickness. However, the result is strongly depending on the humidity content of the carrier gas, as the signal is very much in-

creased by present water vapour. The humidity and butylamine signals are in the same range. The responses to ethanol and toluene are much lower and quite equal. The frequency shift of the thickest layer is around 150 Hz for 1500 ppm of the two chemical species.

**PS** PS layers on QMB sensors show no response to ammonia at all, whereas the butylamine signal is measurable. The response to humidity is very slow and the corresponding time constants large. The response is higher to toluene as to ethanol and in the range of several hundred Hertz. There is hardly any influence of humidity on the signal for all analytes. This attributed to the hydrophobic character of PS.

**PVPh** A change of the sensing properties of PVPh coated QMB sensors was visible with time. The ammonia signal of the aged layers is lower than 100 Hz. The signal for ethanol and toluene are much higher reaching 200 Hz. The ethanol signal is higher than the toluene signal. Humidity decreases the signals for all analytes. This is the only exception, in which a lower signal was measured at higher humidity levels. It is the reason of the poor performance of PVPh coated QMB sensors. The humidity signal is in the order of kilohertz.

**PAB and PCPhS** The ammonia signal of PAB is lower than 40 Hz for 10 ppm in dry air and the humidity influence is substantial. In contrast to the rather low ammonia signal the humidity signal reaches 1.5 kHz. The response of PAB coated QMB sensors is higher to ethanol than to toluene and the signals are comparable to the ammonia response. QMB sensors with PCPhS as sensitive layer have a negligible ammonia signal and a humidity signal in the order of several hundred Hertz.

### 5.7.3. Results Reported by other Authors

To better judge the results obtained with PAA and the other polymers in this work experiments reported by other authors shall be summarized here in short. PAA is rarely used as a gas sensitive layer in chemical gas sensors. It is reported to be used in resonator devices, mainly QMB sensors, and in resistive structures. However, the strong sensitivity towards ammonia has been acknowledged. The data for the other polymers is even more sparse. As only few works report the use of PAA layers, they are summarized here individually.

Fairly recent publications by Nanto et al. [14, 15] describe the use of plasma-polymerized membranes made of acrylic acid on QMB sensors. The thickness of the layers is stated to correspond to a mass load of 6 kHz on 9 MHz QMB sensors. The PAA films were found sensitive to ammonia, methanol and acetaldehyde, but showed no sensitivity towards many other common volatile organic compounds (VOC). The ammonia sensitivity was measured in a range of 500 – 10000 ppm yielding frequency shifts of 100 – 600 Hz in a logarithmic response curve. Unfortunately, no humidity influence is given in the work. Polystyrene films prepared in a similar way were sensitive to all analytes, but little to ammonia. Many other acrylates are said to be sensitive to ammonia as well.

Electrospun nano fibres and multilayer Langmuir-Blodgett (LB) films of PAA plus a varying content of polyvinylalcohol (PVA) are reported by Ding et al. [16]. The deposition was stopped at a mass load of 10 kHz on 10 MHz QMB sensors. The electrospun films were chosen as a larger response due to a high surface area was expected. Pure PVA films do not exhibit a ammonia response: the higher the PAA content the higher is the ammonia signal. The authors present results for a film of 18 per cent PAA in more detail. The ammonia signal at 55% rh is 150 Hz for 50 ppm. The response is slow having long time constants. The response of the multilayer LB film is only 70 Hz. The humidity influence on the ammonia signal is as large as 300 Hz in a variation from 50 to 60% rh. Pure PAA layers prepared by the same technique were tested in a second study by the same authors [17]. The tested ammonia concentration range was then much lower. The signal to 130 ppb ammonia is reported to be 12 Hz showing a linear increase of signal with concentration. There is a linear increase of sensitivity with thickness of the QMB sensor coating. The absorption/desorption times increase as well. A similar influence of humidity as in the first study is reported. The sensitive layer is found to be stable over ten days. PAA is favoured by the authors more or less as a humidity sensing layer.

Other authors report measurements of PAA co-polymerized with isooctylacrylate as sensitive material on self-made resonator devices exposed to ammonia [13]. The thickness of the sensitive films is in the range of micrometres. There is a linear increase of signal with thickness and of the response time as well. The humidity response and the humidity influence on the ammonia signal, shown in a calibration curve for a 1:1 composition of the sensitive layer, are quite low. Only a slight increase of signal is observable. The humidity influence is the lowest for this 1:1 composition of the two compounds. A higher PAA content does not increase the ammonia response, but the humidity cross sensitivity. Thus, the rather hydrophobic isooctylacrylate reduces the humidity influence. They report a almost loga-

rhythmic response to ammonia in a concentration range of 0.1 to 100 v% and a linear response at lower levels. The LOD is 200 ppm for a 20 micrometre film in humid air.

Another work uses again plasma polymerized PAA films [165]. The response to different vapours, unfortunately excluding ammonia, of QMB coated with films of 270 – 1000 nm thickness was tested. Additionally, the plasma polymerized films are compared to cast film of similar thickness. The response and recovery of the cast films is slower, but the response pattern to the different analytes is the same. The longer time constants of the cast films are explained by the higher number of acidic groups in the cast films capable of hydrogen bonding. Hydrogen bonding is also considered the reason for the high response to water vapour, acetic acid, and ethanol. Next the thickness dependency of the signal is presented. Generally, the signal and sensitivity increase with thickness, but not in the case of some analytes. Unfortunately, this topic is not presented in much detail and no explanation is given for the observations.

The last work found relevant deals with cross linked PAA layers with a varying content of polyethyleneglycol (PEG), both pure and co-polymerized with acrylamide, in resistivity measurements during water exposure [159]. The cross linking agent is a diisocyanate species. The high water uptake and the capabilities of PAA of working in humidity sensors is confirmed. A switch type behaviour is reported, where the threshold level depends on the cross linking. The measured resistance changes over 3 – 4 magnitudes in the presence of humidity at the threshold humidity level. More humidity sensing experiments with polymers similar to PAA, mainly acids, are found in [166].

The polymers PS and PVPh are very scarcely used as sensitive layers. They show swelling behaviour and are used in resistive sensors with carbon black composite materials [167]. This sensor type relies on swelling and the mechanism is different and not relevant for this work.

### 5.7.4. Concluding Remarks

Unfortunately, the own QMB results are hardly comparable to the data found in the literature as the conditions and materials are not totally identical. Neither is it possible to compare the found results among each other. However, qualitatively, the trends in the sensor response are the same. The response to ammonia of the PAA layers and related acrylates is large, but normally the response to humidity and the humidity influence of the ammonia signal are overwhelming. PAA also responds to many other analytes. Besides, the response and recovery time constants of cast polymer

films are large, which is not favourable in sensor applications. The data available in the literature gives some strategies to avoid those drawbacks, especially needed for the use in QMB sensors: the use of hydrophobic compounds to minimize the humidity influence and modification of the coating technique to improve the response and recovery times. Plasma polymerized films seem to be superior to compact films in this respect.

The own results have shown that the QMB results are not comparable to the KP results. The initial expectation to use the fast and reliable QMB sensors as a pre-selection tool proved to be *not* possible. It was not possible to predict the response of the KP from the QMB results: sorption into the matrix and a high mass uptake is not enough! The differences are also evident in the response curves, logarithmic for the KP versus Langmuir-Henry for the QMBs, and in the different time behaviour. PAA is a good candidate for the use in GasFETs for the detection and quantification of ammonia judged on the performance in the KP experiments. On the contrast It is unusable in QMB sensors due to the high water response. The low humidity influence in the KP can probably be further improved by cross linking or usage of derivatives like the more hydrophobic poly(methyl acrylic acid) (PMAA). The cross sensitivity is already negligible and needs not many further investigations.

### 5.8. A Model for the Origin of the Observed KP Signals

After the detailed description of the experiments and presentation of the results, the task remains to provide an explanation for the observed effects based on the experimental data. Modelling the KP response of the polymer coated samples used in this work is not as straight forward as for metallic and semiconducting sensitive layers, where well established models can be applied to new materials. There is up to now no general mechanism proposed in the literature. Here, a first comprehensive attempt shall be presented to give an explanation of the mechanism, providing a basis for further investigations.

Chemical background knowledge and understanding the KP method give a starting point for the interpretation and help to understand the origin of the signal. Modelling should be ideally independent of the type of polymer and substrate as well as cover all observations.

In general, there are several possible contributions to the overall KP signal in samples consisting of an insulating polymer layer on top of a conducting substrate: polarization within the polymer layer due to an orientation of permanent dipoles of the polymer, formation of a dipole layer at the

polymer/substrate interface (the double layer (DL) of the substrate) or the polymer layer surface, and a distribution of charges. This was explained in section 2.4.3.2.

The effects observed with the KP on the type of samples used in this work are assumed to originate at the polymer/substrate interface as a result of a modification of the DL. The low thickness dependency of the KP signal supports the assumption of an interface phenomenon at the substrate surface, as well. The polymers under study have no net dipole moment nor can the presence of charges be explained, making the other two aforementioned possibilities seem unlikely. A capacitive effect of water was not observed either, which would be an indication of charges on the surface.

Thus, let us look firstly at the substrates as they play an important role. In section 2.3.2 several possibilities are presented, how gas adsorption or surface modifications can change the DL of a solid. All substrate surfaces are expected to contain surface OH groups due to ageing as hydrolysis takes place over time on most metallic and non metallic surfaces. Gold surfaces are oxidised, alike, but to a lower extent. Untreated gold surfaces used e. g. as gold electrodes are reported to have only a relative OH surface coverage of 0.1%. The  $\text{pH}_{pzc}$  of the same gold electrodes is said to be  $\text{pH} = 4.95$  [168]. These figures cannot be directly applied to the gold substrates in this work, as they depend on the treatment and surface roughness of the gold layer, but they serve as a proof of the existence for surface OH groups. Most metals have 10% surface coverage of OH groups. Also silicone surfaces are easily oxidized and hydrolyzed by water. The density of surface atoms of flat, ideal surfaces is in the range of  $10^{15} \text{ cm}^{-2}$ . Surface atoms not occupied with OH groups are free to interact with analyte molecules directly. The potential change and the work function change is given by the Helmholtz equation, equation (2.29), for all dipolar species at the substrate/polymer interface.

The polymers' influences are normally the result of their sorption capabilities. However, the chemical nature seems of less importance in the KP experiments than in the QMB measurements. In the later case the chemical interactions clearly determine the degree of sorption and thus the response to different analytes. For the KP the effects are not yet understood. Nevertheless, the polymers increase the concentration of analyte molecules in the proximity of the substrate surface over the polymer free substrate. PS can be seen as an exception. However, a KP response is still present.

At last, one has to take into consideration the presence of water molecules, as this seems to be the most influential factor, deciding which processes at the surface are most dominant. Especially, the polar polymers PAA, PVPh, and PAB absorb large amounts of water and they are reported to always

contain residual water, even after long storage times in dry air. Thus, two possible mechanisms are proposed and the two contributions might account for the overall signal, each of which is more dominant in dry and humid air, respectively.

**Experiments in Dry Air** Under dry conditions still a small number of water molecules is presumably present in the polymer layer and at the surface of the substrate. This residual water is not removed by purging with dry air at room temperature. In the nearly absence of water, the surface sites act as predominately as Lewis centres, whereas in the presence of high concentration of water they are more likely to act as Brønstedt centres.

The substrates in this work are not comparable in their surface properties to single crystals, which are mostly used in basic adsorption studies as presented previously. Besides, the measurement conditions are different from ultra high vacuum (UHV) conditions. Consequently, one must consider the effect of oxidization, contaminations, and adsorbed species from the ambient: ammonia adsorption on the substrates used in this work might occur similarly, but only to a lesser extend. Water molecules themselves can participate in Lewis acid-base reactions, too, and they are always present in a physisorbed state on the surfaces. All those adsorption processes influence the potential by changing the intrinsic DL of the substrate and by the dipole moment of the adsorbed layer. It was indicated before that a change in a surface layer of water molecules is able change the surface potential by a high degree.

Water molecules compete with ammonia to occupy surface sites. Addition of ammonia changes the ratio of adsorbed water and ammonia molecules. This accounts for the work function changes. For an illustration of the reaction see the schematic drawing in figure 5.39.

Chemical reactions occurring during chemisorption are considered less likely at room temperature as oxidic surfaces are chemically not very active at low temperatures.

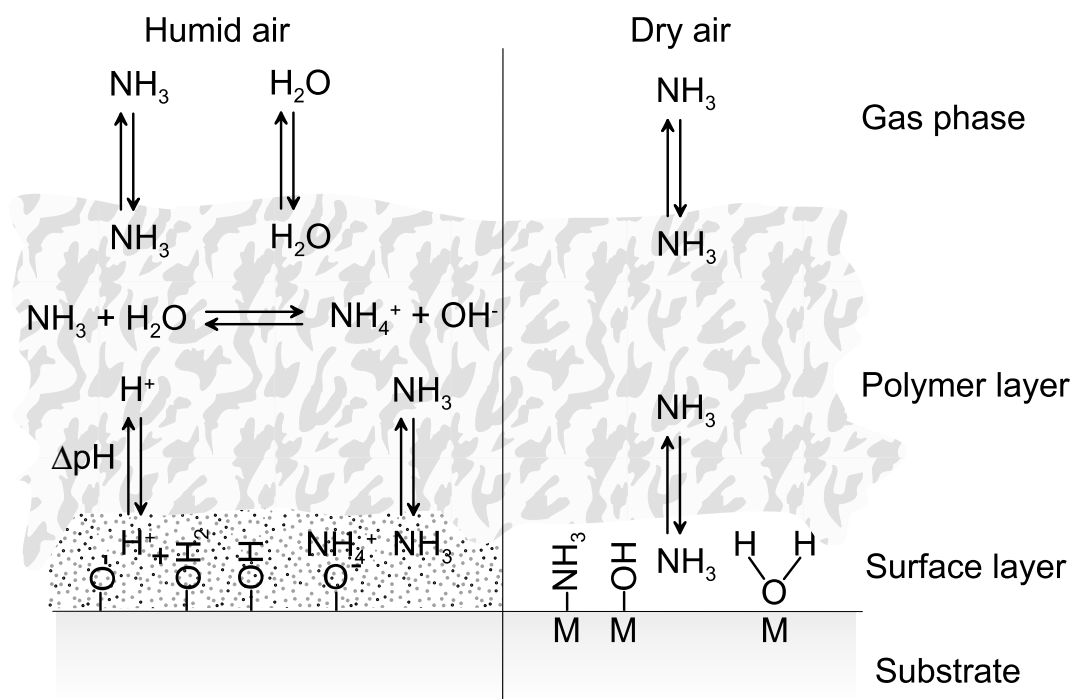


**Figure 5.39.:** Proposed chemical equilibria and chemical species involved in the overall mechanism.

**Experiments in Humid Air** For the explanation of the effects in humid air one should recall the observations made by Nazarov and Thierry [53]. They present KP studies of acidic/basic polymer coated metals and monitor the work function changes due to the polymer deposition. The functional groups of the polymers react with surface OH groups in a Brønstedt acid-base reaction, but only if water molecules are present, i.e. in humid air. The reaction leads to a change in the number and kind of surface dipoles. A formation of different surface species is proposed, for example  $\text{RR}'\text{-NH}_2^+ \text{-OFe}$  or  $\text{RR}'\text{-COO}^- \text{+Fe}$  in the case of steel surfaces. The potential changes reach normally several hundred millivolts. For certain polymer/metal combinations potential changes of 1 V were achieved.

In humid air condensation of water molecules takes place on the substrates and a surface layer of water is formed. This effect is strongly enhanced by the polar polymers. The high water uptake is visible in the high response of the QMB sensors to water vapour and in the IR spectra taken during humidity exposure. A full site-binding model with a Triple Layer Model (TLM) description of the double layer in solution is surely exaggerated, but can help to understand the surface reactions. If any model for a solution is considered a compact capacitor like model seems to be the most



suitable. In the case of PAA, this model is even more favoured as PAA is a strong electrolyte and the ionic strength causes a strongly diminished diffuse layer.

Ammonia is highly soluble in water and it has a high affinity to any condensed water in the polymer matrix and at the substrate surface. The high solubility is supported by the QMB measurements where the ammonia signal is regularly increased by humid air. About 702 l of gaseous ammonia can be dissolved in 1 l of water at a temperature of 20 °C. This is a concentration of 29 mol/l. The Henry constant for ammonia in neutral water is reported to be  $\approx 601$ /mol/bar.

Ammonia molecules absorbed in water get hydrated and react partly as a weak base ( $pK_b = 4.75$ ) in an acid-base reaction with water molecules. The amount of absorbed ammonia and the degree of protonation depends on the pH of the solution. In our case, this chemical reaction changes the pH of the polymer matrix and of the water layer at the surface. Neither one is a real aqueous phase, thus, the term pH has to be used with care. A change in pH due to the ammonia reaction with water influences the concentration of the individual surface OH groups, as the degree of protonation or deprotonation is a function of pH. This mechanism resembles the working principle of a pH sensitive ISFET using e. g. SiO<sub>2</sub> as sensitive material. Additionally, the created ammonium ions can adsorb at the surface.

n-Butylamine is an even stronger base ( $pK_b = 3.2$ ) than ammonia and is highly soluble as ammonia in water. Consequently, the same effects are expected.

Put together these individual stages can explain the observed KP results. An accompanying illustration is presented in figure 5.39.

- The deposition of polymers leads to a new equilibrium distribution of surface species and an initial change of the surface potential. Especially PAA has a highly acidic character and the effect is expected to be large for this polymer. The use of basic polymers is foreseen to be favourable for the detection of acidic chemical species in this respect, as the number of protonated surface species is reduced.
- Added ammonia reacts partly with the absorbed water in the polymer layer to yield ammonium ions. This seems to take place significantly only in PAA, as the IR measurements have proven the existence of ammonium ions only in PAA. Ammonia is dissolved more strongly at low pH and PAA is acidic. A fraction of the ammonium ions reach the surface layer.
- The remaining ammonia molecules, which are not dissolved in the polymer layer, reach partly the substrate surface by diffusion through

the polymer. There hydration and a reaction with water takes place.

- These two reactions change the pH of the surface layer indirectly or directly. The change in pH leads to a new equilibrium of the surface groups similarly to a site-binding model presented in section 2.3.3.2. Besides, the ammonium ions can donate protons directly to surface OH groups depending of the acidic/basic character of the groups in respect the ammonium ions or they can bind to negatively charged surface groups.
- The different dipole moments of all surface species contribute to the surface potential:  $\text{MOH}$ ,  $\text{MO}^-$ ,  $\text{MOH}_2^+$ , and  $\text{MO}^-\text{NH}_4^+$ . Changes in concentration of the individual species with their different dipole moments changes the effective dipole moment and work function of the substrate.
- The second reaction pathway is the direct reaction of ammonia molecules with surface OH groups supported by water molecules. The change of work function is then just the difference of the dipole moments of  $\text{MOH}$  and  $\text{MO}^-\text{NH}_4^+$ .

It was shown that the bare substrate show similar effects. This is an indication that the phenomenon originates at the substrate surface. However, the polymer layer make the effect more reproducible and enhances the effect via the partitioning effect.

Additionally, a few oriented water molecules and some  $\text{M}-\text{NH}_3$  species may be present as in the dry air case adding up to the overall effect. The lower the density of OH groups and the lower the number of water molecules the higher is the contribution of a direct metal–ammonia interaction.

**Humidity Influence** In this model the low influence of humidity on the signal is understandable. It seems sufficient, if a certain level of water is present to prefer the Brønstedt reactions. Water molecules act as a enabler of the reactions of ammonia or protons with surface OH groups. Thus, the humidity influence is low in the KP experiments in contrast to the QMB measurements, because the QMB sensors are sensitive to the total mass load.

**Limited Cross Interference** Ethanol and toluene are not capable of participating in acid-base reactions. Thus, they do not change the pH at the surface. Neither do they react with surface OH groups. The small signal may be the result of some disturbances in the surface water layer. n-Butylamine, on the other hand, is chemically similar to ammonia. It is highly soluble in

water and acts as a Brønstedt base in the same way as ammonia. Consequently, a high KP signal is expected and confirmed by the experiments.

**Time Constants** An explanation of the shorter recovery time and response time of the KP in contrast to the QMB and IR can be proposed. The later two techniques are more sensitive to changes in the bulk, not to changes at the interface to the substrate. Ammonia sorption is fast and already an initial low concentration contributes in a instantaneous reaction with surface groups to the main effect. Humidity uptake is a slower process until equilibrium is reached. The same holds for recovery. Sorption from a PAA layer is even slower due to its acidic character.  $\text{NH}_4^+$  needs to undergo deprotonation for desorption.

**Quantitative Interpretation** To calculate the absolute effect is difficult. Several steps have to be considered leading to the overall response: sorption to the polymer bulk, the acid-base equilibrium, and the different interactions with the substrate surface. Thus, it is not expected to observe a sensitivity in the Nernstian limit. Even in ISFETs this limit is not reached in many cases. It depends on the density and acidity/basicity of the surface OH groups.

**Temperature Dependency** A full quantification of the temperature effect is equally difficult and only some aspect can be given. The temperature influences not only the partition coefficient, but also the equilibria of all involved reactions. It was observed that the sensitivity decreases with increasing temperature. In this picture the temperature dependency can be understood as following: at higher temperatures, the solubility of ammonia in water decreases as well as the amount of water itself on the surface. Therefore, the amount of ammonia which is present at the substrate surface and which is able to react with adsorption sites is reduced and the sensitivity decreases.



## 6. Conclusion and Outlook

### 6.1. General Conclusions

In this work a large variety of Kelvin probe (KP) measurements on polymer coated substrates during gas exposure are presented for the first time. It was discovered that a number of non-conducting polymer layers on conducting substrates show potential changes in the range of 100 mV when exposed to gases like ammonia in very low concentrations.

Prior to the extensive characterisation with the KP, the layers were optimized especially in layer roughness and substrate coverage. The optimal deposition parameters and general observations are reported making one able to prepare the sensitive layers as desired.

It was achieved to identify and to extensively characterize a set of polymers with high responses to ammonia in the Kelvin probe at room temperature, which are to be used in gas sensitive field effect transistor (GasFET) devices. The main focus was set on ammonia as the target analyte. The experiments also cover the humidity influence and cross interferences to ethanol and toluene. Polyacrylic acid (PAA) seems to be most suitable among the different polymers—poly(4-vinylphenol) (PVPh), polystyrene (PS), poly(acrylonitrile-co-butadiene) (PAB), poly(cyanopropylphenyl-siloxane) (PCPhS)—for the ammonia detection with the KP and, presumably, the GasFET. It shows a large signal and sensitivity in addition to low humidity sensitivity. The long time stability is excellent. The initially stated requirements for the gas sensing properties are fully met. The transferability of the KP result to the GasFET has been shown in the meantime by Oprea et al. [164].

The origin of the measured effect is not yet fully clarified and data for model building were gathered by parallel investigations with conventional mass sensitive sensors, the quartz micro balance (QMB), and in infrared (IR) measurements. A comparison of the sensor techniques showed that the QMB, relying purely on mass uptake, and the KP method, sensitive to potential changes, were found not to be comparable. This was much under discussion at the beginning of this work.

Consequently, a first qualitative model for sensing mechanism has been proposed based on the data obtained for several polymer/substrate combinations. It is able to explain the origin of the KP signal for basic analytes

and introduces a first understanding of the observed low humidity influence.

### 6.2. Outlook

The presented results may serve as a starting point and guide for further experiments. The future experiments might follow two directions of equal interest: scientific exploration of the phenomenon and application oriented development.

Firstly, the experiments necessary to fully understand and predict the response of the samples in the KP are only at the very beginning. A broader data base is desired for modelling all aspects of the observed phenomena. Besides, following the ideas presented in this work one needs to focus more on the substrates. The effect of surface modifications will help to support or correct the stated model. The final goal of modelling would include a quantification and prediction of the KP signal for a given polymer/substrate combination.

Secondly, a detailed characterisation and optimisation of the sensitive layer for the application in commercial devices is necessary: qualitative measures for drift, accuracy, noise, and response & recovery times as well as sensitivity and signal height. This cannot be done with the KP only, as the whole sensor device is required to meet the requirements by the application and some measures are different for the GasFET.

Finally, one also might want to focus on the sample preparation procedure and technique. Research in this direction may also help to improve the gas sensing performance as layer prepared by different techniques can have different gas sensing properties.

## A. The Grahame Equation

Grahame derived a relation between the net surface charge  $\sigma$  and the potential  $\psi_0$  at the surface based on the Gouy-Chapman model for the double layer (DL). In the following only monovalent cations and anions are assumed to be present.

The net charge at the surface is compensated by the charges in the diffuse layer  $\sigma_d$  (electroneutrality condition)

$$\sigma = -\sigma_d = -\int_0^{\infty} \rho(x) dx \quad (\text{A.1})$$

The potential  $\psi(x)$  and the charge density  $\rho(x)$  are linked via the Poisson equation in one dimension

$$\frac{d^2\psi(x)}{dx^2} = -\frac{\rho(x)}{\varepsilon\varepsilon_0} \quad (\text{A.2})$$

The charge density can be expressed in terms of the concentration of ions. The concentration of ions in the presence of a potential is linked to the concentration in solution  $c_0$  via a Boltzmann distribution function

$$\rho(x) = e(c_+(x) - c_-(x)) = c_0e\left(e^{-\frac{e\psi(x)}{kT}} - e^{\frac{e\psi(x)}{kT}}\right) \quad (\text{A.3})$$

Given the relation  $2 \sinh y(x) = e^{-y(x)} - e^{y(x)}$  and using the common substitution  $y(x) = \frac{e\psi(x)}{kT}$ ,  $y(x)$  being a dimensionless potential, leads to

$$\frac{d^2y(x)}{dx^2} = \frac{c_0e^2}{\varepsilon\varepsilon_0kT}(e^{y(x)} - e^{-y(x)}) = \kappa^2 \sinh y(x) \quad \kappa = \sqrt{\frac{2c_0e^2}{\varepsilon\varepsilon_0kT}} \quad (\text{A.4})$$

$\kappa$  is a measure for the thickness  $\lambda_d$  of the diffuse layer, as the Debye length is given as the inverse of  $\kappa$ .  $I_c = c_0e^2$  is the ionic strength of the solution. Solving the Poisson-Boltzmann equation for the potential shows that the potential decreases approximately exponentially in the diffuse layer.

Using the Poisson-Boltzmann equation (A.4) becomes

$$\sigma = \varepsilon\varepsilon_0 \int_0^{\infty} \frac{d^2\psi(x)}{dx^2} dx = -\varepsilon\varepsilon_0 \left. \frac{d\psi(x)}{dx} \right|_{x=0} \quad (\text{A.5})$$

### A. The Grahame Equation

---

as the potential vanishes at  $x \rightarrow \infty$  and thus the gradient of the potential at infinity is zero.

Making use of

$$\frac{dy(x)}{dx} = -2\kappa \sinh y(x)/2 \quad (\text{A.6})$$

and substituting back  $y(x)$  for the integration we finally get the Grahame equation

$$\sigma = \sqrt{8\epsilon\epsilon_0 c_0 kT} \sinh \frac{e\psi_d}{2kT} = \frac{4c_0 e}{\kappa} \sinh \frac{e\psi_0}{2kT} \quad (\text{A.7})$$



## Bibliography

- [1] T. Seiyama, A. Kato, K. Fujushi, and M. Nagatani. A new detector for gaseous components using semiconductive thin films. *Analytical Chemistry*, 34:1502, 1962.
- [2] N. Taguchi. Japan Patent 45-38200, 1962.
- [3] W.H. King, Jr. Piezoelectric sorption detector. *Analytical Chemistry*, 36(9):1735–1739, 1964.
- [4] I. Lundström, A.S. Shivaraman, and L. Lundkvist. Hydrogen sensitive MOS field effect transistor. *Applied Physics Letters*, 26:55, 1975.
- [5] M. Fleischer, B. Ostrick, R. Pohle, E. Simon, H. Meixner, C. Bilger, and F. Daeche. Low-power gas sensor based on work-function measurements in low-cost hybrid flip-chip technology. *Sensors and Actuators B*, 80:169–173, 2001.
- [6] M. Fleischer and H. Meixner. *Advanced Gas Sensing*, chapter Markets and industrialisation of low-power sensors based on work function measurements, pages 161–184. Kluwer Academic Publishers, 2003.
- [7] J. Janata. Thirty Years of CHEMFETs – A Personal View. *Electroanalysis*, 16(22):1831, 2004.
- [8] B. Timmer, W. Olthuis, and A. van den Berg. Ammonia sensors and their applications - a review. *Sensors and Actuators B*, 107:666–677, 2005.
- [9] K.T. Lau, S. Edwards, and D. Diamond. Solid-state ammonia sensor based on Berthelot’s reaction. *Sensors and Actuators B*, 98:12–17, 2004.
- [10] M. Bendahan, P. Lauque, J.-L. Seguin, K. Aguir, and P. Knauth. Development of an ammonia gas sensor. *Sensors and Actuators B*, 95: 170–176, 2003.
- [11] B. Ostrick, R. Pohle, M. Fleischer, and H. Meixner. TiN in work function type sensors: A stable ammonia sensitive material for room temperature operation with low humidity cross sensitivity. *Sensors and Actuators B*, 68:234–239, September 2000.
- [12] V. Georgieva, E. Radeva, and L. Spassov. Ammonia sorptive properties of plasma polymer films obtained from hexamethyldisiloxane. *Vacuum*, 58:315–320, 2000.

- [13] Q.Y. Cai, M.K. Jain, and C.A. Grimes. A wireless, remote query ammonia sensor. *Sensors and Actuators B*, 77(3):614–619, 2001.
- [14] H. Nanto, Y. Hamaguchi, Y. Yokoi, S. Kurosawa, T. Oyabu, E. Kusano, and A. Kinbara. A smart ammonia gas sensor using QCM with plasma-polymerized membrane. *Sensors and Materials*, 2(13):69–76, 2001.
- [15] H. Nanto, Y. Hamaguchi, S. Sanada, K. Nobuyama, T. Matsumoto, K. Tanabe, and S Kurosawa. Plasma-polymerized-film coated QCM gas sensor for environmental monitoring. *Chemical Sensors*, 17:363–365, 2001.
- [16] B. Ding, J. Kim, Y. Miyazaki, and S. Shiratori. Electrospun nanofibrous membranes coated quartz crystal microbalance as gas sensor for NH<sub>3</sub> detection. *Sensors and Actuators B*, 101:373–380, 2004.
- [17] B. Ding, M. Yamazaki, and S. Shiratori. Electrospun fibrous polyacrylic acid membrane-based gas sensors. *Sensors and Actuators B*, 106:477–483, 2005.
- [18] V.V. Chabukswar, S. Pethkar, and A.A. Athawale. Acrylic acid doped polyaniline as an ammonia sensor. *Sensors and Actuators B*, 77:657–663, 2001.
- [19] G.K. Prasada, T.P. Radhadkrishnan, D. Sravan Kumar, and M. Ghanashyam Krishna. Ammonia sensing characteristics of thin film based on polyelectrolyte templated polyaniline. *Sensors and Actuators B*, 106:626–631, 2005.
- [20] The Advantagas project, IST 2001-33148: “Advantageous applications of gas sensors for security and consumer applications”.
- [21] Lord Kelvin. Contact electricity of metals. *Philosophical Magazine*, 46: 82, 1898.
- [22] N.F.A. van der Vegt, W.J. Briels, M. Wessling, and H. Strathmann. The sorption induced glass transition in amorphous glassy polymers. *Journal of Chemical Physics*, 110(22):11061–11069, 1999.
- [23] A. Arce, F. Fornasiero, O. Rodriguez, C.J. Radke, and J.M. Prausnitz. Sorption and transport of water vapour in thin polymer films at 35°C. *Physcial Chemistry Chemical Physics*, 6:1003–108, 2004.
- [24] J.W. Grate and M.H. Abraham. Solubility interactions and the design of chemically selective sorbent coatings for chemical sensors and arrays. *Sensors and Actuators B*, 3:85–111, 1991.
- [25] A. Hierlemann, E.T. Zellers, and A.J. Ricco. Use of linear solvation energy relationships for modeling responses from polymer-coated

- acoustic-wave vapor sensors. *Analytical Chemistry*, 2001.
- [26] J.W. Grate. Acoustic wave microsensors arrays for vapor sensing. *Chemical Reviews*, 100:2627–2648, 2000.
- [27] M.H. Abraham, J Andonian-Haftan, C.M. Du, V. Diart, G.S. Whiting, J.W. Grate, and R.A. McGill. Hydrogen bonding. Characterisation of 14 sorbent coatings for chemical microsensors using a new solvation equation. *Journal of the Chemical Society Perkin Transactions*, page 369, 1995.
- [28] S.J. Patrash and E.T. Zellers. Characterization of polymeric surface acoustic wave sensors coating and semiempirical models of sensor responses to organic vapors. *Analytical Chemistry*, 65:2055–2066, 1993.
- [29] R.A. McGill, M.H. Abraham, and J.W. Grate. Choosing polymer coatings for chemical sensors. *CHEMTECH*, 24(9):27–37, 1994.
- [30] R. Srinivasan and I.I. Suni. Differential capacitance studies of the specific adsorption of thiosulfate on silver. *Journal of Applied Electrochemistry*, 25:993–998, 1998.
- [31] C. Fietzek, K. Bodenhöfer, P. Haisch, M. Hess, M. Hanack, S. Steinbrecher, F. Zhou, E. Plies, and W. Göpel. Soluble phthalocyanines as coatings for quartz-microbalances: specific and unspecific sorption of volatile organic compounds. *Sensors and Actuators B*, 57:88, 1999.
- [32] A. Hierlemann, A.J. Ricco, K. Bodenhöfer, and W. Göpel. Effective use of molecular recognition in gas sensing: Results from acoustic wave and in situ FT-IR measurements. *Analytical Chemistry*, 71:3022, 1999.
- [33] F.L. Dickert, A. Haunschild, V. Kuschow, M. Reif, and H. Stathopoulos. Mass-sensitive detection of solvent vapors. Mechanistic studies on host-guest sensors principles by FT-IR spectroscopy and BET adsorption analysis. *Analytical Chemistry*, 68:1058–1061, 1996.
- [34] Y. Miyahara, Tsukada K., and H. Miyagi. Field-effect transistor using a solid electrolyte as a new oxygen sensor. *Journal of Applied Physics*, 63(7):2431–2434, 1988.
- [35] W.I. Cho, C.W. Yi, J.B. Ju, B.W. Cho, and K.S. Yun. Characteristics of a thin-film LaF<sub>3</sub> solid electrolyte for oxygen sensing. *Sensors and Actuators B*, page 149–153, 1991.
- [36] S.K. Choi, C.W. Yi, W.I. Cho, B.C. Cho, J.B. Ju, K.S. Yun, and N. Yamazoe. A MOSFET type sensor for oxygen sensing LaF<sub>3</sub> as a gate material. *Sensors and Actuators B*, 13:45–48, 1993.
- [37] D. Blackwood and M. Josowicz. Work function and spectroscopic studies of interactions between conducting polymers and organic va-

- pors. *Journal of Physical Chemistry*, 95:493, 1991.
- [38] K. Domansky, D.L. Baldwin, J.W. Grate, T.B. Hall, J. Li, M. Josowicz, and J. Janata. Development and calibration of field-effect transistor-based sensor array for measurement of hydrogen and ammonia gas mixtures in humid air. *Analytical Chemistry*, 70:473, 1998.
- [39] J. Janata. Chemical modulation of the electron work function. *Analytical Chemistry*, 63:2546, 1991.
- [40] J. Janata and M. Josowicz. Chemical modulation of work function as a transduction mechanism for chemical sensors. *Accounts of Chemical Research*, 31(5):241, 1998.
- [41] N. Barsan and U. Weimar. Conduction model of metal oxide gas sensors. *Journal of Electroceramics*, 7:143–167, 2001.
- [42] M. Iwamoto and E. Itoh. Nano-electrostatic phenomena in Langmuir-Blodgett films. *Thin Solid Films*, 331:15, 1998.
- [43] E. Itoh and M. Iwamoto. Electronic density of state in metal/polyimide Langmuir-Blodgett film interface and its temperature dependence. *Journal of Applied Physics*, 81:1790, 1997.
- [44] E. Itoh, H. Kokuno, M. Iwamoto, S. Roth, and M. Hanack. Electrostatic phenomena in  $\pi$ -conjugated Langmuir-Blodgett films on metal electrodes. *Journal of Applied Physics*, 37:577, 1008.
- [45] M. Hiramoto, K. Ihara, and M. Yokoyama. Fermi level shift in photoconductive organic pigment films measured by Kelvin vibrating capacitor method. *Japanese Journal of Applied Physics*, 34:3803, 1995.
- [46] T. Manaka, H. Ohta, M. Iwamoto, and M. Fukuzawa. Electrostatic properties of polyethylene LB films on metal electrodes. *Colloids and Surfaces A: Physicochemical and Engineering Aspects*, 257-258:287–290, 2005.
- [47] H. Ishii, N. Hayashi, E. Ito, Y. Washizu, K. Sugi, A. Kimura, M. Niwano, Y. Ouchi, and K. Seki. Kelvin probe study of band bending at organic semiconductor/metal interfaces: examination of Fermi level alignment. *Physica status solidi (a)*, 201(6):1075–1094, 2004.
- [48] A.C. Dillon, P. Gupta, M.B. Robinson, A.S. Bracker, and S.M. George. FTIR studies of water and ammonia decomposition on silicon surfaces. *Journal of Electron Spectroscopy and Related Phenomena*, 54/55: 1085–1095, 1990.
- [49] R.L. Wells and T. Fort. Adsorption of water on clean gold by measurement of work function changes. *Surface Science*, 32:554–560, 1972.
- [50] N.A. Surplice and W. Brearley. Adsorption of carbon monoxide, am-

- monia, and wet air on gold. *Surface Science*, 52(1):62–74, 1975.
- [51] A. Bilic, J.R. Reimers, N.S. Hush, and J. Hafner. Adsorption of ammonia on the gold (111) surface. *Journal of Chemical Physics*, 116(20): 8981–8987, 2002.
- [52] L. Hanley, X. Guo, and J.T. Yates, Jr. Thermal decomposition of chemisorbed azomethane on Pd(111). *Journal of Physical Chemistry*, 93(18):6754–6757, 1989.
- [53] A.P. Nazarov and D. Thierry. Studies in the electrical double layer at metal/polymer interfaces by scanning capacitive probe. *Protection of Metals*, 39(1):55–52, 2003.
- [54] V.J. Novotny and T.E. Karis. Surface potential of thin perfluoropolyether films on carbon. *Applied Physics Letters*, 71(1):52–54, 1997.
- [55] H. Sugimura, K. Hayashi, N. Saito, N. Nakagiri, and O. Takai. Surface potential microscopy for organized molecular systems. *Applied Surface Science*, 188(3-4):403–410, 2002.
- [56] H. McNally, D.B. Janes, B. Kasibhatla, and C.P. Kubiak. Electrostatic investigation into the bonding of poly(phenylene) thiols to gold. *Superlattices and Microstructures*, 31:239–245, 2002.
- [57] J. Guo, N. Koch, J. Schwartz, and S.L. Bernasek. Direct measurement of surface complex loading and surface dipole and their effect on simple device behavior. *Journal of Physical Chemistry B*, 109:3966–3970, 2005.
- [58] L. Zuppiroli, L. Si-Ahmed, K. Kamaras, F. Nüesch, M.N. Bussac, D. Ades, A. Siove, E. Moons, and M. Grätzel. Self-assembled monolayers as interfaces for organic opto-electronic devices. *The European Physical Journal B*, 11:505, 1999.
- [59] S.M. Tadayyon, K. Griffiths, P.R. Norton, C. Tripp, and Z. Popovic. Work function modification of indium-tin-oxide used in organic light emitting devices. *Journal of Vacuum Science Technology A*, 17(4):1773–1778, 1999.
- [60] I.H. Campbell, S. Rubin, Kress J.D., R.L. Martin, D.L. Smith, N.N. Barashakov, and J.P. Ferraris. Controlling Schottky energy barriers in organic electronic devices using self-assembled monolayers. *Physical Review B*, 54:322, 1996.
- [61] A. Vilan, A. Shanzer, and D. Cahen. Molecular control over Au/GaAs diodes. *Nature*, 404:166–168, 2000.
- [62] I. Larson and P. Attard. Surface charge of silver iodide and several metal oxides. Are all surfaces Nernstian? *Journal of Colloid and Interface*

- Science*, 227:152–163, 2000.
- [63] D.E. Yates, S. Levine, and T.W. Healy. Site-binding model of the electrical double layer at the oxide/water interface. *Journal of the Chemical Society: Faraday Transactions I*, 70:1807–1818, 1974.
- [64] J.A. Davis, R.O. James, and J.O. Leckie. Surface ionization and complexation at the oxide/water interface. I. Computation of electrical double layer properties in simple electrolytes. *Journal of Colloid and Interface Science*, 63:480–499, 1978.
- [65] G.H. Bolt and W.H. Van Riemsdijk. *Soil Chemistry, B. Physico-chemical models*, chapter Ion adsorption on organic variable charge constituents, pages 459–503. Elsevier Science, 1982.
- [66] T. Hiemstra, W.H. Van Riemsdijk, and G.H. Bolt. Multisite proton adsorption modeling at the solid/solution interface of (hydr)oxides: A new approach. I. Model description and evaluation of intrinsic reaction constants. *Journal of Colloid and Interface Science*, 183:91–104, 1989.
- [67] G.A. Parks. The isoelectric points of solids oxides, solid hydroxides, and aqueous hydroxo complex systems. *Chemical Review*, 65(2):177–198, 1965.
- [68] Z. Samec, B.W. Johnson, M. Cappadonia, M. Jauch, and K. Doblhofer. Kelvin probe measurements for chemical analysis: interfacial structure of electrodes exposed to the gas phase containing water vapour. *Sensors and Actuators B*, 14:741–742, 1993.
- [69] I.D. Baikie and P.J. Estrup. Low cost PC based scanning Kelvin probe. *Review of Scientific Instruments*, 69(11):3902, 1998.
- [70] I.D. Baikie, P.J.S. Smith, D.M. Porterfield, and P.J. Estrup. Multitip scanning bio-Kelvin probe. *Review of Scientific Instruments*, 70(3):1842, 1999.
- [71] W.A. Zisman. A new method of measuring contact potential differences in metals. *Review of Scientific Instruments*, 3:367, 1932.
- [72] K. Besocke and S. Berger. Piezoelectric driven Kelvin probe for contact potential difference studies. *Review of Scientific Instruments*, 47:840, 1976.
- [73] I.D. Baikie, K.O. van der Wert, H. Oerbekke, J. Broeze, and A. van Silfhout. Automatic Kelvin probe compatible with ultrahigh vacuum. *Review of Scientific Instruments*, 60(2):930, 1989.
- [74] C. Suresh Kumar, A. Subrahmanyam, and J. Majhi. Automated reed-type Kelvin probe for work function and surface photovoltage stud-

- ies. *Review of Scientific Instruments*, 67:805, 1996.
- [75] K. Germanova, Ch. Hardalov, V. Strashilov, and B. Georgiev. An improved apparatus for surface photovoltage studies with a bimorphous piezoelectric Kelvin probe. *Journal of Physics E: Scientific Instruments*, 20:273, 1987.
- [76] M. Schmidt, M. Nohlen, G. Bermes, M. Böhmer, and K. Wandelt. A versatile Kelvin probe for dynamic work function change measurements during gas adsorption and in situ film growth experiments. *Review of Scientific Instruments*, 68:3866, 1997.
- [77] K.B. Johnson and W.N. Hansen. An acoustically driven Kelvin probe for work-function measurements in gas ambient. *Review of Scientific Instruments*, 66(4):2967, 1995.
- [78] S.C. Fain, L.V. Corbin, and J.M. McDavid. Electrostatically driven apparatus for measuring work function differences. *Review of Scientific Instruments*, 47:345–347, 1976.
- [79] S. Saito, T. Soumura, and T. Maeda. Improvements of the piezoelectric driven Kelvin probe. *Journal of Vacuum Science Technology A*, 2:1389, 1984.
- [80] H.A. Engelhardt, P. Feulner, H. Pfnür, and D. Menzel. An accurate and versatile vibrating capacitor for surface and adsorption studies. *Journal of Physics E: Scientific Instruments*, 10:1133, 1970.
- [81] E.S. Zanoria, K. Hammall, S. Danyluk, and A.L. Zharin. The non-vibrating Kelvin probe and its application for monitoring surface wear. *Journal of Testing and Evaluation*, 25(2):233–238, 1997.
- [82] J.P. Belier, J. Lecoœur, and C. Koehler. Improved Kelvin method for measuring contact potential differences between stepped gold surfaces in ultrahigh vacuum. *Review of Scientific Instruments*, 66(12):5544–5547, 1995.
- [83] N.A. Surplice and R.J. D’Arcy. A critique of the Kelvin method of measuring work functions. *Journal of Physics E: Scientific Instruments*, 3:477, 1970.
- [84] L. Kronik and Y. Shapira. Surface photovoltage techniques: theory, experiments and applications. *Surface Science Reports*, 37:1–206, 1999.
- [85] W. Nabhan, B. Equer, A. Broniatowski, and G. De Rosny. A high-resolution scanning Kelvin probe microscope for contact potential measurements on the 100 nm scale. *Review of Scientific Instruments*, 68(8):3108, 1997.
- [86] J. Ren, H.-D. Ließ, R. Mäckel, and H. Baumgärtner. Scanning Kelvin

- Microscope: a new method for surface investigations. *Fresenius' Journal of Analytical Chemistry*, 353:303, 1995.
- [87] H. Baumgärtner and H.D. Liess. Micro Kelvin probe for local work-function measurements. *Review of Scientific Instruments*, 59:802, 1988.
- [88] P.L. Bergstrom, S.V. Patel, J.W. Schrank, and K.D. Wise. A micro-machined surface work-function gas sensor for low-pressure oxygen detection. *Sensors and Actuators B*, 42:195, 1997.
- [89] L.L. Chu, K. Takahata, P. Selvaganapathy, J.L. Shohet, and Y.B. Gianchandani. A micromachined Kelvin probe for surface potential measurements in microfluidic channels and solid-state applications. In *Conference Proceedings 12th Transducers Boston*, page 384, 2003.
- [90] M. Wolff, A.E. Guile, and D.J. Bell. Measurements of localized surface potential differences. *Journal of Physics E: Scientific Instruments*, 2:921, 1969.
- [91] I.D. Baikie, S. Mackenzie, P.J. Estrup, and J.A. Meyer. Noise and the Kelvin method. *Review of Scientific Instruments*, 62:1326, 1991.
- [92] M. Pfeiffer, K. Leo, and N. Karl. Fermi level determination in organic thin films by the Kelvin probe method. *Journal of Applied Physics*, 80: 6880, 1996.
- [93] C.W. Reedyk and M.M. Perlman. The measurement of surface charge. *Journal of the Electrochemical Society: Solid State Science*, 115(1):49, 1968.
- [94] L.B. Harris and J. Fiasson. Direct determination of surface potential on sodium chloride single crystals: I. Analysis of measurements. *Journal of Physical Chemistry: Solid State Physics*, 18:4845–4862, 1985.
- [95] G.-N. Luo, K. Yamaguchi, T. Terai, and M. Yamawaki. Influence of space charge on the performance of the Kelvin probe. *Review of Scientific Instruments*, 72(5):2350–2357, 2001.
- [96] G.-N. Luo, K. Yamaguchi, T. Terai, and M. Yamawaki. Charging effect on work function measurements of lithium ceramics under irradiation. *Journal of Alloys and Compounds*, 349:211–216, 2003.
- [97] B. Ostrick, M. Fleischer, H. Meixner, and C.-D. Kohl. Investigation of the reaction mechanisms, in work function type gas sensors at room temperature by studies of the cross sensitivity to oxygen and water: the carbonate–carbon dioxide system. *Sensors and Actuators B*, 68: 197–202, 2000.
- [98] G.M. Sessler, J.E. West, and D.A. Berkley. Determination of spatial distribution of charges in thin films. *Physical Review Letters*, 38(7): 368–371, 1977.



- [99] J.R. Anderson and A.E. Alexander. Theory of the vibrating condenser converter and application to contact potential measurements. *Australian Journal of Applied Science*, 3:201, 1952.
- [100] P.P. Craig and V. Radeka. Stress dependence of contact potential: The AC Kelvin method. *Review of Scientific Instruments*, 41(2):258, 1970.
- [101] I.D. Baikie, E. Venderbosch, J.A. Meyer, and P.J.Z. Estrup. Analysis of stray capacitance in the Kelvin method. *Review of Scientific Instruments*, 62:725, 1991.
- [102] A. Hadjadj, P. Roca i Cabarrocas, and B. Equer. Analytical compensation of stray capacitance effect in Kelvin probe measurements. *Review of Scientific Instruments*, 66:5272, 1995.
- [103] B. Ritty, F. Wachtel, R. Manquenouille, F. Ott, and J.B. Donnet. Conditions necessary to get meaningful measurements from the Kelvin method. *Journal of Physics E: Scientific Instruments*, 15:310, 1982.
- [104] F. Rossi. Contact potential measurement: Spacing-dependence errors. *Review of Scientific Instruments*, 63:4174, 1992.
- [105] J.S.W. de Boer, H.J. Krusemeyer, and N.C.B. Jaspers. Analysis and improvement of the Kelvin method for measuring differences in work function. *Review of Scientific Instruments*, 44(8):1003, 1973.
- [106] A. Hadjadj, B. Equer, A. Beorchia, and P. Roca i Cabarrocas. Contact potential measurements with a local Kelvin probe. *Philosophical Magazine B*, 82(11):1257–1266, 2002.
- [107] J. Bonnet, L. Soonckindt, and L. Lassabatère. The Kelvin probe method for work function topographies: technical problems and solutions. *Vacuum*, 34(7):693, 1984.
- [108] T. Schwebel, J. Frank, M. Fleischer, H. Meixner, and C.-D. Kohl. A new type of gas sensor based on thermoionic charge carrier emission. *Sensors and Actuators B*, 68:157–161, 2000.
- [109] P. Topart and M. Josowicz. Transient effects in the interaction between polypyrrole and methanol vapor. *Journal of Physical Chemistry*, 96:8662, 1992.
- [110] P. Topart and M. Josowicz. Characterization of the interaction between poly(pyrrole) films and methanol vapor. *Journal of Physical Chemistry*, 96:7824, 1992.
- [111] M. Josowicz and J. Janata. Suspended gate field effect transistor modified with polypyrrole as alcohol sensor. *Analytical Chemistry*, 58:514, 1986.
- [112] J.V. Hatfield, J.A. Covington, and J.W. Gardner. GasFETs incorporat-

- ing conducting polymers as gate materials. *Sensors and Actuators B*, 65:253–256, 2000.
- [113] R. Cabala, V. Meister, and K. Potje-Kamloth. Effect of competitive doping on sensing properties of polypyrrole. *Journal of the Chemical Society, Faraday Transactions*, 93:131, 1997.
- [114] C. Di Natale, R. Paolesse, A. Mantini, A. Macagnano, T. Boschi, and A. D'Amico. Kelvin probe investigation of self-assembled-monolayers of thiol derivatized porphyrins interacting with volatile compounds. *Sensors and Actuators B*, 48:368, 1998.
- [115] A. D'Amico, C. Di Natale, R. Paolesse, A. Macagnano, and A. Mantini. Metalloporphyrins as basic material for volatile sensitive sensors. *Sensors and Actuators B*, 65:209–215, 2000.
- [116] A. D'Amico, C. Di Natale, R. Paolesse, A. Mantini, C. Goletti, F. Davide, and G. Filosofi. Chemical sensing materials characterization by Kelvin probe technique. *Sensors and Actuators B*, 70(1-3):254–262, 2000.
- [117] M. Andersson, M. Holmberg, I. Lundström, A. Lloyd-Spetz, P. Martenson, R. Paolesse, C. Falconi, E. Proiett, C. Di Natale, and A. D'Amico. Development of a ChemFET sensor with molecular films of phorphyrins as sensitive layer. *Sensors and Actuators B*, pages 567–571, 2001.
- [118] M. Bouvet, G. Guillaudb, A. Leroy, A. Maillard, A. Spirkovitch, and F.-G. Tournilhac. Phthalocyanine-based field-effect transistor as ozone sensor. *Sensors and Actuators B*, 73:63–70, 2001.
- [119] C. Gu, L. Sun, T. Zhang, T. Li, and X. Zhang. High-sensitivity phthalocyanine LB film gas sensor based on field effect transistor. *Thin solid films*, 327-329:383–386, 1998.
- [120] E. Simon, M. Fleischer, and H. Meixner. Polyvinylpyrrolidon: A new material for humidity sensing using work function read out. In *Conf. Proc. 8th IMCS Basel*, page 194, July 2000.
- [121] J. Wöllenstein, F. Ihlenfeld, M. Jaegle, G. Köhner, H. Böttner, and W.J. Becker. Gas-sensitive p-GaAs field effect device with catalytic gate. *Sensors and Actuators B*, 68:22–26, 2000.
- [122] N. Barsan, A. Heilig, J. Kappler, U. Weimar, and W. Göpel. CO - water interaction with Pd-doped SnO<sub>2</sub> gas sensors: Simultaneous monitoring of resistances and work functions. In *Conf. Proc. Euroensors XIII*, page 183, 1999.
- [123] B. Flietner, T. Doll, J. Lechner, M. Leu, and I. Eisele. Fabrication of a hybrid field-effect structure for gas detection with diverse sensitive

- materials. *Sensors and Actuators B*, 18-19:632, 1994.
- [124] A. Gurlo, M. Sahm, A. Oprea, N. Barsan, and U. Weimar. A p- to n-transition on  $\alpha$ -Fe<sub>2</sub>O<sub>3</sub>-based thick film sensors studied by conductance and work function change measurements. *Sensors and Actuators B*, 102:291–298, 2004.
- [125] M. Bögner, A. Fuchs, K. Scharnagel, R. Winter, Th. Doll, and I. Eisele. Thin (NO)<sub>1-x</sub> (Al<sub>2</sub>O<sub>3</sub>)<sub>x</sub>, Al doped and Al coated NiO layers for gas detection with HGSFET. *Sensors and Actuators B*, 47:145, 1998.
- [126] A. Karthegeyan, R.P. Gupta, K. Scharnagl, M. Burgmair, S.K. Sharma, and I. Eisele. A room temperature HSGFET ammonia sensor base on iridium oxide thin film. *Sensors and Actuators B*, 85:145–153, 2002.
- [127] U. Lampe, E. Simon, R. Pohle, M. Fleischer, H. Meixner, H.-P. Frerichs, M. Lehmann, and G. Kiss. GasFETs for the detection of reducing gases. In *Technical Digest of Euroensors XVIII*, page 648, 2004.
- [128] T. Doll, K. Scharnagel, R. Winter, I. Bögner, M. Eisele, B. Ostrick, and M. Schöning. Work function gas sensors - reference layers and signal analysis. In *Conference Proceedings Euroensors XII*, pages 143–146, 1998.
- [129] T. Doll, J. Lechner, I. Eisele, K.-D. Schierbaum, and W. Göpel. Ozone detection in the ppb range with work function sensors operating at room temperature. *Sensors and Actuators B*, 34:506–510, 1996.
- [130] B. Ostrick, J. Mühlsteff, M. Fleischer, H. Meixner, T. Doll, and C.-D. Kohl. Adsorbed water as key to room temperature gas sensitive reactions in work function type sensors: The carbonate - carbon dioxide system. *Sensors and Actuators B*, 57:115–119, September 1999.
- [131] B. Ostrick, M. Fleischer, and H. Meixner. The influences of interfaces and interlayers on the gas sensitivity in work function type sensors. *Sensors and Actuators B*, 95:271–274, 2003.
- [132] J. Cassidy, S. Pons, and J. Janata. Hydrogen response of palladium coated gate field effect transistor. *Analytical Chemistry*, 58:1757, 1986.
- [133] M. Zimmer, M. Burgmair, K. Scharnagl, A. Karthigeyan, T. Doll, and I. Eisele. Gold and platinum as ozone sensitive layer in work-function gas sensors. *Sensors and Actuators B*, 80:174–178, 2001.
- [134] D. Filippini, L. Fraigi, R. Aragon, and U. Weimar. Thick film Au-gate field-effect devices sensitive to NO<sub>2</sub>. *Sensors and Actuators B*, 81: 296–300, 2002.
- [135] G. Kiss, E.B. Varhegyi, J. Mizsei, O.H. Krafcsik, K. Kovacs, G. Negyesi, B. Ostrick, H. Meixner, and F. Reti. Examination of the CO/Pt/Cu

- layer structure with Kelvin probe and XPS analysis. *Sensors and Actuators B*, 68:240–243, 2000.
- [136] I. Lundström, A. van den Berg, B. H. van der Schoot, H. H. van den Vlekkert, N. Armgard, and C. I. Nylander. *Sensors - A Comprehensive Survey*, chapter Field effect Chemical Sensors, pages 467–458. VCH Verlagsgesellschaft, 1991.
- [137] S.M. Sze. *Semiconductor Devices - Physics and Technology*. John Wiley & Sons, 2nd edition, 2002.
- [138] P. Bergveld. Development of an ion-selective solid state device for neurophysiological measurements. *IEEE Trans. Biomed Eng.*, 17:70, 1970.
- [139] P. Bergveld. Thirty years of ISFETOLOGY – What happened in the past 30 years and what may happen in the next 30 years. *Sensors and Actuators B*, 88(1):1–20, 2003.
- [140] I. Eisele, T. Doll, and M. Burgmaier. Low power gas detection with FET sensors. *Sensors and Actuators B*, 78:19–25, 2001.
- [141] C. Wilbertz, H.-P. Frerichs, I. Freund, and M. Lehmann. Suspended-gate and Lundstrom-FET integrated on a CMOS-chip. *Sensors and Actuators B*, in press, 2005.
- [142] Z. Gergintschew, P. Kometzky, and D. Schipanski. The capacitively controlled field effect transistor (CCFET) as a new low power gas sensor. *Sensors and Actuators B*, 35-36:285–289, 1996.
- [143] M. Burgmaier, H.-P. Frerichs, M. Zimmer, M. Lehmann, and I. Eisele. Field effect transducers for work function gas measurements: device improvements and comparison of performance. *Sensors and Actuators B*, 95:183–188, 2003.
- [144] L.-G. Ekedahl, M. Eriksson, and I. Lundström. Hydrogen sensing mechanisms of metal-insulator interfaces. *Accounts of Chemical Research*, 31:249–256, 1998.
- [145] P. Kreisl, A. Helwig, A. Friedberger, G. Müller, E. Obermeier, and S. Sotier. Detection of hydrocarbon species using silicon MOS capacitors operated in a non-stationary temperature pulse mode. *Sensors and Actuators B*, 106(2):489–497, 2005.
- [146] A.E. Åbom, E. Comini, G. Sberveglieri, L. Hultmann, and M. Eriksson. Thin oxide films as surface modifiers in MIS field effect gas sensors. *Sensors and Actuators B*, 85:109–119, 2002.
- [147] A.E. Åbom, R.D. Twisten, L. Hultman, and M. Eriksson. Properties of combined TiN and Pt thin films applied to gas sensing. *Journal of*

- Vacuum Science and Technology A*, 20(3):667–673, 2002.
- [148] L. Talazac, F. Barbarin, C. Varenne, L. Mazet, S. Pellier, and C. Soulier. Gas sensing properties of pseudo-Schottky diodes on p-type indium phosphide substrates: application to O<sub>3</sub> and NO<sub>2</sub> monitoring in urban ambient air. *Sensors and Actuators B*, 83:149–159, 2002.
- [149] L.M. Lechuga, A. Calle, D. Golmayo, F. Briones, J. De Abajo, and J.G. De La Campa. Ammonia sensitivity of Pt/GaAs Schottky barrier diodes. improvement of the sensor with an organic layer. *Sensors and Actuators B*, 8(3):249–252, 1992.
- [150] L.M. Lechuga, G. Mier, A. Calle, D. Golmayo, and F. Briones. Urea biosensor based ammonia gas-sensitive Pt/GaAs Schottky diode. *Sensors and Actuators B*, 21(3):205–208, 1994.
- [151] M. Campos, L.O.S. Bulhoes, and C.A. Lindino. Gas-sensitive characteristics of metal/semiconductor polymer Schottky device. *Sensors and Actuators A*, 87:67–71, 2000.
- [152] Andreas Krauß. *Hall-Effekt-Messungen an nanokristallinem Sensormaterial und applikationsspezifische Sensorentwicklung*. PhD thesis, University of Tübingen, <http://w210.ub.uni-tuebingen.de/dbt/volltexte/2001/293/>, 2001.
- [153] J.A. Riddick, W.B. Bunger, and T.K. Sakano. *Organic solvents - Physical Properties and Methods of Purification*, volume 2. John Wiley & Sons, New York, 4th edition, 1986.
- [154] J. Brandrup, E.H. Immergut, and E.A. Grulke, editors. *Polymer Handbook*. John Wiley & Sons, 4 edition, 1999.
- [155] E.S. Wilk, editor. *Industrial Polymer Handbook - Products, Processes, Applications*. Wiley-VCH, 2001.
- [156] The semi-automatic polymer deposition system was designed by A. Oprea.
- [157] G. Sauerbrey. Use of vibrating quartz for thin film weighting and microweighting. *Zeitschrift für Physik*, 155:206, 1959.
- [158] Michael Frank. *Multi-Sensor Systems for VOC: Recalibration and Coating Procedures*. PhD thesis, University of Tübingen, <http://w210.ub.uni-tuebingen.de/dbt/volltexte/2001/250/>, 2001.
- [159] S. Wu, F. Li, Y. Zhu, and J. Shen. The switch-type humidity sensing properties of polyacrylic acid and its copolymers. *Journal of Materials Science*, 35(8):2005–2008, 2000.
- [160] D. Santhiya, S. Subramanian, K. A. Natarajan, and S.G. Malghan. Surface chemical studies on the competitive adsorption of poly(acrylic

- acid) and poly(vinyl alcohol) onto alumina. *Journal of Colloid and Interface Science*, 216:143–153, 1999.
- [161] J.D. Mendelsohn, C.J. Barrett, V.V. Chan, A.J. Pal, A.M. Mayes, and M.F. Rubner. Fabrication of microporous thin films from polyelectrolyte multilayers. *Langmuir*, 16:5071–5023, 2000.
- [162] Mika Harbeck. Austrittsarbeitsänderung bei polymerbeschichteten Sensorstrukturen: Bestimmung mit der Kelvin-Methode. Master's thesis, University of Tübingen, 2000.
- [163] A. Oprea. Personal Communication.
- [164] A. Oprea, E. Simon, M. Fleischer, H.-P. Frerichs, C. Wilbertz, M. Lehmann, and U. Weimar. Flip-chip suspended gate field effect transistors for ammonia detection. In *Technical Digest of Eurosensors XVIII*, pages 18–19, 2004.
- [165] S. Kurosawa, H. Miura, H. Takahashi, J.-W. Park, H. Aizawa, K. Noda, K. Yamada, and M. Hirata. Preparation of long-lifetime gas recognition films by plasma polymerization technique. *Sensors and Actuators B*, 108(1-2):558–563, 2005.
- [166] Y. Li, M.J. Yang, N. Camaioni, and G. Casalbore-Miceli. Humidity sensors based on polymer solid electrolytes: investigation on the capacitative and resistive devices construction. *Sensors and Actuators B*, 39:1–7, 2001.
- [167] M.C. Lonergan, E.J. Severin, B.J. Doleman, S.A. Beaber, R.H. Grubbs, and N.S. Lewis. Array-based vapor sensing using chemically sensitive, carbon black-polymer resistors. *Chemical Materials*, 8:2298–2312, 1996.
- [168] Desiree Barten. *Absorption of Charged Macromolecules on a Gold Electrode*. PhD thesis, Wageningen University, 2003.

## List of Publications and Presentations

### Publications

M. Fleischer, E. Simon, E. Rumpel, H. Ulmer, M. Harbeck, M. Wandel, C. Fietzek, U. Weimar, and H. Meixner. Detection of volatile compounds correlated to human diseases through breath analysis with chemical sensors. *Sensors and Actuators B*, 83:245, 2002.

M. Harbeck, S. Riegelsberger, A. Oprea, N. Barsan, and U. Weimar. Organic non-conducting materials as sensitive layers for field effect gas sensing. In *Dresdner Beiträge zur Sensorik*, w.e.b. Universitätsverlag, Dresden, page 153, 2003.

J. Claußen, C. Fietzek, M. Harbeck, U. Weimar, and H.-G. Mack. Electronic structures of phthalocyanines after exposure to NO<sub>2</sub>. In *Dresdner Beiträge zur Sensorik*, w.e.b. Universitätsverlag, Dresden, page 165, 2003.

A. Oprea, J. Claußen, C. Fietzek, M. Harbeck, H.-G. Mack, and U. Weimar. Bioanalytical and medical trends in sensor applications; organic layers for field effect application. *Technology and Healthcare – International Journal of Health Care Engineering*, 12(2):139, 2004.

### Oral and Poster Presentations

M. Harbeck, M. Wandel, and U. Weimar. Kelvin Probe Measurements: Work Function Changes of Non-conducting Polymers upon Gas Exposure. InCom Symposium, 2001, Dusseldorf (Germany).

M. Fleischer, E. Simon, E. Rumpel, H. Ulmer, M. Harbeck, M. Wandel, C. Fietzek, U. Weimar, and H. Meixner. Detection of volatile compounds correlated to human diseases through breath analysis with chemical sensors. Transducers/Eurosensors 01, 2001, Munich (Germany).

M. Harbeck, M. Wandel, and U. Weimar. Non-Conducting organic polymers as sensitive layers in work function sensors: studies with the Kelvin probe. MATCHEMS Symposium, 2001, Brescia (Italy).

M. Harbeck and U. Weimar. Investigations of work function changes of non-conducting organic polymers upon gas absorption. 9th International Meeting on Chemical Sensors (IMCS), 2002, Boston (USA).

A. Oprea, J. Claußen, C. Fietzek, M. Harbeck, H.-G. Mack, and U. Weimar. Organic layers for field effect application. 7th Conference of the European Society for Engineering and Medicine (ESEM), 2003, Halle (Germany).

M. Harbeck, S. Riegelsberger, A. Oprea, N. Barsan, and U. Weimar. Organic non-conducting materials as sensitive layers for field effect gas sensing. 6. Dresdner Sensor Symposium, 2003, Dresden (Germany).

J. Claußen, C. Fietzek, M. Harbeck, U. Weimar, and H.-G. Mack. Electronic structures of phthalocyanines after exposure to NO<sub>2</sub>. 6. Dresdner Sensor Symposium, 2003, Dresden (Germany).

M. Harbeck and U. Weimar. New Applications of Organic Polymers in Chemical Gas Sensors. Institute Seminary, Faculty of Natural Sciences, Gebze Institute of Technology, 2005, Gebze (Turkey).



Meine akademischen Lehrer waren:

K. Albert, E. Bayer, D. Christen, H. Eckstein, G. Gauglitz, F. Gönnenwein, W. Göpel, G. Häfelinger, H. Hagenmaier, M. Hanack, V. Hoffmann, W. Jäger, G. Jung, S. Kemmler-Sack, W. Koch, B. Koppenhöfer, D. Krug, N. Kuhn, E. Lindner, H.-G. Mack, M. E. Maier, H.-J. Mayer, U. Nagel, H. Oberhammer, D. Oelkrug, H. Pauschmann, G. Pausewang, H. Pommer, G. Reinhardt, K.-D. Schierbaum, D. Schrenk, V. Schurig, E. Schweda, F. F. Seelig, H. Stegmann, J. Strähle, W. Voelter, K.-P. Zeller, C. Ziegler (Tübingen)

Weston T. Borden, C. Campbell, K. Goldberg, H. Jónsson, P. Reid, L.J. Slutsky (Seattle)



# Lebenslauf

## Mika Harbeck

Geburtsdatum

15. Juli 1972

Geburtsort

Kangasniemi (Finnland)

## Hochschulausbildung

09/2000 – 10/2005

Anfertigung der Promotion unter Betreuung von PD Dr. habil. Udo Weimar am Institut für Physikalische und Theoretische Chemie der Universität Tübingen: „Neue Einsatzmöglichkeiten organischer Polymere in chemischen Gassensoren“

05.09.2000

Diplom in Chemie

03/2000 – 09/2000

Diplomarbeit: „Austrittsarbeitsänderung bei polymerbeschichteten Sensorstrukturen: Bestimmung mit der Kelvin-Methode“

09/1996 – 07/1997

Auslandsstudium an der University of Washington in Seattle (USA), Fulbright Reisestipendium

10/1993 – 09/2000

Studium der Chemie an der Universität Tübingen

09/1992 – 05/1993

Studienaufenthalt an der Viittakivi International School, Hauho (Finnland)

## Schulbildung

08/1983 – 06/1992

Hermann-Tast-Schule, Husum

04.06.1992

Abschluss: Allgemeine Hochschulreife

## Aufgabenbereiche während der Promotion

09/2000 – heute

Anstellung als Wissenschaftlicher Angestellter am Institut für Physikalische und Theoretische Chemie der Universität Tübingen:

- Mitwirkung in den Forschungsprojekten LocoMED (BMB+F 16SV1083/6) und Advantagas (IST 2001-33148)
- Koordination des europäischen thematischen Netzwerkes NOSE II (IST 2001-32949)
- Computer- und Netzwerkadministration
- Assistent in den Fortgeschrittenenpraktika für Chemiker und Biochemiker



# Curriculum Vitae

## Mika Harbeck

Date of birth

15 July 1972

Place of birth

Kangasniemi (Finland)

## Education

09/2000 – 10/2005

Work on the doctoral thesis at the Institute of Physical and Theoretical Chemistry, University of Tübingen, directed by PD Dr. habil. Udo Weimar: "New applications of organic polymers in chemical gas sensors"

05/09/2000

Diploma in Chemistry

03/2000 – 09/2000

Diploma thesis: "Work function changes of polymer coated sensor structures: investigations with the Kelvin probe"

09/1996 – 07/1997

Study abroad at the University of Washington, Seattle (USA), Fulbright Travel Grant

10/1993 – 09/2000

Student of Chemistry at the University of Tübingen (Germany)

09/1992 – 05/1993

International studies at the Viittakivi International School, Hauho (Finland)

08/1983 – 06/1992

Hermann-Tast-Gymnasium, Husum (Germany)

04/06/1992

Abitur / German high school diploma

## Work experience

09/2000 – present

Research and Teaching Assistant at the Institute of Physical and Theoretical Chemistry, University of Tübingen:

- Involvement in the research projects LocoMED (BMB+F 16SV1083/6) and Advantagas (IST 2001-33148)
- Coordination of the European thematic network NOSE II (IST 2001-32949)
- Computer and network administrator
- Teaching assistant for graduate students in chemistry and biochemistry



## Danksagungen

Mein größter Dank geht an PD Dr. Udo Weimar für die Überlassung des interessanten Themas und die hervorragenden Arbeitsbedingungen in seiner Arbeitsgruppe. Unschätzbar waren die Möglichkeiten neben der Doktorarbeit vielfältige Erfahrungen zu sammeln, die weit über die eigentliche Tätigkeit hinausgingen.

Herrn Prof. Dr. Günter Gauglitz danke ich für die Übernahme des Koreferats und zusammen mit Prof. Dr. Lars Wesemann (Vorsitz), Prof. Dr. Heinz Oberhammer und Prof. Dr. Günter Häfelinger für die Bereitschaft, die Prüfungskommission bei der Verteidigung zu bilden.

Dr. Alexandru Oprea danke ich für seine wertvolle Hilfe und Unterstützung bei der Planung, dem Aufbau und der Durchführung der Experimente sowie seinen Anmerkungen bei der Korrektur dieser Arbeit.

Ein weiterer Dank geht an Mihail Croitoru (Institut für Angewandte Physik) für die Aufnahme der REM- und AFM-Messungen und an Dr. Serpil Harbeck für die Hilfe bei den IR-Messungen.

Ute Harbusch und Egon Merz danke ich für ihre Unterstützung bei den administrativen Tätigkeiten, die vor allem bei NOSE II angefallen sind. Ihre freundliche Art war jedes Mal eine große Ermunterung bei diesem meist ungeliebten Teil der Arbeit.

Den Projektpartnern in Locomed, Advantagas und auch NOSE II gilt mein Dank für die gute Zusammenarbeit, und allen Geldgebern gebührt Dank für die Finanzierung meiner Arbeit.

Erst meine Freunde, Studien- und Arbeitskollegen und Zimmergenossen in VG 2.110 haben meine Zeit in Tübingen unvergesslich gemacht. Besonders erwähnen möchte ich an dieser Stelle Georg Belge, Jan und Susanne Claußen, Christopher Fietzek, Michael Frank, Martin Herold, Andreas Krauß, Almuth Liebich, Mathias Nagel, Jan Mitrovics, Nikos Papamichail, Wolf Schmid, Stefan und Astrid Strathmann, Matthias Vollprecht, Michael Wandel, Christine Weinl und Olaf Wurzinger. Es war wirklich eine schöne Zeit mit Euch hier in Tübingen.

Allen bisher nicht genannten Kollegen im Arbeitskreis und am ganzen Institut möchte ich zusammenfassend danken. Sie hätten es sicherlich verdient, hier gebührender gewürdigt zu werden. Doch fallen mir noch besonders Götz Reinhardt und seine Mitstreiter im 10. Stock des B-Gebäudes sowie Hans-Joachim Egelhaaf und Prof. Volker Hoffmann ein.

Zu guter Letzt möchte ich auch meiner ganzen Familie und insbesondere meiner Frau Serpil für ihre vielfältige Unterstützung während des Studiums und der Doktorarbeit danken.